SUSPENSIONS:

MICROSTRUCTURE, DIFFUSION, AND INHOMOGENEOUS FLOW

Dissertation by

Jeffrey Franklin Morris

In Partial Fulfillment of the Requirements

for the Degree of

Doctor of Philosophy

California Institute of Technology

Division of Chemistry and Chemical Engineering

Pasadena, California

1996

(Defended 19 May 1994)

To my parents

and

To the memory of Chara Economou

Acknowledgments

My decision to come to Caltech would not have been made were it not for the efforts of Professor John Brady, who subsequently became my thesis advisor. Those efforts were successful for the promise of an environment which is openminded yet critical. This promise has been kept: Caltech is a place rare for the quality and integrity of its people. For his continuous excitement for science, willingness to lend his mind to investigations of alternative viewpoints, and dedication to truth, John Brady is an exemplar of these attributes. I have experienced no hour of regret for my decision to study at Caltech.

To the others who have served on my candidacy and thesis committees, many thanks are given: to Professor Roberto Mauri of the City College of New York, and to Professors Rudolph Marcus, George Gavalas, Julia Kornfield, and Zhen-Gang Wang of Caltech. To the final three, I am deeply grateful for the additional efforts made on my behalf as I have sought a career in science.

My groupmates — Roger Bonnecaze, John Bauer, Ivan Claeys, Thanh Phung, Phil Lovalenti, Yvette Baxter, Yevgeny Yurkovetsky, Mike Vicic, Douglas Varela, Willem Boersma, Prabhu Nott, and Mehrzad Tabatabaian — have filled the days with challenge, laughter, and smiles. To Roger and Phil, thanks for guidance and special friendship. To Zhenya and Prabhu, thanks for so much laughter and good conversation. Paul Rider, in his brief stay with us above the equator, added great pleasure to my life.

The years in Pasadena were made rich through the uncommon friendship of Rich

Barrett, Thanh Phung, Chara Economou, and Michael Tsapatsis.

For the love of Neena Imam through it all, I shall be ever grateful.

Abstract

A theory of self-diffusivity in sheared suspensions valid for any particle volume fraction ϕ, Péclet number Pe, and lengthscale of disturbance in ϕ is developed. The theory is applied to the determination of the full tensor self-diffusivity in a weakly-sheared ($Pe \ll 1$) suspension of hydrodynamically-interacting hard spheres and a strongly-sheared ($Pe \gg 1$) suspension of hard spheres without hydrodynamic interactions, both at $\phi \ll 1$.

The influence of weak Brownian motion alone and in conjunction with a repulsive interparticle force of hard-sphere type upon the pair-distribution function, $g(\boldsymbol{r})$ where $\boldsymbol{r}$ is the separation vector of a pair of particles, is analyzed for a suspension of spheres at $Pe \gg 1$ and $\phi \ll 1$. At large Pe, the radial fluxes of pair probability due to advection and Brownian diffusion balance in a thin $O(a\,Pe^{-1})$ boundary layer at contact, with a the sphere radius. The boundary-layer analyses demonstrate that Brownian diffusion renders g finite at contact in the absence of interparticle forces, and that within the boundary layer there is generally a large excess of pair probability along the compressional axes. By calculation of the bulk normal stress differences in the case with repulsive forces, it is shown how this asymmetry of the microstructure yields nonNewtonian constitutive behavior in the limit $Pe^{-1} = 0$.

Hydrodynamic resistance functions relating the particle and bulk motions to the bulk isotropic stress are developed. Application of these functions is demonstrated by calculations of the shear-induced correction to the osmotic pressure and the particle contribution to the pressure in a sheared lattice.

Pressure-driven flow in a channel at vanishing Reynolds number of a suspension of particles denser than the suspending fluid has been dynamically simulated by Stokesian Dynamics over ranges of the particle fraction, channel width, and a buoyancy parameter characterizing the relative strength of the buoyancy to shearing forces. The predictions of the flow by the suspension-balance model* are in good agreement with simulation results.

*Nott, P. R. & J. F. Brady 1994 *J. Fluid Mech.* **275**, 157.

Contents

List of Figures

List of Tables

Chapter 1

Introductory discussion

This volume describes several investigations of the properties and behavior of suspensions. In this discussion, we describe the various studies with the goal of indicating our motivations for the work, as well as to establish the relations between the investigations. Suspensions of spherical particles in Newtonian fluid under conditions of small Reynolds number are studied. The significance of the analyses and conclusions is not necessarily limited to suspensions of spheres, but in all calculations spherical particles are considered.

As the perspective in the final chapter is rather different from the others, we note at the outset how the other studies have contributed to or are related to this work. In Chapters 2, 3, and 4, we consider the particle dynamics to elucidate certain aspects of the microscopic basis for the bulk flow behavior in suspensions. In Chapter 5, bulk flow itself is the central subject, as we describe a study of pressure-driven channel flow of a suspension in which the particles, being denser than the fluid, tend to settle. In this flow, shear-induced migration caused by the inhomogeneous shear rate (Leighton & Acrivos 1987*b*) competes with gravitational settling, leading to the phenomenon of heavy material flowing stably above light over a wide range of the relevant parameters. Our study shows that this complicated flow behavior can be described by the flow model of Nott & Brady (1994), which uses the notion of the particle pressure in a noncolloidal suspension. The resistance functions necessary to evaluate the particle pressure are described in Chapter 4. Important justification for nonNewtonian constitutive relations employed in this model are provided by Chapter 3, in which the microstructure of a strongly-sheared suspension is analyzed. In addi-

tion, we have shown in Chapter 3, using the theory of Chapter 2, that the bulk stress due to particle interactions, the driving force for the migration, and the self-diffusivity are linearly related.

Determination of macroscopic properties from the microscopic dynamics is a statistical mechanical problem. Suspensions, like many other well-studied systems of statistical mechanics, consist of assemblies of many particles whose precise locations are not known, and equilibrium properties of suspensions, *e.g.* the osmotic pressure, are described by familiar equilibrium statistical mechanical formulae (Russel, Saville & Schowalter 1989). We do not, however, remain upon the familiar ground of equilibrium suspensions, but rather devote ourselves to the study of nonequilibrium suspensions. The work is primarily concerned with suspensions under shear, although much of the formal theory of Chapters 2-4 may be applied to sedimentations.

There are two separate problems in the statistical description of material properties. The first is to determine the probability distribution of the phase variables, and the second is to describe the property of interest in terms of the probability distribution and the relevant particle-scale and bulk parameters. In each of Chapters 2-4, the dual nature of the problem of property determination is reflected, with the problem of primary emphasis differing in the various investigations. We are fortunate in studying low-Reynolds-number flow because here the particle configuration, and not the configuration plus momentum, is the complete set of phase variables, because the velocities are strictly position-dependent. This is no longer true if the particles or the fluid have momentum. Thus it is possible, at least at the pair level, to determine

the nonequilibrium particle microstructure (the average configuration) analytically.

Particle dynamics based upon the Smoluchowski equation (Russel 1993) is the common theme of Chapters 2 and 3. The Smoluchowski equation describes the evolution of the configurational probability of suspended particles on timescales long relative to the time required for Brownian momentum impulses to decay, with Brownian motion included as a diffusive flux. The relative strengths of the bulk flow, Brownian diffusion, and interparticle forces determine the microstructure, and hence the bulk behavior. The Péclet number, Pe, is a measure of the relative strength of the shear flow to that of Brownian motion and plays an important role in our work.

We begin by studying self diffusion, the most basic transport mechanism in a suspension. For self diffusion, the microstructural problem must be considered in full generality, as not only the average microstructure at the conditions of interest, but also the perturbation to this structure caused by the motion of a diffusing particle, are necessary for evaluation of self-diffusivity. The theory is applied in Chapter 2 to a weakly-sheared ($Pe \ll 1$) suspension to obtain the full tensor self-diffusivity of a dilute suspension of spheres with and without hydrodynamic interactions. In Chapter 3, the theory is applied to the determination of the self-diffusivity of a large-Pe suspension of hard spheres without hydrodynamic interactions.

Before applying the theory of self-diffusion at $Pe \gg 1$, the steady microstructure in the strongly-sheared suspension is determined. We have considered suspensions in which the particles interact hydrodynamically and through a repulsive hard-sphere force at $|\boldsymbol{r}| = 2b \geq 2a$, with a the particle radius and $\boldsymbol{r}$ the pair sep-

aration. (In a hydrodynamically-interacting suspension, $b = a$ corresponds to no interparticle forces.) The microstructure under these conditions is characterized by large excesses—$O(Pe^{0.78})$ if $b = a$ and $O(Pe)$ if $b > a$—of particles within a narrow $O(a\,Pe^{-1})$ boundary layer at $r = 2b$ in the compressional quadrants, *i.e.* where a pair of particles are approaching one another. Batchelor & Green (1972*b*) showed that the pair-distribution function, $g(\boldsymbol{r})$, of a suspension in pure straining flow at $Pe^{-1} = 0$ is spherically symmetric if nonhydrodynamic forces between particles are absent, and that this symmetry results in Newtonian rheology, despite the fact that g diverges at particle contact. Our study shows how weak residual Brownian motion and short-ranged repulsive interparticle forces lead to the asymmetry, and we determine the dependence of g upon both Pe and b/a. This allows us to determine the manner in which the rheological behavior tends toward Newtonian as $Pe \to \infty$ and $b/a - 1 \to 0$. For $b = a$, we find that in hydrodynamically-interacting suspensions, the normal stress differences as $Pe \to \infty$ are $O(Pe^{-0.22})$. For any $b > a$, the normal stress differences are independent of Pe in the limit $Pe^{-1} = 0$, and scale as $(b/a-1)^{0.22}$ for $b/a-1 \to 0$. We believe that the slow vanishing of the nonNewtonian effects as $Pe \to \infty$ provides at least a partial explanation (partial only because the analysis is for dilute suspensions) for the sizeable normal stress differences found in Stokesian Dynamics (Brady & Bossis 1988) simulations of suspensions at $Pe = 10^4$ by Phung (1993), despite the absence of interparticle forces. For $b > a$, the slow decay as $b/a - 1 \to 0$ suggests that normal stress differences will be measurable even for suspensions with extremely short-ranged forces. The work of Chapter 3 thus provides

theoretical justification for modeling the normal stresses of noncolloidal suspensions as being dependent on the strain rate, as is done indirectly in the model of Nott & Brady (1994).

The notion of a particle pressure was employed in the suspension community (Batchelor 1988; Jenkins & McTigue 1990) without theoretical justification until the work of Chapter 4 appeared as Jeffrey, Morris & Brady (1993). This work describes the hydrodynamic resistance functions which relate the pressure moments on particle surfaces to the particle and bulk motions in a low-Reynolds-number suspension. Examples of the application of the functions to the calculation of the shear-induced correction to the osmotic pressure and the suspension pressure in a sheared lattice are presented.

Chapter 5 is a combined simulational and modeling study, in which the influence of particle buoyancy upon the bulk flow in pressure-driven channel flow of a suspension is investigated. This resuspension-type flow involves a competition between gravitational settling and shear-induced migration which leads to the interesting flow with relatively dense material flowing above lighter. Stokesian Dynamics simulations were used as numerical experiments to generate information about the bulk flow under a variety of conditions. The suspension-balance model of Nott & Brady (1994) was used to predict the flow and the model predictions were compared in order to determine the success of the model and determine potential directions for improvement. The agreement between model predictions and simulational results is very good.

We reiterate that a common theme throughout this volume is that the inter-

play of forces at the particle scale—these forces include Brownian or thermal forces, electrostatic forces, hydrodynamic forces, and the forces of an external field such as gravity—yields a nonequilibrium microstructure. The anisotropy in the microstructure influences the bulk behavior in a fundamental and often striking manner, with a good example being shear-induced migration and the resulting macroscopically nonuniform particle concentrations. From either an engineering or scientific persective, the success in modeling the bulk flow of a suspension over the range of conditions described in Chapter 5 is encouraging, and it is hoped that further study devoted to the flow of suspensions finds its impetus in this work.

Chapter 2

Self diffusion in sheared suspensions

Abstract

Self diffusion in a suspension of spherical particles in steady linear shear flow is investigated by following the time evolution of the correlation of number density fluctuations. Expressions are presented for the evaluation of the self-diffusivity in a suspension which is either macroscopically quiescent or in linear flow at arbitrary Péclet number $Pe = \dot{\gamma}a^2/2D$, where $\dot{\gamma}$ is the shear rate, a is the particle radius, and $D = k_BT/6\pi\eta a$ is the diffusion coefficient of an isolated particle. Here, k_B is Boltzmann's constant, T is the absolute temperature, and η is the viscosity of the suspending fluid. The short-time self-diffusion tensor, $\boldsymbol{D}_0^s$, is given by k_BT times the microstructural average of the hydrodynamic mobility of a particle, and depends on the volume fraction $\phi = \frac{4}{3}\pi a^3 n$ and Pe only when hydrodynamic interactions are considered. As a tagged particle moves through the suspension, it perturbs the average microstructure, and the long-time self-diffusion tensor, $\boldsymbol{D}_\infty^s$, is given by the sum of $\boldsymbol{D}_0^s$ and the correlation of the flux of a tagged particle with this perturbation. In a flowing suspension both $\boldsymbol{D}_0^s$ and $\boldsymbol{D}_\infty^s$ are anisotropic, in general, with the anisotropy of $\boldsymbol{D}_0^s$ due solely to that of the steady microstructure. The influence of flow upon $\boldsymbol{D}_\infty^s$ is more involved, having three parts: the first is due to the nonequilibrium microstructure, the second is due to the perturbation to the microstructure caused by the motion of a tagged particle, and the third is by providing a mechanism for diffusion that is absent in a quiescent suspension through correlation of hydrodynamic velocity fluctuations.

The self-diffusivity in a simply-sheared suspension of identical hard spheres is determined for $Pe \ll 1$ and $\phi \ll 1$, both with and without hydrodynamic interactions

between the particles. The leading dependence upon flow of $\boldsymbol{D}_0^s$ is $0.22D\phi Pe\hat{\boldsymbol{E}}$, where $\hat{\boldsymbol{E}}$ is the rate-of-strain tensor made dimensionless with $\dot{\gamma}$. Regardless of whether or not the particles interact hydrodynamically, flow influences $\boldsymbol{D}_\infty^s$ at $O(\phi Pe)$ and $O(\phi Pe^{3/2})$. In the absence of hydrodynamics, the leading correction is proportional to $\phi PeD\hat{\boldsymbol{E}}$. The correction of $O(\phi Pe^{3/2})$, which results from a singular advection-diffusion problem, is proportional, in the absence of hydrodynamic interactions, to $\phi Pe^{3/2}D\boldsymbol{I}$; when hydrodynamics are included, the $O(\phi Pe^{3/2}D)$ correction is given by two terms, one proportional to $\hat{\boldsymbol{E}}$, and the second a nonisotropic tensor.

At high ϕ a scaling theory based on the approach of Brady (1994) is used to approximate $\boldsymbol{D}_\infty^s$. For weak flows the long-time self-diffusivity factors into the product of the long-time self-diffusivity in the absence of flow and a nondimensional function of $\bar{Pe} = \dot{\gamma}a^2/2D_0^s(\phi)$. At small $\bar{Pe}$, the dependence on $\bar{Pe}$ is the same as at low ϕ.

2.1 Introduction

This work addresses the problem of calculating the self-diffusivity in a suspension undergoing steady shear at small Reynolds number. Self diffusion is one of the most basic transport processes occurring in a suspension, and self-diffusivity in a quiescent system is among the most intensely studied properties in colloid and polymer science. Determining the influence of shearing flow upon self diffusion poses intriguing and challenging questions. In addition to the fundamental issues of formulation and application of the theory of diffusivity under nonequilibrium conditions, interest is motivated by the phenomena of shear-induced self diffusion and bulk migration of particles in noncolloidal suspension flows. The limited theoretical study of the diffusivity in a sheared suspension has followed a different course from that taken in the study of quiescent suspensions. This difference proves unnecessary and aspects of the problem that are common to both quiescent and flowing suspensions are emphasized as we develop a methodology for determining the self-diffusivity in a linear flow.

In a suspension, the trajectory of a particle is typically tortuous and unpredictable whether the particle moves as the result of Brownian motion, because of a bulk flow, or through the influence of both factors. Brownian motion can, of course, only be described statistically. However, even in a noncolloidal suspension the trajectory cannot, for any practical purposes, be specified exactly. In general, if the location of a given particle is known at some time, the best that one may hope at a later time is to determine the positional probability distribution, and from this the expected position of the particle. This indicates that to properly describe the temporal variation of

the expected position requires accounting for dispersion about the average trajectory. This is evident in a macroscopically quiescent suspension, but is equally true in a flowing suspension. In a quiescent suspension, it has been established in numerous studies (see the review by Pusey 1991) that the variance in position of a particle subject to Brownian forces grows linearly on two separate time scales, and the Brownian diffusivity of a quiescent suspension is thus characterized by both a short-time and long-time diffusion coefficient. Successful theory, based upon the experimental technique of dynamic light scattering (Berne & Pecora 1976), has been developed to calculate these coefficients (Russel & Glendinning 1981; Jones & Burfield 1982; Rallison & Hinch 1986; Brady 1994). The technique is based upon observation of the temporal decay of correlation in number density fluctuations, which may be related to the diffusivity because decorrelation of the scattered light arises from the uncorrelated, and hence over appropriate time scales diffusive, motions of the particles. The relationship between the rate at which number density fluctuations decay and the self- and collective-diffusivities lies at the center of the analytical theory of diffusivity in quiescent suspensions and is shown in this investigation to have the same role in the theory of self diffusion in a sheared suspension.

In a suspension subjected to a bulk linear flow, a spherical particle centered at $\boldsymbol{x}$ has expected velocity

$$\langle \boldsymbol{u} \rangle(\boldsymbol{x}) = \dot{\boldsymbol{\Gamma}} \cdot \boldsymbol{x},$$

where $\langle\ \rangle(\boldsymbol{x})$ denotes a position-dependent ensemble average, and $\dot{\boldsymbol{\Gamma}}$ is the velocity-gradient tensor of the bulk flow. The flow is chosen to vanish at the origin. In a

given realization, a particle may have a velocity quite different from $\langle \boldsymbol{u} \rangle$, as Brownian motion, interparticle forces, and hydrodynamic interactions cause deviation from the streamline specified by integrating $\dot{\boldsymbol{\Gamma}} \cdot \boldsymbol{x}(t)$ in time. Finite correlation of fluctuations about the mean velocity generates diffusive motion, and the techniques of light scattering provide a convenient analytical basis to describe the diffusion, regardless of the relative strength of the bulk flow to that of Brownian motion, which is characterized by the Péclet number $Pe = \dot{\gamma} a^2 / 2D$, where $\dot{\gamma}$ is the magnitude of the shear rate, a the particle size, and D the diffusion coefficient of an isolated particle.

Analysis of diffusion within the light-scattering formalism amounts to a study of the temporal dependence of the Fourier transform of the number density autocorrelation, denoted $F(\boldsymbol{k}, t)$, where $\boldsymbol{k}$ is the wavevector and t is time. For self-diffusivity, we are interested only in the portion of F due to correlation of the position of a particle with its own prior values, given in Fourier representation by the self-intermediate scattering function $F_s(\boldsymbol{k}, t)$ (Berne & Pecora 1977; Rallison & Hinch 1986), which is simply the Fourier transform of the conditional positional probability of a given particle. For an isolated Brownian particle in a linear flow, the problem for this distribution has been solved (Novikov 1958; Elrick 1962; Batchelor 1979). In §2.2 we introduce the governing equation for F_s for an isolated particle, allowing us to demonstrate the simplicity with which the diffusivity may be identified by the Fourier-transform method.

Coupling of diffusive spreading with a nonuniform flow leads to advectively-enhanced, or Taylor, dispersion (Taylor 1953). At sufficiently long time in a qui-

escent suspension, the root-mean-square position of a particle (or the positional variance) grows linearly with time at a rate which is proportional to the long-time self-diffusivity. By contrast, the temporal growth of the positional variance in a suspension in simple shear is cubic in the flow direction, while the temporal growth of the variance along a principal axis in a straining flow is exponential. Although the dispersive motion in a linear flow does not in general grow linearly in time, an underlying diffusive motion (*e.g.* molecular diffusivity) is, nevertheless, present and necessary to give the observed variance. Thus, to determine the dispersivity in a suspension, one needs to first determine the self-diffusivity. The Fourier-transform method allows one to do this very simply by identifying the self-diffusivity as the (tensor) coefficient of the $O(k^2)$ term in $\partial \ln F_s/\partial t$. The initial $O(k^2)$ decay of F_s may be identified with the short-time self-diffusivity, which is simply the thermal energy k_BT times the average of the mobility of a particle within the microstructure, whereas the $O(k^2)$ decay at long times is identified with the long-time self-diffusivity.

A different method was applied to investigate dispersion in flowing suspensions by Frankel & Brenner (1991). In their development for an isolated particle with internal degrees of freedom in unbounded linear flows, a transformation of the time coordinate was used to remove the bulk linear motion. It may be possible to extend this analysis to multi-particle systems, but the complexity of the analysis for an isolated particle indicates that this would be an extremely difficult task. While the problems we must consider within the light-scattering formalism are analytically complex, their physical content is readily understood and the method, formally, is quite simple.

To evaluate the self-diffusivity, we must determine the microstructure at some initial time, which we choose as the steady microstructure at the conditions of interest, and the microstructural perturbation caused by a given particle as it moves through a suspension, which we denote by the function f_N (whose definition given by (2.28) is a generalization of that of Brady (1994) for linear flows). As it moves, a particle forces the neighboring particles to adopt new configurations, and this perturbation to the microstructure in turn influences the motion of the particle of interest. We show that for all conditions of bulk flow and concentration, evaluation of the long-time self-diffusivity requires determination of the average microstructure and the microstructural perturbation f_N, with subsequent evaluation of the correlation between f_N and the flux of the tagged particle. We note that because the short-time self-diffusivity requires only the microstructural average of the hydrodynamic mobility of a particle, it is the correlation of f_N with the flux of the particle that leads to the difference between the short- and long-time self-diffusivities.

The equation governing the microstructure in a suspension at low particle Reynolds number is the Smoluchowski equation. Reduced to its pair form, this equation was first studied for weak straining flow by Batchelor (1977). The bulk of the analytical effort of this study is thus devoted to development of the governing equation for the perturbation function f_N and determination of the steady small-k solution of the pair-perturbation function, f, obtained by reduction of f_N. Derivation of the governing equations is presented in §2.3, where a nonlinear integro-differential equation governing f_N valid for all times and all wavelengths (*i.e* all $\boldsymbol{k}$) at any particle volume

fraction or Péclet number is obtained. The integro-differential equation governing f_N is indicative of the complexity of the physical process of self-diffusion in general, and especially in a sheared suspension. Simplification is possible, however, for the study of the long-time self-diffusivity, as only its small-k form, given in §2.3.5, is needed. The equation and boundary conditions governing the pair perturbation are given in §2.3.6, completing the theoretical development of the problem for the self-diffusivity in a linearly-flowing suspension.

The general theory is applied to a dilute suspension in simple shear for $Pe \ll 1$, considering the cases of particles with and without hydrodynamic interactions separately. The steady pair-distribution function $g(\boldsymbol{r})$ is analyzed in §2.4.1, followed by the study of the pair perturbation, $f(\boldsymbol{r})$. Exact analytical results are available for the case in which hydrodynamics are neglected, and we find that most conclusions gleaned from this analysis apply to the full problem as well. The only qualitative influence of hydrodynamic interactions is the introduction of velocity fluctuations whose correlation provides a mechanism of self diffusion absent if hydrodynamics are neglected; otherwise, the effects of hydrodynamics are only quantitative. In contrast to what one might expect from prior work on generalized Taylor dispersion (Frankel & Brenner 1991), which gives a first correction of $O(Pe^2)$, the first effects of weak shear on the self-diffusivity are $O(Pe)$. The $O(Pe)$ distortion of the pair-distribution function g (Batchelor 1977) leads to a correction to $\boldsymbol{D}_0^s$ proportional to $\phi Pe D\hat{\boldsymbol{E}}$, where $\hat{\boldsymbol{E}}$ is the dimensionless rate-of-strain tensor. (The next correction to g, and hence to $\boldsymbol{D}_0^s$, is $O(\phi Pe^2)$, as shown by Brady & Vicic (1995*a*), but we do not consider this

contribution.) The $O(\phi Pe)$ correction to $\boldsymbol{D}^s_\infty$ from its value of $D^s_0(\phi)\boldsymbol{I}$ in the quiescent suspension is also proportional to $\hat{\boldsymbol{E}}$, regardless of whether or not hydrodynamics are included. It is important to note that the $O(\phi Pe)$ corrections to $\boldsymbol{D}^s_0$ and $\boldsymbol{D}^s_\infty$ are valid for general linear flows.

In simple shear, the $O(Pe)$ correction does not contribute to the diffusivity in the velocity-gradient direction, and to capture the leading correction in all directions, we must go to the next order in the perturbation. As is familiar in analogous problems in heat and mass transfer, the effect of weak advection is singular, with a balance of advection and diffusion at large separations $r/a \sim O(Pe^{-1/2})$, and the next correction is $O(Pe^{3/2})$, found by matched asymptotic expansions (Proudman & Pearson 1957; Acrivos & Taylor 1962; Leal 1992). Specifically, the next correction to $\boldsymbol{D}^s_\infty$ is $O(\phi Pe^{3/2})$ and its tensor form depends upon whether or not hydrodynamics are included. In the absence of hydrodynamics the $O(\phi Pe^{3/2})$ correction is isotropic, whereas with hydrodynamics it is given by the sum of a nonisotropic tensor and a tensor proportional to $\hat{\boldsymbol{E}}$.

Leal (1973) studied the effective thermal conductivity in a dilute suspension of spherical drops or rigid particles in weak simple shear. By considering the influence of a single particle or drop upon the temperature field, the conductivity in the direction of the velocity gradient was determined, with the first dependence upon Pe being $O(\phi Pe^{3/2})$, which is the same as the first Pe-dependence of the corresponding component of $\boldsymbol{D}^s_\infty$. Considering the case of hydrodynamically-interacting particles, the detailed problem for the temperature disturbance due to a particle and f of the

present study are the same in most of their salient features, except for the fact that the relative diffusivity of suspended particles depends upon their separation. Had Leal's (1973) study considered the full tensor conductivity, an $O(\phi Pe)$ contribution proportional to $\hat{\boldsymbol{E}}$ would have been found. This contribution is due to the coupling of the velocity disturbance caused by a particle with the dipolar temperature disturbance in the absence of flow.

Experimental data on the diffusivity in suspensions at conditions corresponding to those of the present study are not presently available. Qiu *et al.* (1988) have measured the long-time self-diffusivity in a simple-shear flow for a suspension of polystyrene particles at $\phi \approx 0.003$. Their particles were electrostatically repulsive, and their effective radii could be varied by changing the ionic strength of the suspending fluid. The self-diffusivity was shown to have an expected strong dependence upon the effective radius. Unfortunately, the Péclet number based upon the effective radius of these particles was of $O(10)$, and our results are not directly applicable. We are not aware of any other experimental study at small Péclet number.

At the other extreme of large Péclet number, there have been a number of studies of shear-induced self diffusion, for example by Eckstein, Bailey & Shapiro (1977) and Leighton & Acrivos (1987). These studies showed that hydrodynamic dispersion occurs with the self-diffusivity scaling as $\dot{\gamma}a^2$ (or as Pe in dimensionless form). Recently Acrivos *et al.* (1992) studied the self-diffusivity of hydrodynamically-interacting hard spheres in simple-shear flow and determined the $O(\phi)$ coefficient of $\dot{\gamma}a^2$ in the flow direction by a trajectory calculation. A similar trajectory calculation (Mauri *et al.*

1995) has determined the $O(\phi^2)$ coefficient in the velocity-gradient direction. (The symmetry of the relative motion of two identical particles in Stokes flow necessitates that three particle interactions be included to determine the self-diffusivity in the velocity-gradient direction.) Although the results we have obtained for weak shear flow do not apply at high Péclet number, the Fourier-transform method remains applicable. In the following chapter, the effects of strong shear upon the microstructure of a suspension and the implications for the rheology and self-diffusivity are addressed. In particular, we show that the methodology developed here can be applied at high Péclet numbers and use it to predict the $O(\dot{\gamma}a^2)$ long-time self-diffusivity in a general linear flow as $Pe \to \infty$.

Simulations by Stokesian Dynamics of hydrodynamically-interacting suspensions in shear flow by Phung (1993) have shown that $\boldsymbol{D}^s_\infty$ is generally nonisotropic in the plane perpendicular to the mean flow; as in an experiment, the diagonal component of $\boldsymbol{D}^s_\infty$ in the direction of the mean flow and the off-diagonal terms are not readily determined owing to the nonlinear temporal growth of the variance dominating the dispersion. The complete particle mobility tensor, and thus the complete short-time self-diffusivity for the simulated conditions, is also available from these simulations (Phung 1993). Simulations of the shear flow of a monolayer suspension of identical particles by Bossis & Brady (1987) demonstrated that residual Brownian motion may have a profound influence upon the correlation time and the self-diffusivity at large Péclet number. Simulations at small particle fraction and small Péclet number would provide a desirable check on the results of this analysis. Unfortunately, they require a

large computational expenditure in order to gather sufficient data to give confidence in the results.

In the study of the long-time self-diffusivity of concentrated quiescent suspensions by Brady (1994), a method for determining the scaling of $D_0^{\infty}(\phi)$ in good agreement with experiment for all ϕ was obtained by factoring the diffusivity into a hydrodynamic term and a microstructural term. The approach is applied in §2.4.4 to a sheared suspension at small Pe to determine the scaling of the advectively-influenced diffusivity as $\phi \rightarrow \phi_m$, where ϕ_m is the particle volume fraction at maximum packing. It is shown for weak flows that the long-time self-diffusivity can be written as the product of the long-time self-diffusivity in the absence of flow and a nondimensional function of the Péclet number scaled by the short-time self-diffusivity, $\bar{Pe} = \dot{\gamma}a^2/2D_0^s(\phi)$. At small $\bar{Pe}$ the scaling with $\bar{Pe}$ is the same as at low ϕ.

In the next section, the Fourier-transform method in terms of the isolated particle problem is presented. This is followed, in §2.3, by development of a framework for the description of self-diffusivity valid for a quiescent or linearly-flowing suspension at arbitrary Péclet number. Application of the theory to a weakly-sheared and dilute suspension of hard spheres is presented in §2.4, along with the scaling theory near maximum packing. We conclude with a summary and discussion.

2.2 Advection and diffusion of an isolated particle

Self-diffusivity in a macroscopically quiescent suspension is directly related to the rate at which the variance in a particle's position grows with time:

$$\langle \boldsymbol{x}\boldsymbol{x} \rangle \sim 2D\boldsymbol{I}t,$$

where D is the magnitude of the isotropic diffusion tensor, and we have presumed that sufficient time has elapsed to achieve the long-time asymptotic limit. A suspension in linear flow presents a different and richer situation, as the variance in position does not necessarily grow linearly in time owing to the position-dependent velocity field, and therefore the variance in the particle position is not so readily related to the diffusivity. An extreme example occurs in pure straining motion where the variance grows exponentially in time (Foister & van de Ven 1980). In simple shear there is a balance of straining and rotation, and the coupled effects of advection and diffusion lead to a variance in particle position proportional to t^3 in the flow direction. The pioneering work of Taylor (1953) and its generalizations by Brenner and coworkers (*e.g.*, Brenner 1980, Frankel & Brenner 1991) based upon this coupling have led to the well-developed theory of generalized Taylor dispersion.

To understand how the coupling between advection and diffusion leads to dispersion and then how to *define* the diffusivity in shearing flows, consider the equation

flow, which is mathematically identical to the equation describing the evolution of an impulse of dye or heat released into the same flow:

$$\frac{\partial G}{\partial t} + \dot{\boldsymbol{\Gamma}}\cdot\boldsymbol{x}\cdot\nabla G + \boldsymbol{U}\cdot\nabla G - D\nabla^2 G = 0, \tag{2.1}$$

where $\dot{\boldsymbol{\Gamma}}$ is the constant velocity-gradient tensor, $\boldsymbol{U}$ is a uniform velocity, and D is the diffusion coefficient. For a spherical Brownian particle of radius a, $D = k_B T/6\pi\eta a$, where η is the viscosity of the suspending fluid and $k_B T$ is the thermal energy. We assume that the particle (or dye) is released at the origin so that $G(\boldsymbol{x}, t)$ satisfies the initial condition

$$G(\boldsymbol{x}, 0) = \delta(\boldsymbol{x}).$$

The spatial Fourier transform of (2.1) is

$$\frac{\partial F_s}{\partial t} - \boldsymbol{k}\cdot\dot{\boldsymbol{\Gamma}}\cdot\nabla_k F_s - i\boldsymbol{k}\cdot\boldsymbol{U}F_s + k^2 D F_s = 0, \tag{2.2}$$

while the initial condition transforms to

$$F_s(\boldsymbol{k}, 0) = 1,$$

where $\boldsymbol{k}$ is the Fourier-space position vector (wavevector), and the Fourier transform of G is given by

$$F_s(\boldsymbol{k}, t) = \int G(\boldsymbol{x}, t) e^{i\boldsymbol{k}\cdot\boldsymbol{x}} d\boldsymbol{x}.$$

We use this notation for the transform of G because it is equivalent to the self-

intermediate scattering function of dynamic light scattering (Berne & Pecora 1976).

In the absence of flow, it is well-known that the self-diffusivity is related to the scattering function by

$$D^s = -\frac{\dot{F}_s}{k^2 F_s}, \tag{2.3}$$

for time scales over which the right-hand side is a constant. Here, the overdot denotes differentiation with respect to time. While not an issue for an isolated particle, the motion of a particle in a quiescent suspension is, in general, diffusive only on time scales that are alternately much shorter and much longer than the time required for a particle to wander a distance comparable to its own size, $t \ll a^2/D$ and $t \gg a^2/D$, respectively. At intermediate times, correlated interaction of a particle with neighboring particles renders its motion nondiffusive (for a lucid discussion of the physical significance of the short- and long-time self-diffusivities in quiescent suspensions, see Rallison & Hinch 1986). The same time scales apply to a weakly-sheared suspension, while at large Péclet number long-time diffusion in a shear flow may be expected to occur on time scales $t \gg \dot{\gamma}^{-1}$, although some caution should be exercised in making a definitive statement about this time scale. For diffusion to occur, a particle must make a large number of essentially uncorrelated motions, and for large Péclet number motions are generated predominantly by configuration-dependent hydrodynamic interactions (perhaps also by nonhydrodynamic interparticle forces). Hence, to move diffusively, a particle must experience a large number of configurations, with the rate at which new configurations are encountered proportional to the shear rate. While the estimate of $t \gg \dot{\gamma}^{-1}$ is therefore reasonable, the correlation time can be ex-

tremely large in shear flow of a suspension at low Reynolds number (Bossis & Brady 1987), and the time scale at which diffusion will be observed for general conditions remains unknown, but will depend upon concentration, residual Brownian motion, and nonhydrodynamic interparticle forces.

Despite these issues, (2.3) suggests that one may *define* the self-diffusivity as the coefficient of k^2 in $\partial \ln F_s/\partial t$ under any flow conditions. That this definition is correct may be appreciated by observing that in (2.2) diffusive variation of F_s is $O(k^2)$, while linear and uniform flow cause rates of variation which are independent of k and $O(k)$, respectively. The governing equation for the probability distribution of a tagged particle in a suspension is the many-particle generalization of (2.1), and the equation for F_s for a suspension retains the essential structure exhibited by (2.2). It is thus conceptually simple to identify the self-diffusivity of a suspension in linear flow. Although the diffusion coefficient is simply identifiable in (2.2), this does not imply that the variance in particle position necessarily grows linearly in time in a flowing suspension.

For $\boldsymbol{U} = 0$, Novikov (1958) and Elrick (1962) solved (2.1) for the case of simple-shear flow, and these solutions were generalized by Batchelor (1979), who demonstrated that the solution to (2.2) could be written for any linear flow as

$$F_s(\boldsymbol{k}, t) = \exp\left(-Dk_i k_j B_{ij}\right), \tag{2.4}$$

where $\boldsymbol{B}(t)$ is a symmetric tensor satisfying

$$\frac{\partial B_{ij}}{\partial t} = \delta_{ij} + \dot{\Gamma}_{il} B_{jl} + \dot{\Gamma}_{jl} B_{il},$$

with the initial condition

$$B_{ij} \sim \delta_{ij} t, \quad \text{as} \quad t \to 0.$$

The physical space solution obtained by transforming (2.4) is

$$G(\boldsymbol{x}, t) = \frac{1}{(4\pi D)^{3/2} \Delta^{1/2}} \exp\left(\frac{-x_i x_j b_{ij}}{4D\Delta}\right), \tag{2.5}$$

where $\Delta(t)$ is the determinant of the matrix $\boldsymbol{B}$, and $b_{ij}(t)$ is the cofactor of the ij element of $\boldsymbol{B}$. (Note that the solution (2.5) can be straightforwardly generalized for a tensorial diffusion coefficient.)

In the case of the simple-shear flow $u_x = \dot{\gamma} y$, denoting $\boldsymbol{x} = (x_1, x_2, x_3)$ as (x, y, z), the components of $\boldsymbol{B}$ are

$$B_{11} = t(1 + \tfrac{1}{3}\dot{\gamma}^2 t^2), \quad B_{22} = t, \quad B_{33} = t, \quad B_{12} = \tfrac{1}{2}\dot{\gamma} t^2,$$

and

$$B_{13} = B_{23} = 0,$$

the determinant Δ is

$$\Delta = t^3(1 + \tfrac{1}{12}\dot{\gamma}^2 t^2),$$

and the solution is

$$G(\boldsymbol{x},t) = \frac{1}{(4\pi Dt)^{3/2}(1+\dot{\gamma}^2t^2/12)^{1/2}} \exp[-\frac{(x-\dot{\gamma}yt/2)^2}{4Dt(1+\dot{\gamma}^2t^2/12)} - \frac{(y^2+z^2)}{4Dt}]. \quad (2.6)$$

For reference, note that when $\dot{\gamma} = 0$ the diffusive solution with $\boldsymbol{B} = \boldsymbol{I}t$ is obtained. The t^3 dependence of B_{11} in simple shear indicates the coupling between advection and diffusion discussed earlier. In §2.4, (2.6) will be used to construct solutions to problems encountered in the study of self-diffusivity in shear flow.

Other treatments of diffusion in sheared systems (Duffy 1984; san Miguel & Sancho 1979; Frankel & Brenner 1991) have not used the Fourier transform approach, but rather have transformed to a coordinate system moving with the shearing motion to remove the linear shear flow from the governing equation (2.1). While such an approach is possible, it unnecessarily complicates the analysis. Seeking a solution in the form of a Fourier transform places the analysis of quiescent and flowing suspensions on the same footing with an easy identification of the diffusivity. Advectively enhanced, or Taylor, dispersion with nonlinear temporal growth in the variance is then contained in (2.5).

2.3 Theoretical development

2.3.1 The self-intermediate scattering function

The self-intermediate scattering function was introduced in a purely mathematical fashion in the previous section. Here, its connection to the motion of a particle

in a suspension is established. We consider N spherical particles, each of radius a, immersed in a Newtonian fluid at small Reynolds number. The full N-particle configuration is denoted $\boldsymbol{x}^N$, while the center of particle α is located at $\boldsymbol{x}_\alpha$. The number density at any point $\boldsymbol{x}$ is

$$n(\boldsymbol{x},t) = \sum_{\alpha=1}^{N} \delta(\boldsymbol{x} - \boldsymbol{x}_\alpha),$$

with Fourier transform given by

$$\tilde{n}(\boldsymbol{k},t) = \int e^{i\boldsymbol{k}\cdot\boldsymbol{x}} \sum_{\alpha=1}^{N} \delta(\boldsymbol{x} - \boldsymbol{x}_\alpha) d\boldsymbol{x} = \sum_{\alpha=1}^{N} e^{i\boldsymbol{k}\cdot\boldsymbol{x}_\alpha}.$$

In dynamic light scattering, the intermediate scattering function $F(\boldsymbol{k},t)$ (also known as the dynamic structure factor) is a quantity of interest for its relation to the auto-correlation in number density (Berne & Pecora 1976):

$$\begin{aligned} F(\boldsymbol{k},t) = \frac{1}{N}\langle \tilde{n}(\boldsymbol{k},t)\tilde{n}^*(\boldsymbol{k},0)\rangle &= \langle \tilde{n}(\boldsymbol{k},t)\tilde{n}(-\boldsymbol{k},0)\rangle \\ &= \sum_{\alpha=1}^{N}\sum_{\beta=1}^{N} \langle e^{i\boldsymbol{k}\cdot(\boldsymbol{x}_\alpha(t) - \boldsymbol{x}_\beta(0))}\rangle, \end{aligned}$$

where * indicates a complex conjugate and the second equality follows from the fact that $n(\boldsymbol{x},t)$ is real. The indistinguishability of particles allows F to be expressed as

$$F(\boldsymbol{k},t) = \langle e^{i\boldsymbol{k}\cdot(\boldsymbol{x}_1(t) - \boldsymbol{x}_1(0))}\rangle + (N-1)\langle e^{i\boldsymbol{k}\cdot(\boldsymbol{x}_2(t) - \boldsymbol{x}_1(0))}\rangle. \tag{2.7}$$

The first term on the right-hand side of (2.7) is the self-intermediate scattering function,

$$F_s(\boldsymbol{k},t) = \langle e^{i\boldsymbol{k}\cdot(\boldsymbol{x}_1(t)-\boldsymbol{x}_1(0))}\rangle; \tag{2.8}$$

in this investigation of the self-diffusivity we are concerned only with F_s and hereafter the remainder of F will not be considered. The temporal behavior of the complete scattering function can be related to the collective diffusivity (Pusey 1991).

2.3.2 Probability distributions and the ensemble average

In (2.7-2.8), the angle brackets $\langle\ \rangle$ denote an ensemble average taken with respect to both the initial, $\boldsymbol{x}^N(0)$, and present, $\boldsymbol{x}^N(t)$, configurations of the particles. We denote as $\mathcal{P}_N$ the joint probability distribution of finding the two configurations, and write this probability as

$$\mathcal{P}_N(\boldsymbol{x}^N(t),\boldsymbol{x}^N(0)) = P_N(\boldsymbol{x}^N(t)|\boldsymbol{x}^N(0))P_N^0(\boldsymbol{x}^N(0)), \tag{2.9}$$

where $P_N^0(\boldsymbol{x}^N(0))$ is the distribution function for the initial configuration $\boldsymbol{x}^N(0)$, and $P_N(\boldsymbol{x}^N(t)|\boldsymbol{x}^N(0))$ is the conditional (or transition) probability of the configuration being $\boldsymbol{x}^N(t)$, given that the configuration was initially $\boldsymbol{x}^N(0)$. Thus, F_s can be written

$$\begin{aligned} F_s(\boldsymbol{k},t) &= \int\int e^{i\boldsymbol{k}\cdot(\boldsymbol{x}_1(t)-\boldsymbol{x}_1(0))}\mathcal{P}_N(\boldsymbol{x}^N(t),\boldsymbol{x}^N(0))d\boldsymbol{x}^N(t)d\boldsymbol{x}^N(0) \\ &= \int\int e^{i\boldsymbol{k}\cdot(\boldsymbol{x}_1(t)-\boldsymbol{x}_1(0))}P_N(\boldsymbol{x}^N(t)|\boldsymbol{x}^N(0))P_N^0(\boldsymbol{x}^N(0))d\boldsymbol{x}^N(t)d\boldsymbol{x}^N(0). \end{aligned} \tag{2.10}$$

In this work, P_N^0 denotes the steady initial distribution for the conditions of interest (*cf.* Eq. (2.35)). The transition probability is governed by the conservation equation

$$\frac{\partial P_N}{\partial t} + \sum_{\alpha=1}^{N} \nabla_\alpha \cdot \boldsymbol{j}_\alpha = 0, \tag{2.11}$$

and satisfies the initial condition

$$P_N(t=0) = \delta(\boldsymbol{x}^N - \boldsymbol{x}^N(0)). \tag{2.12}$$

In (2.11), $\boldsymbol{j}_\alpha$ is the probability flux associated with particle α, given by

$$\boldsymbol{j}_\alpha = \boldsymbol{U}_\alpha P_N - \sum_{\beta=1}^{N} \boldsymbol{D}_{\alpha\beta} P_N \cdot \nabla_\beta \left(\ln P_N + V \right), \tag{2.13}$$

where $\boldsymbol{D}_{\alpha\beta} = k_B T \boldsymbol{M}_{\alpha\beta}$, with $\boldsymbol{M}_{\alpha\beta}$ the hydrodynamic mobility of particle α due to a force on particle β, and V is the interparticle potential energy made dimensionless by $k_B T$. In the absence of Brownian motion and interparticle forces, particle α moves with the hydrodynamic velocity $\boldsymbol{U}_\alpha$, which may include the influence of a buoyancy or external force acting upon the particles.

We write $\boldsymbol{U}_\alpha$ as

$$\begin{aligned} \boldsymbol{U}_\alpha &= \boldsymbol{U}^\infty(\boldsymbol{x}_0) + \dot{\boldsymbol{\Gamma}} \cdot (\boldsymbol{x}_\alpha - \boldsymbol{x}_0) + \boldsymbol{U}'_\alpha(\boldsymbol{x}_N) \\ &= \boldsymbol{U}^*(\boldsymbol{x}_0) + \dot{\boldsymbol{\Gamma}} \cdot \boldsymbol{x}_\alpha + \boldsymbol{U}'_\alpha(\boldsymbol{x}_N), \end{aligned} \tag{2.14}$$

where $\boldsymbol{U}^\infty(\boldsymbol{x}_0)$ is the bulk average velocity measured at an arbitrary field point, $\boldsymbol{x}_0$,

from which the bulk shear velocity is referenced, and $\boldsymbol{U}^*(\boldsymbol{x}_0)$ is

$$\boldsymbol{U}^*(\boldsymbol{x}_0) = \boldsymbol{U}^\infty(\boldsymbol{x}_0) - \dot{\boldsymbol{\Gamma}}\cdot\boldsymbol{x}_0.$$

The fluctuation velocity $\boldsymbol{U}'_\alpha$ is simply

$$\boldsymbol{U}'_\alpha = \boldsymbol{U}_\alpha - (\boldsymbol{U}^*(\boldsymbol{x}_0) + \dot{\boldsymbol{\Gamma}}\cdot\boldsymbol{x}_\alpha). \tag{2.15}$$

The bulk flow is divergence-free, thus satisfying $\dot{\Gamma}_{ii} = 0$.

Inserting (2.13) to (2.11), yields the Smoluchowski equation governing P_N,

$$\frac{\partial P_N}{\partial t} + \sum_{\alpha=1}^{N} \nabla_\alpha\cdot\left[\boldsymbol{U}_\alpha P_N - \sum_{\beta=1}^{N} \nabla_\alpha\cdot\{\boldsymbol{D}_{\alpha\beta}P_N\cdot\nabla_\beta(\ln P_N + V)\}\right] = 0. \tag{2.16}$$

Following Rallison & Hinch (1986), we integrate over the initial coordinates $\boldsymbol{x}^N(0)$, defining

$$\hat{P}_N(\boldsymbol{x}^N, t; \boldsymbol{k}) \equiv \int P_N(\boldsymbol{x}^N|\boldsymbol{x}^N(0))P_N^0(\boldsymbol{x}^N(0))e^{-i\boldsymbol{k}\cdot\boldsymbol{x}_1(0)}d\boldsymbol{x}^N(0). \tag{2.17}$$

The operator in (2.16) depends only on present variables, and thus replacing P_N with $\hat{P}_N$ in (2.16) yields the governing equation for $\hat{P}_N$, which satisfies the initial condition

$$\hat{P}_N(\boldsymbol{x}^N, 0; \boldsymbol{k}) = P_N^0(\boldsymbol{x}^N)e^{-i\boldsymbol{k}\cdot\boldsymbol{x}_1}. \tag{2.18}$$

In terms of $\hat{P}_N$, the scattering function is

$$F_s(\boldsymbol{k},t) = \int \hat{P}_N e^{i\boldsymbol{k}\cdot\boldsymbol{x}_1} d\boldsymbol{x}^N. \tag{2.19}$$

Reduced forms of $\hat{P}_N$ are given by

$$\hat{P}_M(\boldsymbol{x}_1,\ldots,\boldsymbol{x}_M,t;\boldsymbol{k}) = \frac{N!}{(N-M)!}\int \hat{P}_N d\boldsymbol{x}_{M+1}\cdots d\boldsymbol{x}_N, \quad \text{for} \quad M<N.$$

In particular, we have

$$\hat{P}_1 = N\int \hat{P}_N d\boldsymbol{x}_2\cdots d\boldsymbol{x}_N, \tag{2.20}$$

so that

$$F_s(\boldsymbol{k},t) = \frac{1}{N}\int \hat{P}_1 e^{i\boldsymbol{k}\cdot\boldsymbol{x}_1} d\boldsymbol{x}_1. \tag{2.21}$$

As discussed in §2.2, the self-diffusivity is the coefficient—in general, a non-isotropic tensor—of the $O(k^2)$ term in $\partial \ln F_s/\partial t$. The time derivative of F_s is

$$\begin{aligned}
\frac{\partial F_s}{\partial t}(\boldsymbol{k},t) &= \int e^{i\boldsymbol{k}\cdot\boldsymbol{x}_1}\frac{\partial \hat{P}_N}{\partial t} d\boldsymbol{x}^N \\
&= -\int \sum_{\alpha=1}^{N} \nabla_\alpha\cdot(\hat{\boldsymbol{j}}_\alpha e^{i\boldsymbol{k}\cdot\boldsymbol{x}_1}) d\boldsymbol{x}^N + i\boldsymbol{k}\cdot\int \hat{\boldsymbol{j}}_1 e^{i\boldsymbol{k}\cdot\boldsymbol{x}_1} d\boldsymbol{x}^N \\
&= i\boldsymbol{k}\cdot\int \hat{\boldsymbol{j}}_1 e^{i\boldsymbol{k}\cdot\boldsymbol{x}_1} d\boldsymbol{x}^N,
\end{aligned} \tag{2.22}$$

where use has been made of the divergence theorem and the requirement that the probability flux from the system is zero. Upon inserting the constitutive law for the

flux (*i.e.*, (2.13) with $\hat{P}_N$ replacing P_N) into (2.22), we obtain

$$\begin{aligned}(\dot{\ln F_s})(\boldsymbol{k},t) &= \boldsymbol{k}\cdot\dot{\boldsymbol{\Gamma}}\cdot\nabla_k \ln F_s + i\boldsymbol{k}\cdot\boldsymbol{U}^* \\ &\quad + \frac{i\boldsymbol{k}}{F_s}\cdot\int[\boldsymbol{U}_1'\hat{P}_N - \sum_{\alpha=1}^{N}\boldsymbol{D}_{1\alpha}\hat{P}_N\cdot\nabla_\alpha(\ln\hat{P}_N + V)]e^{i\boldsymbol{k}\cdot\boldsymbol{x}_1}d\boldsymbol{x}^N,\end{aligned} \tag{2.23}$$

where the notation

$$\frac{\partial \ln F_s}{\partial t} = (\dot{\ln F_s})$$

is employed. It was possible to evaluate the first two terms on the right of (2.23) directly because neither $\boldsymbol{U}^*$ nor $\dot{\boldsymbol{\Gamma}}$ is configuration-dependent.

2.3.3 Initial value of $(\dot{\ln F_s})$: short-time self-diffusivity and mean velocity

Using the known initial value of $\hat{P}_N$ given by (2.18), we find

$$(\dot{\ln F_s})(\boldsymbol{k},0) = \boldsymbol{k}\cdot\dot{\boldsymbol{\Gamma}}\cdot\nabla_k \ln F_s + i\boldsymbol{k}\cdot\langle\boldsymbol{U}_1\rangle^0 - \boldsymbol{k}\cdot\langle\boldsymbol{D}_{11}\rangle^0\cdot\boldsymbol{k}, \tag{2.24}$$

where $\langle\ \rangle^0$ denotes the unconditional average with respect to the initial distribution P_N^0. Recalling that $\boldsymbol{D}_{11} = k_BT\boldsymbol{M}_{11}$, where $\boldsymbol{M}_{11}$ is the mobility of particle 1 due to a force exerted upon it, (2.24) shows that the initial diffusive, *i.e.* $O(k^2)$, variation of $(\dot{\ln F_s})$ is determined by the average mobility of the tagged particle within the microstructure. The short-time self-diffusion tensor, in a quiescent or a flowing

suspension, is

$$\boldsymbol{D}_0^s = \langle \boldsymbol{D}_{11} \rangle^0 = k_B T \langle \boldsymbol{M}_{11} \rangle^0. \tag{2.25}$$

The short-time self-diffusivity will generally be nonisotropic in a nonequilibrium suspension, and the full tensor $\boldsymbol{D}_{11}$ must be retained in (2.24).

The $O(\boldsymbol{k})$ term in (2.24), $\langle \boldsymbol{U}_1 \rangle^0$, is the average velocity of the tagged particle:

$$\langle \boldsymbol{U}_1 \rangle^0 = \boldsymbol{U}^* + \langle \boldsymbol{U}_1' \rangle^0 - \int \sum_{\alpha=1}^{N} \boldsymbol{D}_{1\alpha} \cdot \nabla_\alpha (\ln P_N^0 + V) P_N^0 d\boldsymbol{x}_N. \tag{2.26}$$

In (2.26), $\langle \boldsymbol{U}_1' \rangle^0$ is the average velocity of a particle due to hydrodynamic interactions or due to an external force acting on the particle. For the linear flow considered here, $\langle \boldsymbol{U}_1' \rangle^0 = 0$. The last term on the right-hand side of (2.26) is the mean velocity of particle 1 arising from the initial distribution. Had the initial distribution been chosen to be the equilibrium Boltzmann distribution, *i.e.* $P_N^0 = P_N^{eq} \sim \exp(-V)$, this last term would vanish identically. However, there is no need in general, and particularly at high Péclet number, to choose the initial distribution to be the equilibrium one, and the final term in (2.26) may contribute to the mean velocity of a tagged particle, although in the linear flow considered here the last term in (2.26) is zero, as may be seen from symmetry arguments. The mean velocity of a particle must be proportional to $\dot{\boldsymbol{\Gamma}}$ which drives the flow. However, there is no vector with which to multiply $\dot{\boldsymbol{\Gamma}}$ to form a vector, and thus the term is zero.

2.3.4 Perturbation function

To evaluate the rate of decay of number density correlation at arbitrary times requires a solution for $\hat{P}_N$. Noting that $\boldsymbol{x}_1$ is a coordinate that plays a special role due to the initial condition (2.18), we write $\hat{P}_N$ as*

$$\hat{P}_N = \frac{1}{N}\hat{P}_1 P^0_{(N-1)|1}[1 + f_N], \tag{2.28}$$

thus defining a perturbation function f_N. The function $P^0_{(N-1)|1}$ is the conditional probability for $N-1$ particles given particle 1 fixed, at the initial time. The coordinate dependences are given explicitly by

$$\hat{P}_N(\boldsymbol{x}_1, \boldsymbol{r}^N, t), \quad \hat{P}_1(\boldsymbol{x}_1, t), \quad P^0_{(N-1)|1}(\boldsymbol{r}^N), \quad \text{and} \quad f_N(\boldsymbol{r}^N, t),$$

indicating a change of coordinates to

$$\boldsymbol{x}_1 \quad \text{and} \quad \boldsymbol{r}^N \equiv (\boldsymbol{r}_2, \ldots, \boldsymbol{r}_N),$$

*The form of $\hat{P}_N$ given by (2.28) is in the same spirit as

$$\hat{P}_N = P^0_N e^{-i\boldsymbol{k}\cdot\boldsymbol{x}_1} F_s[1 + f_N], \tag{2.27}$$

which was used by Brady (1994). Employing (2.28) in place of (2.27) for a quiescent suspension, f_N and its reduced forms satisfy the governing equations found by Brady (1994). However, application of f_N as defined by (2.27) for a suspension in linear flow fails to generate the linear-velocity convective derivative of F_s in Fourier space, *i.e.* $-\boldsymbol{k}\cdot\dot{\boldsymbol{\Gamma}}\cdot\nabla_k F_s$, which is known from (2.2) should appear, and thus results in more complicated analysis for f_N.

related to the original coordinates, which we denote using a superscript prime, by

$$\boldsymbol{x}_1 = \boldsymbol{x}_1', \quad \text{and} \quad \boldsymbol{r}_\alpha = \boldsymbol{x}_\alpha' - \boldsymbol{x}_1',$$

with the gradient operators in the original coordinates replaced by

$$\nabla_1' = \nabla_1 - \sum_{\alpha=2}^{N} \nabla_\alpha, \quad \text{and} \quad \nabla_\alpha' = \nabla_\alpha,$$

with $2 \leq \alpha \leq N$.

We take the potential to be an interparticle potential, which is independent of absolute position and may be written as $V(\boldsymbol{r}^N)$. The effect of an external force derivable from a potential can be included directly into $\boldsymbol{U}_\alpha$. Thus, the flux of particle α is given by

$$\hat{\boldsymbol{j}}_\alpha = \boldsymbol{U}_\alpha \hat{P}_N - \boldsymbol{D}_{\alpha 1} \cdot \nabla_1 \hat{P}_N - \sum_{\beta=2}^{N} (\boldsymbol{D}_{\alpha\beta} - \boldsymbol{D}_{\alpha 1}) \hat{P}_N \cdot \nabla_\beta (\ln \hat{P}_N + V), \quad 1 \leq \alpha \leq N, \tag{2.29}$$

and the Smoluchowski equation for $\hat{P}_N(\boldsymbol{x}_1, \boldsymbol{r}^N)$ is

$$\begin{aligned} \frac{\partial \hat{P}_N}{\partial t} \; &+ \; \nabla_1 \cdot \boldsymbol{U}_1 \hat{P}_N - \boldsymbol{D}_{11} : \nabla_1 \nabla_1 \hat{P}_N \\ &- \sum_{\alpha=2}^{N} \nabla_1 \cdot (\boldsymbol{D}_{1\alpha} - \boldsymbol{D}_{11}) \hat{P}_N \cdot \nabla_\alpha (\ln \hat{P}_N + V) \\ &+ \sum_{\alpha=2}^{N} \nabla_\alpha \cdot [\boldsymbol{U}_\alpha^r \hat{P}_N - (\boldsymbol{D}_{\alpha 1} - \boldsymbol{D}_{11}) \cdot \nabla_1 \hat{P}_N] \\ &- \sum_{\alpha,\beta=2}^{N} \nabla_\alpha \cdot \boldsymbol{D}_{\alpha\beta}^r \hat{P}_N \cdot \nabla_\beta (\ln \hat{P}_N + V) = 0, \end{aligned} \tag{2.30}$$

where we have defined

$$\boldsymbol{U}_\alpha^r \equiv \boldsymbol{U}_\alpha - \boldsymbol{U}_1, \tag{2.31}$$

and

$$\boldsymbol{D}_{\alpha\beta}^r \equiv \boldsymbol{D}_{\alpha\beta} - \boldsymbol{D}_{\alpha 1} - \boldsymbol{D}_{1\beta} + \boldsymbol{D}_{11}. \tag{2.32}$$

The temporal variation of F_s in terms of f_N is found by substituting (2.28) into (2.23). Making the necessary alterations for the change of coordinates and performing the integration with respect to $\boldsymbol{x}_1$, we obtain

$$\begin{aligned}
(\ln \dot{F}_s) \;=\; & \boldsymbol{k}\cdot\dot{\boldsymbol{\Gamma}}\cdot\nabla_k \ln F_s + i\boldsymbol{k}\cdot\langle \boldsymbol{U}_1\rangle^0 - \boldsymbol{k}\cdot\langle \boldsymbol{D}_{11}\rangle^0\cdot\boldsymbol{k} \\
& -\boldsymbol{k}\cdot\int(\boldsymbol{D}_{11} - \langle \boldsymbol{D}_{11}\rangle^0)\cdot\boldsymbol{k} f_N P^0 d\boldsymbol{r}^N \\
& +i\boldsymbol{k}\cdot\int(\boldsymbol{U}_1 - \dot{\boldsymbol{\Gamma}}\cdot\boldsymbol{x}_1 - \langle \boldsymbol{U}_1\rangle^0) f_N P^0 d\boldsymbol{r}^N \\
& -i\boldsymbol{k}\cdot\int\sum_{\alpha=2}^{N}[(\boldsymbol{D}_{1\alpha} - \boldsymbol{D}_{11})\cdot\nabla_\alpha f_N + (\boldsymbol{D}_{1\alpha} - \boldsymbol{D}_{11}) f_N\cdot\nabla_\alpha \bar{V}] P^0 d\boldsymbol{r}^N,
\end{aligned} \tag{2.33}$$

where we denote $P^0_{(N-1)|1}$ as P^0 and define

$$\bar{V} \equiv \ln P^0 + V$$

to simplify notation. Note that $\bar{V}$ results from the departure of the steady distribution from the equilibrium Boltzmann distribution. In obtaining (2.33) we have made use

of the fact that, since both $\hat{P}_N$ and P_N^0 are normalized,

$$\int f_N P^0_{(N-1)|1} d\boldsymbol{r}^N = \int f_N P^0 d\boldsymbol{r}^N = 0.$$

2.3.5 Equation governing the perturbation function f_N

The equation governing f_N is obtained by inserting (2.28) to (2.30), multiplying the equation by $e^{i\boldsymbol{k}\cdot\boldsymbol{x}_1}$, and integrating over $\boldsymbol{x}_1$ to yield

$$\begin{aligned} P^0\frac{\partial f_N}{\partial t} \;+\; & P^0\sum_{\alpha=2}^{N}[\boldsymbol{U}^r_\alpha - \sum_{\beta=2}^{N}\boldsymbol{D}^r_{\alpha\beta}\cdot\nabla_\beta\bar{V}]\cdot\nabla_\alpha f_N - \sum_{\alpha,\beta=2}^{N}\nabla_\alpha\cdot\boldsymbol{D}^r_{\alpha\beta}P^0\cdot\nabla_\beta f_N \\ = \;& -Q[(\ln F_s) - \boldsymbol{k}\cdot\dot{\boldsymbol{\Gamma}}\cdot\nabla_k \ln F_s - i\boldsymbol{k}\cdot(\boldsymbol{U}^* - \boldsymbol{U}'_1) + \boldsymbol{k}\cdot\boldsymbol{D}_{11}\cdot\boldsymbol{k}] \\ & + i\boldsymbol{k}\cdot\left(\sum_{\alpha=2}^{N}\{\nabla_\alpha\cdot[(\boldsymbol{D}_{\alpha 1} - \boldsymbol{D}_{11})Q] + (\boldsymbol{D}_{1\alpha} - \boldsymbol{D}_{11})Q\cdot\nabla_\alpha(\ln Q + V)\}\right), \end{aligned} \tag{2.34}$$

where we write $Q = P^0[1 + f_N]$ to simplify notation. In writing (2.34) we have made use of the fact that the initial distribution satisfies the steady equation

$$\sum_{\alpha=2}^{N}\nabla_\alpha\cdot\left[\boldsymbol{U}^r_\alpha P^0 - \sum_{\beta=2}^{N}\boldsymbol{D}^r_{\alpha\beta}P^0\cdot\nabla_\beta[\ln P^0 + V]\right] = 0. \tag{2.35}$$

In the absence of flow, the initial distribution reduces to the equilibrium Boltzmann distribution, $P_N^{eq} \sim^{-V}$. Note that we could have used a time-dependent initial distribution by including $\partial P/\partial t$ in (2.35) with no change to the subsequent equations.

Finally, we make use of (2.33) for $(\ln \dot{F}_s)$ to rewrite (2.34) as

$$\begin{aligned} P^0\frac{\partial f_N}{\partial t} \;+\; & P^0\sum_{\alpha=2}^{N}[\boldsymbol{U}_\alpha^r - \sum_{\beta=2}^{N}\boldsymbol{D}_{\alpha\beta}^r\cdot\nabla_\beta\bar{V}]\cdot\nabla_\alpha f_N - \sum_{\alpha,\beta=2}^{N}\nabla_\alpha\cdot\boldsymbol{D}_{\alpha\beta}^r P^0\cdot\nabla_\beta f_N \\ = \; & -Q[i\boldsymbol{k}\cdot(\boldsymbol{U}_1 - \dot{\boldsymbol{\Gamma}}\boldsymbol{x}_1 - \langle\boldsymbol{U}_1\rangle^0) + \boldsymbol{k}\cdot(\boldsymbol{D}_{11} - \langle\boldsymbol{D}_{11}\rangle^0)\cdot\boldsymbol{k}] \\ & +i\boldsymbol{k}\cdot\sum_{\alpha=2}^{N}\{\nabla_\alpha\cdot[(\boldsymbol{D}_{\alpha 1} - \boldsymbol{D}_{11})Q] + (\boldsymbol{D}_{1\alpha} - \boldsymbol{D}_{11})Q\cdot\nabla_\alpha(\ln Q + V)\} \\ & -Q\Big[i\boldsymbol{k}\cdot\int(\boldsymbol{U}_1 - \dot{\boldsymbol{\Gamma}}\cdot\boldsymbol{x}_1 - \langle\boldsymbol{U}_1\rangle^0)f_N P^0 d\boldsymbol{r}^N \\ & \quad - \boldsymbol{k}\cdot\int(\boldsymbol{D}_{11} - \langle\boldsymbol{D}_{11}\rangle^0)\cdot\boldsymbol{k} f_N P^0 d\boldsymbol{r}^N \\ & \quad - i\boldsymbol{k}\cdot\int\sum_{\alpha=2}^{N}[(\boldsymbol{D}_{1\alpha} - \boldsymbol{D}_{11})\cdot\nabla_\alpha f_N + (\boldsymbol{D}_{1\alpha} - \boldsymbol{D}_{11})f_N\cdot\nabla_\alpha\bar{V}]P^0 d\boldsymbol{r}^N\Big]. \end{aligned} \tag{2.36}$$

The initial condition for f_N is

$$f_N(\boldsymbol{r}^N, t = 0) = 0. \tag{2.37}$$

Equation (2.36) is a nonlinear integro-differential equation for f_N, showing that departures from the initial distribution are driven by fluctuations in velocity and diffusivity. Equation (2.36) is valid for all times and for all linear flows, regardless of the value of the Péclet number. Used in conjunction with (2.33) the diffusivity can be determined at any time and for any lengthscale (*i.e.* any $\boldsymbol{k}$) of perturbation.

To determine the long-time self-diffusivity, the small k, *i.e.* long wavelength, form of (2.36) is sufficient. Because P^0 is the steady nonequilibrium probability distribution, examination of (2.36) shows that f_N is $O(k)$. Thus, keeping terms to

$O(k)$ only on the right-hand side of (2.36) we have

$$\begin{aligned} P^0\frac{\partial f_N}{\partial t} \;+\; & P^0\sum_{\alpha=2}^{N}[\boldsymbol{U}_\alpha^r - \sum_{\beta=2}^{N}\boldsymbol{D}_{\alpha\beta}^r\cdot\nabla_\beta\bar{V}]\cdot\nabla_\alpha f_N - \sum_{\alpha,\beta=2}^{N}\nabla_\alpha\cdot\boldsymbol{D}_{\alpha\beta}^r P^0\cdot\nabla_\beta f_N \\ = \;& i\boldsymbol{k}\cdot\Big(P^0(\boldsymbol{U}_1 - \dot{\boldsymbol{\Gamma}}\cdot\boldsymbol{x}_1 - \langle\boldsymbol{U}_1\rangle^0) \\ & - \sum_{\alpha=2}^{N}\{\nabla_\alpha\cdot[(\boldsymbol{D}_{\alpha 1} - \boldsymbol{D}_{11})P^0] - (\boldsymbol{D}_{1\alpha} - \boldsymbol{D}_{11})P^0\cdot\nabla_\alpha\bar{V}\}\Big) + o(k). \end{aligned} \tag{2.38}$$

2.3.6 The pair problem

To make analytical progress we define the pair-perturbation function,

$$f(\boldsymbol{r}_2) = \int P_{N-2|2}^0(\boldsymbol{r}_3,\ldots,\boldsymbol{r}_N|\boldsymbol{r}_2)f_N(\boldsymbol{r}^N)\,d\boldsymbol{r}_3\cdots d\boldsymbol{r}_N, \tag{2.39}$$

whose governing equation is found by integrating (2.38) with respect to $N-2$ of the relative coordinates, thus reducing to an equation depending only upon the separation between a pair of particles. Hereafter, we write $\boldsymbol{r}$ in place of $\boldsymbol{r}_2$ and the gradient with respect to $\boldsymbol{r}_2$ as simply ∇. Also, we write

$$\boldsymbol{U}_r = \boldsymbol{U}_2 - \boldsymbol{U}_1, \quad \text{and} \quad \boldsymbol{D}_r = \boldsymbol{D}_{22} - \boldsymbol{D}_{21} - \boldsymbol{D}_{12} + \boldsymbol{D}_{11}.$$

Quantities are scaled as

$$\boldsymbol{r}\sim a, \quad \boldsymbol{U}\sim\dot{\gamma}a, \quad \boldsymbol{k}\sim a^{-1}, \quad \boldsymbol{D}_r\sim 2D, \quad \text{and} \quad t\sim\frac{a^2}{D}, \tag{2.40}$$

and the Péclet number is defined as

$$Pe \equiv \frac{\dot{\gamma} a^2}{2D}, \tag{2.41}$$

where $\boldsymbol{U}$ indicates velocities in general, $\dot{\gamma} \equiv (\dot{\boldsymbol{\Gamma}}{:}\dot{\boldsymbol{\Gamma}})^{1/2}$, and D is the diffusion coefficient of an isolated particle. In this nondimensionalization, $\boldsymbol{D}_r \sim \boldsymbol{I}$ as $r \to \infty$. As we do not employ alternate symbols to denote dimensionless quantities, it should be borne in mind that all quantities are dimensionless unless noted otherwise in the following.

Integrating (2.38) with respect to $N-2$ of the relative coordinates, we find the dimensionless governing equation for f in the limit of small k,

$$\begin{aligned} \frac{1}{2} g \frac{\partial f}{\partial t} \;&+\; Pe\, g\langle \boldsymbol{U}_r{\cdot}\nabla f_N\rangle_2^0 - g\langle \boldsymbol{D}_r{\cdot}\nabla\bar{V}{\cdot}\nabla f_N\rangle_2^0 \\ &-\; \nabla{\cdot}g\langle \boldsymbol{D}_r{\cdot}\nabla f_N\rangle_2^0 - \nabla{\cdot}g\int P_{3|2}^0\langle \boldsymbol{D}_{23}^r{\cdot}f_N\rangle_3^0 d\boldsymbol{r}_3 \\ &=\; \tfrac{1}{2} i\boldsymbol{k}{\cdot}\{-Pe\, g\langle \boldsymbol{U}_r'\rangle_2^0 + \nabla{\cdot}g\langle \boldsymbol{D}_r\rangle_2^0 + g\langle \boldsymbol{D}_r{\cdot}\nabla\bar{V}\rangle_2^0\} + o(k), \end{aligned} \tag{2.42}$$

where the steady pair-distribution function $g(\boldsymbol{r})$ is defined by $P_{1|1}^0 = ng(\boldsymbol{r})$, and $\langle\ \rangle_2^0$ stands for the conditional average over the initial distribution with two particles fixed as defined in (2.39). The boundary condition at the pair level is obtained by requiring the relative flux $\hat{\boldsymbol{j}}_2 - \hat{\boldsymbol{j}}_1$ to vanish at particle contact,

$$\begin{aligned} \hat{\boldsymbol{r}}{\cdot}[-\langle \boldsymbol{D}_r{\cdot}\nabla f_N\rangle_2^0 \;&-\; \langle[\boldsymbol{D}_r{\cdot}\nabla\bar{V}]f_N\rangle_2^0 - \int\langle \boldsymbol{D}_{23}^r{\cdot}\nabla_3 f_N\rangle_3^0 P_{3|2}^0 d\boldsymbol{r}_3 + Pe\langle \boldsymbol{U}_r f_N\rangle_2^0] \\ &=\; \tfrac{1}{2}\hat{\boldsymbol{r}}{\cdot}\langle \boldsymbol{D}_r\rangle_2^0{\cdot}i\boldsymbol{k} \quad \text{at} \quad r=2, \end{aligned} \tag{2.43}$$

where $\hat{\boldsymbol{r}} = \boldsymbol{r}/|\boldsymbol{r}|$. At large separation the perturbation vanishes,

$$f \sim 0 \quad \text{as} \quad r \to \infty, \tag{2.44}$$

and the initial condition is unchanged,

$$f = 0 \quad \text{at} \quad t = 0. \tag{2.45}$$

A similar reduction of the expression for $(\ln \dot{F}_s)$ is performed by integrating over $N-2$ of the relative coordinates in (2.33). Since $(\ln \dot{F}_s)$ pertains to a single particle, we scale the diffusivities by D rather than $2D$ to obtain

$$\begin{aligned}(\ln \dot{F}_s) \;=\; & 2Pe(\boldsymbol{k}\cdot\dot{\boldsymbol{\Gamma}}\cdot\nabla_k \ln F_s + i\boldsymbol{k}\cdot\langle \boldsymbol{U}_1\rangle^0) - \boldsymbol{k}\cdot\boldsymbol{D}_0^s\cdot\boldsymbol{k} \\ & + \phi\frac{3}{4\pi} i\boldsymbol{k}\cdot\int\{\langle[-2Pe\,\boldsymbol{U}_r' + \boldsymbol{D}_r\cdot\nabla\bar{V}]\hat{f}_N\rangle_2^0 + \langle \boldsymbol{D}_r\cdot\nabla f_N\rangle_2^0\} g(\boldsymbol{r})d\boldsymbol{r}, \\ & + O(k^3),\end{aligned} \tag{2.46}$$

where $\boldsymbol{U}_r' = \boldsymbol{U}_2^r - \dot{\boldsymbol{\Gamma}}\cdot\boldsymbol{r}$ and we have introduced the volume fraction $\phi = \frac{4}{3}\pi a^3 n$, with n the number density of particles. Note that $\boldsymbol{D}_r = 2(\boldsymbol{D}_{11} - \boldsymbol{D}_{21})$ and $\boldsymbol{U}_r' = -2(\boldsymbol{U}_1' - \dot{\boldsymbol{\Gamma}}\cdot\boldsymbol{x}_1 - \langle \boldsymbol{U}_1\rangle^0)$ for identical particles; the factor of 2 in front of Pe arises because Pe has been defined relative to $2D$.

2.4 Diffusivity in a weakly-sheared suspension

The expressions derived in the preceding section, which are valid for all shear rates, are applied to the determination of self-diffusivity in a sheared suspension at small Péclet number. To obtain a rigorous solution we assume the particle fraction to be dilute and consider the dual limit of $Pe \ll 1$ and $\phi \ll 1$. Diluteness allows us to neglect nonlinear averages of fluctuational quantities as well as third-particle effects to obtain a closed equation for f. The diluteness assumption, however, limits the results to small ϕ, and to remedy this restriction, the method of Brady (1994) for determining the scaling of $D^s_\infty(\phi)$ with respect to ϕ near maximum packing in a quiescent suspension is applied.

Weak shear flow alters the diffusivity in a suspension relative to its value at equilibrium in three ways. The first is through its alteration of the steady microstructure, an effect reflected most directly in an $O(Pe)$ contribution to the short-time self-diffusion tensor, but important also to the long-time self-diffusivity. The second effect is also microstructural in nature, as f_N now satisfies an advection/diffusion, rather than a diffusion, equation. Third, the bulk flow generates velocity fluctuations in a suspension of hydrodynamically-interacting particles, and correlation of these velocity fluctuations provides a diffusive mechanism absent in a quiescent suspension. Of these effects, only the last requires that the particles interact hydrodynamically, although hydrodynamics influence each effect.

Expanding $g(\boldsymbol{r})$ and $f(\boldsymbol{r})$ as asymptotic series in Pe allows ready identification of the first influence of flow upon the diffusion tensors. The initial pair-distribution

function is expanded as

$$g(\boldsymbol{r}) = g^{eq}(r)[1 + Pe\, p(\boldsymbol{r}) + O(Pe^2)], \tag{2.47}$$

where $g^{eq}(r)$ is the equilibrium radial-distribution function. The problem for p, first solved for hydrodynamically-interacting particles by Batchelor (1977), is outlined in §2.4.1. The next correction to the steady initial distribution is $O(Pe^2)$ and has recently been determined by Brady & Vicic (1995*a*). This term will not be necessary as we determine the self-diffusivities only to $O(Pe^{3/2})$, which requires expanding f to $O(Pe^{3/2})$. We shall first determine, in §2.4.2, the perturbation function and the self-diffusivities in the absence of hydrodynamic interactions. In §2.4.3, we complete the determination with hydrodynamic interactions included. Finally, in §2.4.4 we apply the scaling ideas of Brady (1994) to estimate the effects of weak flow on the self-diffusivity near maximum packing. Except where necessary to make a point about correlations, the angle brackets will be omitted, with all quantities implicitly assumed to have their average value conditioned on the separation of a pair of particles.

2.4.1 Steady microstructure and the short-time self-diffusivity in a dilute suspension

For small volume fraction, the equilibrium pair distribution is assumed to be uniform for all separations, *i.e.* $g^{eq}(r) = 1$ for all r. Under this assumption, Batchelor (1977)

showed that p satisfies (a reduction of (2.35))

$$\nabla\cdot(\boldsymbol{D}_r\cdot\nabla p) = \nabla\cdot\boldsymbol{U}_r, \tag{2.48}$$

with boundary conditions

$$\hat{\boldsymbol{r}}\cdot\boldsymbol{D}_r\cdot\nabla p \;=\; 0 \quad \text{at} \quad r=2, \tag{2.49}$$

$$\text{and} \quad p \;\to\; 0, \quad \text{as} \quad r\to\infty. \tag{2.50}$$

The problem for p is forced by the straining motion and thus

$$p(\boldsymbol{r}) = -\hat{\boldsymbol{r}}\cdot\hat{\boldsymbol{E}}\cdot\hat{\boldsymbol{r}}\; q(r),$$

where $\hat{E}_{ij} = (\dot{\Gamma}_{ij} + \dot{\Gamma}_{ji})/2\dot{\gamma}$ is the rate-of-strain tensor made dimensionless with $\dot{\gamma}$. The function q satisfies

$$\frac{1}{r^2}\frac{d}{dr}\left(r^2 G\frac{dq}{dr}\right) - \frac{6Hq}{r^2} = -W(r),$$

where $G(r)$ and $H(r)$ are defined by

$$\boldsymbol{D}_r = G(r)\hat{\boldsymbol{r}}\hat{\boldsymbol{r}} + H(r)(\boldsymbol{I} - \hat{\boldsymbol{r}}\hat{\boldsymbol{r}}),$$

and $W(r)$ is defined by

$$\nabla\cdot\boldsymbol{U}_r = \hat{\boldsymbol{r}}\cdot\hat{\boldsymbol{E}}\cdot\hat{\boldsymbol{r}}W(r).$$

The functions G and H may be expressed in terms of mobility functions (Kim & Karrila 1991) relating the velocity to applied force as

$$G(r) = x^a_{11}(r) - x^a_{12}(r), \quad \text{and} \quad H = y^a_{11}(r) - y^a_{12}(r),$$

while W is expressed in terms of the functions $A(r)$ and $B(r)$ (Batchelor & Green 1972) describing the radial and transverse components of the relative velocity due to pair hydrodynamic interaction:

$$W(r) = 3[B(r) - A(r)] - r\frac{dA}{dr},$$

where

$$\boldsymbol{U}_r - \dot{\boldsymbol{\Gamma}}\cdot\boldsymbol{r} = -\boldsymbol{r}\cdot\hat{\boldsymbol{E}}\cdot[A(r)\hat{\boldsymbol{r}}\hat{\boldsymbol{r}} + B(r)(\boldsymbol{I} - \hat{\boldsymbol{r}}\hat{\boldsymbol{r}})].$$

For equal-sized spheres, A and B are given in terms of nondimensional mobility functions as

$$A(r) = \frac{4}{r}(x^g_{11} - x^g_{12}) = \frac{4}{3r}(X^G_{11} - X^G_{12})(x^a_{11} - x^a_{12}),$$

and

$$B(r) = \frac{8}{r}(y^g_{11} - y^g_{12}) = \frac{8}{r}\left(\frac{1}{3}(y^a_{11} - y^a_{12})(Y^G_{11} - Y^G_{12}) + (y^a_{11} - y^a_{12})(Y^G_{11} - Y^G_{12})\right),$$

with $x^g_{\alpha\beta}$ and $y^g_{\alpha\beta}$ the functions relating the stresslet of particle α to the force on particle β in the formulation of Kim & Mifflin (1985), while $X^G_{\alpha\beta}$ and $Y^G_{\alpha\beta}$ are resistance functions relating force to rate of strain and so forth. Using the more precise values

of hydrodynamic functions now available, the problem for p was solved here for use in evaluation of the diffusivity with only minor variation of the solution from the values reported originally.

The problem for p in the absence of hydrodynamic interactions is

$$\nabla^2 p = 0, \tag{2.51}$$

with

$$\hat{\boldsymbol{r}}\cdot\nabla p = 2\hat{\boldsymbol{r}}\cdot\hat{\boldsymbol{E}}\cdot\hat{\boldsymbol{r}} \quad \text{at} \quad r = 2, \tag{2.52}$$

and $p \to 0$ for large r. Note that in the absence of hydrodynamic interactions neither $\boldsymbol{U}_r$ nor $\boldsymbol{D}_r$ vanish at contact, and the boundary condition at contact is modified accordingly. The solution of (2.51) is simply

$$p = -\frac{32}{3}\frac{1}{r^3}\,\hat{\boldsymbol{r}}\cdot\hat{\boldsymbol{E}}\cdot\hat{\boldsymbol{r}}. \tag{2.53}$$

The quadrupolar decay of p as r^{-3} also holds for hydrodynamically-interacting particles when r is large.

In the absence of hydrodynamic interactions the short-time self-diffusivity is unaffected by the microstructure and remains the constant $D = k_B T/6\pi\eta a$ in dimensional form. With hydrodynamics, however, $\boldsymbol{M}_{11}$ depends upon $\boldsymbol{r}$, and from (2.25) the short-time self-diffusivity is $k_B T$ times the average mobility of a particle in the

steady microstructure, so that with the diffusivities nondimensionalized by D we have

$$\begin{aligned} \boldsymbol{D}_0^s &= \boldsymbol{I} + \phi\frac{3}{4\pi}\int \boldsymbol{D}_{11} g(\boldsymbol{r}) d\boldsymbol{r} \\ &= \boldsymbol{I} + \phi\frac{3}{4\pi}\int \boldsymbol{D}_{11} g^{eq}(r)(1 + Pe\, p(\boldsymbol{r})) d\boldsymbol{r}. \end{aligned} \tag{2.54}$$

The integral over g^{eq} produces an isotropic $O(\phi)$ correction to the diffusivity, first determined by Batchelor (1983). We denote this equilibrium correction by $D_0^s(\phi)$:

$$D_0^s(\phi) = (1 - 1.83\phi). \tag{2.55}$$

The $O(Pe)$ disturbance to the structure gives

$$\begin{aligned} \phi\frac{3}{4\pi} Pe \int \boldsymbol{D}_{11}(\boldsymbol{r}) p(\boldsymbol{r}) d\boldsymbol{r} &= -\frac{2}{5}\phi Pe \hat{\boldsymbol{E}} \int_2^\infty (x_{11}^a(s) - y_{11}^a(s)) q(s) s^2 ds \\ &= 0.22\phi Pe D \hat{\boldsymbol{E}}. \end{aligned}$$

Thus, we find

$$\boldsymbol{D}_0^s = D_0^s(\phi)\boldsymbol{I} + 0.22\phi Pe \hat{\boldsymbol{E}} + O(\phi^2, Pe^2), \tag{2.56}$$

with D_0^s given by (2.55), a result which has been available since the work of Batchelor (1977) to evaluate the microstructural distortion by a weak straining flow.

2.4.2 The long-time self-diffusivity in a dilute suspension: no hydrodynamics

To determine the long-time self-diffusivity we need the limit as $t \to \infty$, or only the steady solution, for f_N. The analysis is simplest if we consider separately the cases with and without hydrodynamic interactions. In the absence of hydrodynamics the analytical analysis is considerably simplified, although the general features are the same in the two cases. In this section the case without hydrodynamic interactions is studied; hydrodynamic interactions are treated in §2.4.3. A suspension without hydrodynamic interactions can be realized with particles interacting through a long-range repulsive force. If the repulsive force is hard-sphere-like, with characteristic length $b \gg a$, then the following analysis will apply with all lengths scaled by b instead of a, except in the isolated particle diffusivity; D remains $k_BT/6\pi\eta a$ because it is the true hydrodynamic radius a that sets the single particle diffusivity.

Closure for f

For small ϕ, $g^{eq} = 1$ and the nonlinear averages appearing in (2.42) are approximated as

$$\begin{aligned}
\langle \boldsymbol{U}_r \cdot \nabla f_N \rangle_2^0 &\approx \dot{\boldsymbol{\Gamma}} \cdot \boldsymbol{r} \cdot \nabla f, \\
\langle \boldsymbol{D}_r \cdot \nabla \tilde{V} \cdot \nabla f_N \rangle_2^0 &\approx \nabla (\ln g + \langle V \rangle_2^0) \cdot \nabla f = Pe \nabla p \cdot \nabla f, \\
\langle \boldsymbol{D}_r \cdot \nabla f_N \rangle_2^0 &\approx \nabla f,
\end{aligned}$$

with an error of $O(\phi)$ in each case; a similar small error is incurred by neglecting the integral over $\boldsymbol{r}_3$. With averaging again implicit, the steady form of (2.42) is given by

$$\nabla\cdot(1+Pe\,p)\nabla f - Pe(\dot{\boldsymbol{\Gamma}}\cdot\boldsymbol{r} - \nabla p)\cdot\nabla f = -Pe\,i\boldsymbol{k}\cdot\nabla p + O(Pe^2). \tag{2.57}$$

The boundary conditions become

$$\hat{\boldsymbol{r}}\cdot\nabla f = -\tfrac{1}{2}\hat{\boldsymbol{r}}\cdot i\boldsymbol{k} + O(Pe^2) \quad \text{at} \quad r = 2, \tag{2.58}$$

and

$$f \to 0 \quad \text{as} \quad r \to \infty. \tag{2.59}$$

Asymptotic expansion of f

The condition of $Pe \ll 1$ indicates advection is weak on the lengthscale of the particle. However, as is usual in problems involving a balance of diffusion with weak advection, it is not a uniformly valid approximation to neglect the flow in the entire domain. In this case of a linear flow, advection balances diffusion for $r \sim Pe^{-1/2}$, and we construct f by matched asymptotic expansions, which is now standard for problems of this type (Proudman & Pearson 1957; Acrivos & Taylor 1962; Leal 1992).

The governing equation for f is forced by a term linear in $i\boldsymbol{k}$, and thus we write

$$f = i\boldsymbol{k}\cdot\boldsymbol{b}(\boldsymbol{r}). \tag{2.60}$$

This defines the wavevector-independent field $\boldsymbol{b}$, which is analogous to the so-called 'B-field' introduced by Brenner (1980). We now write $\boldsymbol{b}$ in two separate regions as

$$\begin{aligned} \boldsymbol{b} &= \boldsymbol{b}(\boldsymbol{r}), \quad r = O(1), \\ \text{and} \quad \boldsymbol{b} &= \boldsymbol{B}(\boldsymbol{R}), \quad R = Pe^{1/2} r = O(1), \end{aligned} \tag{2.61}$$

which are to be matched in the domain of mutual validity. In (2.61), we use the outer variable $\boldsymbol{R}$, defined as $\boldsymbol{R} \equiv Pe^{1/2}\boldsymbol{r}$. Both $\boldsymbol{b}$ and $\boldsymbol{B}$ are expressed as series in Pe, with the inner expansion given by

$$\boldsymbol{b}(\boldsymbol{r}) = \sum_{n=0}^{\infty} h_n(Pe)\boldsymbol{b}_n(\boldsymbol{r}), \tag{2.62}$$

and the outer expansion by

$$\boldsymbol{B}(\boldsymbol{R}) = \sum_{n=0}^{\infty} H_n(Pe)\boldsymbol{B}_n(\boldsymbol{R}). \tag{2.63}$$

The first three h_n and H_0 will be seen to be

$$h_0 = 1, \quad h_1 = Pe, \quad h_2 = Pe^{3/2}, \quad \text{and} \quad H_0 = Pe. \tag{2.64}$$

The leading term of the inner expansion is governed by

$$\nabla^2 \boldsymbol{b}_0 = 0, \quad \text{and} \quad \hat{\boldsymbol{r}}\cdot\nabla\boldsymbol{b}_0 = -\tfrac{1}{2}\hat{\boldsymbol{r}} \quad \text{at} \quad r = 2. \tag{2.65}$$

With $h_1 = Pe$, the governing equation at $O(Pe)$ is

$$\nabla^2 \boldsymbol{b}_1 = (\dot{\boldsymbol{\Gamma}}\cdot\boldsymbol{r} - 2\nabla p)\cdot\nabla \boldsymbol{b}_0 - \nabla p, \tag{2.66}$$

with the condition of

$$\hat{\boldsymbol{r}}\cdot\nabla \boldsymbol{b}_1 = 0 \quad \text{at} \quad r = 2. \tag{2.67}$$

The far-field conditions on $\boldsymbol{b}_0$ and $\boldsymbol{b}_1$ are those of matching with the outer solution. Here, and at many later points, it is more convenient to maintain the analysis in terms of a general $\dot{\boldsymbol{\Gamma}}$; when necessary to be specific, the dimensionless velocity gradient will be for simple shear, $\dot{\Gamma}_{ij} = \delta_{i1}\delta_{j2}$.

The solution to (2.65) is

$$\boldsymbol{b}_0 = \frac{2\hat{\boldsymbol{r}}}{r^2}, \tag{2.68}$$

where a constant (in r) vector solution is set to zero to agree with the known solution for $Pe \equiv 0$. Inserting $\boldsymbol{b}_0$ and p into (2.66) yields

$$\begin{aligned} \nabla^2 \boldsymbol{b}_1 = \quad & 2\hat{\boldsymbol{\Omega}}\cdot\hat{\boldsymbol{r}} r^{-2} + \hat{\boldsymbol{E}}\cdot\hat{\boldsymbol{r}}\left(2r^{-2} + \frac{64}{3}r^{-4} + \frac{256}{3}r^{-7}\right) \\ + \quad & \hat{\boldsymbol{r}}\cdot\hat{\boldsymbol{E}}\cdot\hat{\boldsymbol{r}}\hat{\boldsymbol{r}}\left(-6r^{-2} - \frac{160}{3}r^{-4} + \frac{512}{3}r^{-7}\right), \end{aligned}$$

which has the particular solution

$$b^p_{1,k} = -\hat{\Omega}_{kj}\hat{r}_j + \hat{r}_i\hat{E}_{ij}\hat{r}_j\hat{r}_k\left(\frac{1}{2} + \frac{16}{3r^2} + \frac{64}{3r^5}\right),$$

where $\hat{\Omega}_{ij} = (\Gamma_{ij} - \Gamma_{ji})/2\dot{\gamma}$ is the dimensionless vorticity tensor. The harmonic homogeneous solution is determined by application of the boundary condition at $r = 2$ to yield the complete $\boldsymbol{b}_1$,

$$b_{1,k} = \hat{r}_i \hat{E}_{ij} \hat{r}_j \hat{r}_k (\frac{1}{2} + \frac{16}{3} r^{-2} - 24 r^{-4} + \frac{64}{3} r^{-5}) + \hat{E}_{kj} \hat{r}_j (-\frac{36}{5} r^{-2} + \frac{72}{5} r^{-4}) - \hat{\Omega}_{jk} \hat{r}_j. \quad (2.69)$$

Proceeding to a consideration of the outer expansion, the choice of $H_0 = Pe$ is now clear, because $\boldsymbol{b}_0$ and part of $Pe\boldsymbol{b}_1$ are $O(Pe)$ for $r = O(Pe^{-1/2})$. The governing equation for $\boldsymbol{B}_0$ is

$$\bar{\nabla}^2 \boldsymbol{B}_0 - Y \frac{\partial \boldsymbol{B}_0}{\partial X} = 0, \quad (2.70)$$

where $\bar{\nabla}$ denotes the gradient with respect to $\boldsymbol{R} = (X, Y, Z)$, and $\boldsymbol{B}_0$ must also satisfy

$$\boldsymbol{B}_0 \to 0 \quad \text{as} \quad R \to \infty, \quad (2.71)$$

and match the inner solution as $R \to 0$. We construct $\boldsymbol{B}_0$ using the solution for an instantaneous point source in the simple-shear flow, which satisfies

$$\frac{\partial G}{\partial t} - \bar{\nabla}^2 G + Y \frac{\partial G}{\partial X} = 4\pi \delta(\boldsymbol{R}) \delta(t), \quad (2.72)$$

and was given by Elrick (1962) as

$$G(\boldsymbol{R}, t) = \frac{1}{2\sqrt{\pi}\, t^{3/2} (1 + t^2/12)^{1/2}} \exp[-\frac{(X - Yt/2)^2}{4t(1 + t^2/12)} - \frac{(Y^2 + Z^2)}{4t}]. \quad (2.73)$$

The inner solution to be matched is a Y-directed dipole, requiring that

$$\begin{aligned} \boldsymbol{B}_0(\boldsymbol{R}) &= -\alpha_d \int_0^\infty (\bar{\nabla} + t\mathbf{1}_Y \frac{\partial}{\partial X}) G(\boldsymbol{R}, t) dt \\ &= -\frac{\alpha_d}{2\sqrt{\pi}} \int_0^\infty \boldsymbol{V}(\boldsymbol{R}, t) \frac{e^{-R^2/4t} e^{\mathcal{E}}}{t^{3/2}(1 + t^2/12)^{1/2}} dt, \end{aligned} \tag{2.74}$$

where α_d denotes the coefficient of the r^{-2} dependence of the inner solution (*i.e.* the dipole strength) and $\mathcal{E}$ is given by

$$\mathcal{E}(X, Y, t) = \frac{(X^2 - 3Y^2)t/12 + XY}{4(1 + t^2/12)}. \tag{2.75}$$

The components of $\boldsymbol{V}(\boldsymbol{R}, t)$ are

$$V_X = -\frac{X}{2t} + \frac{Y + Xt/6}{4(1 + t^2/12)}, \quad V_Y = -\frac{Y}{2t} + \frac{-X + Yt/2}{4(1 + t^2/12)}, \quad \text{and} \quad V_Z = -\frac{Z}{2t}. \tag{2.76}$$

The solution (2.74) agrees with the dipole solution of Blawzdziewicz & Szamel (1993), who have given the solution to the steady advection/diffusion equation for simple-shear flow and general dipolar forcing. The operator

$$\bar{\nabla} + t\mathbf{1}_Y \partial/\partial X,$$

which is the gradient in the frame following the deformation of the material, commutes with the operator on the left-hand side of (2.72).

We see from the inner solution that $\alpha_d = 2$, and thus the asymptotic form of $\boldsymbol{B}_0$

as $R \to 0$ needed for matching to the inner solution is given by

$$\boldsymbol{B}_0 \sim \boldsymbol{R}(2R^{-3} + A_1) - \hat{\boldsymbol{\Omega}}\cdot\boldsymbol{R}(R^{-1} + A_2) + \tfrac{1}{2}R^{-3}\boldsymbol{R}\cdot\hat{\boldsymbol{E}}\cdot\boldsymbol{R}\boldsymbol{R} + O(R^2), \tag{2.77}$$

where

$$A_1 = \frac{1}{2\sqrt{\pi}}\int_0^\infty \frac{1-(1+t^2/12)^{1/2}}{t^{5/2}(1+t^2/12)^{1/2}}dt = -\frac{0.192}{2\sqrt{\pi}}, \tag{2.78}$$

$$\text{and} \quad A_2 = \frac{1}{2\sqrt{\pi}}\int_0^\infty \frac{1-(1+t^2/12)^{1/2}}{t^{3/2}(1+t^2/12)^{3/2}}dt = -\frac{1.37}{2\sqrt{\pi}}. \tag{2.79}$$

In inner variables, terms of (2.77) which are linear in R generate terms in $H_0\boldsymbol{B}_0$ proportional to $rPe^{3/2}$ which can not be matched by $h_0\boldsymbol{b}_0 + h_1\boldsymbol{b}_1$. Thus, $h_2 = Pe^{3/2}$, and the governing equation and boundary condition for $\boldsymbol{b}_2$ are homogeneous:

$$\nabla^2\boldsymbol{b}_2 = 0, \quad \text{and} \quad \hat{\boldsymbol{r}}\cdot\nabla\boldsymbol{b}_2 = 0 \quad \text{at} \quad r = 2. \tag{2.80}$$

From the matching condition, we deduce that $\boldsymbol{b}_2$ is a combination of harmonic solutions linear in $\boldsymbol{r}$,

$$\boldsymbol{b}_2 = \boldsymbol{r}(a_1 + a_3 r^{-3}) + \hat{\boldsymbol{\Omega}}\cdot\boldsymbol{r}(a_2 + a_4 r^{-3}),$$

and this condition also shows

$$a_1 = A_1, \quad \text{and} \quad a_2 = A_2.$$

The boundary condition in (2.80) yields

$$a_3 = 4A_1, \quad \text{and} \quad a_4 = 4A_2.$$

This completes the solution of $\boldsymbol{b}$ to $O(Pe^{3/2})$ in the absence of hydrodynamic interactions.

Evaluation of the long-time self-diffusivity

Consistent with the closure of the equation for f, for small ϕ we neglect correlations in (2.46). Inserting $f = i\boldsymbol{k}\cdot\boldsymbol{b}$ and rearranging, we obtain

$$\begin{aligned}(\ln \dot{F}_s) &= 2Pe(\boldsymbol{k}\cdot\dot{\boldsymbol{\Gamma}}\cdot\nabla_k \ln F_s + i\boldsymbol{k}\cdot\langle \boldsymbol{U}_1\rangle^0) - \boldsymbol{k}\cdot\boldsymbol{D}_0^s\cdot\boldsymbol{k} \\ &\quad - \phi\frac{3}{4\pi}\boldsymbol{k}\boldsymbol{k}:\int(\nabla\boldsymbol{b} + Pe\,\boldsymbol{b}\nabla p)g(\boldsymbol{r})d\boldsymbol{r} + O(k^3, Pe^2). \qquad (2.81)\end{aligned}$$

Thus, to $O(Pe^2)$ the long-time self-diffusivity in the dilute limit is given by

$$\begin{aligned}\boldsymbol{D}_\infty^s &= \boldsymbol{D}_0^s + \phi\frac{3}{4\pi}\int(\nabla\boldsymbol{b} + Pe\boldsymbol{b}\nabla p)g(\boldsymbol{r})d\boldsymbol{r}, \\ &= \boldsymbol{D}_0^s + \phi\frac{3}{4\pi}\int\nabla[(1 + Pe\,p)\boldsymbol{b}]d\boldsymbol{r},\end{aligned}$$

where we have made use of the perturbation to the steady microstructure. Finally, integrating by parts and substituting in the expansion for $\boldsymbol{b}$ to $O(Pe^{3/2})$ we have

$$\boldsymbol{D}_\infty^s = \boldsymbol{D}_0^s - \phi\frac{3}{\pi}\left[\oint_{r=2}\hat{\boldsymbol{r}}\boldsymbol{b}_0 d\Omega + Pe\oint_{r=2}\hat{\boldsymbol{r}}(\boldsymbol{b}_0 p + \boldsymbol{b}_1)d\Omega + Pe^{3/2}\oint_{r=2}\hat{\boldsymbol{r}}\boldsymbol{b}_2 d\Omega\right], \quad (2.82)$$

where $d\Omega$ is the element of solid angle.

From the solutions for $\boldsymbol{b}$ we have

$$\begin{aligned}
\oint_{r=2} \hat{\boldsymbol{r}}\boldsymbol{b}_0 d\Omega &= \frac{2\pi}{3}\boldsymbol{I}, \\
\oint_{r=2} \hat{\boldsymbol{r}}(\boldsymbol{b}_0 p + \boldsymbol{b}_1) d\Omega &= \frac{16\pi}{45}\hat{\boldsymbol{E}} + \frac{2\pi}{3}\hat{\boldsymbol{E}}, \\
\oint_{r=2} \hat{\boldsymbol{r}}\boldsymbol{b}_2 d\Omega &= -\frac{12\pi}{3}A_1\boldsymbol{I},
\end{aligned}$$

giving a long-time self-diffusivity in dimensional form of

$$\boldsymbol{D}^s_\infty = D[(1-2\phi)\boldsymbol{I} + \frac{46}{15}\phi Pe\hat{\boldsymbol{E}} + 0.65\phi Pe^{3/2}\boldsymbol{I}] + O(\phi^2, Pe^2), \qquad (2.83)$$

using the numerical value $A_1 \approx -0.054$. The $O(Pe^{3/2})$ term is valid only for simple-shear flow, while the $O(Pe)$ term is valid for a general linear flow.

In integrating by parts to obtain (2.82) we have neglected the surface integral at infinity. Since the dipolar solution $\boldsymbol{b}_0$ decays as r^{-2}, neglecting this surface integral needs to be justified. That it is proper to discard this integral can be seen by noting that the small k expansion of the governing equation for f_N, (2.38), is not valid when $r \sim k^{-1}$. There is an outer region where the $O(k^2)$ term, $i\boldsymbol{k}\cdot\nabla f_N$, from the right-hand side of (2.36) cannot be neglected. Here $i\boldsymbol{k}$ acts like a uniform velocity and, as is common in all problems of diffusion and weak uniform advection, this outer region changes the decay from algebraic to exponential, thus justifying the neglect of the surface integral at large r.

2.4.3 The long-time self-diffusivity in a dilute suspension: hydrodynamics

We now turn to the problem for the long-time self-diffusivity with hydrodynamic interactions. The analysis proceeds much as before. The only qualitatively new feature is the presence of hydrodynamic velocity fluctuations as a source of diffusive behavior.

Closure for f

With hydrodynamic interactions, the nonlinear averages appearing in (2.42) are approximated as

$$\begin{aligned}
\langle \boldsymbol{U}_r \cdot \nabla f_N \rangle_2^0 &\approx \langle \boldsymbol{U}_r \rangle_2^0 \cdot \nabla f, \\
\langle \boldsymbol{D}_r \cdot \nabla \bar{V} \cdot \nabla f_N \rangle_2^0 &\approx \langle \boldsymbol{D}_r \rangle_2^0 \cdot \nabla (\ln g + \langle V \rangle_2^0) \cdot \nabla f = Pe \langle \boldsymbol{D}_r \rangle_2^0 \cdot \nabla p, \\
\text{and} \quad \langle \boldsymbol{D}_r \cdot \nabla f_N \rangle_2^0 &\approx \langle \boldsymbol{D}_r \rangle_2^0 \cdot \nabla f,
\end{aligned}$$

with $O(\phi)$ errors as before. The steady form of (2.42) becomes

$$\begin{aligned}
\nabla \cdot [\boldsymbol{D}_r (1 + Pe\, p) \cdot \nabla f] &- Pe(\boldsymbol{U}_r - \boldsymbol{D}_r \cdot \nabla p) \cdot \nabla f \\
&= \tfrac{1}{2} i \boldsymbol{k} \cdot [Pe(\boldsymbol{U}_r' - 2\boldsymbol{D}_r \cdot \nabla p) - (1 + Pe\, p) \nabla \cdot \boldsymbol{D}_r] \\
&\quad + O(Pe^2), \qquad (2.84)
\end{aligned}$$

with

$$\hat{\boldsymbol{r}}\cdot\boldsymbol{D}_r\cdot\nabla f = 0 \quad \text{at} \quad r = 2, \tag{2.85}$$

and

$$f \to 0 \quad \text{as} \quad r \to \infty. \tag{2.86}$$

Asymptotic expansion of f

The asymptotic expansion of $f = i\boldsymbol{k}\cdot\boldsymbol{b}$ with hydrodynamic interactions proceeds as before with the same inner and outer regions and the same scale functions (2.64). In the inner region, the leading-order governing equation is

$$\nabla\cdot(\boldsymbol{D}_r\cdot\nabla\boldsymbol{b}_0) = -\tfrac{1}{2}\nabla\cdot\boldsymbol{D}_r, \tag{2.87}$$

with boundary condition

$$\hat{\boldsymbol{r}}\cdot\boldsymbol{D}_r\cdot\nabla\boldsymbol{b}_0 = 0 \quad \text{at} \quad r = 2. \tag{2.88}$$

At $O(Pe)$, $\boldsymbol{b}_1$ is governed by

$$\nabla\cdot(\boldsymbol{D}_r\cdot\nabla\boldsymbol{b}_1) = (\boldsymbol{U}_r - 2\boldsymbol{D}_r\cdot\nabla p)\cdot\nabla\boldsymbol{b}_0 + \tfrac{1}{2}\boldsymbol{U}_r' - \boldsymbol{D}_r\cdot\nabla p, \tag{2.89}$$

with boundary condition

$$\hat{\boldsymbol{r}}\cdot\boldsymbol{D}_r\cdot\nabla\boldsymbol{b}_1 = 0 \quad \text{at} \quad r = 2. \tag{2.90}$$

Because the relative diffusivity varies spatially and the relative velocity deviates from $\dot{\boldsymbol{\Gamma}}\cdot\boldsymbol{r}$, solutions are not available in closed form and in the inner region must be determined numerically. However, the basic findings with regard to the influence of shear upon the long-time self-diffusivity for hydrodynamically noninteracting particles are unchanged by hydrodynamics: the leading influence of the flow upon the diffusion tensor is $O(\phi Pe)$ and mirrors the geometry of $\hat{\boldsymbol{E}}$, and the next dependence is $O(\phi Pe^{3/2})$.

At large r, $\boldsymbol{D}_r \sim \boldsymbol{I}$ and $\nabla_r\cdot\boldsymbol{D}_r$ scales as r^{-5}, so that the particular solution to (2.89) is proportional to r^{-3}, while the homogeneous solution is dipolar and thus proportional to r^{-2}. Including the first variation of $\boldsymbol{D}$ at large r,

$$G = 1 - \tfrac{3}{2}r^{-1} + O(r^{-3}) \quad \text{and} \quad H = 1 - \tfrac{3}{4}r^{-1} + O(r^{-3}),$$

we find

$$\boldsymbol{b}_0 = \hat{\boldsymbol{r}}\, b_0(r) \sim \hat{\boldsymbol{r}}\left(\frac{\alpha_d}{r^2} + \frac{9\alpha_d - 15}{8r^3}\right), \tag{2.91}$$

which satisfies (2.87) to terms in r^{-5}. The coefficient α_d denoting the strength of the dipole created by the pair interaction must be chosen so that a logarithmically-divergent term in the general solution at $r = 2$ vanishes; the appropriate value is found by trial to be $\alpha_d = 1.07$, which differs from the value of 2 for the coefficient of r^{-2} in the equivalent problem without hydrodynamics. The solution for $b_0(r)$ is presented in Figure 2.1. The combined asymptotic and numerical procedure used to determine $\boldsymbol{b}_0$, which was outlined by Batchelor (1977) for the determination of the

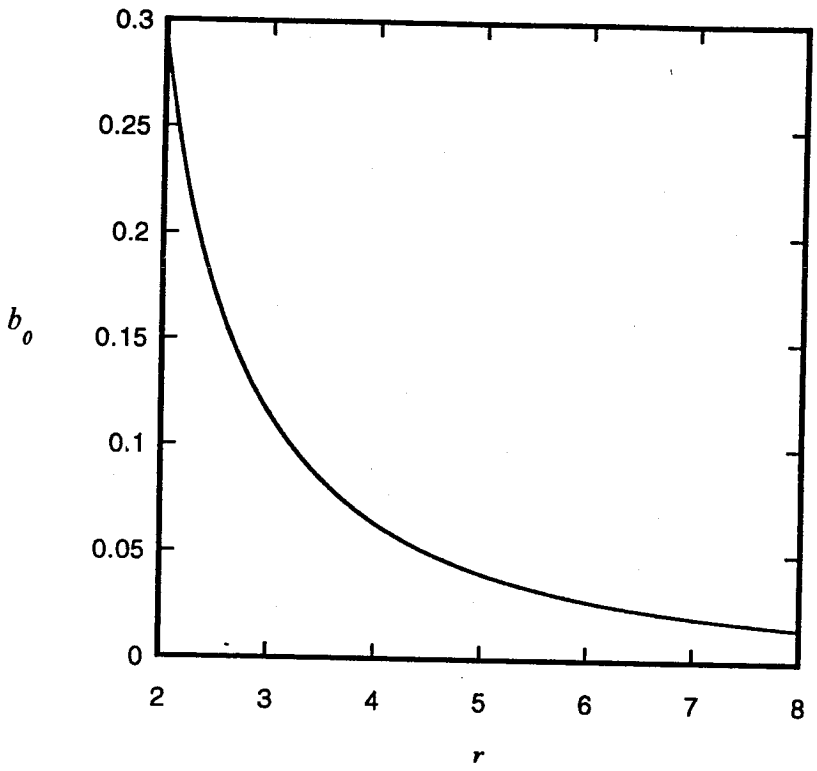

Figure 2.1: The function $b_0(r)$ specifying the radial dependence of $\boldsymbol{b}_0$.

microstructural distortion p satisfying equations (2.48-2.50) of the present work, is used also for the solution of the other problems in the inner region.

The homogeneous outer solution $\boldsymbol{B}_0^h$ satisfies the same governing equation as in the absence of hydrodynamics, and the solution differs only through the magnitude of the induced dipole. The fluctuation velocity $\boldsymbol{U}_r'$ caused by the force dipoles (stresslets) of the particles is proportional to r^{-2} and thus the leading-order outer problem is inhomogeneous,

$$-\bar{\nabla}^2\boldsymbol{B}_0 + Y\frac{\partial \boldsymbol{B}_0}{\partial X} = -\frac{1}{2}\boldsymbol{U}_r'(\boldsymbol{R}); \tag{2.92}$$

it is only the dominant portion of $\boldsymbol{U}_r'$ that enters the outer problem at leading order in Pe, *i.e* (Batchelor & Green 1972)

$$\boldsymbol{U}_r' \sim -\frac{5}{r^2}\hat{\boldsymbol{r}}\cdot\hat{\boldsymbol{E}}\cdot\hat{\boldsymbol{r}}\hat{\boldsymbol{r}} = -\frac{5}{R^2}Pe\hat{\boldsymbol{R}}\cdot\hat{\boldsymbol{E}}\cdot\hat{\boldsymbol{R}}\hat{\boldsymbol{R}}. \tag{2.93}$$

The particular solution to (2.92) is constructed by weighting the Green's function for the problem, given by (2.73) integrated over t, by $\boldsymbol{U}_r'/2$ to yield

$$\boldsymbol{B}_0^p(\boldsymbol{R}) = -\frac{1}{2}\frac{1}{4\pi}\int \boldsymbol{U}_r'(\boldsymbol{S})\int_0^\infty G(\boldsymbol{R}-\boldsymbol{S},t)dtd\boldsymbol{S}, \tag{2.94}$$

which is given in component form by

$$\begin{aligned} B_i^p(\boldsymbol{R}) &= \frac{5}{16\pi^{3/2}}E_{jk}\int\frac{S_iS_jS_k}{S^5}d\boldsymbol{S}\int_0^\infty\frac{e^{-|\boldsymbol{R}-\boldsymbol{S}|^2/4t}\exp[\mathcal{E}(\boldsymbol{R}-\boldsymbol{S},t)]dt}{t^{3/2}(1+t^2/12)^{1/2}} \\ &= \frac{5}{16\pi^{3/2}}\int\frac{S_xS_yS_i}{S^5}d\boldsymbol{S}\int_0^\infty\frac{e^{-|\boldsymbol{R}-\boldsymbol{S}|^2/4t}\exp[\mathcal{E}(\boldsymbol{R}-\boldsymbol{S},t)]dt}{t^{3/2}(1+t^2/12)^{1/2}} \end{aligned} \tag{2.95}$$

where $\boldsymbol{S} = (S_x, S_y, S_z)$ and the subscript of $\boldsymbol{B}_0^p$ is omitted for simplicity of notation.

To completely determine the solution in the inner region up to and including terms of $O(Pe^{3/2})$, (2.95) is expanded for small R to give

$$\begin{aligned} B_i^p(\boldsymbol{R}) &\sim \frac{5}{16\pi^{3/2}} E_{jk} \int \frac{S_i S_j S_k}{S^5} d\boldsymbol{S} \int_0^\infty t^{-3/2} e^{-|\boldsymbol{R}-\boldsymbol{S}|^2/4t} dt + O(R^2) \\ &\sim \frac{5}{8\pi} E_{jk} \int \frac{S_i S_j S_k}{S^5 |\boldsymbol{R}-\boldsymbol{S}|} d\boldsymbol{S} + O(R^2). \end{aligned} \tag{2.96}$$

The integral of (2.96) may be evaluated by observing that it is of the form

$$\int \frac{y_i y_j y_k}{y^5 |\boldsymbol{x}-\boldsymbol{y}|} d\boldsymbol{y} = C_1(\delta_{ij}\hat{\boldsymbol{x}}_k + \delta_{ik}\hat{\boldsymbol{x}}_j + \delta_{jk}\hat{\boldsymbol{x}}_i) + C_2 \hat{\boldsymbol{x}}_i \hat{\boldsymbol{x}}_j \hat{\boldsymbol{x}}_k.$$

Contractions of the integral with $\boldsymbol{I}\hat{\boldsymbol{x}}$ and $\hat{\boldsymbol{x}}\hat{\boldsymbol{x}}\hat{\boldsymbol{x}}$, with θ the angle between $\boldsymbol{R}$ and $\boldsymbol{S}$, yield

$$2\pi \int_0^\infty \int_0^\pi \frac{\cos\theta \sin\theta}{\sqrt{R^2 + S^2 - 2RS\cos\theta}} d\theta dS = 2\pi = 5C_1 + C_2,$$

and

$$2\pi \int_0^\infty \int_0^\pi \frac{\cos^3\theta \sin\theta}{\sqrt{R^2 + S^2 - 2RS\cos\theta}} d\theta dS = \frac{4\pi}{3} = 3C_1 + C_2,$$

respectively, where the factor of 2π is due to integration of the angle about the axis of symmetry, and thus $C_1 = C_2 = \pi/3$.

The homogeneous $\boldsymbol{B}_0^h$ is obtained by multiplying $\boldsymbol{B}_0$ determined in the absence of hydrodynamics, given in asymptotic form for small R by (2.77), by $\alpha_d/2$ to account for the different dipole strength in the problem with hydrodynamic interactions. Thus,

the complete outer solution asymptotes to

$$\begin{aligned} \boldsymbol{B}_0 \sim \quad & \frac{\alpha_d}{2}\boldsymbol{R}(2R^{-3}+A_1) - \frac{\alpha_d}{2}\hat{\boldsymbol{\Omega}}\cdot\boldsymbol{R}(R^{-1}+A_2) \\ & +(\frac{\alpha_d}{4}+\frac{5}{24})R^{-3}\boldsymbol{R}\cdot\hat{\boldsymbol{E}}\cdot\boldsymbol{R}\boldsymbol{R} + \frac{5}{12}R^{-1}\hat{\boldsymbol{E}}\cdot\boldsymbol{R} + O(R^2), \end{aligned} \tag{2.97}$$

where A_1 and A_2 are given by (2.78) and (2.79), respectively. Because the remainder in (2.96) is $O(R^2)$, the $O(Pe^{3/2})$ inner solution $h_2\boldsymbol{b}_2$ will match only with terms from the homogeneous outer solution, and is identical in functional form to, but differs in magnitude from, the leading-order outer solution found when hydrodynamic interactions are neglected.

Consideration of the forcing of (2.89) indicates that $\boldsymbol{b}_1$ may be written

$$\boldsymbol{b}_1 = M_1(r)\hat{\boldsymbol{r}}\cdot\hat{\boldsymbol{E}}\cdot\hat{\boldsymbol{r}}\hat{\boldsymbol{r}} + M_2(r)\hat{\boldsymbol{E}}\cdot\hat{\boldsymbol{r}} + M_3(r)\hat{\boldsymbol{\Omega}}\cdot\hat{\boldsymbol{r}},$$

with the $M_i(r)$ satisfying

$$\begin{aligned} \frac{d}{dr}\left(r^2 G\frac{dM_1}{dr}\right) - 12HM_1 &= r^2 L_1(r) \\ \frac{d}{dr}\left(r^2 G\frac{dM_2}{dr}\right) - 2HM_2 &= r^2 L_2(r) - 4H(r)M_1, \\ \frac{d}{dr}\left(r^2 G\frac{dM_3}{dr}\right) - 2HM_3 &= r^2 b_0(r), \end{aligned}$$

where

$$L_1 = -(1-B)b_0 \;+\; (1+B-A)rb_0' + \frac{(B-A)r}{2} \;+\; 2[Gb_0'q' - \frac{2Hb_0q}{r^2}] + Gq' - \frac{2Hq}{r},$$

and

$$L_2 = \left[1 - B + \frac{2Hq}{r^2}\right] b_0 - \frac{Br}{2} + \frac{2Hq}{r}.$$

At large r, the forcings are

$$\begin{aligned} L_1 &\sim (-3\alpha_d - \frac{5}{2})r^{-2} - \frac{(9\alpha_d - 15)}{2}r^{-3}, \\ L_2 &\sim b_0 \sim \alpha_d r^{-2} + \frac{9\alpha_d - 15}{8}r^{-3}, \end{aligned}$$

from which we find the asymptotic solutions

$$\begin{aligned} M_1(r) &\sim \frac{\alpha_d}{4} + \frac{5}{24} + \frac{18\alpha_d - 25}{32r}, \\ M_2(r) &\sim \frac{5}{12} + \frac{3\alpha_d}{16r}, \\ M_3(r) &\sim -\frac{\alpha_d}{2} + \frac{15}{16r}(1-\alpha), \end{aligned}$$

whose constant portions match with the small-R asymptote (2.97) of the outer solution $\boldsymbol{B}_0$. Starting at $r = 10$ and integrating back to $r = 2$ yields a complete solution for $\boldsymbol{b}_1$; small additive corrections to the asymptotic solutions determined by trial were sufficient to determine the solution which satisfies the boundary condition at contact. The solution curves for M_1, M_2, and M_3 are presented in Figure 2.2 (a-c), respectively.

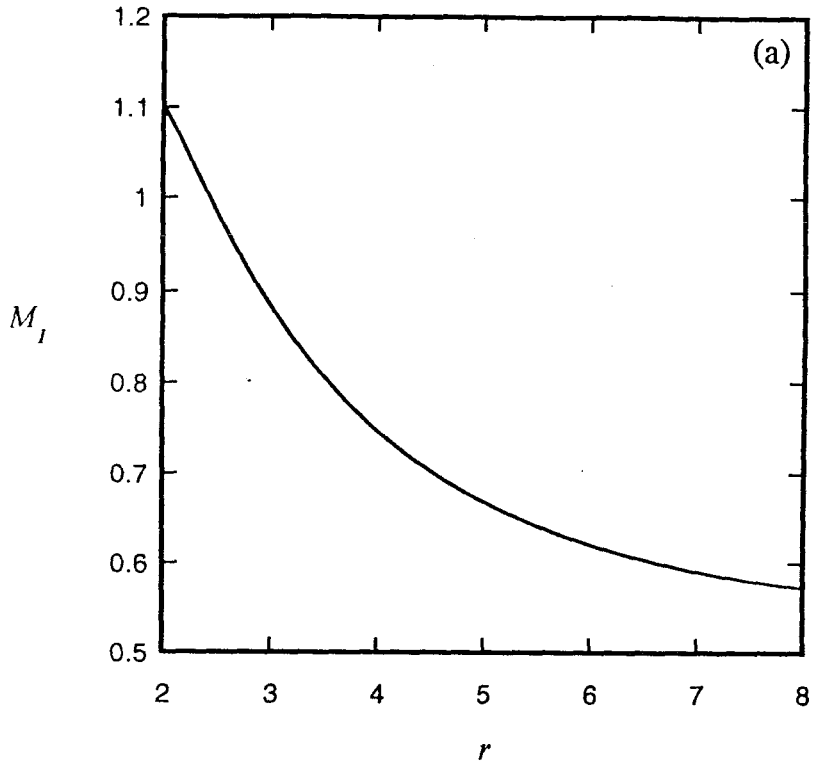

Figure 2.2: The functions (*a*) $M_1(r)$, (*b*) $M_2(r)$, and (*c*) $M_3(r)$ specifying the radial dependence of b_1; (*b*) and (*c*) are on the following page.

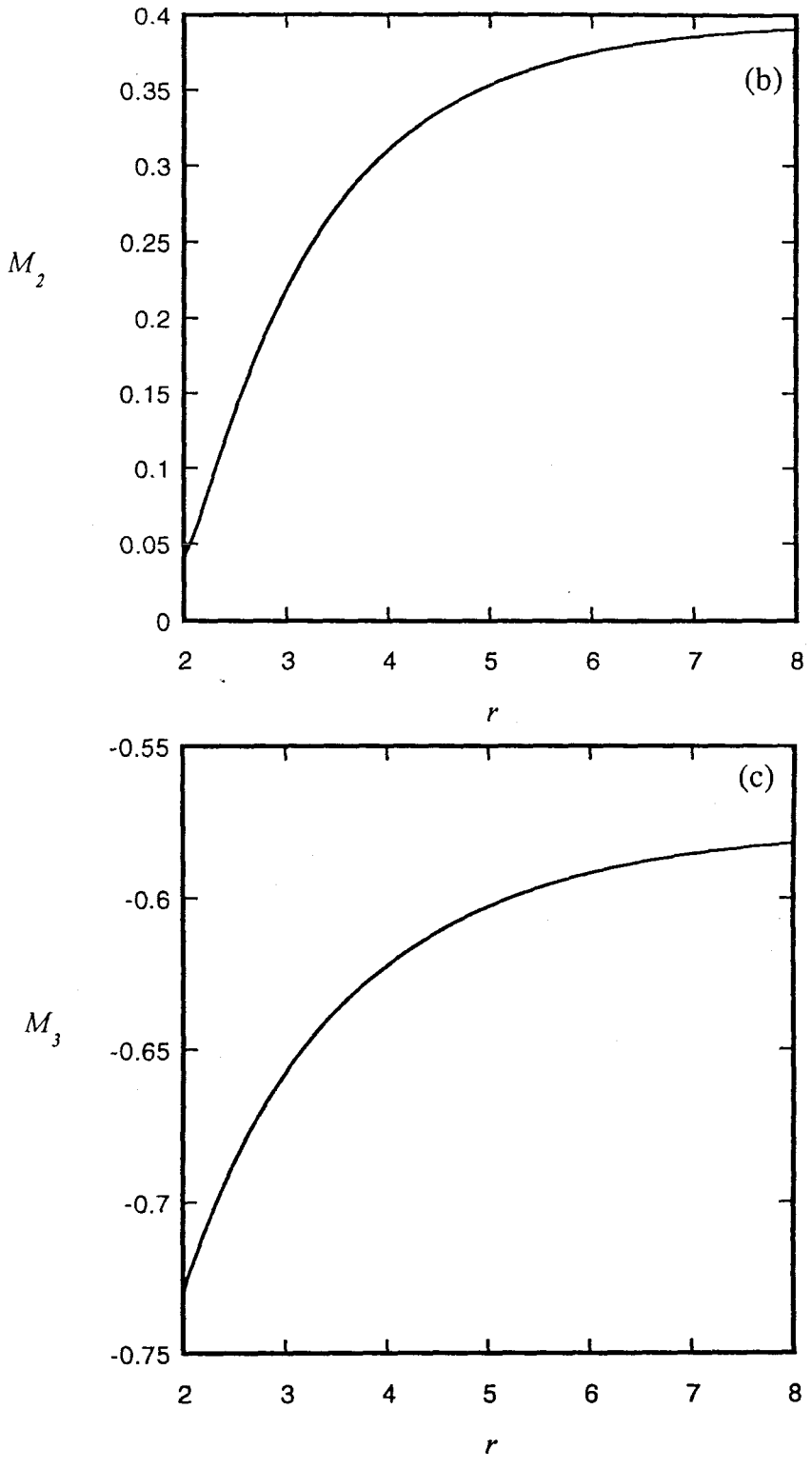

For caption, see previous page.

The equation for $\boldsymbol{b}_2$ is homogeneous,

$$\nabla\cdot(\boldsymbol{D}_r\cdot\nabla\boldsymbol{b}_2) = 0, \tag{2.98}$$

with the boundary condition

$$\hat{\boldsymbol{r}}\cdot\boldsymbol{D}_r\cdot\nabla\boldsymbol{b}_2 = 0, \quad \text{at} \quad r = 2. \tag{2.99}$$

To find $\boldsymbol{b}_2$, we note that it matches with terms which are linear in R of (2.97), and may thus be written

$$\boldsymbol{b}_2 = N_1(r)\hat{\boldsymbol{r}} + N_2(r)\hat{\boldsymbol{\Omega}}\cdot\hat{\boldsymbol{r}}, \tag{2.100}$$

where, as $r \to \infty$,

$$N_1 \sim \frac{\alpha_d}{2}a_1 r, \quad \text{and} \quad N_2 \sim \frac{\alpha_d}{2}a_3 r,$$

with the next terms constant in r to satisfy the equation including the first variation of $\boldsymbol{D}_r$ with r^{-1}. These asymptotic solutions were used as estimates to start integration of the equations governing N_1 and N_2 toward $r = 2$ from large r. Small additive corrections found by trial were sufficient to satisfy the boundary condition at contact. The solutions for N_1 and N_2 are presented in Figure 2.3 (a) and (b), respectively.

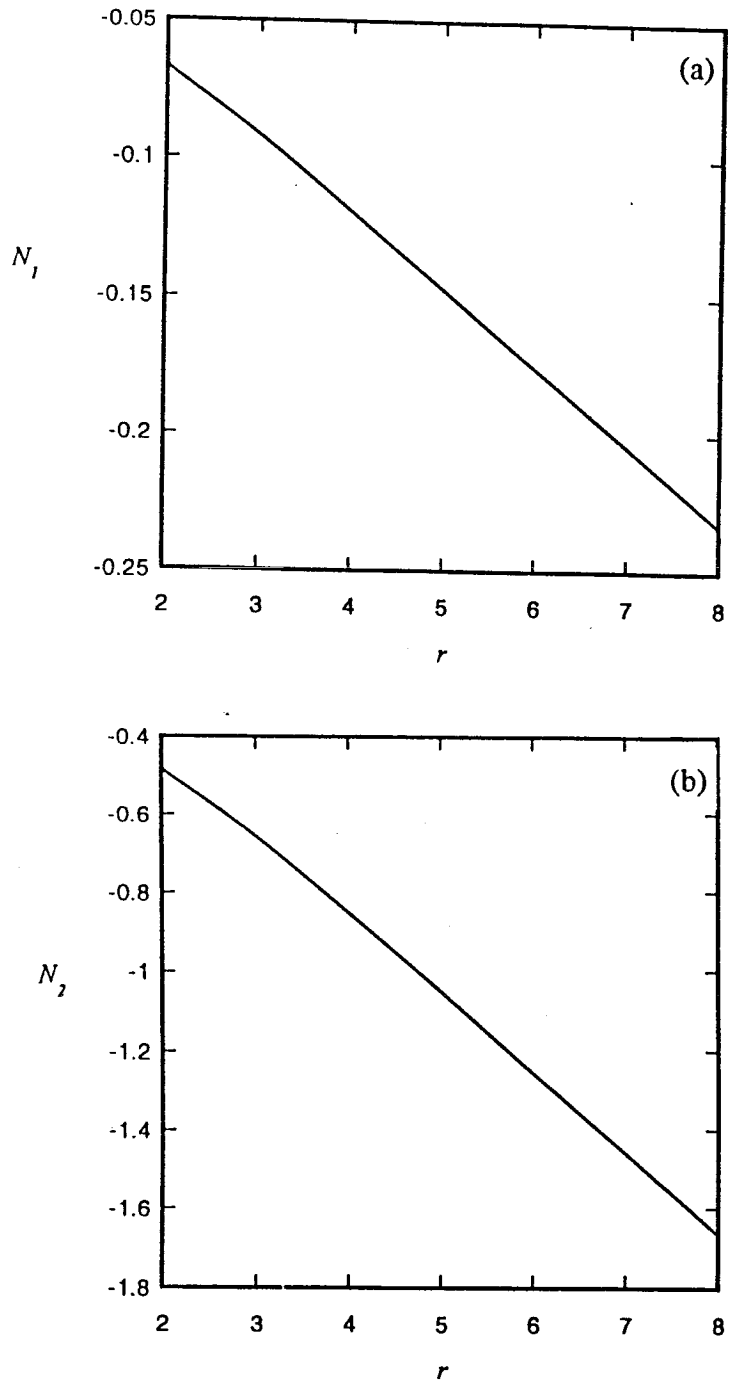

Figure 2.3: The functions (a) $N_1(r)$ and (b) $N_2(r)$ specifying the radial dependence of b_2.

Evaluation of the long-time self-diffusivity

With hydrodynamic interactions and $g^{eq} = 1$, the equation to determine the long-time self-diffusivity, (2.46), becomes

$$\begin{aligned}(\ln \dot{F}_s) &= 2Pe(\boldsymbol{k}\cdot\dot{\boldsymbol{\Gamma}}\cdot\nabla_k \ln F_s + i\boldsymbol{k}\cdot\langle \boldsymbol{U}_1\rangle^0) - \boldsymbol{k}\cdot\boldsymbol{D}_0^s\cdot\boldsymbol{k} \\ &\quad +\phi\frac{3}{4\pi}\boldsymbol{kk}:\int \boldsymbol{D}_r\cdot\nabla\boldsymbol{b}\,d\boldsymbol{r} + \phi\frac{3}{4\pi}Pe\,\boldsymbol{kk}:\int \nabla\cdot[\boldsymbol{D}_r\,p\,\boldsymbol{b}]d\boldsymbol{r} \\ &\quad -\phi\frac{3}{4\pi}Pe\,\boldsymbol{kk}:\int[2\boldsymbol{U}_r' + p\nabla\cdot\boldsymbol{D}_r]\,\boldsymbol{b}\,d\boldsymbol{r} + O(k^3, Pe^2). \qquad (2.101)\end{aligned}$$

Hence, the long-time self-diffusivity with hydrodynamic interactions is given by

$$\begin{aligned}\boldsymbol{D}_\infty^s &= \boldsymbol{D}_0^s + \phi\frac{3}{4\pi}\int \boldsymbol{D}_r\cdot\nabla\boldsymbol{b}\,d\boldsymbol{r} + \phi\frac{3}{4\pi}Pe\int \nabla\cdot[\boldsymbol{D}_r\,p\,\boldsymbol{b}]d\boldsymbol{r} \\ &\quad -\phi\frac{3}{4\pi}Pe\int[2\boldsymbol{U}_r' + p\nabla\cdot\boldsymbol{D}_r]\,\boldsymbol{b}\,d\boldsymbol{r}.\end{aligned}$$

The first two integrals on the right-hand side can be integrated by the divergence theorem, with the surface integrals at infinity discarded as discussed before, and since with hydrodynamic interactions $\hat{\boldsymbol{r}}\cdot\boldsymbol{D}_r = 0$ at contact, the contact contributions are zero. Thus, the long-time self-diffusivity reduces to

$$\boldsymbol{D}_\infty^s = \boldsymbol{D}_0^s - \phi\frac{3}{4\pi}\int(1 + Pe\,p)\boldsymbol{b}\nabla\cdot\boldsymbol{D}_r\,d\boldsymbol{r} - \phi\frac{3}{2\pi}Pe\int \boldsymbol{U}_r'\boldsymbol{b}\,d\boldsymbol{r}. \qquad (2.102)$$

We first consider the ϕ-dependence of $\boldsymbol{D}_\infty^s$ for $Pe \equiv 0$, which requires knowledge of $\boldsymbol{b}_0$ only. Batchelor (1976, 1982) found $\boldsymbol{D}_\infty^s = (1 - 2.10\phi)\boldsymbol{I}$, for $\phi \ll 1$. Rallison & Hinch (1986) obtained $\boldsymbol{D}_\infty^s = (1 - 2.06\phi)\boldsymbol{I}$ using improved hydrodynamic functions

(Jeffrey & Onishi 1984). Here, it is determined as the correlation of $\boldsymbol{b}_0$, the $\boldsymbol{b}$-field at $Pe = 0$, with the divergence of $\boldsymbol{D}_r$,

$$\nabla\cdot\boldsymbol{D} \equiv \hat{\boldsymbol{r}}\, Z(r), \quad \text{where} \quad Z(r) = G'(r) + 2\frac{G(r) - H(r)}{r},$$

and is calculated as

$$\phi\frac{3}{4\pi}\int \boldsymbol{b}_0(\boldsymbol{r})\hat{\boldsymbol{r}}Z(r)d\boldsymbol{r} = -0.24\phi\,\boldsymbol{I}.$$

This result sums with $\boldsymbol{D}_0^s$ given by (2.55) to yield in dimensional form

$$\boldsymbol{D}_\infty^s = D(1 - 2.07\phi)\boldsymbol{I}, \tag{2.103}$$

a result sufficiently close to previous findings to provide confidence in the accuracy of the hydrodynamic data employed.

The first advective effects on the diffusivity arise from the correlation of $\boldsymbol{b}$ with $\nabla\cdot\boldsymbol{D}_r$ in (2.102):

$$\begin{aligned} -\phi\frac{3}{4\pi}Pe\int Z(r)p(\boldsymbol{r})\hat{\boldsymbol{r}}\boldsymbol{b}_0(\boldsymbol{r})d\boldsymbol{r} &= \frac{2}{5}\phi Pe\hat{\boldsymbol{E}}\int_2^\infty Z(s)q(s)b_0(s)s^2ds \\ &= 0.09\phi Pe\hat{\boldsymbol{E}}; \end{aligned} \tag{2.104}$$

$$\begin{aligned} -\phi\frac{3}{4\pi}Pe\int Z(r)\hat{\boldsymbol{r}}\boldsymbol{b}_1(\boldsymbol{r})d\boldsymbol{r} &= -\phi Pe\hat{\boldsymbol{E}}\int_2^\infty Z(s)[\tfrac{2}{5}M_1(s) + M_2(s)]s^2ds \\ &= -0.75\phi Pe\hat{\boldsymbol{E}}; \end{aligned} \tag{2.105}$$

and

$$-\phi\frac{3}{4\pi}Pe^{3/2}\int Z(r)\hat{\boldsymbol{r}}\boldsymbol{b}_2(\boldsymbol{r})d\boldsymbol{r} = -\phi Pe^{3/2}\boldsymbol{I}\int_2^\infty Z(s)N_1(s)s^2ds$$
$$= 0.13\phi Pe^{3/2}\boldsymbol{I}. \qquad (2.106)$$

At large s, $\boldsymbol{b}_1(s)$ and $\boldsymbol{b}_2(s)$ are constant and linear in s, respectively, while $Z(s) \sim 15s^{-5}$; thus, the integrals converge.

Contributions to $\boldsymbol{D}^s_\infty$ from the correlation integral

$$-\phi\frac{3}{2\pi}Pe\int \boldsymbol{U}'_r\boldsymbol{b}\,d\boldsymbol{r}$$

are present only when hydrodynamic interactions are considered. We calculate these contributions to $O(Pe^{3/2})$. The first is from the integral over the inner region, yielding

$$-\phi\frac{3}{2\pi}Pe\int \boldsymbol{U}'_r(\boldsymbol{r})\boldsymbol{b}_0(\boldsymbol{r})d\boldsymbol{r} = \frac{1}{5}\phi PeD^s_0\int[2A(s)+3B(s)]b_0(s)s^3ds$$
$$= 0.96\phi Pe\hat{\boldsymbol{E}}. \qquad (2.107)$$

There is also an $O(\phi Pe^{3/2})$ contribution from integration of $\boldsymbol{U'b}$ over the *outer* region. In terms of outer variables, the correlation integral is

$$-Pe\int \boldsymbol{U}'_r(\boldsymbol{r})\boldsymbol{b}(\boldsymbol{r})d\boldsymbol{r} \sim Pe^3\int \boldsymbol{U}'_r(\boldsymbol{R})\boldsymbol{B}_0(\boldsymbol{R})(Pe^{-3/2}d\boldsymbol{R}) + o(Pe^{3/2});$$

recalling that the velocity fluctuation is proportional to r^{-2}, which introduces one factor of Pe, while $H_0 = Pe$ introduces another, the scaling of an $O(Pe^{3/2})$ contribu-

tion becomes clear. However, because the contribution to $\boldsymbol{D}^s_\infty$ from the correlation of $\boldsymbol{U}'$ with $\boldsymbol{b}_0$ has already been determined in the inner region, we must integrate

$$\int \boldsymbol{U}'_r[\boldsymbol{B}_0 - \boldsymbol{b}_0(\boldsymbol{R})]d\boldsymbol{R},$$

where $\boldsymbol{b}_0(\boldsymbol{R})$ indicates the dipolar $\boldsymbol{b}$-field in the absence of flow expressed in outer variables. To show explicitly the contributions associated with the homogeneous and particular portions of $\boldsymbol{B}_0$, we express the integrations yielding $O(Pe^{3/2})$ contributions as

$$\mathcal{D}^h = sym\frac{1}{2}\int \boldsymbol{U}'_r[\boldsymbol{B}^h_0 - \boldsymbol{b}_0(\boldsymbol{R})]d\boldsymbol{R}, \quad \text{and} \quad \mathcal{D}^p = sym\frac{1}{2}\int \boldsymbol{U}'_r\boldsymbol{B}^p_0 d\boldsymbol{R}, \qquad (2.108)$$

where the forms of $\boldsymbol{B}^h_0$ and $\boldsymbol{B}^p_0$ are given by (2.74) and (2.95), respectively. Although neither integral in (2.108) is symmetric, it is only the symmetric portions which contribute to the diffusivity. The 4-fold integration ($d\boldsymbol{R}$ and dt) for $\mathcal{D}^h$ and the 7-fold integration ($d\boldsymbol{R}$, $d\boldsymbol{S}$, and dt) for $\mathcal{D}^p$ were reduced analytically to 2-fold and 3-fold integrations, respectively, with the remaining integrations performed numerically. Analytical reduction of the integrals follows from the observation that the exponential in the solution has the form of a generalized Gaussian, and may, through a time-dependent change of coordinates, be rewritten as a sum of quadratic terms, allowing the spatial integrals to be evaluated. Each volumetric integration requires integration over an introduced parameter because we replace R^5 in the denominator of the asymptotic form of the disturbance velocity (see Equation (2.93)) by the

integral relation

$$R^{-5} = \frac{1}{\Gamma(\frac{5}{2})} \int \alpha^{3/2} e^{-\alpha R^2} d\alpha = \frac{4}{3\sqrt{\pi}} \int \alpha^{3/2} e^{-\alpha R^2} d\alpha,$$

where Γ denotes the gamma function and, in the second equality, we use $\Gamma(\frac{5}{2}) = 3\sqrt{\pi}/4$. With this replacement, the spatial integrations in the new coordinates reduce to familiar Gaussian integrals, albeit with coefficients dependent on t and the introduced parameters. The remaining integrations were performed numerically. By symmetry, $\mathcal{D}^{h,p}_{i3} = \mathcal{D}^{h,p}_{3i} \equiv 0$ for $i \neq 3$. We find

$$\mathcal{D}^h_{11} = -\mathcal{D}^h_{22} \approx 6 \times 10^{-5},$$

while the components $\mathcal{D}^h_{12}$, $\mathcal{D}^h_{21}$, and $\mathcal{D}^h_{33}$ are all found to be smaller than 10^{-10}; thus, $\mathcal{D}^h$ is essentially zero. The particular integral yields

$$\mathcal{D}^p = \begin{pmatrix} 3.83 & 0.93 & 0 \\ 0.93 & 1.74 & 0 \\ 0 & 0 & 0.39 \end{pmatrix}. \tag{2.109}$$

Bringing together all the contributions to $\boldsymbol{D}^s_\infty$, we have

$$\boldsymbol{D}^s_\infty = (1 - 2.07\phi)\boldsymbol{I} + 0.30\phi Pe\hat{\boldsymbol{E}} + (0.13\boldsymbol{I} + \mathcal{D}^h + \mathcal{D}^p)\phi Pe^{3/2} + O(\phi^2, Pe^2). \tag{2.110}$$

Again, the $O(Pe)$ term is valid for a general linear flow, while the $O(Pe^{3/2})$ term is restricted to simple shear.

This completes the evaluation of the leading flow-dependent components of the self-diffusivity for $Pe \ll 1$ and $\phi \ll 1$. In the general case, a non-hard-sphere interparticle potential will generate an $O(Pe)$ and an $O(Pe^{3/2})$ diffusivity contribution. Proper evaluation of these contributions requires inclusion of the potential-driven flux in the governing equations for g and $\boldsymbol{b}$.

2.4.4 Scaling prediction for the long-time self-diffusivity near maximum packing

For concentrated quiescent colloidal dispersions, Brady (1994) showed that a prediction of the long-time self-diffusivity in very good agreement with experiment for all ϕ could be obtained by factoring the diffusivity into a hydrodynamic and a structural (or thermodynamic) term. The idea behind this approach is the recognition that the appropriate scale for the diffusivity, both in the equation for the perturbation function and the time derivative of the structure factor, is the short-time self-diffusivity, $D_0^s(\phi)$, at the volume fraction of interest, rather than the infinite dilution value D. In this scaling, the diffusivity of a pair asymptotes to $\boldsymbol{I}$ for widely-separated particles regardless of ϕ, and it is clear that the appropriate Péclet number is $\bar{Pe} = \dot{\gamma}a^2/2D_0^s(\phi)$. With this scaling all of the above equations are unchanged, showing that the long-time self-diffusivity factors into the product of the short-time self-diffusivity times the nondimensional correlation integrals of the perturbation function.

The short-time self-diffusivity for equilibrium colloidal dispersions of hard spheres has been determined theoretically for all ϕ (Beenakker & Mazur 1984), by Stokesian

Dynamics simulations (Phillips, Brady & Bossis 1988; Ladd 1990), and experimentally (Pusey & van Megen 1983; Ottewill & Williams 1987); all are in excellent agreement with one another.

The second step in the approach is to derive a self-consistent formulation by rewriting the long-time self-diffusivity, (2.46), as

$$-\boldsymbol{k}\cdot\bar{\boldsymbol{D}}^s_\infty\cdot\boldsymbol{k} = (\ln\dot{F}_s) - 2\bar{Pe}(\boldsymbol{k}\cdot\dot{\boldsymbol{\Gamma}}\cdot\nabla_k \ln F_s + i\boldsymbol{k}\cdot\langle\boldsymbol{U}_1\rangle^0) = i\boldsymbol{k}\cdot\bar{\boldsymbol{j}}_1, \tag{2.111}$$

where the constant flux of particle 1 is

$$\bar{\boldsymbol{j}}_1 = \bar{\boldsymbol{D}}^s_0\cdot i\boldsymbol{k} + \phi\frac{3}{4\pi}\int\{\langle[-2\bar{Pe}\,\boldsymbol{U}'_r + \bar{\boldsymbol{D}}_r\cdot\nabla\bar{V}]f_N\rangle^0_2 + \langle\bar{\boldsymbol{D}}_r\cdot\nabla f_N\rangle^0_2\}g(\boldsymbol{r})d\boldsymbol{r}. \tag{2.112}$$

The overbars denote normalization with $D^s_0(\phi)$. Equation (2.112) can be solved for $i\boldsymbol{k}$ in terms of $\bar{\boldsymbol{j}}_1$, and the $i\boldsymbol{k}$ forcing on the right-hand side of (2.42) can be replaced by $\bar{\boldsymbol{j}}_1$ to give a self-consistent equation for the perturbation function f_N. This suggests that we now write f_N as

$$f_N = \bar{\boldsymbol{j}}_1\cdot\bar{\boldsymbol{b}},$$

where the new $\bar{\boldsymbol{b}}$ field satisfies the self-consistent version of (2.42). In terms of $\bar{\boldsymbol{b}}$, the long-time self-diffusivity becomes

$$\boldsymbol{D}^s_\infty = \boldsymbol{D}^s_0\cdot\left[\boldsymbol{I} + \phi\frac{3}{4\pi}\int\{\langle[-2\bar{Pe}\,\boldsymbol{U}'_r + \bar{\boldsymbol{D}}_r\cdot\nabla\bar{V}]\bar{\boldsymbol{b}}\rangle^0_2 + \langle\bar{\boldsymbol{D}}_r\cdot\nabla\bar{\boldsymbol{b}}\rangle^0_2\}g(\boldsymbol{r})d\boldsymbol{r}\right]^{-1}. \tag{2.113}$$

Integrating by parts, (2.113) can be rewritten as

$$\boldsymbol{D}^s_\infty = \boldsymbol{D}^s_0 \cdot \left[\boldsymbol{I} - \phi \frac{3}{4\pi} \oint_{r=2} \hat{\boldsymbol{r}} \cdot \bar{\boldsymbol{D}}_r \, \bar{\boldsymbol{b}} \, g \, dS \right. \\ \left. - \phi \frac{3}{4\pi} \int \langle [2\bar{Pe}\, \boldsymbol{U}'_r + \nabla \cdot \bar{\boldsymbol{D}}_r - \bar{\boldsymbol{D}}_r \cdot \nabla V] \bar{\boldsymbol{b}} \rangle^0_2 g(\boldsymbol{r}) d\boldsymbol{r} \right]^{-1} . \quad (2.114)$$

For hard spheres in the absence of hydrodynamic interactions $\boldsymbol{U}'_r$ and $\nabla \cdot \bar{\boldsymbol{D}}_r$ are zero. Further, the contact integral becomes

$$\phi \frac{3}{4\pi} \oint_{r=2} \hat{\boldsymbol{r}} \cdot \bar{\boldsymbol{D}}_r \, \bar{\boldsymbol{b}} \, g \, dS = \phi g^{eq}(2;\phi) \frac{3}{\pi} \oint \hat{\boldsymbol{r}} (1 + \bar{Pe}\, p) \bar{\boldsymbol{b}} \, d\Omega,$$

with $g^{eq}(2;\phi)$ the equilibrium pair distribution at contact. As maximum packing is approached, $\phi \to \phi_m \approx 0.63$, the equilibrium pair-distribution function diverges as $g^{eq}(2;\phi) \sim 1.2(1 - \phi/\phi_m)^{-1}$ (Woodcock 1981), and the contact integral dominates; the volume integral is less singular as $\phi \to \phi_m$. This implies that only the contact values of g^{eq}, p, and $\bar{\boldsymbol{b}}$ are needed to estimate the long-time self-diffusivity. Brady (1994) showed that in a quiescent suspension a good estimate for the contact value could be obtained with the low-ϕ limit of $\bar{\boldsymbol{b}}$. If we use this same approximation here, then we have the estimate

$$\boldsymbol{D}^s_\infty \sim \boldsymbol{D}^s_\infty(\phi; \bar{Pe} = 0) \cdot \left[\boldsymbol{I} - \frac{23}{15} \bar{Pe} \hat{\boldsymbol{E}} - 0.325 \bar{Pe}^{3/2} \boldsymbol{I} \right]^{-1}, \quad \text{as} \quad \phi \to \phi_m,$$

where the long-time self-diffusivity in the absence of flow is given by

$$\boldsymbol{D}^s_\infty(\phi;\bar{Pe}=0) \approx \frac{\boldsymbol{D}^s_0}{\phi 2g(2;\phi)}. \tag{2.115}$$

For small $\bar{Pe}$[†], we can expand the denominator and $D^s_0(\phi;\bar{Pe})$ from (2.56) to obtain

$$\boldsymbol{D}^s_\infty \sim D^s_\infty(\phi;\bar{Pe}=0)\left[\boldsymbol{I}+\frac{23}{15}\bar{Pe}\hat{\boldsymbol{E}}+0.325\bar{Pe}^{3/2}\boldsymbol{I}+O(\bar{Pe}^2)\right], \quad \text{as} \quad \phi\to\phi_m. \tag{2.116}$$

The coefficients of the $O(\bar{Pe})$ and $O(\bar{Pe}^{3/2})$ terms are, of course, approximate, but the general form displayed by (2.116) is not sensitive to the approximations made.

With hydrodynamic interactions, the contact integrals are identically zero as discussed before. However, Brady (1994) argued that at large ϕ a contact integral again appears because $\nabla\cdot\bar{\boldsymbol{D}}_r$ is singular at contact. Physically, the variation in the relative mobility of two particles at close packing is small at all separations not near contact, because the relative motion is resisted by the effective viscosity of the suspension, which diverges at close packing. Near contact, however, the relative motion is resisted by the viscosity of the solvent, not that of the suspension, and this results in $\nabla\cdot\bar{\boldsymbol{D}}_r$ having a delta function at contact. Thus, the long-time self-diffusivity is given by the estimate (2.116) whether or not there are hydrodynamic interactions. The only effect of hydrodynamic interactions is through $D^s_0(\phi)$ and $\bar{Pe}$.

[†]Note that the requirement for the perturbation analysis is now that $\dot{\gamma}a^2/2D^s_0(\phi) \ll 1$, which is a very severe restriction on the shear rate because $D^s_0(\phi)$ vanishes near maximum packing for hydrodynamically-interacting particles as $D^s_0(\phi)\sim 0.85(1-\phi/\phi_m)$ (Phung 1993).

Unfortunately, there are no data with which to compare the above predictions. Simulation data of Phung (1993), while at low Pe, are not at sufficiently low $\bar{P}e$ to extract the $\bar{P}e$ dependence. The prediction that for weak flows the long-time self-diffusivity normalized by the long-time self-diffusivity at $\bar{P}e = 0$ should be a function of $\bar{P}e$ may be used to collapse the data for all volume fractions onto a single universal curve. The limited data of Phung (1993) do seem to conform to this scaling. It would be interesting to see if this prediction is borne out by experiment and if the first correction to the long-time self-diffusivity in the velocity-gradient direction in simple shear behaves as $\bar{P}e^{3/2}$.

2.5 Summary and concluding remarks

We have investigated the self-diffusivity of a suspension of spherical particles in a linear flow. Using the Fourier-transform method based upon dynamic light scattering we have developed a theory for the identification and evaluation of the short- and long-time self-diffusion tensors for suspensions at all particle fractions in linear flow at arbitrary Péclet number, with any nonhydrodynamic interparticle and external forces acting upon the particles. Although our application of the theory in the present work is limited to small-wavevector variations corresponding to disturbances with large spatial extent, the theory is applicable for all $\boldsymbol{k}$.

The theory was applied to determine $\boldsymbol{D}_0^s$ and $\boldsymbol{D}_\infty^s$ in a dilute suspension in weak simple-shear flow, *i.e.*, in the dual limit $\phi \ll 1$ and $Pe \ll 1$. A general feature of self diffusion in suspensions, which is brought clearly into focus by this study, is the

dual nature of the role of microstructure in the process. To evaluate the diffusivities the microstructure at a chosen "initial" instant (we have chosen this as the steady microstructure at the conditions of interest as the most natural, but by no means the only, choice) and the perturbation to this microstructure caused by the motion of a tagged particle must be determined for the evaluation of $\boldsymbol{D}_{\infty}^{s}$, whereas $\boldsymbol{D}_{0}^{s}$ requires knowledge only of the initial microstructure. This had been established for equilibrium conditions by Rallison & Hinch (1986) and Brady (1994), where the concept of a perturbation function was developed. In this work we have generalized the definition of the perturbation function given by Brady (1994) to apply to linear bulk flows and shown that the definitions and formulae also hold for nonequilibrium conditions. One consequence is that $\boldsymbol{D}_{0}^{s}$ is defined as k_BT times the average hydrodynamic mobility of a particle within the microstructure for any bulk conditions. This definition is not arbitrary, but follows directly from the identification of the self-diffusivity with the tensor coefficient of the $O(k^2)$ term in $\partial \ln F_s/\partial t$, when this identification is made at the initial instant. Under all conditions, it is the coupling of the perturbed microstructure with the flux of the tagged particle that leads to the difference between $\boldsymbol{D}_{0}^{s}$ and $\boldsymbol{D}_{\infty}^{s}$. The coupling of a straining flow with a diffusive spreading leads to Taylor dispersion (Taylor 1953), and the positional variance of a particle will never, at least in certain directions, grow linearly with time. Thus, one can not identify the self-diffusivity in terms of the growth rate of the variance as is possible for quiescent suspensions, and the simplicity of the identification of the self-diffusivity in the Fourier-transform method is very useful for the investigation of this property in

a flowing suspension.

We have considered the self-diffusivity in a weakly-sheared suspension both with and without hydrodynamic interactions. When hydrodynamic interactions are neglected, the governing equations are simplified but maintain their essential structure, and this problem may be regarded as a model for suspensions of highly electrostatically repulsive particles. Direct correspondence between terms in the self-diffusivity for the cases with and without hydrodynamics demonstrates clearly the influence of the microstructure upon $\boldsymbol{D}^s_\infty$. We see from (2.82) that the self-diffusivity may be written strictly in terms of microstructural functions when hydrodynamic interactions are neglected. Hydrodynamic interactions have a quantitative effect upon the microstructure and thus upon the diffusivity contributions determined in their absence, and a qualitative influence through the introduction of hydrodynamic velocity fluctuations which provide another mechanism for diffusion. Dominant features of the shear-induced diffusion process, even in the limit of $Pe \gg 1$, may thus be obtained from the relatively simple study of noninteracting hard spheres as we demonstrate in the following chapter.

The steady governing equations for the pair-distribution function, $g(\boldsymbol{r})$, and pair-perturbation function, $f(\boldsymbol{r})$, were solved and their solutions used to evaluate the diffusivities. The short-time self-diffusivity is altered from the Stokes-Einstein value of $D = k_B T/6\pi\eta a$ when hydrodynamic interaction are considered, with an $O(\phi Pe)$ correction proportional to $\hat{\boldsymbol{E}}$ resulting from the distortion of the steady pair-distribution from spherical symmetry by straining flow (Batchelor 1977). The long-time self-

diffusivity has first corrections of $O(\phi Pe)$ and $O(\phi Pe^{3/2})$, regardless of whether hydrodynamic interactions are considered. The $O(\phi Pe)$ contribution is proportional $\hat{\boldsymbol{E}}$ and, like the correction to $\boldsymbol{D}_0^s$ of the same order, is valid for arbitrary linear flow, whereas the $O(\phi Pe^{3/2})$ we determine is specific to simple-shear flow. Although $\boldsymbol{D}_\infty^s$ will have a correction of $O(\phi Pe^{3/2})$ in other linear flows, not only the numerical value but also the tensorial character of the contribution will differ: the $O(\phi Pe)$ corrections are determined from the solution of the $O(Pe)$ problem for f in the inner region only, with no information from the outer solution (matching this inner solution does not require use of a degree of freedom), whereas the $O(\phi Pe^{3/2})$ correction requires the detailed form of the first term in the series solution in the outer region.

The $O(\phi Pe^{3/2})$ contribution to $\boldsymbol{D}_\infty^s$ is isotropic in the absence of hydrodynamic interactions. When hydrodynamic interactions are included, this contribution is given by the sum of a tensor proportional to $\hat{\boldsymbol{E}}$, with component form in simple shear of $\hat{E}_{ij} = (\delta_{i1}\delta_{j2} + \delta_{i2}\delta_{j1})/2$, and a nonisotropic tensor. The $O(\phi Pe^{3/2})$ self-diffusivity corrections are equivalent in their order with respect to ϕ and Pe to those found by Leal (1973) for the influence of a weak simple-shear flow upon the cross-stream effective conductivity of a passive scalar in a dilute suspension of spherical drops or rigid particles. A direct analogy exists between the singular problem for the temperature fluctuation in that study with that for f when hydrodynamics are considered in the present work, and we can deduce form this analogy that the correlation of velocity disturbance with temperature disturbance yields an $O(\phi Pe)$ correction proportional to $\hat{\boldsymbol{E}}$ to the effective conductivity.

The isotropy of the self-diffusivity contribution determined at $O(\phi Pe^{3/2})$ neglecting hydrodynamics prompts an interesting comparison with the results of Qiu *et al.* (1988). These authors used forced Rayleigh scattering to measure the self-diffusivity in a charge-stabilized suspension of polystyrene spheres of average actual radius $a = 0.037\mu$m subjected to large-amplitude oscillating shear ($\dot{\gamma}/\omega < 10$ where $\dot{\gamma}$ is the shear rate and ω is the temporal rate of oscillation). For highly-repulsive spheres, the particles have an effective radius a_E with $a_E \gg a$, and hydrodynamics may be neglected in a first analysis. Qiu *et al.* (1988) measured the self-diffusivity in the vorticity-direction of a simple-shear flow, denoted as $D_{s\perp}(\dot{\gamma})$. The value of a_E was varied by changing the ionic strength of the suspending fluid, and Taylor dispersion along the flow direction, denoted $D_{s||}$, was well-correlated by the expression

$$D_{s||} = D_{s\perp}(1 + \frac{\dot{\gamma}^2}{2\omega^2}),$$

which the authors show is precisely the result which one would expect if the diffusion coefficient in the velocity-gradient-direction were also given by $D_{s\perp}$. Although further experimental study is warranted, this is evidence for isotropic diffusivity perpendicular to the mean flow. The argument advanced by the authors to explain this isotropy is that each encounter with another particle induces in a test particle a random displacement which scales with the effective radius of the spheres. It must be noted that these experiments were performed at a Péclet number $a_E^2\dot{\gamma}/D = O(10)$, with D the bare diffusivity, and the results of the present study are not applicable at this condition. Nonetheless, we note these results because it is possible that the microstructural

anisotropy necessary to obtain an advectively-driven diffusivity has similar character (but different magnitude) over a wide range of Pe, and if so, fundamental geometric similarity between the advective contribution to the diffusivity over a wide range of conditions will exist.

Self-diffusivity in a monodisperse suspension of spherical particles in simple shear including full hydrodynamic interactions has been investigated by Stokesian Dynamics for monolayers by Brady & Bossis (1987) and for fully three-dimensional suspensions by Phung (1993). Most of these results are for values of ϕ well outside the dilute regime for which our analysis is valid. We may note, however, that these results do not generally show the long-time self-diffusivity in the plane perpendicular to the bulk flow to be isotropic, although the approximation of isotropy is not a poor one for $\phi > 0.3$.

Flow-dependent corrections to the self-diffusivity at $\phi \rightarrow \phi_m$ have been shown to follow the same scaling with respect to ϕ as in the case of $\bar{P}e = 0$, for sufficiently small $\bar{P}e$; these scalings were obtained using the method developed by Brady (1994) for the determination of the scaling with ϕ in a concentrated suspension which factorizes $\boldsymbol{D}^s_\infty$ into a hydrodynamically-influenced term, which is simply $\boldsymbol{D}^s_0$, and a microstructural term which can be written as $(g(2)f(2))^{-1}$ in the general case as $\phi \rightarrow \phi_m$ (the argument of 2 is shorthand for $|\boldsymbol{r}| = 2$). The analysis shows that for weak flows the appropriate Péclet number is that based on the short-time self-diffusivity at the volume fraction of interest, $\bar{P}e = \dot{\gamma}a^2/2D^s_0(\phi)$, and that $\boldsymbol{D}^s_\infty$ can be expressed as the product of $\boldsymbol{D}^s_\infty$ at $\bar{P}e = 0$ times the same function of $\bar{P}e$ as at small ϕ.

The phenomenon of shear-induced diffusion of noncolloidal particles (Eckstein, Bailey, & Shapiro 1977; Leighton & Acrivos 1987; Acrivos *et al.* 1992) may also be treated by the Fourier-transform method. This problem requires the evaluation of both g and f (or the $\boldsymbol{b}$-field as we have formulated the problem) for $Pe \gg 1$ and will be treated in the following Chapter where the microstructure of a strongly-sheared suspension is studied.

Chapter 3

Microstructure, rheology, and self diffusion in a strongly-sheared suspension

Abstract

The effects of Brownian motion alone and in combination with an interparticle force of hard-sphere type upon the particle configuration in a strongly-sheared suspension have been analyzed. In the limit $Pe \to \infty$ under the influence of hydrodynamic interactions alone, the pair-distribution function has symmetry properties that yield a Newtonian constitutive behavior and a zero self-diffusivity. Here, $Pe = \dot{\gamma}a^2/2D$ is the Péclet number with $\dot{\gamma}$ the shear rate, a the particle size, and D the diffusivity of an isolated particle. Fore-aft symmetry, in which a second sphere is equally likely to lie on an approaching (fore) or receding (aft) trajectory relative to the reference sphere, holds under these conditions, and although the steady pair-distribution function diverges at contact for pure straining motion, the rheology is Newtonian. At small particle fraction ϕ, where $\phi = \frac{4}{3}\pi a^3 n$ with n the number density of particles, Brownian diffusion at large Pe gives rise to an $O(aPe^{-1})$ thin boundary layer at contact in which the effects of Brownian diffusion and advection balance, and the pair-distribution function is asymmetric within the boundary layer with a contact value of $O(Pe^{0.78})$; nonNewtonian effects, which scale as the product of the contact value and the $O(a^3Pe^{-1})$ layer volume, vanish as $Pe^{-0.22}$ as $Pe \to \infty$. If, however, particles are maintained at a minimum separation of $2b$, with $b > a$, there is a boundary layer of thickness aPe^{-1} leading to an asymmetry of the pair-distribution function which is $O(Pe)$, with an excess of particles along the compressional axes. The product of the asymmetric pair-distribution function and the thin boundary layer is $O(1)$ (dependent on b/a) as $Pe \to \infty$ yielding nonNewtonian rheology, with normal

stresses scaling as $\eta\dot{\gamma}$. For a dilute suspension without hydrodynamic interactions in a general linear flow, the bulk stress resulting from pair interactions, denoted $\boldsymbol{\Sigma}'$, and the associated normal stress differences are proportional to $\eta\dot{\gamma}\phi_b^2(a/b)$, where $\phi_b = \frac{4}{3}\pi b^3 n$ is the thermodynamic volume fraction. Including hydrodynamic interactions, the hydrodynamic normal stress difference is $O(\eta\dot{\gamma}\phi^2)$. The broken symmetry and boundary-layer structure also yields a shear-induced self-diffusivity of $O(\dot{\gamma}a^2\phi)$ as $Pe \to \infty$. For dilute suspensions of hard spheres without hydrodynamics, the self-diffusivity is predicted to be $\boldsymbol{D}^s = -\frac{a^2}{\eta}\frac{2}{27}\frac{1}{\phi}\boldsymbol{\Sigma}'$.

3.1 Introduction

This paper addresses the microstructure of low-Reynolds-number suspensions of spheres in strong shearing flow where the influence of Brownian motion is weak. We have analyzed the pair-distribution function under the combined influence of weak Brownian motion and an interparticle force of hard-sphere type. The study is motivated by a number of observations in nonequilibrium suspensions. When particles are added to a Newtonian solvent, the suspension is often nonNewtonian, and thus the particles cause a more striking alteration of rheological properties than the simple and familiar increase in the effective viscosity. The effects in suspensions of spherical particles include normal stress differences, which have been observed experimentally (Gadala-Maria 1979) and in simulations (Phung 1993), and a contribution to the isotropic stress (or particle pressure), which has been described and determined in simulation by Jeffrey, Morris & Brady (1993). It is therefore generally inappropriate to apply a Newtonian constitutive relation in modeling suspension flow, as this can yield predictions of velocity and particle fraction fields in marked disagreement with experiment and simulation for flows far from equilibrium. Far from equilibrium here implies large values of the Péclet number, Pe, which is a measure of the relative strength of shear and Brownian forces. Rational constitutive modeling of suspension rheology for arbitrary flows requires understanding the microscopic basis for bulk behavior at large Pe. It is the goal of this work to analytically determine the microstructure of a strongly-sheared suspension and demonstrate certain consequences of the microstructure for the suspension rheology and self-diffusivity.

The rheology of suspensions is related to the spatial distribution of particles, termed the microstructure, and qualitative features of the rheology may be ascribed to symmetry properties of the microstructure. For a suspension of spheres in the limits of $Pe = 0$ and $Pe^{-1} = 0$, the pair-distribution function, $g(\boldsymbol{r})$, is spherically symmetric (at least for pure straining flows), *i.e.*, $g(\boldsymbol{r}) = g(r)$, and this microstructural isotropy is associated with Newtonian constitutive behavior. Here, $\boldsymbol{r}$ is the vector separation between the centers of a pair of spheres. We focus upon whether the pair-distribution function possesses "fore-aft," rather than the more restrictive spherical symmetry. Fore-aft symmetry is characterized by equal probability of a second particle lying on a trajectory where it is approaching (fore) or receding (aft) relative to a reference particle, and is relevant for flows in which the approaching and receding portions of the pair trajectory are mirror images. This is true of simple-shear and planar (two-dimensional) extensional flow. If fore-aft symmetry of $g(\boldsymbol{r})$ holds, the rheology is Newtonian in the sense that normal stresses are zero. This work will demonstrate how the combined effects of Brownian motion and an interparticle force of hard-sphere type give rise to the microstructural asymmetry necessary to yield nonNewtonian behavior at large Pe. Broken fore-aft symmetry at $Pe^{-1} = 0$ is reflected also in a finite self-diffusivity of $O(\phi)$ in the dilute limit, which we calculate using the theory of self-diffusivity in sheared suspensions developed in Chapter 2.

Analytical study of the pair-distribution function in flowing suspensions was initiated by Batchelor & Green (1972*b*) who showed that under the action of hydrodynamic interactions alone in pure straining flow, at $Pe^{-1} \equiv 0$, $g(\boldsymbol{r})$ is spherically

symmetric. This is a remarkable symmetry considering the angular dependence of the relative velocity of two particles, whereas isotropic microstructure at equilibrium $Pe \equiv 0$ is, of course, expected. In simple-shear flow there is a region of closed trajectories, and therefore one cannot conclude that $g(\boldsymbol{r})$ is isotropic, although this is a possible structure. At finite Pe, flow distorts g from spherical symmetry as shown by Batchelor (1977) in his study of a weakly-strained ($Pe \ll 1$) suspension, although his determination of g to $O(Pe)$ was insufficient for calculation of nonNewtonian effects. To determine the normal stress requires the next correction to g, which is $O(Pe^2)$ (Brady & Vicic 1995*a*). Numerous studies of the pair-distribution function at small Pe have followed Batchelor's (1977) work, most with the aim of incorporating many-body effects present in suspensions at higher concentrations. Russel (1993) reviews much of the statistical mechanical work which has been performed for colloidal dispersions.

Although the present study is devoted to microstructure in linear flows, it is worth noting the microstructural studies of sedimenting particles. Batchelor (1982) studied the pair-distribution function in sedimentation, showing that for $Pe^{-1} \equiv 0$, $g(\boldsymbol{r})$ is, as in linear flow, spherically symmetric. Using theory developed by Batchelor (1982), Batchelor & Wen (1982) evaluated g numerically for dilute sedimentation at large Pe, but did not resolve the solution up to particle contact, and thus were unable to determine the manner in which the singular contact value of g is made finite by Brownian motion. The influence of surface roughness on the trajectories of sedimenting spherical particles has been investigated by Tabatabaian & Cox (1991)

followed either by rigid-body (both studies) or frictional-sliding (Davis) motion while particle surfaces were in contact. The microstructure was not determined by either study, but Tabatabaian & Cox demonstrated the loss of fore-aft symmetry of the trajectory when surfaces made contact, while Davis calculated the self-diffusivity caused by the loss of symmetry.

At equilibrium, the probability of a configuration is proportional to the Boltzmann factor $\exp[-V]$, where V is the potential energy for the configuration made dimensionless by the thermal energy kT. In a flowing suspension, however, the interplay of Brownian motion, interparticle forces, and hydrodynamic interactions leads to a nonequilibrium microstructure that can only be determined analytically by solution of the Smoluchowski equation governing the configurational probability. The primary factor determining the microstructure in a flowing suspension is the relative strength of the shear-driven flux to the diffusive Brownian flux, *i.e.*, Pe. Often, suspended particles are of micron size or larger, which for typical shear rates yields $Pe > O(1)$, and the microstructure is determined predominantly by hydrodynamic effects.

The effect of flow at large Péclet number upon the pair-distribution function has been demonstrated by experiment and simulation. In Figure 3.1, adapted from Phung (1993), and Figure 3.2, reproduced from Parsi & Gadala-Maria (1987), are plots of the steady $g(\boldsymbol{r})$ found at large values of Pe. Phung determined g from Stokesian Dynamics (Brady & Bossis 1988) simulation of a suspension in shear flow $u_x = \dot{\gamma}y$; the projections of g onto the plane of shear, x-y, and the plane perpendicular to the bulk flow, y-z, are shown. These were fully three-dimensional simulations at

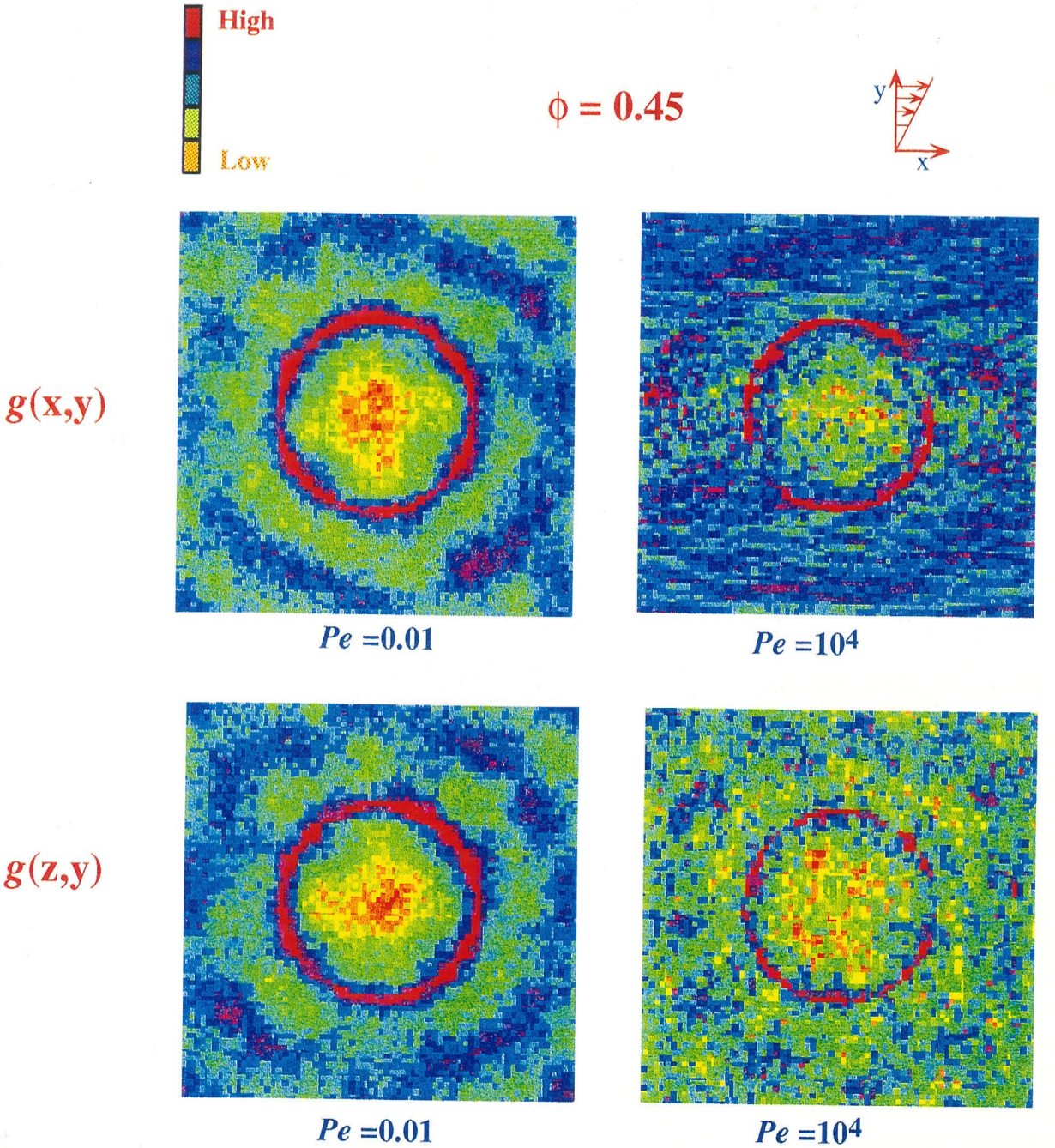

Figure 3.1: Projections of the pair-distribution function g onto the x-y and y-z planes for a monodisperse suspension at $\phi = 0.45$ in simple shear, $u_x = y$, simulated by Stokesian Dynamics. The reference sphere is centered at the center of the square and the scale at the top indicates the relative density of sphere centers. Note the distortion in the nearest-neighbor ring in the x-y plane and the narrowing of this ring in both the x-y and y-z planes for $Pe = 10^4$ relative to $Pe = 0.01$ From Phung (1993).

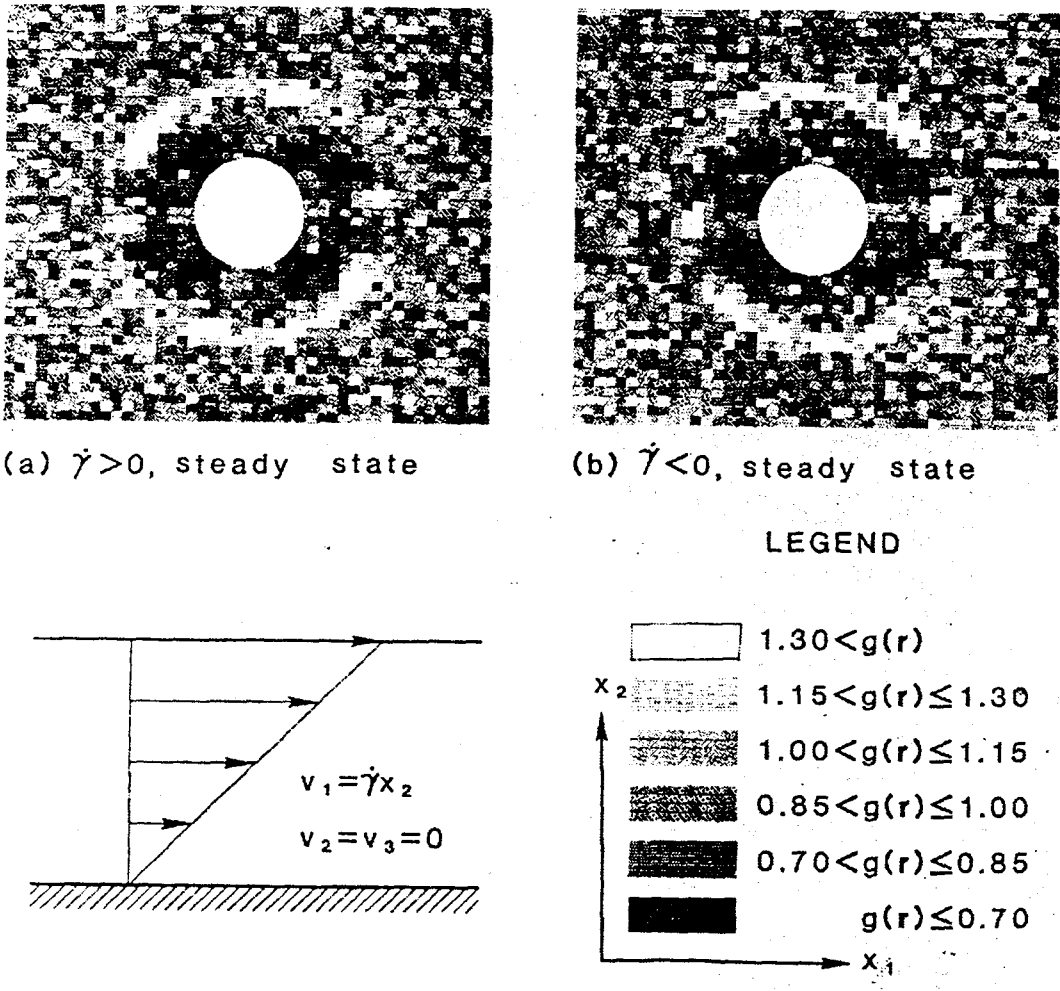

Figure 3.2: Pair-distribution function g, in the plane of shear, for a suspension of polystyrene spheres in silicone oil at particle volume fraction $\phi = 0.4$ in simple shear at $Pe = 3.0 \times 10^5$ and $Re = 3.2 \times 10^{-7}$. The shear rate is opposite in the two plots. Note the fore-aft asymmetry of the pair distribution and the reversal of the asymmetry for reversal of the shear rate. From Parsi & Gadala-Maria (1987).

zero Reynolds number of a monodisperse suspension of spheres at a particle volume fraction of $\phi = 0.45$; there are no interparticle forces. The pair-distribution function from $Pe = 0.01$ is presented for purposes of comparison with that for $Pe = 10^4$, with the Péclet number defined as $Pe \equiv 6\pi\eta\dot{\gamma}a^3/kT$ with a denoting the sphere radius. At $Pe = 10^4$, there is narrowing of the nearest-neighbor ring in both projections relative to the near-equilibrium condition of $Pe = 0.01$. Distortion of this ring from circular is scarcely discernible in the plane perpendicular to the flow, but is obvious in the plane of shear. Parsi & Gadala-Maria (1987) performed simple-shear flow experiments with a suspension of spherical polystyrene particles in silicone oil at $\phi = 0.4$, $Pe = 3.0 \times 10^5$ and $Re = 3.2 \times 10^{-7}$. The particle radii were in the range of $20-25\mu$m, a size for which colloidal forces are typically considered negligible. The pair-distribution function, determined by analysis of video images of the particle position, is illustrated by the projection of g in the plane of shear in Figure 3.2. The pair-distribution functions determined by Parsi & Gadala-Maria (1987) and Phung (1993) have the common feature of an excess of particle pairs along the compressional axes, as g takes on large values adjacent to the reference particle in the compressional quadrants of the plane of shear, and relatively small values in the extensional quadrants. With flow reversal, the compressional and extensional quadrants are interchanged and, as demonstrated by the results of Parsi & Gadala-Maria (1987), the fore-aft asymmetry is reversed after a period of microstructural rearrangement.

Normal stress differences resulting from the asymmetry of $g(\boldsymbol{r})$ have been observed in strongly-sheared suspensions both experimentally by Gadala-Maria (1979) and in

Stokesian Dynamics simulation by Phung (1993). In a parallel-plate geometry using suspensions identical to those of Parsi & Gadala-Maria (1987), Gadala-Maria found normal stress differences that scaled roughly as $\eta\dot{\gamma}$ for $\phi = 0.3 - 0.5$. In suspensions of Brownian particles interacting only through hydrodynamics, Phung found normal stress differences for values of Pe as large as 10^4 for $\phi = 0.31 - 0.51$.* As an example, for $\phi = 0.45$ and Pe in the range $2 \times 10^2 < Pe < 10^4$, Phung found $N_1/\dot{\gamma}\eta \approx 2$ while $N_2/\eta\dot{\gamma}$ increased from roughly 2 to 2.5 in this range, where N_1 and N_2 are normal stress differences defined $N_1 = \langle \Sigma_{22} - \Sigma_{11} \rangle$ and $N_2 = \langle \Sigma_{33} - \Sigma_{22} \rangle$, with $\boldsymbol{\Sigma}$ the bulk stress of the suspension. Interparticle forces are absent in Phung's simulations, and these results demonstrate that residual Brownian diffusion creates microstructural asymmetry sufficient to yield measurable nonNewtonian effects for $Pe \gg 1$. Further experimental evidence of the asymmetry of $g(\boldsymbol{r})$ at large Pe is given by the work of Gadala-Maria & Acrivos (1980), where for suspensions of $\phi > 0.3$, the torque required to generate an oscillatory torsional flow in a parallel-plate viscometer went through a marked transient before reaching steady state at each reversal of the flow direction.

These examples are ample evidence of nonNewtonian behavior in suspensions at large Péclet number, and yet when Brownian motion and interparticle forces vanish, it has been shown analytically for dilute suspensions that the microstructure is symmetric and the rheology Newtonian. Considering only Stokes flows, we shall term the condition where Brownian motion and interparticle forces are absent the hydrodynamic limit. A simple argument based upon the reversibility of Stokes flow

*Phung (1993) reported normal stress differences for Pe as large as 10^6, but the data show too much scatter for confidence in the values at $Pe > 10^4$.

shows that fore-aft symmetry should hold also for nondilute suspensions in the hydrodynamic limit: supposing an initially isotropic microstructure, development of an asymmetric structure due to shearing is incompatible with the fact that upon reversal of the shear rate all trajectories are reversed and the structure vanishes to reproduce the original isotropic stucture. Thus, the experimental and simulational results seem to contradict the analytical reasoning. To clarify this situation and to predict the rheology of noncolloidal suspensions, we have analyzed the pair-distribution function of a monodisperse suspension of spheres under conditions of weak Brownian motion ($Pe \gg 1$). Under these conditions, there is a balance between advection and Brownian diffusion in a narrow boundary layer of $O(a\,Pe^{-1})$ at minimum separation, analogous to boundary layers encountered in heat or mass transfer from surfaces, and it is within the boundary layer that the symmetry properties of g are determined. Two cases, distinguished by the minimum separation of a pair of particles, denoted $2b$ so that b is the effective radius of the particles, have been studied. In the first case, the particles interact only hydrodynamically, and the minimum separation is at actual contact, *i.e.*, $b = a$. In the second case, a repulsive force of hard-sphere type maintains a minimum separation of $2b > 2a$.

We study the steady pair equation at $\phi \ll 1$ considering only pair interactions. Investigation of the problem with hydrodynamics and weak Brownian motion, but no nonhydrodynamic forces ($b \equiv a$), is presented in §3.3. Under these conditions, the boundary-layer equation for g for pure straining motion is solved by similarity reduction to find $g(2) = O(Pe^{0.78})$, where $g(2)$ is the contact value of $g(\boldsymbol{r})$. Although

the solution is not fore-aft symmetric, the product of the $O(a^3 Pe^{-1})$ volume of the boundary layer and the $O(Pe^{0.78})$ magnitude of g scales as $Pe^{-0.22}$ as $Pe \to \infty$, and thus nonNewtonian effects vanish in the hydrodynamic limit. In §3.4, the influence of a repulsive interparticle force of hard-sphere type is analyzed by considering the pair equation for particles maintained at a minimum separation $2b > 2a$. The problem is first studied without hydrodynamic interactions to simplify the boundary-layer analysis, then with full pair hydrodynamics. Fundamental features of the microstructure are the same regardless of whether or not particles interact hydrodynamically: the radial balance between advection and Brownian diffusion yields an asymmetric $g(\boldsymbol{r})$ of $O(Pe)$ within the boundary layer. In the limit $Pe \to \infty$, the product of the $O(Pe)$ asymmetry and the $O(a^3\, Pe^{-1})$ boundary-layer volume is finite, yielding nonNewtonian rheology that is independent of Pe, as illustrated by dilute-limit calculation of the average normal stress differences which, for $b - a$ small, scale as $\eta\dot{\gamma}\phi^2$. It should be noted that with hydrodynamics, nonNewtonian effects scale as $(b/a - 1)^{0.22}$ as $b - a \to 0$. The exponent of 0.22 arises from a grouping of the contact values of the hydrodynamic functions which also yields the $Pe^{-0.22}$ scaling of nonNewtonian effects under the influence of hydrodynamics alone. The asymmetry in the boundary-layer solution for $b > a$ is also reflected in an $O(\phi)$ cross-stream self-diffusivity in simple shear, which we calculate in §3.5 for the case of hard spheres without hydrodynamics using the theory developed in Chapter 2. Finally, we discuss the work and possible extensions.

3.2 Governing equations

3.2.1 Smoluchowski equation

We consider a suspension of N identical spheres homogeneously dispersed in a Newtonian fluid. The suspension is subjected to a linear incompressible flow with the constant velocity-gradient tensor $\dot{\boldsymbol{\Gamma}}$. The probability distribution function for the N-particle configuration, $\boldsymbol{x}^N$, is denoted $P_N(\boldsymbol{x}^N, t)$ and satisfies the Smoluchowski equation

$$\frac{\partial P_N}{\partial t} + \sum_{\alpha=1}^{N} \nabla_\alpha \cdot \boldsymbol{j}_\alpha = 0, \tag{3.1}$$

with the flux of particle α

$$\boldsymbol{j}_\alpha = \boldsymbol{U}_\alpha P_N - \sum_{\beta=1}^{N} \boldsymbol{D}_{\alpha\beta} P_N \cdot \nabla_\beta (\ln P_N + V), \tag{3.2}$$

where $\boldsymbol{U}_\alpha$ is the hydrodynamic velocity, V is the particle potential energy made dimensionless with kT, and the Brownian diffusivity is given by $\boldsymbol{D}_{\alpha\beta} = kT\boldsymbol{M}_{\alpha\beta}$, where $\boldsymbol{M}_{\alpha\beta}$ is the hydrodynamic mobility of particle α to a force exerted on particle β. We take V to be an interparticle potential depending only upon the relative configuration of the particles. A potential dependent upon absolute position, and hence the influence of particle buoyancy for example, may be included without altering the basic formulation; the flux from such a potential is appropriately grouped with the hydrodynamic velocity because both generate a nonequilibrium microstructure.

Fixing the separation vector between a pair of particles, (3.1) is integrated with

respect to the center-of-mass coordinate of the pair and the positions of the remaining $N-2$ particles to arrive at the equation for $P_{1|1}(\boldsymbol{r})$, the probability distribution for finding a particle at $\boldsymbol{r}$ given that a particle lies at the origin:

$$\frac{\partial P_{1|1}}{\partial t} + \nabla_r\cdot(\langle \boldsymbol{U}\rangle_2 P_{1|1}) - \nabla_r\cdot\left[P_{1|1}\langle \boldsymbol{D}\cdot\nabla_r(\ln P_N + V)\rangle_2\right] \tag{3.3}$$
$$-\nabla_r P_{1|1}\cdot\int P_{3|2}(\boldsymbol{x}_3|\boldsymbol{r})\langle(\boldsymbol{D}_{13}-\boldsymbol{D}_{23})\cdot\nabla_3(\ln P_N + V)\rangle_3 d\boldsymbol{x}_3 = 0,$$

where $\nabla_r = \nabla_2 = -\nabla_1$, and $P_{3|2}$ is the probability of finding a third particle at $\boldsymbol{x}_3$ given the positions of a pair of particles at the origin and at $\boldsymbol{r}$. In (3.3), the relative velocity and relative diffusivity are given by

$$\boldsymbol{U} = \boldsymbol{U}_2 - \boldsymbol{U}_1, \quad \text{and} \qquad \boldsymbol{D} = \boldsymbol{D}_{11} - \boldsymbol{D}_{12} - \boldsymbol{D}_{21} + \boldsymbol{D}_{22},$$

respectively. The notation $\langle\ \rangle_2$ indicates a conditional average with two particles fixed.

To make analytical progress, we consider dilute particle volume fraction, $\phi = 4\pi n a^3/3 \ll 1$ with n the average number density of particles. Thus, with an $O(\phi)$ error the nonlinear averages and integral over the position of a third particle in (3.3) are neglected. Quantities are made dimensionless by scaling as

$$\boldsymbol{r} \sim a, \quad \boldsymbol{U} \sim \dot{\gamma} a, \quad \boldsymbol{D} \sim 2D, \quad \text{and} \quad t \sim \dot{\gamma}^{-1}, \tag{3.4}$$

where $\dot{\gamma}$ is a characteristic magnitude of $\dot{\boldsymbol{\Gamma}}$, and the scaling of the relative diffusivity is

with its far-field asymptotic value, $2D$, with D the diffusivity of an isolated particle. The Péclet number is defined by

$$Pe \equiv \frac{\dot{\gamma} a^2}{2D}. \tag{3.5}$$

In order to investigate the behavior under the action of interparticle forces, we consider a simple hard-sphere interparticle force at a variable distance $r = 2b$. This force may be incorporated through a no-flux condition rather than in the flux itself. Thus, the dimensionless equation for the pair-distribution function $g(\boldsymbol{r})$, defined by $P_{1|1}(\boldsymbol{r}) = n\, g(\boldsymbol{r})$, is

$$\frac{\partial g}{\partial t} + \nabla\cdot(\boldsymbol{U}g) - Pe^{-1}\nabla\cdot(\boldsymbol{D}\cdot\nabla g) = 0, \tag{3.6}$$

with boundary conditions of

$$\hat{\boldsymbol{r}}\cdot(\boldsymbol{j}_2 - \boldsymbol{j}_1) = 0 \quad \text{at} \quad r = 2b/a, \tag{3.7}$$

$$g \sim 1 \quad \text{as} \quad r \to \infty, \tag{3.8}$$

where $\hat{\boldsymbol{r}} = \boldsymbol{r}/r$ is the unit vector projecting from particle 1 to particle 2. To simplify notation in (3.6) and hereafter, we write ∇ for ∇_r and the angle brackets indicating averaging are omitted. Setting $b = a$ corresponds to no interparticle forces.

We are interested in the condition $Pe \gg 1$, for which the steady solution of (3.6) over most of the domain is well-approximated by the solution to

$$\nabla\cdot(\boldsymbol{U}g) = 0, \tag{3.9}$$

with the far-field condition of

$$g \sim 1 \quad \text{as} \quad r \to \infty. \tag{3.10}$$

Batchelor & Green (1972*b*) solved (3.9) and (3.10), demonstrating that when the trajectory of the second sphere relative to the reference sphere comes from infinitely far away, where it is assumed that all positions of the second sphere are equally likely, g is a function of scalar separation only. The solution under these assumptions, denoted $g(\boldsymbol{r}) = p(r)$, is

$$p(r) = \frac{1}{1-A} \exp\left[\int_r^\infty \frac{3(B-A)}{r(1-A)} dr\right]. \tag{3.11}$$

The scalar functions $A(r)$ and $B(r)$ specify the radial dependence of the disturbance of the relative velocity from $\dot{\boldsymbol{\Gamma}} \cdot \boldsymbol{r}$ due to the pair hydrodynamic interaction (Batchelor & Green 1972*a*),

$$\boldsymbol{U} - \dot{\boldsymbol{\Gamma}} \cdot \boldsymbol{r} = -\boldsymbol{r} \cdot \hat{\boldsymbol{E}} \cdot [A(r)\hat{\boldsymbol{r}}\hat{\boldsymbol{r}} + B(r)(\boldsymbol{I} - \hat{\boldsymbol{r}}\hat{\boldsymbol{r}})],$$

where $\hat{\boldsymbol{E}}$ is the dimensionless rate-of-strain tensor. In terms of the standard mobility and resistance functions (Kim & Karrila 1991), A and B are given by

$$A(r) = \frac{4}{r}(x_{11}^g - x_{12}^g) = \frac{4}{3r}(X_{11}^G - X_{12}^G)(x_{11}^a - x_{12}^a),$$

and

$$B(r) = \frac{8}{r}(y_{11}^g - y_{12}^g) = \frac{8}{r}\left[\frac{1}{3}(y_{11}^a - y_{12}^a)(Y_{11}^G - Y_{12}^G) - (y_{11}^b - y_{12}^b)(Y_{11}^H + Y_{12}^H)\right],$$

where $x_{\alpha\beta}^g$ and $y_{\alpha\beta}^g$ are the functions relating the stresslet on particle α to the force on particle β in the formulation of Kim & Mifflin (1985), $X_{\alpha\beta}^G$ and $Y_{\alpha\beta}^G$ are the resistance functions relating force to rate of strain, and so forth. Both $A(r)$ and $B(r)$ tend to zero with large r so that $p(r)$ tends to unity. Beyond its purely radial dependence, the main feature of note regarding p is that it diverges at particle contact, as $(r/a-2)^{-0.78}$ with a logarithmic correction (Batchelor & Green 1972b; see (3.28) below). While p is not forced to satisfy the condition of no flux through the inner boundary ($b = a$), it nevertheless does so because the radial velocity is linear in $r/a - 2$, and thus $\boldsymbol{U}p$ vanishes at contact.

The spherically symmetric solution for the pair-distribution function is only strictly valid when all particle trajectories come from infinity, as is the case in pure straining flow. In simple-shear flow, however, there are regions of closed streamlines, and there is no guarantee that $g(\boldsymbol{r}) = p(r)$ in the region of closed streamline. Thus, the familiar problem of simple-shear flow requires special treatment. With repulsive interparticle forces of sufficient range ($b/a - 1 \approx 10^{-4}$), however the closed streamline region is destroyed and the analysis we present below is valid.

3.3 Pair-distribution function: weak Brownian motion, no interparticle forces

We first investigate the behavior in the absence of interparticle forces ($b \equiv a$). The result that the pair-distribution function of spheres in pure straining is a function of scalar separation only, (3.11), is a strong statement. However, the divergence of p at contact is incompatible with any level of Brownian motion because this would result in a finite relative flux at contact. Brownian diffusion, no matter how weak, displaces particle pairs and leads to a finite value of g at contact. Weak diffusion is important only in a boundary layer over which a steep gradient in pair probability exists, a concept familiar in transport of heat or mass (Leal 1992). The spherically symmetric p is valid to $O(Pe^{-1})$ except at small separations. Asymmetry in the pair configuration of magnitude greater than $O(Pe^{-1})$ thus lies solely within the boundary layer, and we focus attention upon this region.

We restrict the investigation to pure straining flows, because for an isolated pair of spheres in simple shear there is a region of closed trajectories (Batchelor & Green 1972*a*), as noted above. The analysis for the region of closed trajectories is not straightforward, in part because the pair-distribution function in the limit $Pe^{-1} = 0$ is indeterminate (Batchelor & Green 1972*b*). Analysis is further restricted to the specific flow of planar extension because of the obvious symmetry properties of this flow. For concreteness, we take the dimensional rate of strain of the undisturbed flow

to have the components

$$E_{ij} = \frac{\dot{\gamma}}{2}(\delta_{i1}\delta_{j2} + \delta_{i2}\delta_{j1}),$$

corresponding to the rate of strain in the simple-shear flow $u_1 = \dot{\gamma}x_2$.

The relative diffusivity may be written as (Batchelor 1976)

$$\boldsymbol{D} = G(r)\hat{\boldsymbol{r}}\hat{\boldsymbol{r}} + H(r)(\boldsymbol{I} - \hat{\boldsymbol{r}}\hat{\boldsymbol{r}}), \tag{3.12}$$

where $G(r)$ and $H(r)$ are known functions given for equal-sized spheres by

$$G(r) = 2[x^a_{11}(r) - x^a_{12}(r)], \quad \text{and} \quad H(r) = 2[y^a_{11}(r) - y^a_{12}(r)],$$

with the hydrodynamic mobility functions $x^a_{\alpha\beta}$ and $y^a_{\alpha\beta}$ describing the velocity of sphere α due to a force on particle β along and transverse to the line of centers of the pair, respectively (Kim & Karrila 1991). Introducing (3.12) for $\boldsymbol{D}$ to (3.6), the steady pair equation in spherical coordinates is

$$\begin{aligned}\frac{1}{r^2}\frac{\partial}{\partial r}\left[r^2 G(r)\frac{\partial g}{\partial r}\right] + \frac{H}{r^2\sin\varphi}\left[\frac{\partial}{\partial\varphi}\sin\varphi\frac{\partial g}{\partial\varphi} + \frac{1}{\sin\varphi}\frac{\partial^2 g}{\partial\theta^2}\right] \\ -Pe\left[U_r\frac{\partial g}{\partial r} + \frac{U_\varphi}{r}\frac{\partial g}{\partial\varphi} + \frac{U_\theta}{r\sin\varphi}\frac{\partial g}{\partial\theta} + g\nabla\cdot\boldsymbol{U}\right] = 0,\end{aligned} \tag{3.13}$$

where φ is the azimuthal angle measured from the x_3 axis, and θ is the polar angle measured from the x_1 axis. The components of the relative velocity are

$$U_r = r\,[1 - A(r)]\,\gamma_r, \quad U_\varphi = r\,[1 - B(r)]\,\gamma_\varphi, \quad \text{and} \quad U_\theta = r\,[1 - B(r)]\,\gamma_\theta,$$

(3.14)

and the divergence of $\boldsymbol{U}$ is

$$\nabla\cdot\boldsymbol{U} = W(r)\gamma_r, \tag{3.15}$$

with

$$W = 3(B-A) - r\frac{dA}{dr}. \tag{3.16}$$

In equations (3.14) and (3.15), the angular dependences given by γ_r, γ_φ, and γ_θ are defined as

$$\gamma_r = \hat{\boldsymbol{r}}\cdot\hat{\boldsymbol{E}}\cdot\hat{\boldsymbol{r}} = \tfrac{1}{2}\sin^2\varphi\sin 2\theta, \quad \gamma_\varphi = \hat{\boldsymbol{\varphi}}\cdot\hat{\boldsymbol{E}}\cdot\hat{\boldsymbol{r}} = \tfrac{1}{4}\sin 2\varphi\sin 2\theta,$$
$$\text{and} \quad \gamma_\theta = \hat{\boldsymbol{\theta}}\cdot\hat{\boldsymbol{E}}\cdot\hat{\boldsymbol{r}} = \tfrac{1}{2}\sin\varphi\cos 2\theta, \tag{3.17}$$

where $\hat{\boldsymbol{\varphi}}$ and $\hat{\boldsymbol{\theta}}$ are the unit vectors in the φ and θ directions, respectively.

At large Péclet number, the influence of Brownian diffusion is comparable to that of advection only for particles near contact. Thus, for $r-2 \ll 1$, the radial coordinate is stretched according to

$$y = Pe(r-2),$$

with $y = O(1)$ resulting in a balance between advection and diffusion. The radial diffusivity and radial velocity are approximated by Taylor expansions to linear terms about their values at $r = 2$. At leading order in Pe the governing equation for g

within the boundary layer is

$$y\frac{\partial^2 g}{\partial y^2} + [1 + \gamma_r A'(2) y]\frac{\partial g}{\partial y} - \left[\frac{1}{2}(1 - B(2))\left(\gamma_\varphi \frac{\partial g}{\partial \varphi} + \frac{\gamma_\theta}{\sin\varphi}\frac{\partial g}{\partial \theta}\right)\right] + \frac{1}{2}W(2)\gamma_r g = 0, \tag{3.18}$$

where a prime denotes differentiation of a hydrodynamic function with respect to r, and we have used $A(2) = 1$, $G(2) = 0$, and $G'(2) = 2$. Values of other quantities appearing in (3.18) are

$$A'(2) = -4.08, \quad B(2) = 0.406, \quad \text{and} \quad W(2) = 6.38.$$

The boundary conditions on g are

$$y\frac{\partial g}{\partial y} = 0 \quad \text{at} \quad y = 0, \tag{3.19}$$

$$g \sim p \quad \text{as} \quad y \to \infty. \tag{3.20}$$

The system of equations (3.18-3.20) admits the similarity transformation

$$g(y, \theta, \varphi) = u(\eta) h(\theta, \varphi), \quad \text{where} \quad \eta = y/Y(\theta, \varphi). \tag{3.21}$$

The equation governing u is

$$\eta u'' + (1 + a_1\eta)u' - a_2 u = 0, \tag{3.22}$$

with the boundary conditions

$$\eta u' = 0 \quad \text{at} \quad \eta = 0, \tag{3.23}$$

$$uh \sim p(r) \quad \text{as} \quad \eta \to \infty. \tag{3.24}$$

The equations governing Y and h are

$$\gamma_\varphi \frac{\partial Y}{\partial \varphi} + \frac{\gamma_\theta}{\sin\varphi}\frac{\partial Y}{\partial \theta} + \gamma_r \frac{4A'(2)}{1-B(2)} Y = \frac{4a_1}{1-B(2)}, \tag{3.25}$$

and

$$\gamma_\varphi \frac{\partial h}{\partial \varphi} + \frac{\gamma_\theta}{\sin\varphi}\frac{\partial h}{\partial \theta} + \gamma_r \frac{2W(2)}{1-B(2)} h = \frac{4a_2 h}{Y(1-B(2))}. \tag{3.26}$$

Without loss of generality[†] we set $a_1 = 1$, while a_2 is determined by matching uh to p, a condition which requires the angular dependence of uh to vanish at large η. With $a_1 = 1$, the asymptotic form of (3.22) at large η shows that

$$u \sim \text{constant} \times \eta^{a_2}. \tag{3.27}$$

Near particle contact, Batchelor & Green (1972*b*) determined

$$p \sim 0.234(r-2)^{-0.78}[\log(r-2)^{-1}]^{-0.29} \quad \text{as} \quad r \to 2, \tag{3.28}$$

[†]A study of (3.25) shows that a_1 must be positive, but is otherwise arbitrary, in order that Y, and hence the boundary-layer thickness, be positive. At the stagnation points in the compressional quadrants, *e.g.*, $\varphi = \pi/2$ and $\theta = 3\pi/4$, both γ_φ and γ_θ vanish, while the radial velocity is negative, $\gamma_r < 0$. Thus, at this point $Y = a_1/A'(2)\gamma_r$, and because $A' < 0$ we must have $a_1 > 0$.

and up to a weak logarithmic error, matching of the radial dependence of u and p is accomplished by taking $a_2 = -0.78$. This value of a_2 also satisfies the requirement of vanishing angular dependence of the product uh, as is verified by inserting $h = Y^{a_2}$ to (3.26), which yields an equation identical to (3.25) when we choose

$$a_2 = \frac{1}{2}\frac{W(2)}{A'(2)} = -0.78. \tag{3.29}$$

Note that (3.29) shows the genesis of the divergence in p in terms of hydrodynamic functions.

A change of variables to $\zeta = -\eta$ yields the standard form known as Kummer's equation for $u(\zeta)$,

$$\zeta u'' + (1-\zeta)u' + a_2 u = 0,$$

which has the general solution (Abramowitz & Stegun 1972)

$$u(\zeta) = \lambda_1 M(-a_2, 1, \zeta) + \lambda_2 U(-a_2, 1, \zeta),$$

where M and U are confluent hypergeometric functions, and λ_1 and λ_2 are arbitrary constants. For second argument of unity, U is logarithmically singular at $\zeta = 0$ and is therefore discarded. The argument ζ is negative, and

$$M(-a_2, 1, \zeta) \sim K(-\zeta)^{a_2} = K\eta_2^a \quad \text{as} \quad \eta \to \infty,$$

with K a constant. This far-field form of M agrees with the asymptotic form of u

given by (3.27) which was shown to satisfy the boundary condition (3.24) of matching the radial dependence of p. The condition (3.23) at contact is satisfied because $M'(-a_2, 1, 0) = -a_2$ and thus the product $\zeta M'(-a_2, 1, \zeta)$ vanishes at $\zeta = 0$.

To complete the solution for g within the boundary layer, we determine the scaling function $Y(\varphi, \theta)$, which has the physical meaning of a variable boundary-layer thickness. It is sufficient, due to symmetry of the pair configuration and bulk flow, to determine Y in the restricted domain $0 < \varphi < \pi/2$ and $3\pi/4 < \theta < 5\pi/4$. The solution elsewhere may be obtained from the symmetry relations

$$Y(\pi - \varphi, \theta) = Y(\varphi, \theta), \quad Y(\varphi, \theta) = Y(\varphi, \theta + \pi), \quad \text{and} \quad Y(\varphi, \theta) = Y(\varphi, \frac{3\pi}{2} - \theta).$$

Two conditions on Y are required, which we choose to be finiteness of Y at $\theta = 3\pi/4$ and $\partial Y/\partial\varphi = 0$ at $\varphi = \pi/2$.

The solution to (3.25) is found by the method of characteristics (Carrier & Pearson 1988). Rewriting (3.25) as

$$\frac{\partial Y}{\partial \theta} + v(\varphi, \theta)\frac{\partial Y}{\partial \varphi} = w(Y, \varphi, \theta), \tag{3.30}$$

where

$$v(\varphi, \theta) = \frac{\gamma_\varphi}{\gamma_\theta}\sin\varphi, \quad \text{and} \quad w(Y, \varphi, \theta) = 4\frac{\sin\varphi}{\gamma_\theta}\frac{1 - \gamma_r Y}{1 - B(2)}, \tag{3.31}$$

we may interpret w as the complete derivative $w = dY/ds$ with $d\theta/ds = 1$ and

$d\varphi/ds = v$. For $\theta = 3\pi/4$, (3.25) reduces to

$$\frac{dY(\varphi, \frac{3\pi}{4})}{d\varphi} + (k_1 \tan\varphi)Y = -k_2 \sec\varphi \csc\varphi,$$

with solution

$$Y(\varphi, \frac{3\pi}{4}) = k_2(\cos\varphi)^{k_1} \int_{\varphi}^{\frac{\pi}{2}} (\cos x)^{-(1+k_1)} \csc x \, dx, \tag{3.32}$$

where

$$k_1 = \frac{2A'(2)}{1 - B(2)} \approx -13.7, \quad \text{and} \quad k_2 = \frac{4}{1 - B(2)} \approx 6.7.$$

Similarly, for $\varphi = \pi/2$, (3.25) reduces to

$$\frac{dY(\frac{\pi}{2}, \theta)}{d\theta} + (k_1 \tan 2\theta)Y = k_2 \csc 2\theta,$$

with solution

$$Y(\frac{\pi}{2}, \theta) = k_2(\cos 2\theta)^{k_1/2} \int_{3\pi/4}^{\theta} (\cos 2x)^{-(1+k_1/2)} dx. \tag{3.33}$$

To illustrate the asymmetry of the boundary-layer solution, we present plots of (3.32) and (3.33) in Figure 3.3 and Figure 3.4, respectively. Figure 3.3 illustrates that Y grows from a minimum at the stagnation point and diverges as $\varphi \to 0$ and $\varphi \to \pi$, where the relative velocity vanishes. The plot of (3.33) in Figure 3.4 illustrates that the boundary-layer thickness grows rapidly in the extensional quadrants ($\theta < \pi/2$ and $\theta > \pi$) and diverges along the extensional axes. In Figure 3.5, $Y(\varphi, \theta)$ is plotted along the curve $\theta = 3\pi/4$ and three characteristic curves (here only within the restricted domain). The curves indicate the three-dimensional structure of the boundary layer.

Note that while it diverges at $\varphi = 0$ and $\varphi = \pi$ and grows rapidly as we enter the extensional quadrant, Y is small over most of the compressional quadrant.

The functional form and Pe-dependence of the pair-distribution function in the boundary layer are given by

$$g = k(\varphi, \theta) \left[\frac{Pe}{Y(\varphi, \theta)} \right]^{0.78} M(0.78, 1, -y/Y(\varphi, \theta)). \tag{3.34}$$

The weak logarithmic dependence of the outer solution p is neglected in writing (3.34), but may be included in the angularly-dependent coefficient $k(\varphi, \theta)$ if matching is performed. Matching to p occurs at different r for varying φ and θ, and thus the magnitude of k will vary with angular position so that the logarithm may be absorbed.

The physical implications of this analysis are readily understood. Competition between the oppositely-directed advective and diffusive fluxes causes an accumulation of pair probability adjacent to $r = 2$ in the compressional quadrants, while in the extensional quadrants, both advection and diffusion displace pairs from contact. Because there is no competition in the extensional quadrants, the boundary layer grows and eventually diverges along the extensional axes. Though detailed matching to p is not performed, (3.34) demonstrates that weak Brownian diffusion removes the singularity at contact to yield an asymmetric $g(\boldsymbol{r})$ of large $O(Pe^{0.78})$ but finite magnitude. The normal stress differences for hydrodynamically-interacting hard spheres scale as the boundary-layer volume $O(a^3\, Pe^{-1})$ times $g(2)$, and thus nonNewtonian effects scale as $Pe^{-0.22}$ as $Pe \to \infty$. This slow decay suggests measurable normal stress differences may be expected even at large Pe. Ultimately, however, as $Pe \to \infty$ the structure

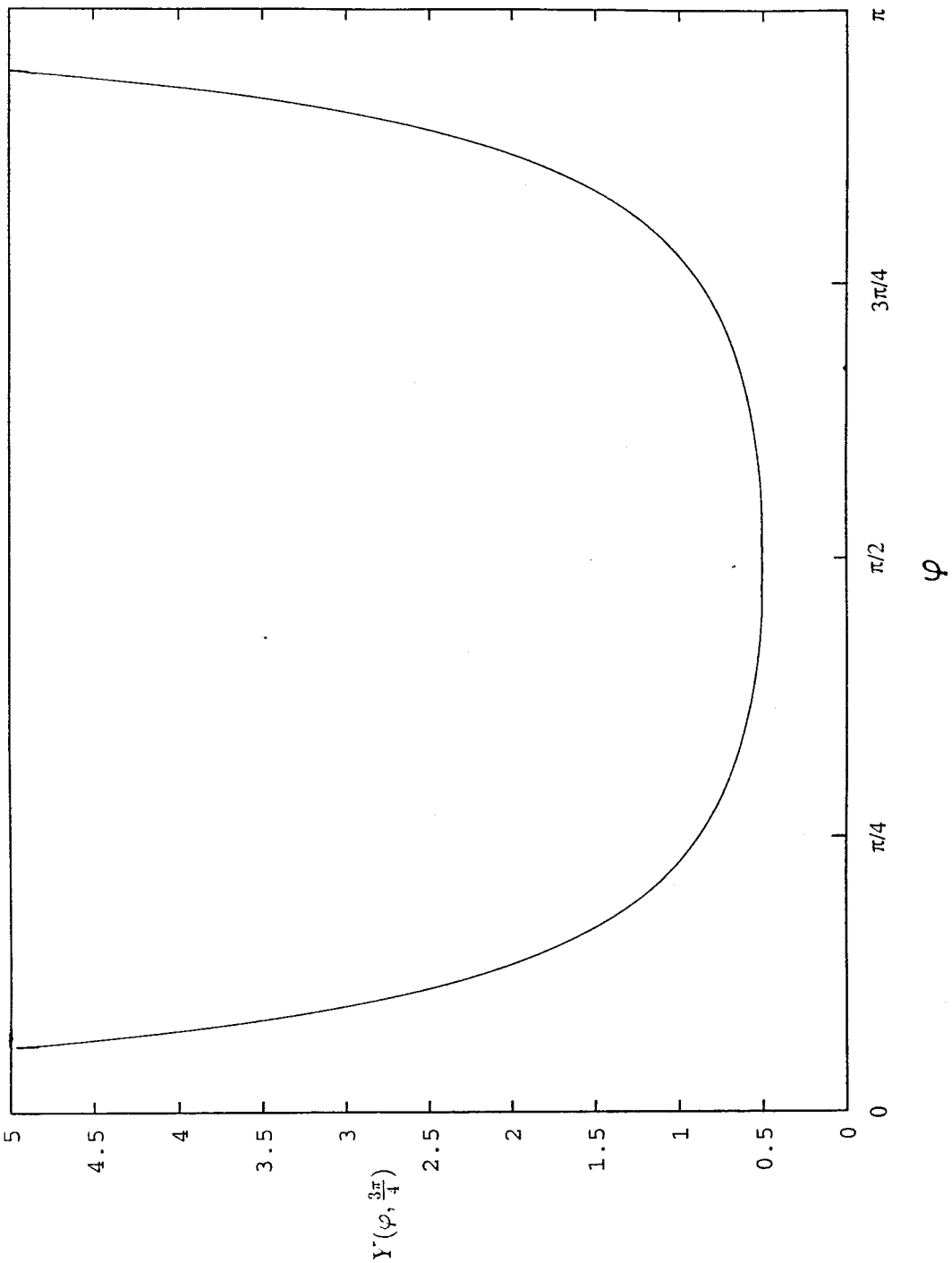

Figure 3.3: The boundary-layer scaling function Y plotted as a function of φ for $\theta = 3\pi/4$. Note that Y diverges as $\varphi \to 0$ and $\varphi \to \pi$.

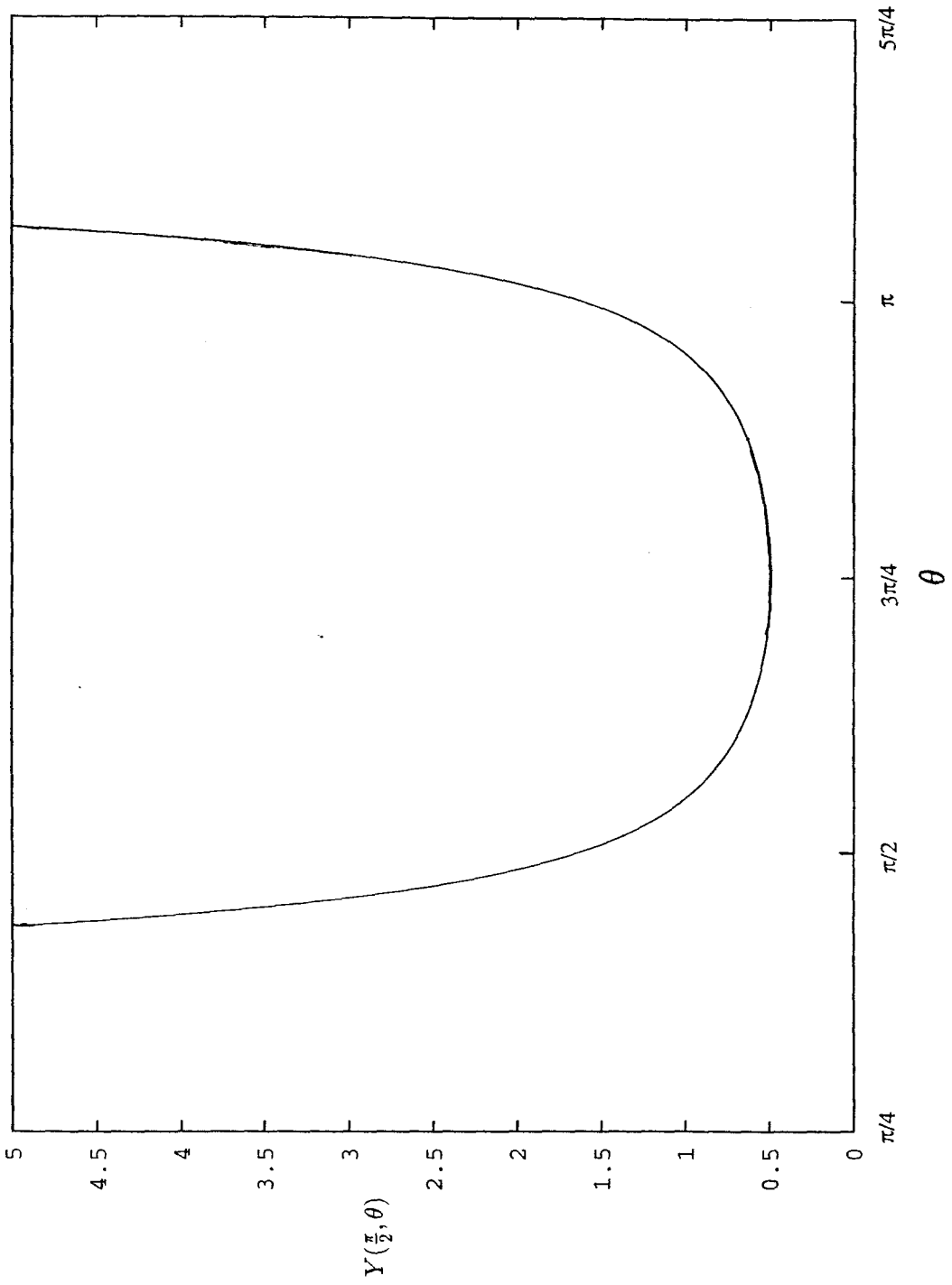

Figure 3.4: The boundary-layer scaling function Y plotted as a function of θ for $\varphi = \pi/2$, illustrating that Y grows rapidly in the extensional quadrants and diverges at $\theta = 5\pi/4$ and $\theta = \pi/4$, the θ-coordinates of the extensional axes.

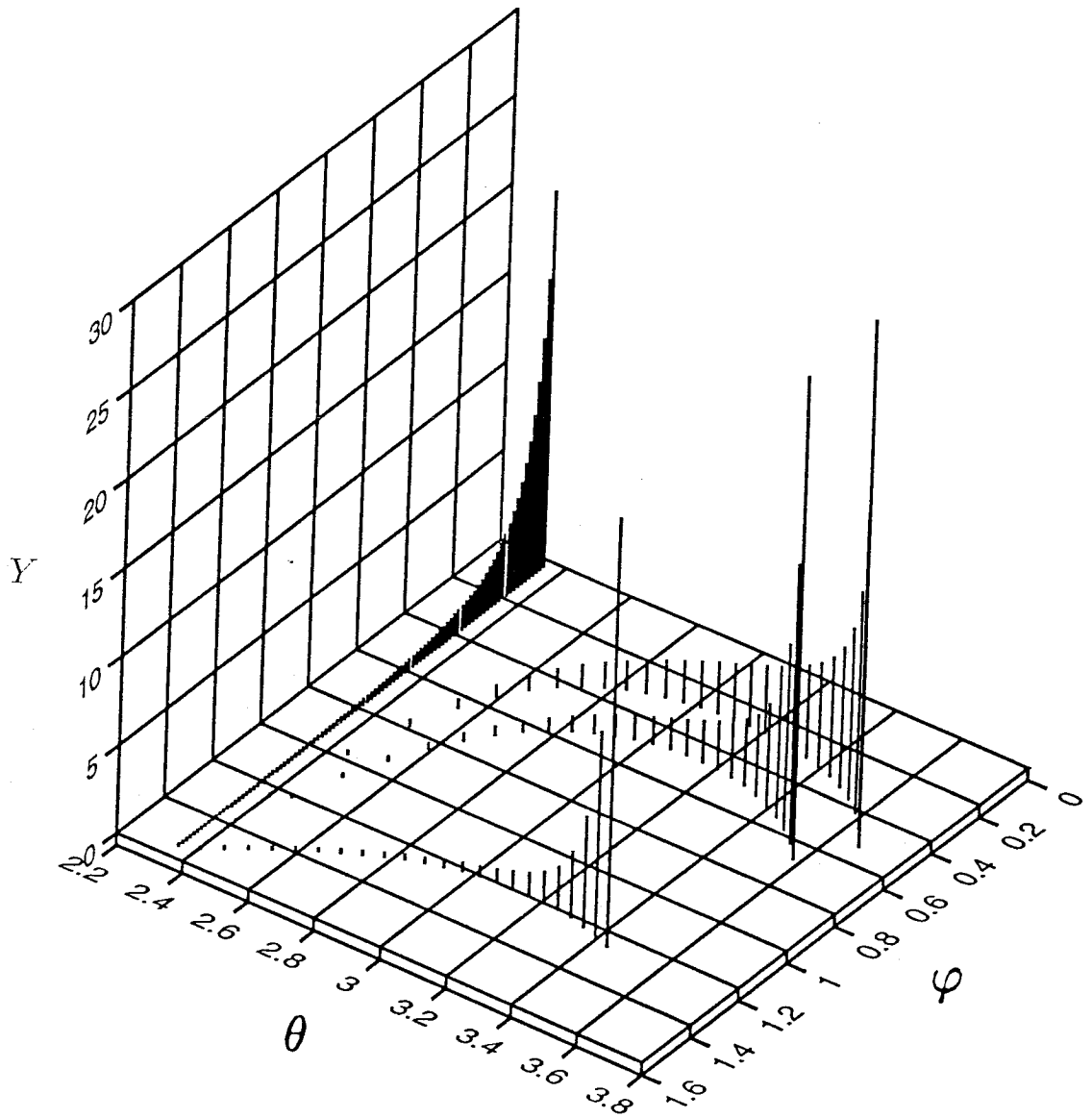

Figure 3.5: The boundary-layer scaling function Y within the restricted domain $0 < \varphi < \pi/2$ and $3\pi/4 < \theta < 5\pi/4$. The function is plotted along the boundary curve specified by $\theta = 3\pi/4$ and along three characteristic curves.

becomes symmetric and the rheology Newtonian. Although we have only carried out a detailed analysis for planar extensional flow, we expect the same conclusion to hold for general linear flows.

3.4 Pair-distribution function: weak Brownian motion and interparticle forces

The vanishing of nonNewtonian effects in the hydrodynamic limit was expected based upon general symmetry considerations and prior work. In this section, we investigate the large-Péclet-number problem for $g(\boldsymbol{r})$ in a suspension of spheres that interact through a hard-sphere force which maintains a minimum separation of $2b > 2a$. Unlike the problem for g of weakly Brownian particles interacting only through hydrodynamics, there is no similarity solution of the boundary-layer equation $b > a$. To obtain a tractable equation which contains the essential physical elements giving rise to a boundary-layer structure, we consider only the radial terms in the pair equation. Our justification is that it is the competition between radial advection and radial diffusion that sets the magnitude of g near contact. Results of this analysis therefore have the correct qualitative features of magnitude and asymmetry of the pair-distribution function, but may not give accurate numerical values. We first study the problem neglecting hydrodynamics to simplify and clarify the analysis, without altering most of the basic conclusions, and then include pair hydrodynamic interactions. Calculation of nonNewtonian particle stress contributions are presented in

each case.

3.4.1 No hydrodynamics

In the absence of hydrodynamic interactions, $\boldsymbol{U} = \dot{\boldsymbol{\Gamma}}\cdot\boldsymbol{r}$ and the pair-distribution function is governed by

$$\nabla^2 g - Pe\dot{\boldsymbol{\Gamma}}\cdot\boldsymbol{r}\cdot\nabla g = 0, \tag{3.35}$$

with the boundary conditions

$$\frac{\partial g}{\partial r} = 2Pe\gamma_r g \quad \text{at} \quad r = 2, \tag{3.36}$$

$$g \sim 1 \quad \text{as} \quad r \to \infty. \tag{3.37}$$

Except near contact, (3.35) reduces to $\dot{\boldsymbol{\Gamma}}\cdot\boldsymbol{r}\cdot\nabla g = 0$, *i.e.*, on a streamline g is a constant, which the far-field condition dictates to be unity. Near contact, we stretch r according to

$$y = Pe(r-2).$$

The equation for g in the stretched coordinates is

$$\frac{\partial^2 g}{\partial y^2} - 2\gamma_r\left[1 - \frac{1}{2\gamma_r}Pe^{-1} + \frac{1}{2}Pe^{-1}y\right]\frac{\partial g}{\partial y} = Pe^{-1}\left[\gamma_\varphi\frac{\partial g}{\partial \varphi} + \frac{\gamma_\theta}{\sin\varphi}\frac{\partial g}{\partial \theta}\right] + O(Pe^{-2}), \tag{3.38}$$

with the boundary conditions

$$\frac{\partial g}{\partial y} = 2\gamma_r g \quad \text{at} \quad y = 0, \tag{3.39}$$

$$g \sim 1 \quad \text{as} \quad y \to \infty. \tag{3.40}$$

The leading-order balance,

$$\frac{\partial^2 g}{\partial y^2} - 2\gamma_r \frac{\partial g}{\partial y} = 0,$$

has the general solution

$$g(y) = 1 + \text{ constant } \times \int_y^\infty e^{\gamma_r z} dz$$

which asymptotes to unity as $y \to \infty$, but fails to satisfy the boundary condition at $y = 0$, and thus terms of $O(Pe^{-1})$ must be maintained. This failure may be explained by noting that the leading-order governing equation is the radial derivative of the boundary condition at $y = 0$, so that either the governing equation or the boundary condition is redundant. Radial advection and diffusion compete to generate the large gradients in g characteristic of the boundary layer, which prompts us to maintain only those terms of $O(Pe^{-1})$ which appear in the divergence of the radial flux. That is, we solve the equation obtained by discarding the right-hand side of (3.38). The solution,

$$g(y) = \frac{1 + 2\gamma_r \int_0^y e^{s(z)} dz}{1 + 2\gamma_r \int_0^\infty e^{s(z)} dz}, \tag{3.41}$$

where $s(z)$ is given by

$$s(z) = 2\gamma_r \left[\left(1 - \frac{1}{2\gamma_r} Pe^{-1} \right) z + \frac{1}{4} Pe^{-1} z^2 \right], \tag{3.42}$$

is valid only for $\gamma_r < 0$. In the extensional quadrants, where $\gamma_r > 0$, g remains $O(1)$; there is no boundary layer. Note also that since there are no regions of closed streamlines, the analysis applies to any linear flow. Rewriting g as

$$g(y) = g(0)\left[1 + 2\gamma_r \int_0^y e^{s(z)} dz\right], \tag{3.43}$$

with

$$g(0) = -\frac{4}{3} Pe\gamma_r + O(1) \quad \text{as} \quad Pe \to \infty, \tag{3.44}$$

shows that there is an $O(Pe)$ excess of particles in the compressional quadrants.

The solution (3.41) for g is readily extended to validity for all b. (We have assumed now that $b = a$, but there were no hydrodynamic interactions.) Scaling lengths by b rather than a, and replacing Pe by

$$\bar{Pe} \equiv \frac{\dot{\gamma} b^2}{2D} = \frac{3\pi\eta\dot{\gamma} a b^2}{kT}, \tag{3.45}$$

the problem and solution for g for arbitrary b are identical to those given above. We have noted in the second equality of (3.45) that $D = kT/6\pi\eta a$ and thus there is residual dependence upon the hydrodynamic radius.

Macroscopic stress without hydrodynamics

The particle stress is given by (Brady 1993)

$$\langle \boldsymbol{\Sigma}_p \rangle = -nkT\boldsymbol{I} + n(\langle \boldsymbol{S}^B \rangle + \langle \boldsymbol{S}^P \rangle + \langle \boldsymbol{S}^H \rangle), \tag{3.46}$$

where $nkT\boldsymbol{I}$ is the familiar kinetic contribution which yields the dilute osmotic pressure, and

$$\langle \boldsymbol{S}^B \rangle = -kT\langle \nabla\cdot(\boldsymbol{R}_{SU}\cdot\boldsymbol{R}_{FU}^{-1})\rangle, \tag{3.47a}$$

$$\langle \boldsymbol{S}^P \rangle = -\langle(\boldsymbol{x}\boldsymbol{I} + \boldsymbol{R}_{SU}\cdot\boldsymbol{R}_{FU}^{-1})\cdot\boldsymbol{F}^P\rangle, \tag{3.47b}$$

$$\text{and} \quad \langle \boldsymbol{S}^H \rangle = -\langle \boldsymbol{R}_{SU}\cdot\boldsymbol{R}_{FU}^{-1}\cdot\boldsymbol{R}_{FE} - \boldsymbol{R}_{SE}\rangle:\langle \boldsymbol{E}\rangle, \tag{3.47c}$$

are, respectively, the expressions for the Brownian, interparticle force, and hydrodynamic stresslets. The particle stress may be recast as

$$\langle \boldsymbol{\Sigma}_P\rangle = -nkT\boldsymbol{I} - nkTa\oint_{r=2a}\hat{\boldsymbol{r}}\hat{\boldsymbol{r}}P_{1|1}(\boldsymbol{r})dS - n\langle \boldsymbol{x}\boldsymbol{F}^P\rangle \tag{3.48}$$
$$-n\langle \boldsymbol{R}_{SU}\cdot\boldsymbol{R}_{FU}^{-1}\cdot\boldsymbol{R}_{FE} - \boldsymbol{R}_{SE}\rangle:\langle \boldsymbol{E}\rangle + nkT\langle \boldsymbol{R}_{SU}\cdot\boldsymbol{R}_{FU}^{-1}\cdot\nabla[V + \ln P_N]\rangle,$$

by decomposing $\langle \boldsymbol{S}^B\rangle$ into the contact integral and the final term involving $\nabla \ln P_N$. In (3.48), the subscripts on the resistance tensors $\boldsymbol{R}_{FU}$ and $\boldsymbol{R}_{SE}$ denote the relation of force to velocity and stress to rate of strain, respectively, and the others are clear from these. Recall that V has been made dimensionless with kT. The influence of a hard-sphere force for arbitrary $b \geq a$ is given by a 'contact' integral identical in form to that in (3.48) with b replacing a. For $b > a$ or for $b = a$ without hydrodynamics, this integral represents the nonhydrodynamic hard-sphere stress, rather than a hydrodynamic Brownian stress.

In the absence of hydrodynamics, $\langle \boldsymbol{\Sigma}_P \rangle$ reduces to

$$\langle \boldsymbol{\Sigma}_P \rangle = -nkT \left[1 + \phi_b \frac{3}{\pi} \int \hat{\boldsymbol{r}}\hat{\boldsymbol{r}} g(2b\hat{\boldsymbol{r}}) d\Omega \right] + 5\eta\phi \langle \boldsymbol{E} \rangle, \tag{3.49}$$

where $5\eta\phi\langle \boldsymbol{E} \rangle = 2\eta_E \langle \boldsymbol{E} \rangle$ is the shear stress due to the Einstein viscosity correction, $\eta_E = \frac{5}{2}\eta\phi$. The particle pressure is defined mechanically as

$$\Pi = -\frac{1}{3}\boldsymbol{I}:\langle \boldsymbol{\Sigma}_P \rangle, \tag{3.50}$$

so that in equilibrium (3.49) yields the familiar hard-sphere fluid equation of state (see, *e.g.*, Hansen & McDonald 1986),

$$\frac{\Pi}{nkT} = 1 + 4\phi_b g(2b).$$

We shall denote the stress due to particle interactions $\boldsymbol{\Sigma}'$. Specifically, $\boldsymbol{\Sigma}'$ is the particle stress less $(-nkT)\boldsymbol{I}$ and the Einstein viscosity contribution. Inserting the contact value of $g(\boldsymbol{r})$ given by $g(0)$ of (3.44) to (3.49) yields

$$\langle \boldsymbol{\Sigma}' \rangle = \eta\dot{\gamma}\phi_b^2 \frac{a}{b}\frac{9}{\pi} \int_{\gamma_r<0} \hat{\boldsymbol{r}}\hat{\boldsymbol{r}}\gamma_r d\Omega + O\left(\eta\dot{\gamma}\phi_b^2 \frac{a}{b}\bar{P}e^{-1}\right), \tag{3.51}$$

for a dilute suspension.

With our choice of coordinates, the first normal stress difference, $N_1 = \langle \Sigma'_{11} - \Sigma'_{22} \rangle$, vanishes because of symmetry about the compressional axis. This conclusion is true for general linear flow. For planar extensional flow, the second normal stress difference

is nonzero:

$$N_2 = \langle \Sigma'_{22} - \Sigma'_{33} \rangle = -\eta\dot{\gamma}\phi_b^2 \frac{a}{b}\frac{12}{5\pi} + O\left(\eta\dot{\gamma}\phi_b^2 \frac{a}{b}\bar{P}e^{-1}\right). \tag{3.52}$$

The pressure due to particle interactions is given by

$$\Pi' = \eta\dot{\gamma}\phi_b^2 \frac{a}{b}\frac{4}{\pi} + O\left(\eta\dot{\gamma}\phi_b^2 \bar{P}e^{-1}\frac{a}{b}\right). \tag{3.53}$$

In simple-shear flow, $u_1 = \dot{\gamma}x_2$, the first normal stress difference is again zero due to symmetry about the compressional axis. The second normal stress difference is

$$N_2 = -\eta\dot{\gamma}\phi_b^2 \frac{a}{b}\frac{9}{5\pi},$$

The particle pressure

$$\Pi' = \eta\dot{\gamma}\phi_b^2 \frac{a}{b}\frac{3}{\pi},$$

and the shear viscosity

$$\eta_r = 1 + \frac{5}{2}\phi + \phi_b^2 \frac{a}{b}\frac{9}{20}.$$

In obtaining (3.41) we have neglected the $O(Pe^{-1})$ terms on the right-hand side of (3.38) while retaining terms of the same size in the radial balance on the left-hand side. This is generally not valid, and the RHS does affect the angular structure of $g(2)$. The magnitude of $g(2)$ of $O(Pe)$ is not affected, however. Recent work solving (3.35) for all Pe shows the boundary-layer structure exhibited by (3.41) (Brady & Vicic 1995*b*). The stress predictions from the radial balance for simple-shear flow are within 10% for all quantities except the first normal stress differences. The precise symmetry

about the compressional axis is broken and finite first normal stress differences occur as $Pe \to \infty$.

3.4.2 Pair hydrodynamics

The relatively simple analysis without hydrodynamics showed that there is a large $O(Pe)$ excess of particle pairs along the compressional axes, leading to nonNewtonian rheology in the limit $Pe \to \infty$. We now include hydrodynamic interactions and show that a similar microstructure is found for all nonzero $b-a$. The more complete solution presented here shows the dependence of g—and consequently of the rheology—upon b which results from evaluation of the hydrodynamic functions at $r = 2b$ for use in the boundary-layer equation. Thus, we are able to determine the manner in which the rheology approaches Newtonian behavior as $b/a - 1 \to 0$. The effective radius $b > a$ introduces a second lengthscale in the problem, and for hydrodynamically-interacting particles both b and a are relevant. We continue to scale lengths with a, applying this scaling also to b and denoting the dimensionless radius $\hat{b} \equiv b/a$.

When hydrodynamics are included, the outer solution for dilute ϕ is $p(r)$, and it is convenient to consider $f(\boldsymbol{r}) \equiv g(\boldsymbol{r}) - p(r)$, because f vanishes to $O(Pe^{-1})$ outside the boundary layer[‡]. As in §3.3, we stretch the radial coordinate near contact as

$$y = Pe(r - 2\hat{b}).$$

[‡]It is of no benefit to consider the deviation $f = g - p$ for hydrodynamically-interacting particles without interparticle forces as addressed in §3.3, because f would diverge at $r = 2a$ in that problem.

Expanding the hydrodynamic functions to linear terms about their values at $r = 2\hat{b}$, we find the equation for f in the stretched coordinates,

$$(1+\alpha_1 Pe^{-1}y)\frac{\partial^2 f}{\partial y^2} - \alpha_2\gamma_r(1-\frac{\alpha_3}{\gamma_r}Pe^{-1}+\alpha_4 Pe^{-1}y)\frac{\partial f}{\partial y} - \alpha_5 Pe^{-1}\gamma_r f =$$

$$Pe^{-1}\frac{(1-\bar{B})}{2\bar{G}}\left[\gamma_\varphi\frac{\partial f}{\partial\varphi}+\frac{\gamma_\theta}{\sin\varphi}\frac{\partial f}{\partial\theta}\right]+O(Pe^{-2}), \qquad (3.54)$$

with the boundary conditions

$$\left[\frac{\partial f}{\partial y}-\alpha_2\gamma_r f\right]_{y=0} = \left[-Pe^{-1}p'(r)+\alpha_2\gamma_r p(r)\right]_{r=2\hat{b}} \equiv R(\hat{b},Pe) \qquad (3.55)$$

$$f \sim 0 \quad \text{as} \quad y\to\infty. \qquad (3.56)$$

In (3.54) and (3.55), α_1-α_5 are given by

$$\alpha_1 = \frac{\bar{G}'}{\bar{G}}, \quad \alpha_2 = \frac{2\hat{b}(1-\bar{A})}{\bar{G}}, \quad \alpha_3 = \frac{\bar{G}'+\bar{G}/\hat{b}}{2\hat{b}(1-\bar{A})}$$

$$\alpha_4 = \frac{1-\bar{A}-2\hat{b}\bar{A}'}{2\hat{b}(1-\bar{A})}, \quad \text{and} \quad \alpha_5 = \frac{\bar{W}}{\bar{G}}, \qquad (3.57)$$

where overbars are used to denote the hydrodynamic functions evaluated at $r = 2\hat{b}$, *e.g.*, $\bar{G} = G(2\hat{b})$. Note that the α_i are positive and independent of both Pe and $\dot{\gamma}$. We divide (3.54) by $(1+\alpha_1 Pe^{-1}y)$, discarding terms of $O(Pe^{-2})$ and the entire

right-hand side to yield the radial balance

$$\frac{\partial^2 f}{\partial y^2} - \alpha_2\gamma_r\left[1 - \frac{\alpha_3}{\gamma_r}Pe^{-1} + (\alpha_4 - \alpha_1)Pe^{-1}y\right]\frac{\partial f}{\partial y} - \alpha_5\gamma_r Pe^{-1}f = 0. \tag{3.58}$$

The boundary conditions are unchanged, but it is worth noting that

$$R(\hat{b}, Pe) \sim \alpha_2\gamma_r p(2\hat{b}) \quad \text{as} \quad Pe \to \infty,$$

indicating that the flux associated with p tends to become purely convective at large Pe.

As in the problem without hydrodynamics, a solution satisfying the leading-order balance, *i.e.*,

$$\frac{\partial^2 f}{\partial y^2} - \alpha_2\gamma_r\frac{\partial f}{\partial y} = 0,$$

and the boundary conditions does not exist, making it necessary to maintain $O(Pe^{-1})$ terms in (3.58) to obtain a solution. The equation obtained by discarding the term $-\alpha_5\gamma_r Pe^{-1}f$, associated with the divergence of the relative velocity,

$$\frac{\partial^2 f}{\partial y^2} - \alpha_2\gamma_r\left[1 - \frac{\alpha_3}{\gamma_r}Pe^{-1} + (\alpha_4 - \alpha_1)Pe^{-1}y\right]\frac{\partial f}{\partial y} = 0, \tag{3.59}$$

has the solution

$$f = f(0)\frac{\int_y^\infty e^{S(z)}dz}{\int_0^\infty e^{S(z)}dz}, \quad \gamma_r < 0, \tag{3.60}$$

where

$$S(z) = \alpha_2\gamma_r\left[\left(1 - \frac{\alpha_3}{\gamma_r}Pe^{-1}\right)z + \frac{(\alpha_4 - \alpha_1)}{2}Pe^{-1}z^2\right], \tag{3.61}$$

and

$$f(0) = -R(\hat{b}, Pe)\frac{\int_0^\infty e^{S(z)}dz}{1 + \alpha_2\gamma_r\int_0^\infty e^{S(z)}dz} \tag{3.62}$$

$$\sim -\alpha_2\gamma_r Pe\; p(2\hat{b})\left(\frac{1}{\alpha_4 + \alpha_2\alpha_3 - \alpha_1}\right), \quad as \quad Pe \to \infty. \tag{3.63}$$

There is no solution to (3.59) for $\gamma_r > 0$. The integral in the numerator of (3.60) is easily seen to be $O(1)$ with respect to Pe, and thus the deviation of the pair-distribution function from the spherically symmetric p is $O(Pe)$ in the compressional quadrants.

The $O(Pe^{-1})$ coefficients of $\partial f/\partial y$ in (3.54) were retained while discarding other terms of $O(Pe^{-1})$. We now consider (3.58) which includes also the term representing the velocity divergence, *i.e.*, $-\alpha_5 f$, with angular derivatives again neglected. Analysis presented in the Appendix shows that the solution to (3.58) is given by

$$f(y) = f(0)e^{-\eta_1 y}[1 + \alpha_1 Pe^{-1}y]^{\eta_2}, \quad \gamma_r < 0, \tag{3.64}$$

with $f(0)$ given in this case by

$$f(0) = -PeR(\hat{b}, Pe)\left[\frac{\alpha_1\alpha_5}{\alpha_2\alpha_4} + \alpha_2\alpha_3\right]^{-1} \tag{3.65}$$

$$\sim -\alpha_2\gamma_r Pe\; p(2\hat{b})\left[\frac{\alpha_1\alpha_5}{\alpha_2\alpha_4} + \alpha_2\alpha_3\right]^{-1} \quad \text{as} \quad Pe \to \infty, \tag{3.66}$$

and η_1 and η_2 are given by

$$\eta_1 = -\alpha_2\gamma_r + \alpha_2\alpha_3 Pe^{-1}, \quad \text{and} \qquad \eta_2 = -Pe^{-1}\frac{\alpha_1\alpha_5}{\alpha_2\alpha_4}.$$

The requirement on (3.64) of $\gamma_r < 0$ shows that inclusion of the $O(Pe^{-1})$ velocity divergence term does not alter the primary conclusion that under the combined influence of a hard-sphere force and Brownian motion there is an $O(Pe)$ excess of particles along the compressional axes. Presumably, the small angular derivative terms also have only a quantitative influence upon the solution for f. As discussed in the Appendix, (3.64) is obtained by a change of variable which is invalid without hydrodynamic interactions. Thus, it is not appropriate to simply set the influence of hydrodynamics to zero in this solution, while (3.60) does tend to the no-hydrodynamics solution at $\hat{b} \gg 1$.

That a solution for the pair-distribution function at leading order in Pe may be obtained only in the compressional quadrants agrees with the expectation that competition between radial advection and diffusion occurs in the compressional but not in the extensional quadrants. The important distinguishing feature from the case of $b \equiv a$ is that the radial velocity of the pair does not vanish at the minimum separation. The positive radial velocity may be said heuristically to sweep the extensional quadrants of second particles, and thus a large accumulation of pair probability does not occur there, and Brownian diffusion remains only perturbative.

Macroscopic stress with hydrodynamics

The particle stress is again evaluated using (3.46) - (3.48). With hydrodynamics included, there are several contributions of $O(\eta\dot{\gamma})$ as $Pe \to \infty$. First, we note that since $\nabla\cdot(\boldsymbol{R}_{SU}\cdot\boldsymbol{R}_{FU}^{-1})$ is $O(1)$ everywhere and the product of $g(\boldsymbol{r})$ and the boundary-layer volume is also $O(1)$, the Brownian stress (3.47a) remains $O(kT)$, in agreement with the simulations of Phung (1993). Both the hydrodynamic and interparticle force stress contributions are $O(\eta\dot{\gamma})$. For the hydrodynamic stress this is obvious, while for the interparticle-force contribution we note that the hard-sphere force is

$$\boldsymbol{F}^p = \frac{1}{2}kT\hat{\boldsymbol{r}}\delta(r-2b),$$

with the kT amplitude necessary to give the correct equilibrium structure. Hence,

$$n\langle\boldsymbol{S}^P\rangle = -n^2kT\oint_{r=2b}(b\,\hat{\boldsymbol{r}}\hat{\boldsymbol{r}} + \boldsymbol{R}_{SU}\cdot\boldsymbol{R}_{FU}^{-1}\cdot\hat{\boldsymbol{r}})g(\boldsymbol{r})dS. \tag{3.67}$$

Since $g(2b)$ is $O(Pe)$ this "contact" integral will give an $O(\eta\dot{\gamma})$ contribution to the stress. Making use of the known hydrodynamic functions, (3.67) can be rewritten as

$$n\langle\boldsymbol{S}^P\rangle = -n^2kT\,b(1-\overline{A})\oint_{r=2b}\hat{\boldsymbol{r}}\hat{\boldsymbol{r}}g(\boldsymbol{r})dS. \tag{3.68}$$

Using (3.66) for $f(0)$ the interparticle force contribution to the stress becomes

$$n\langle\boldsymbol{S}^P\rangle = \eta\dot{\gamma}\phi^2\left(\frac{b}{a}\right)^3(1-\overline{A})\alpha^*\bar{p}\,\frac{27}{4\pi}\int_{\gamma_r<0}\hat{\boldsymbol{r}}\hat{\boldsymbol{r}}\gamma_r d\Omega, \tag{3.69}$$

when $\bar{p} = p(2b/a)$ and

$$\alpha^*(b/a) = \alpha_2 \left[\frac{\alpha_1 \alpha_5}{\alpha_2 \alpha_4} + \alpha_2 \alpha_3 \right]^{-1}. \tag{3.70}$$

Note that the dependence on flow type is the same as in absence of hydrodynamics, with only the coefficient modified by hydrodynamics.

In the limit of large b/a, the interparticle force stress reduces to (3.51), the result found in the absence of hydrodynamics, but it is not appropriate to simply set hydrodynamic effects identically zero in f given by (3.64) as we noted above. We have applied the solution for f including the influence of $\nabla \cdot \boldsymbol{U}$ because this solution should be more accurate for $b/a - 1 \ll 1$, and we wished to investigate the impact of short-ranged symmetry-breaking effects. If one wishes to see the residual influence of hydrodynamics when $b \gg a$, the simpler solution (3.60) for f should be used, in which replacement of the coefficients with their no-hydrodynamics values is valid. For b/a near unity we can estimate the behavior by noting that

$$(1 - \overline{A}) \sim (b/a - 1),\ \alpha^* \sim (b/a - 1) \quad \text{and} \quad \bar{p} \sim (b/a - 1)^{-0.78} \quad \text{as} \quad b/a \to 1, \tag{3.71}$$

so that

$$n\langle \boldsymbol{S}^p \rangle \sim \eta \dot{\gamma} \phi^2 (b/a - 1)^{1.22} \int_{\gamma_r} \hat{\boldsymbol{r}} \hat{\boldsymbol{r}} \gamma_r d\Omega \quad \text{as} \quad b/a \to 1. \tag{3.72}$$

Unlike $\langle \boldsymbol{\Sigma}^P \rangle$, where the integration is restricted to the boundary layer on the compressive axes, the hydrodynamic stresslet, $\langle \boldsymbol{\Sigma}^H \rangle = n\langle \boldsymbol{S}^H \rangle$ the hydrodynamic stress is always $O(\eta\dot{\gamma})$ and thus contributions arise from the whole domain $r > 2b$. Thus,

we cannot make general statements about the form of the hydrodynamic stress with regard to the asymmetry caused by the boundary layer because there is presumably an $O(1)$ angular variation on the extensional axes that we have not determined.

Nevertheless, we can illustrate the consequences of the interparticle forces in creating an asymmetric structure by computing the second normal stress difference for planar extensional flow from the compressional quadrant only. Batchelor & Green (1972*b*) showed that for $b = a$, the hydrodynamic stress associated with the spherically symmetric $p(r)$ is Newtonian; despite the divergence of p at $r = 2a$, the viscosity is finite and the symmetry of the microstructure leads to zero normal stress differences. Scaling the stresslet as

$$\boldsymbol{S}^H = \frac{20}{3}\pi\eta\dot{\gamma}a^3\hat{\boldsymbol{S}}^H,$$

the second normal stress difference for the hydrodynamic stresslet, N_2^H, is given by

$$N_2^H = \langle\Sigma_{22}^H - \Sigma_{33}^H\rangle = \eta\dot{\gamma}\phi^2\frac{15}{4\pi}I_2(b/a, Pe). \tag{3.73}$$

The dimensionless integral I_2, given by

$$I_2(b/a, Pe) = \int(\hat{S}_{22}^H - \hat{S}_{33}^H)f(\boldsymbol{\rho})d\boldsymbol{\rho}$$

with $\boldsymbol{\rho} = \boldsymbol{r}/a$ used to emphasize the nondimensionality, was evaluated by Stokesian Dynamics. In Figure 3.6, $I_2(1.025, Pe)$ is plotted, showing that I_2 becomes indepen-

dent of Pe as $Pe \to \infty$, with an asymptotic value of of the stress difference reached when $Pe = 10^4$. Variation of N_2^H with b/a is demonstrated in Figure 3.7 by plotting $I_2(b/a, 10^6)$ against $b/a - 1$. For $b/a - 1 \to 0$, N_2^H vanishes as $(b/a - 1)^{0.22}$ because f is proportional to $(b/a - 1)^{0.22}$. This slow decay as $b \to a$ suggests that even for very short-ranged forces, the normal stress differences of a noncolloidal suspension should be measurable.

At large b/a, the hydrodynamic particle stress reduces to the Einstein viscosity correction $(5\phi/2)\boldsymbol{E}$. Interestingly, the two stress differences N_2^P and N_2^H both scale as $\eta\dot{\gamma}\phi^2$ as $b/a \to \infty$. The independence of the result from b/a is surprising, but results simply from the fact that the boundary-layer volume is proportional to b^3 while the stress experienced by one particle due the straining field of a second scales as $(b/a)^{-3}$. Recall, however, that as b/a increases, the maximum true particle fraction ϕ_m decreases rapidly, as $\phi_m = (a/b)^3\phi_{b,m}$ where $\phi_{b,m}$ denotes the maximum packing fraction based on the effective radius. Hence, the hydrodynamic normal stress differences decay in importance relative to N_2^P as $(a/b)^5$.

3.5 Shear-induced self-diffusivity of hard spheres

A theory to describe the self-diffusivity of a sheared suspension at arbitrary ϕ, Pe, and lengthscale of the particle-fraction disturbance has been developed in Chapter 2. The theory is based upon the experimental technique of light-scattering (Berne & Pecora 1976) and amounts to a study of the Fourier-transformed equation governing the configurational transition probability. This method has been extensively used in

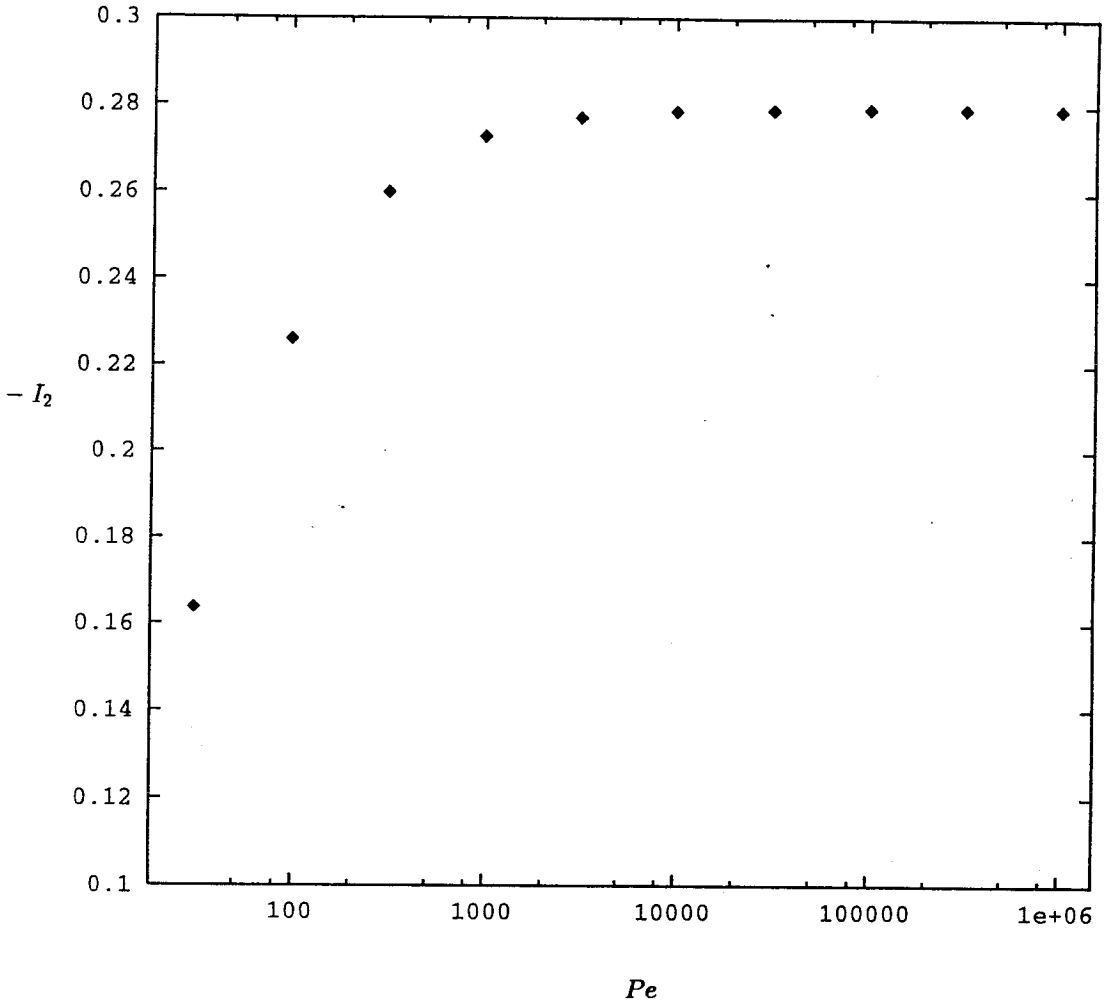

Figure 3.6: The dimensionless integral I_2 specifying the hydrodynamic second normal stress difference, $N_2^H = (15/4\pi)I_2\eta\dot{\gamma}\phi^2$, as a function of Pe for $b/a = 1.025$.

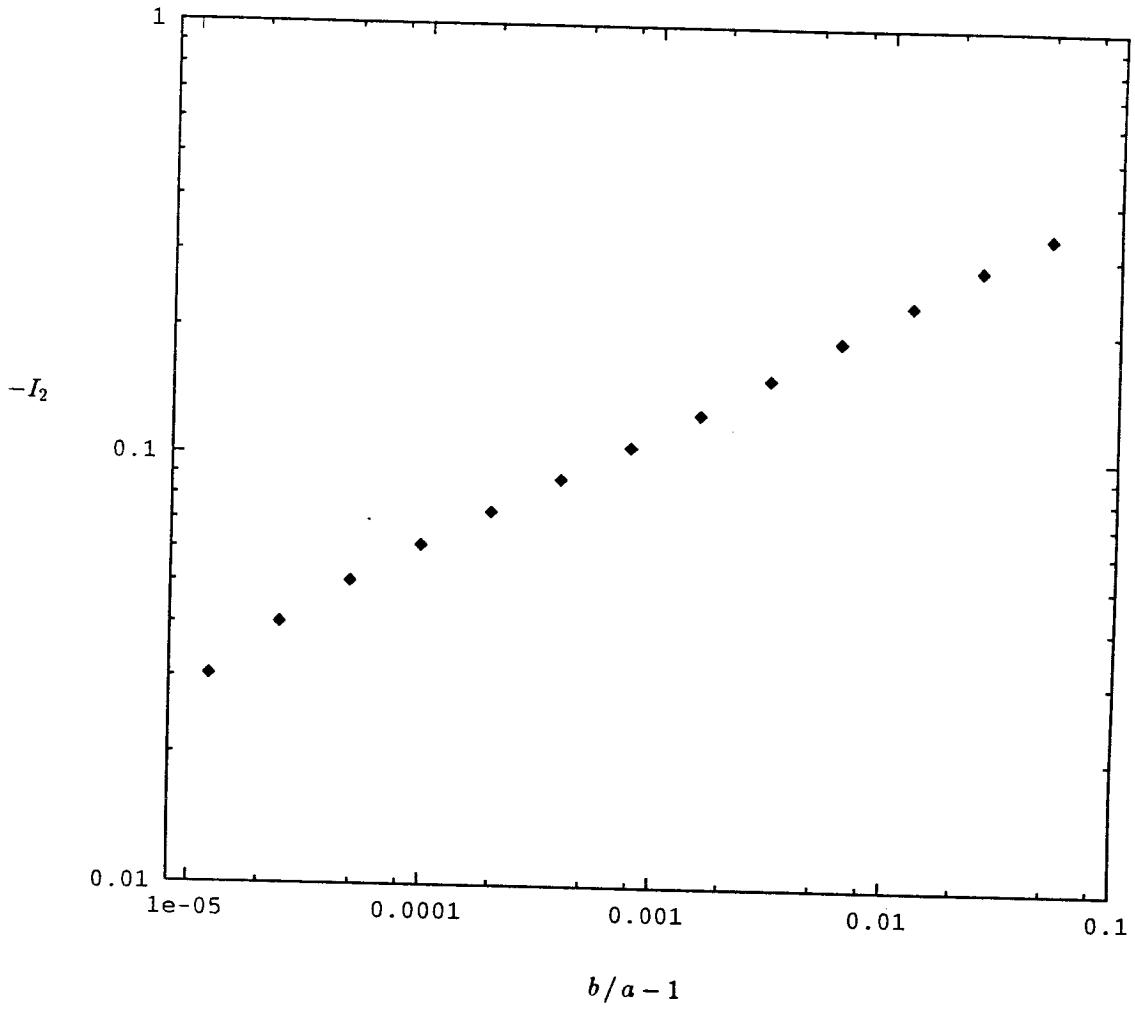

Figure 3.7: The dimensionless integral I_2 specifying the hydrodynamic second normal stress difference, $N_2^H = (15/4\pi)I_2\eta\dot{\gamma}\phi^2$, as a function of $b/a - 1$ for $Pe = 10^6$.

the evaluation of diffusion in quiescent colloidal dispersions (Jones & Burfield 1982; Rallison & Hinch 1986; Pusey 1991). We apply the theory to the determination of the self-diffusivity of a sheared suspension of hard spheres with no hydrodynamic interactions at $\bar{P}e \gg 1$.

We first outline those aspects of the theory necessary for the present calculation. The self-diffusivity is determined from the temporal evolution of spatial correlation. The self-intermediate scattering function, F_s, which represents the Fourier transform of the spatial autocorrelation function, is given by

$$\begin{aligned} F_s &= \langle e^{i\boldsymbol{k}\cdot[\boldsymbol{x}_1(t)-\boldsymbol{x}_1(0)]}\rangle \\ &= \int\int e^{i\boldsymbol{k}\cdot[\boldsymbol{x}_1(t)-\boldsymbol{x}_1(0)]} P_N(\boldsymbol{x}^N(t)|\boldsymbol{x}^N(0)) P_N^0(\boldsymbol{x}^N(0) d\boldsymbol{x}^N(t) \boldsymbol{x}^N(0), \end{aligned}$$

where $\boldsymbol{k}$ is the wavelength of the scattered light and P_N here denotes the probability for the configuration to undergo the transition from $\boldsymbol{x}^N(0)$ to $\boldsymbol{x}^N(t)$, and P_N^0 is the probability distribution for the configuration at the initial time, which we take to be the steady distribution at the conditions of interest. For arbitrary flow conditions, the self-diffusivity may be defined as the coefficient of $-k^2$ in the derivative

$$\frac{\partial \ln F_s}{\partial t} \equiv (\dot{\ln F_s}).$$

In the general case, $(\dot{\ln F_s})$ is given by

$$(\dot{\ln F_s}) = \boldsymbol{k}\cdot\dot{\boldsymbol{\Gamma}}\cdot\nabla_k \ln F_s + i\boldsymbol{k}\cdot\boldsymbol{U}^*\boldsymbol{k}\cdot\langle \boldsymbol{D}_{11}\rangle^0\cdot\boldsymbol{k} \tag{3.74}$$

$$-\boldsymbol{k}\cdot\int(\boldsymbol{D}_{11}-\langle\boldsymbol{D}_{11}\rangle^0)\cdot\boldsymbol{k}f_NP^0d\boldsymbol{r}^N+i\boldsymbol{k}\cdot\int[\boldsymbol{U}_1'f_NP^0d\boldsymbol{r}^N$$
$$-i\boldsymbol{k}\cdot\int\sum_{\alpha=2}^{N}\left[(\boldsymbol{D}_{1\alpha}-\boldsymbol{D}_{11})\cdot\nabla_\alpha f_N+(\boldsymbol{D}_{1\alpha}-\boldsymbol{D}_{11})f_N\cdot\nabla_\alpha(lnP^0+V)\right]P^0d\boldsymbol{r}^N,$$

where $\boldsymbol{r}^N$ is the relative configuration vector giving the positions of the other particles relative to particle 1, which lies at the origin, and $P^0=P^0_{N-1|1}$ is the probability for the configuration. Also, $\boldsymbol{U}^*$ is the velocity at an arbitrary field point from which the shear velocity with constant gradient $\dot{\boldsymbol{\Gamma}}$ is measured, and

$$\boldsymbol{U}_1'=\boldsymbol{U}_1-\dot{\boldsymbol{\Gamma}}\cdot\boldsymbol{x}_1-\langle\boldsymbol{U}_1\rangle^0$$

is the hydrodynamic disturbance velocity relative to the bulk flow (uniform plus shear) of the tagged particle. The scalar function f_N, which describes the perturbation to the microstructure caused by the motion of a tagged particle, is central to the theory of the long-time self-diffusivity, because the difference between the short-time self-diffusivity, $kT\langle\boldsymbol{M}_{11}\rangle$, and the long-time self-diffusivity is due to the correlation of the flux of the tagged particle with f_N.

In the general case, f_N is governed by a complex integro-differential equation (see Eqn (2.36) of Chapter 2) which we do not reproduce. For self-diffusion, the steady f_N is sufficient, and the conditions we consider, *i.e.*, a dilute suspension of hard spheres with no hydrodynamics for $k\ll 1$ ($\boldsymbol{k}$ is made dimensionless with a^{-1}), allow several simplications. We reduce the general equation for f_N to that governing the steady

pair perturbation f_2. Recognizing the linearity of the problem in $i\boldsymbol{k}$, we write f_2 as

$$f_2(\boldsymbol{r}) = i\boldsymbol{k}\cdot\boldsymbol{b}, \tag{3.75}$$

thus defining a wavevector-independent field $\boldsymbol{b}$ analogous to the B-field of Brenner (1980). The steady equation for $\boldsymbol{b}$ for a dilute suspension of hard spheres without hydrodynamic interactions is

$$\nabla^2\boldsymbol{b} - (\bar{Pe}\dot{\boldsymbol{\Gamma}}\cdot\boldsymbol{r} - 2\nabla \ln g)\cdot\nabla\boldsymbol{b} = -\nabla \ln g, \tag{3.76}$$

and the boundary conditions are

$$\hat{\boldsymbol{r}}\cdot\nabla\boldsymbol{b} = 2\bar{Pe}\gamma_r\boldsymbol{b} \quad \text{at} \quad r = 2 \tag{3.77}$$

$$\boldsymbol{b} \sim 0 \quad \text{as} \quad r \to \infty. \tag{3.78}$$

Here, all lengths have been made dimensionless with b. The expression for the long-time self-diffusivity of hard spheres can be expressed using $\boldsymbol{b}$ as simply

$$\boldsymbol{D}^s_\infty = \boldsymbol{I} - \phi\frac{3}{\pi}\int_{r=2}\hat{\boldsymbol{r}}\boldsymbol{b}g\,d\Omega. \tag{3.79}$$

Thus, only the contact value of $\boldsymbol{b}$ is needed for the evaluation of hard-sphere diffusivity.

The steady $g(\boldsymbol{r})$ for hard spheres at $Pe \gg 1$ was determined in §3.4 by a boundary-layer analysis, and there is a similar boundary-layer problem for $\boldsymbol{b}$. Only the radial

portion of $\boldsymbol{b}$ is required and we write

$$\boldsymbol{b} = q(r)\hat{\boldsymbol{r}}. \tag{3.80}$$

Substituting (3.80) to (3.76), we obtain the governing equation for $q(y)$, where $y = Pe(r-2)$,

$$\frac{\partial^2 q}{\partial y^2} - \left[2\gamma_r\left(1 - \frac{1}{2\gamma_r} + \frac{1}{2}\bar{P}e^{-1}y\right) - 2\frac{\partial \ln g}{\partial y}\right]\frac{\partial q}{\partial y} = -\bar{P}e^{-1}\frac{\partial \ln g}{\partial y}, \tag{3.81}$$

with the conditions

$$\frac{\partial q}{\partial y} = -\frac{1}{2}\bar{P}e^{-1} \quad \text{at} \quad y = 0 \tag{3.82}$$

$$q \sim 0 \quad \text{as} \quad y \to \infty. \tag{3.83}$$

The solution to this system is

$$q(y) = \bar{P}e^{-1}\int_y^\infty \left[\frac{1}{2}\frac{g^2(0)}{g^2}e^{s(z)} + \frac{e^{s(z)}}{g^2(z)}\int_0^z e^{-s(x)}g^2(x)\frac{d\ln g}{dx}dx\right]dz \tag{3.84}$$

where we recall that s was defined previously by (3.42). For the determination of $\boldsymbol{D}^s_\infty$, we need only the contact value of q,

$$q(0) = \bar{P}e^{-1}\int_0^\infty \left[\frac{1}{2}\frac{g^2(0)}{g^2}e^{s(z)} + \frac{e^{s(z)}}{g^2(z)}\int_0^z e^{-s(x)}g^2(x)\frac{d\ln g}{dx}dx\right]dz,$$

which upon evaluation of the integrals yields

$$q(0) = -\frac{1}{3} + O(\bar{P}e^{-1}). \tag{3.85}$$

Hence, the long-time self-diffusivity is given in dimensional form for general b/a by

$$\boldsymbol{D}^s_\infty = D\boldsymbol{I} - \dot{\gamma} b^2 \phi_b \frac{2}{3\pi} \int_{\gamma_r<0} \hat{\boldsymbol{r}}\hat{\boldsymbol{r}}\gamma_r d\Omega. \tag{3.86}$$

In simple shear flow $U_1 = \dot{\gamma} x_2$, we have

$$\boldsymbol{D}_{11} = \boldsymbol{D}_{22} = 2\boldsymbol{D}_{33} = \frac{4}{15\pi}\dot{\gamma} b^2 \phi_b. \tag{3.87}$$

A comparison of (3.86) and (3.51) shows that $\boldsymbol{D}^s_\infty$ may be expressed in terms of $\boldsymbol{\Sigma}'$ as

$$\boldsymbol{D}^s_\infty = -\eta\dot{\gamma}\frac{1}{\phi}\frac{9}{\pi}\boldsymbol{\Sigma}', \tag{3.88}$$

or alternatively in a form which is of interest because it agrees with the idea of self-diffusion being driven by a partial or osmotic pressure,

$$\boldsymbol{D}^s_\infty = -\frac{a^2}{\eta}\frac{2}{27}\frac{\partial}{\partial\phi}\boldsymbol{\Sigma}'. \tag{3.89}$$

3.6 Summary and concluding remarks

We have analyzed the influence of weak Brownian motion and repulsive interparticle forces of hard-sphere type on the pair-distribution function of a suspension. In strong flow, *i.e.*, at $Pe \gg 1$, g varies rapidly in a narrow $O(aPe^{-1})$ boundary layer near particle contact.

In the case of hard spheres subject only to hydrodynamic interactions, we have solved the boundary-layer problem for g by a similarity transformation. This analysis, which includes the influence of the spatial variation of the hydrodynamic interactions, shows that Brownian motion renders the contact value of g finite, with $g(2) = O(Pe^{0.78})$. Despite the fact that this large g lacks fore-aft symmetry, its magnitude is not quite large enough to generate normal stress differences in the hydrodynamic limit because the product of $g(2)$ and the $O(Pe^{-1})$ boundary-layer volume is $O(Pe^{-0.22})$ and thus vanishes as $Pe \to \infty$. However, when the effective radius of a particle is $b > a$, as when particles interact by a strong repulsive force, we have shown through a boundary-layer analysis of the radial terms in the pair equation (there is no similarity solution in this case) that $g(\boldsymbol{r})$ is $O(Pe)$ in the compressional quadrants and $O(1)$ in the extensional quadrants. Thus, the product of the asymmetry and the boundary-layer volume, again $O(a^3Pe)$, is finite as $Pe \to \infty$, and normal stress differences scaling as $\eta\dot{\gamma}\phi^2$ and a shear-induced self-diffusivity scaling as $\eta a^2\phi$ are predicted in this limit. We find that as $b/a - 1 \to 0$, the asymmetric portion of g depends on the separation as $(b/a-1)^{0.22}$, and hence the normal stress differences vanish as expected when $b = a$. The exponents of $(b/a-1)^{0.22}$ and $Pe^{-0.22}$ are given

by a combination of the contact values of hydrodynamic functions,

$$1 + \frac{W(2a)}{2A'(2a)} = 1 + a_2 = 0.22,$$

where a_2 arose in the solution of the similarity problem for g in the case of $b = a$.

These results go far toward explaining the observation of nonNewtonian behavior in noncolloidal suspensions. The abundant evidence, some of which we have detailed in the introduction, that the pair interaction at large Pe is markedly asymmetric in sheared suspensions may now be understood in qualitative and quantitative terms. Both cases studied show a large asymmetry, and the slow decay of the influence of this asymmetry upon the rheology either as $Pe \to \infty$ for $b = a$ or as $b/a - 1 \to 0$ for $Pe^{-1} = 0$ indicates that, due to the always-present weak Brownian motion and irreversible surface interactions caused by roughness or a finite-ranged force, we may expect to find measurable nonNewtonian effects.

We have considered primarily pure straining flow when hydrodynamic interactions are important ($b \approx a$), because of the uncertainty about how to deal rigorously with the region of closed trajectories in the two-body analysis for simple shear. For sufficiently long-ranged interparticle forces, there are no longer closed trajectories, and our analysis applies to any linear flow. At moderate to high concentrations, closed streamlines cease to be an issue because multi-particle interactions are common, and these will result in displacement of particles from the region where closed streamlines occur in the dilute system. As the balance between the radial advection and radial Brownian diffusion gives rise to the boundary-layer structure in g regardless of ϕ,

the present analyses have significance at conditions beyond those for which they are rigorously valid.

A potential extension of the work presented here is the equivalent analyses using average two-particle hydrodynamic functions in a nondilute suspension, available from Stokesian Dynamics simulations. The work of Brady & Bossis (1985) showed the average relative velocity (with the average over both approach and recession) of a pair in a concentrated suspension of hydrodynamically-interacting spheres to be larger in magnitude than for an isolated pair, by a factor which scaled as $[1-(\phi_A/\phi_{A,m})^{1/2}]^{-1}$ (monolayer suspensions were studied, thus the areal fraction of particles, ϕ_A, and maximum areal fraction, $\phi_{A,m}$, appear). From this result, it is clear that the function $\langle A(r)\rangle$ in the description of the average radial relative velocity (see Eqn. (3.14)) is a strong function of ϕ, and we may expect $\langle a_2\rangle \approx \langle W(2)\rangle/2\langle A'(2)\rangle$ to also be ϕ-dependent. The decay of nonNewtonian behavior, if the scaling $Pe^{-(1+\langle a_2\rangle)}$ for $Pe \to \infty$ holds at nondilute ϕ, will thus depend on ϕ.

Evaluation of the pair-distribution function in a large-Péclet-number sedimentation of spheres may be performed by a boundary-layer analysis similar to that for linear flow. If there is nonzero dispersity in particle size or density so that relative velocity exists and the analysis can be performed at the two-particle level (under the influence of hydrodynamics alone, two identical particles settle at the same velocity for all separations and a third particle is necessary to cause a relative velocity), the boundary-layer problem for sedimentation can be seen to be much like that for linear flow: in both cases, the relative velocity and diffusivity vary with separation

and the pair-distribution function in the hydrodynamic limit is spherically symmetric. Spherical symmetry of the microstructure for sedimentation of nonBrownian particles was demonstrated by Batchelor (1982), in work where the boundary-layer problem is suggested.

Appendix. Boundary-layer solution: influence of velocity divergence.

In §3.4.2, we reported two approximate boundary-layer solutions for $f(\boldsymbol{r}) = g(\boldsymbol{r}) - p(r)$ neglecting angular derivatives, but maintaining other terms of similar order. The first analysis, detailed in the text, neglected the term representing the velocity divergence from the equation governing f. Here, we present the analysis leading to the solution for f including the influence of $\nabla \cdot U$, reported in the text by (3.64). We have not obtained a boundary-layer solution including angular derivatives as this problem is no simpler than solving the complete equation for all Pe.

As the only derivatives maintained are in the stretched radial coordinate, we denote differentiation by a prime, and write (3.54) as

$$[1 + c_1 y]f'' + [c_2 + c_3 y]f' + c_4 f = 0, \tag{3.90}$$

with

$$c_1 = \alpha_1 Pe^{-1}, \quad c_2 = -\alpha_2 \gamma_r + \alpha_2 \alpha_3 Pe^{-1},$$

$$c_3 = -\alpha_2\alpha_4\gamma_r Pe^{-1}, \quad \text{and} \quad c_4 = \alpha_5 Pe^{-1}\gamma_r, \tag{3.91}$$

where $\alpha_1 - \alpha_5$ are given by (3.57). Note that $c_4 f$ represents the influence of the velocity divergence.

We apply the transformation

$$\xi = -\frac{c_3}{c_1}\left(\frac{1}{c_1} + y\right) = \gamma_r\left(\frac{1 - \bar{A} - 2\hat{b}\bar{A}'}{\bar{G}'}\right)\left[Pe\frac{\bar{G}}{\bar{G}'} + y\right]. \tag{3.92}$$

This transformation is valid only if $c_1 \neq 0$ (*i.e.*, $\bar{G}' \neq 0$), and thus we should not neglect hydrodynamics in the resulting solution. The equation for $f(\xi)$ is

$$\xi f'' + (\beta - \xi)f' - \alpha f = 0, \tag{3.93}$$

where

$$\alpha = \frac{c_4}{c_3} = -\frac{\alpha_5}{\alpha_2\alpha_4}, \quad \text{and} \quad \beta = \frac{1}{c_1}\left(1 - \frac{c_3}{c_1^2}\right).$$

Thus, $f(\xi)$ satisfies Kummer's equation and has the general solution

$$f(\xi) = \mu M(\alpha, \beta, \xi) + \lambda U(\alpha, \beta, \xi),$$

where M and U are confluent hypergeometric functions and μ and λ are arbitrary constants (Abramowitz & Stegun 1972; section 13.1). We must set $\mu = 0$ because M grows without bound whether ξ is positive or negative for α and β of this study. Note that ξ has the sign of γ_r, and for $\xi > 0$, $U \sim \xi^{-\alpha}$ and is unbounded. Thus we find

a solution only for $\gamma_r < 0$, which is consistent with the analysis when the influence of the velocity divergence was neglected. We use the fact that $e^{\xi}U(\beta-\alpha,\beta,-\xi)$ is also a solution to (3.93) and apply $U(\beta-\alpha,\beta,-\xi) \sim (-\xi)^{\alpha-\beta}$ for large $|\xi|$ (we may use this relation over the entire range as $\xi(y=0) = O(Pe) \gg 1$). to write f in the original boundary-layer variable y as

$$f(y) = C(\varphi,\theta)\exp\left[-\frac{c_3 y}{c_1}\right]\left(1+\alpha_1 Pe^{-1}y\right)^{c_4/c_3}, \tag{3.94}$$

where we have noted that the leading coefficient is in general dependent on φ and θ. Enforcing the boundary condition at $y=0$ and consideration of the asymptotic form of the final factor in (3.94) yields

$$f(y) \sim f(0)e^{-c_2 y}\left[1+\alpha Pe^{-1}y\right]^{c_4/c_3}, \quad \text{as} \quad Pe \to \infty, \tag{3.95}$$

where in this case

$$f(0) = -PeR\left[\frac{\alpha_a\alpha_5}{\alpha_2\alpha_4} - \alpha_2\alpha_3\right]^{-1}. \tag{3.96}$$

We see that the primary finding of the simpler study neglecting the velocity divergence, *i.e.*, that there is an $O(Pe)$ excess of particles along the compressional axes, is unchanged. We conclude that the influence of the velocity divergence upon f is primarily quantitative, increasing the contact value of f from that given by (3.60) by a factor which tends to $1-a_2 \approx 1.78$ as $b-a \to 0$.

As noted above, the transformation of variables we have used here is not valid when hydrodynamics is neglected. It may be of interest for some purposes to know

the residual influence of hydrodynamics when $b/a \gg 1$. A study of (3.58) for large b/a shows that the appropriate balance to consider is (3.59), because $\nabla \cdot \boldsymbol{U}$ decays as r^{-6} for large r, and thus scales as r^{-4} relative to the derivative of the radial diffusivity G.

Chapter 4

The pressure moments for two rigid spheres in low-Reynolds-number flow

This chapter is taken from the reference Jeffrey, Morris & Brady (1993)

Abstract

The trace of the first moment of the stress for a rigid sphere—the pressure moment—is determined for a sphere in the presence of a second sphere when both are immersed in a linear ambient flow. The spheres may be of different radii and the Reynolds number is low. The pressure moment of either sphere is expressed using resistance functions, as in other studies, and these functions are determined for all separations. The pressure moment is essential for determining the bulk or macroscopic stress of a suspension of hydrodynamically-interacting particles. The osmotic pressure of colloidal dispersions is related to the pressure moment and the application of the resistance functions determined here to this system is given as an illustration. The suspension or particle-phase pressure needed in two-phase flow modeling is also determined by the pressure moment and the results for a sheared cubic lattice are reported.

4.1 Introduction

A mechanical definition of the osmotic pressure in a colloidal dispersion has been given by Brady (1993) in terms of the hydrodynamic interactions among the suspended particles. In addition to the interactions already familiar in low-Reynolds-number hydrodynamics, a new 'pressure interaction' must be defined. This new interaction is also needed in models of particulate two-phase systems, where particle-phase momentum balances necessitate the concept of a solid-phase pressure (Wallis 1969, Batchelor 1988, Koch 1990, Nott & Brady 1994) in order to complete the specification of the bulk stress. The 'suspension pressure' thus introduced requires for its determination—by Stokesian Dynamics simulations (Brady & Bossis 1988) for example—the hydrodynamic pressure interactions between particles. Example calculations of the osmotic pressure and suspension pressure are given at the end of this chapter, after we have defined the pressure interaction precisely and established how it can be calculated.

In low-Reynolds-number hydrodynamics, interactions between particles are frequently specified by using the moments of the surface stress acting on each particle. The first moment of the stress has been decomposed in the past into an antisymmetric part, which equals the couple acting on the particle, and a traceless symmetric part called the stresslet. These two quantities have been tabulated for two rigid spheres in a series of papers summarized in Jeffrey & Onishi (1984), Jeffrey (1992) and Kim & Karrila (1991). It is the trace of the first moment, however, that is needed for the pressure interactions, and this has not been studied before. We denote it by S and

define it for a specified particle as

$$S = -\int \boldsymbol{x}' \cdot \boldsymbol{\sigma} \cdot \boldsymbol{n}\, dA,$$

where $\boldsymbol{x}'$ is the position vector measured relative to the particle center, and the integration is over the surface of the particle. The minus sign is included because the previous studies used it in their definitions; the integral can then be interpreted as the moment exerted *by* the sphere *on* the fluid. Such an interpretation and sign will be used in this work in order to keep the equations similar to those already developed. Before we proceed with the calculations, it is important to pause for a moment and consider terminology. We should decide whether the term stresslet, which until now has referred to a traceless quantity, is to be expanded to include the trace of the first moment, or whether it should be left as the traceless quantity. After considering the equations that arise in the applications described later in this study, we think that it is most convenient to make an analogy with the terminology used for the stress tensor. Thus the stress tensor has a non-zero trace, and when the traceless part of the stress tensor is referred to separately it is called the deviatoric stress. In the same way, a stresslet should have a non-zero trace, and if a traceless quantity is needed, it can be called either the traceless part of the stresslet, or the deviatoric stresslet.

4.2 Expressions for the pressure moment of a sphere

We first derive a Faxén law for the pressure moment by using the reciprocal theorem. We start by recalling (Kim & Karrila 1991, Ladyzhenskaya 1963) that the pressure field $p(\boldsymbol{x})$ produced by a point force $\boldsymbol{F}$ acting at a point $\boldsymbol{y}$ is $p(\boldsymbol{x}) = \boldsymbol{F}\cdot\boldsymbol{P}(\boldsymbol{x}-\boldsymbol{y})$, where

$$\boldsymbol{P}(\boldsymbol{x}) = \frac{1}{4\pi}\frac{\boldsymbol{x}}{x^3} .$$

Next we note that the velocity field $\boldsymbol{v}(\boldsymbol{x})$ around a point source of fluid of strength Q located at the origin is

$$\boldsymbol{v} = \frac{Q}{4\pi}\frac{\boldsymbol{x}}{x^3} = Q\boldsymbol{P}(\boldsymbol{x}) .$$

The reciprocal theorem is used in the form (Kim & Karrila 1991)

$$\int \boldsymbol{v}_1 \cdot (\boldsymbol{\sigma}_2 \cdot \boldsymbol{n}) dA + \int \boldsymbol{v}_1 \cdot (\nabla \cdot \boldsymbol{\sigma}_2) dV = \int \boldsymbol{v}_2 \cdot (\boldsymbol{\sigma}_1 \cdot \boldsymbol{n}) dA + \int \boldsymbol{v}_2 \cdot (\nabla \cdot \boldsymbol{\sigma}_1) dV ,$$

where $\boldsymbol{n}$ is directed outward from the particle surface into the fluid. We take $\boldsymbol{v}_1$ to be the flow outside an expanding sphere whose radius is a and whose rate of volume increase is Q; the sphere center is at the origin. For $\boldsymbol{v}_2$, we take the flow generated by a point force $\boldsymbol{F}$ at $\boldsymbol{y}$ when there is a sphere of constant size stationary at the origin. The reciprocal theorem becomes

$$\int \frac{Q}{4\pi}\frac{\boldsymbol{x}'}{a^3} \cdot (\boldsymbol{\sigma}_2 \cdot \boldsymbol{n}) dA + \int Q\boldsymbol{P}(\boldsymbol{x}) \cdot (-\boldsymbol{F})\delta(\boldsymbol{x}-\boldsymbol{y}) dV(\boldsymbol{x}) = 0 .$$

Simplifying further, we obtain

$$\frac{Q}{4\pi a^3}(-S_2) - Q\boldsymbol{F}\cdot\boldsymbol{P}(\boldsymbol{y}) = 0 \ ,$$

and this gives an expression for the pressure moment as

$$S_2 = -4\pi a^3 \boldsymbol{F}\cdot\boldsymbol{P}(\boldsymbol{y}) \ .$$

Now we observe that $-\boldsymbol{F}\cdot\boldsymbol{P}(\boldsymbol{y}) = \boldsymbol{F}\cdot\boldsymbol{P}(-\boldsymbol{y})$ is the pressure that would exist at the origin if the point force were acting in the absence of the sphere. This is the 'ambient' pressure as seen by the sphere, usually denoted $p^\infty(\boldsymbol{x}=0)$. Thus we obtain a Faxén law in the form

$$S = 4\pi a^3 p^\infty(\boldsymbol{x}=0) \ . \tag{4.1}$$

The extension of this result to an arbitrary ambient flow follows by echoing Hinch's argument cited in Kim & Karrila (1991) that any ambient flow can be modeled by a suitable superposition of point forces.

We next obtain an exact expression for the pressure moment of one sphere in the presence of another in terms of multipole expansions. We follow the notation of Jeffrey & Onishi (1984) throughout; equations taken from their paper will be labeled by JO. In terms of spherical coordinates $(\rho_\alpha, \theta_\alpha, \phi)$ centered on sphere α, the quantity

we wish to calculate is

$$S = -a_\alpha \int\int (-p + \mu \frac{\partial u}{\partial \rho_\alpha}) a_\alpha^2 \sin\theta_\alpha d\theta_\alpha d\phi \,,$$

where $u = \boldsymbol{u} \cdot \hat{\boldsymbol{\rho}}_\alpha$. Using (JO 2.3) and (JO 2.1), we obtain

$$a_\alpha^3 \int p \sin\theta_\alpha d\theta_\alpha d\phi = 4\pi a_\alpha^2 \mu \sum_{n=0}^{\infty} p_{0n}^{(3-\alpha)} t_\alpha t_{3-\alpha}^n \,. \tag{4.2}$$

A similar calculation based on (JO 2.4, 2.7, 2.1) shows that the $\partial u/\partial \rho$ term in the integrand integrates to 0. We should remember when comparing (4.2) with (4.1) that the coefficients p_{mn} have the dimensions of velocity. Also, it is worth noting that the integration leads to a contribution p_{00} from the sphere to its own pressure moment; however, this coefficient must always be zero, because it implies logarithmic velocities far from the sphere. The only contribution, then, is the pressure environment created by the second sphere. Since only $m = 0$ terms appear in the expression, we can see that only axisymmetric motions will lead to non-zero pressure moments. This fact can also be deduced from general vector considerations.

4.3 Resistance functions

As with the other interactions between spheres, the pressure moment can be expressed as a function of the velocities of the spheres and the ambient velocity field, given by

$$\boldsymbol{U}(\boldsymbol{x}) = \boldsymbol{U}_\infty + \boldsymbol{\Omega}_\infty \times \boldsymbol{x} + \boldsymbol{E}_\infty \cdot \boldsymbol{x} \,,$$

with constant $\boldsymbol{U}_\infty$, $\boldsymbol{\Omega}_\infty$, and $\boldsymbol{E}_\infty$, in which case we are led to functions analogous to the resistance functions defined in earlier papers. We write

$$\begin{pmatrix} S_1 \\ S_2 \end{pmatrix} = \mu \begin{pmatrix} \boldsymbol{P}_{11} & \boldsymbol{P}_{12} & \boldsymbol{Q}_{11} & \boldsymbol{Q}_{12} \\ \boldsymbol{P}_{21} & \boldsymbol{P}_{22} & \boldsymbol{Q}_{21} & \boldsymbol{Q}_{22} \end{pmatrix} \cdot \begin{pmatrix} \boldsymbol{U}_1 - \boldsymbol{U}(\boldsymbol{x}_1) \\ \boldsymbol{U}_2 - \boldsymbol{U}(\boldsymbol{x}_2) \\ \boldsymbol{E}_1 - \boldsymbol{E}_\infty \\ \boldsymbol{E}_2 - \boldsymbol{E}_\infty \end{pmatrix} . \tag{4.3}$$

The rotations of the spheres do not appear in the equation because it can be shown that they do not contribute to the trace. Since the only vector in the problem is $\boldsymbol{d}$, where

$$\boldsymbol{d} = (\boldsymbol{x}_2 - \boldsymbol{x}_1)/|\boldsymbol{x}_2 - \boldsymbol{x}_1|$$

is the unit vector along the line of centers directed from particle 1 to particle 2, clearly we have (including non-dimensionalizing factors)

$$\boldsymbol{P}_{\alpha\beta} = \pi(a_\alpha + a_\beta)^2 X^P_{\alpha\beta} \boldsymbol{d}, \tag{4.4}$$

$$\boldsymbol{Q}_{\alpha\beta} = \pi(a_\alpha + a_\beta)^3 X^Q_{\alpha\beta} (\boldsymbol{dd} - \tfrac{1}{3}\boldsymbol{I}), \tag{4.5}$$

and $X^P_{\alpha\beta}$, $X^Q_{\alpha\beta}$ are functions only of $s \equiv 2r/(a_\alpha + a_\beta)$, where $r = |\boldsymbol{x}_2 - \boldsymbol{x}_1|$. The other resistance functions which are contracted with the rate of strain have been made traceless, so it seems reasonable to follow this practice here. The only symmetries obeyed by the functions are labeling ones:

$$X^P_{\alpha\beta}(s,\lambda) = -X^P_{(3-\alpha)(3-\beta)}(s,\lambda^{-1}) \quad \text{and} \quad X^Q_{\alpha\beta}(s,\lambda) = X^Q_{(3-\alpha)(3-\beta)}(s,\lambda^{-1}).$$

4.4 The functions $X^P_{\alpha\beta}$

4.4.1 Method of reflections

We start by deriving the first few terms by the method of reflections. Suppose sphere 1 is moving with velocity $\boldsymbol{U}_1 = U\boldsymbol{d}$ toward sphere 2. The pressure field at the center of sphere 2 is

$$p = \tfrac{3}{2}a_1\mu U_1/r^2\,;$$

hence,

$$S_2 = .\pi(a_1+a_2)^2\mu X^P_{21}U_1 = 4\pi a_2^3\,\tfrac{3}{2}a_1\mu U_1/r^2\,,$$

and therefore

$$X^P_{21} = \frac{4}{(1+\lambda)^2}\frac{6\lambda^3}{(1+\lambda)^2 s^2}\,.$$

From the above relations, we have

$$X^P_{12} = -\frac{4}{(1+\lambda)^2}\frac{6\lambda}{(1+\lambda)^2 s^2}\,.$$

Sphere 2 responds to the ambient velocity induced near it by sphere 1 by exerting a force on the fluid; hence,

$$S_1 = 4\pi a_1^2\mu X^P_{11}U_1 = 4\pi a_1^3(3/2)(a_2/r^2)\mu(3a_1/2r)U_1\,,$$

and

$$X_{11}^P = \frac{18\lambda}{(1+\lambda)^3 s^3}.$$

4.4.2 Twin multipole expansions

These functions can be calculated using the results obtained in JO section 3. In terms of P_{npq} defined in (JO 3.4—3.9) we have

$$X_{11}^P - \tfrac{1}{4}(1+\lambda)^2 X_{12}^P = \sum_{n=1}^{\infty}\sum_{p=0}^{\infty}\sum_{q=0}^{\infty} \tfrac{3}{2} P_{npq} t_2^{p+n} t_1^{q+1}.$$

For the complementary problem defined in (JO 3.11) we have

$$X_{11}^P + \tfrac{1}{4}(1+\lambda)^2 X_{12}^P = \sum_{n=1}^{\infty}\sum_{p=0}^{\infty}\sum_{q=0}^{\infty} (-1)^{n+p+q+2} \tfrac{3}{2} P_{npq} t_2^{p+n} t_1^{q+1}.$$

From these equations, we see that the pattern observed with the earlier functions continues to hold, namely that the even and odd powers of s divide between the functions. Thus

$$\begin{aligned} X_{11}^P(s,\lambda) &= \sum_{\substack{m=1 \\ m \text{ odd}}}^{\infty} \sum_{q=1}^{m-1} \sum_{n=1}^{(q+1)/2} \tfrac{3}{2} P_{n(q-n)(m-q-1)} \lambda^q \frac{2^m}{(1+\lambda)^m s^m} \\ &= \sum_{\substack{m=1 \\ m \text{ odd}}}^{\infty} \frac{f_m(\lambda)}{(1+\lambda)^m s^m}, \end{aligned} \tag{4.6}$$

and

$$X_{12}^P(s,\lambda) = \frac{-4}{(1+\lambda)^2} \sum_{\substack{m=2 \\ m \text{ even}}}^{\infty} \frac{f_m(\lambda)}{(1+\lambda)^m s^m}, \tag{4.7}$$

where

$$f_0 = f_1 = 0, f_2 = 6\lambda, f_3 = 18\lambda,$$

$$f_4 = 54\lambda^2, f_5 = -24\lambda + 162\lambda^2 + 216\lambda^3,$$

$$f_6 = 216\lambda^2 + 486\lambda^3 + 576\lambda^4,$$

$$f_7 = 432\lambda^2 + 498\lambda^3 + 2592\lambda^4 + 1440\lambda^5,$$

$$f_8 = 864\lambda^2 + 3888\lambda^3 + 7446\lambda^4 + 7128\lambda^5 + 3456\lambda^6.$$

4.4.3 Lubrication theory

The flow between nearly-touching spheres has been studied in Jeffrey & Corless (1988) and Jeffrey (1989). Solutions based on an expansion in the small parameter ϵ were given there. In the latter paper it was shown that, when higher orders are included, not all quantities can be approximated successfully by considering only the flow in the gap. We follow the method given there to circumvent that difficulty by writing the pressure moment as

$$S_1 = -\int \boldsymbol{x}' \cdot \boldsymbol{\sigma} \cdot \boldsymbol{n} dA = a_1 \boldsymbol{F} \cdot \boldsymbol{d} - a_1 \int (\boldsymbol{n} + \boldsymbol{d}) \cdot \boldsymbol{\sigma} \cdot \boldsymbol{n} dA \,.$$

Using the known result for $\boldsymbol{F}$ and integrating the previously obtained solution (which had been found using the algebra system *Maple*, and was therefore easy to reprogram) we obtain

$$X_{11}^P = g_1 \xi^{-1} + g_2 \ln \xi^{-1} + P_{11}^X(\lambda) + g_3 \xi \ln \xi^{-1} + O(\xi)\,, \tag{4.8}$$

λ	P_{11}^X	P_{12}^X	P_{21}^X	P_{22}^X
1	-0.0118	-0.1435	0.1435	0.0118
2	0.0930	-0.1279	0.2581	-0.0634
3	0.3236	-0.1283	0.3199	-0.0963
4	0.5662	-0.1186	0.3337	-0.1024
5	0.7925	-0.1059	0.3249	-0.0988
10	1.6347	-0.0576	0.2286	-0.0653
20	2.5543	-0.0237	0.1193	-0.0322
100	4.0499	-0.0016	0.0114	-0.0029

Table 4.1: Values of the function $P_{\alpha\beta}^X(\lambda)$, with λ the size ratio of the two spheres, appearing in the asymptotic form of $X_{\alpha\beta}^P$ for small separation.

and

$$\tfrac{1}{4}(1+\lambda)^2 X_{12}^P = -g_1\xi^{-1} - g_2 \ln \xi^{-1} + \tfrac{1}{4}(1+\lambda)^2 P_{12}^X(\lambda) - g_3 \xi \ln \xi^{-1} + O(\xi)\,, \qquad (4.9)$$

where

$$g_1 = 3\lambda^2/(1+\lambda)^3\,,$$

$$g_2 = \tfrac{3}{10}(\lambda - 4\lambda^2)/(1+\lambda)^2\,,$$

$$g_3 = \frac{5 - 97\lambda + 64\lambda^2 - 44\lambda^3 + \lambda^4}{140(1+\lambda)^2}\,, \qquad (4.10)$$

and the $P_{\alpha\beta}^X$ are functions which we shall tabulate here (*cf.* Table 4.1). We can notice that, as with the X^A functions, the singular terms cancel if the two spheres have the same velocity.

4.4.4 Arbitrary separations

The singularities cause slow convergence of the series (4.6)–(4.7) when s is near 2. We remove them from the series by giving the g_i appearing in (4.8)–(4.9) the values defined by (4.10) and then adding the left-hand side of (4.8) to (4.6) while at the same time subtracting the right-hand side of (4.8) from (4.6). If $\tilde{f}(\lambda) = 2^{-m} f(\lambda)$, we write

$$X_{11}^P = g_1 \frac{2s}{s^2-4} + [g_2 + g_3(\tfrac{1}{4}s^2 - 1)] \ln \frac{s+2}{s-2} - g_3 s + \sum_{\substack{m=1 \\ m \text{ odd}}}^{\infty} \left[\frac{\tilde{f}_m(\lambda)}{(1+\lambda)^m} - g_1 - \frac{2g_2}{m} + \frac{4g_3}{m(m+2)} \right] \left(\frac{2}{s}\right)^m . \quad (4.11)$$

Mathematically this is equivalent to (4.6), but numerically the rate of convergence has improved because the coefficients of s^{-m} now decay faster by a factor m^{-2} owing to cancellation. Similarly,

$$\frac{(1+\lambda)^2}{4} X_{12}^P = -g_1 \frac{4}{s^2-4} - [g_2 + g_3(\tfrac{1}{4}s^2 - 1)] \ln \frac{s^2}{s^2-4} + g_3 - \sum_{\substack{m=2 \\ m \text{ even}}}^{\infty} \left[\frac{\tilde{f}_m(\lambda)}{(1+\lambda)^m} - g_1 - \frac{2g_2}{m} + \frac{4g_3}{m(m+2)} \right] \left(\frac{2}{s}\right)^m . \quad (4.12)$$

Numerical tabulations of $X_{\alpha\beta}^P$ are not given because the expressions and data given above are accurate to at least two significant digits for all s. We do tabulate the $P_{\alpha\beta}^X(\lambda)$, however, because they provide a good test of the convergence of the series, as well as being useful in studies of nearly-touching spheres. Expanding the leading

terms in (4.11) and comparing with (4.8), we obtain

$$P_{11}^X = \tfrac{1}{4}g_1 + g_2 \ln 4 - 2g_3 + \sum_{\substack{m=1 \\ m \text{ odd}}}^{\infty} \left[\frac{\tilde{f}_m(\lambda)}{(1+\lambda)^m} - g_1 - \frac{2g_2}{m} + \frac{4g_3}{m(m+2)} \right], \qquad (4.13)$$

and similarly

$$\frac{(1+\lambda)^2}{4} P_{12}^X = \tfrac{1}{4}g_1 + g_3 - \sum_{\substack{m=2 \\ m \text{ even}}}^{\infty} \left[\frac{\tilde{f}_m(\lambda)}{(1+\lambda)^m} - g_1 - \frac{2g_2}{m} + \frac{4g_3}{m(m+2)} \right]. \qquad (4.14)$$

4.4.5 Results for $X_{\alpha\beta}^P$

To illustrate the behavior of the pressure moment, in Figure 4.1 we plot X_{11}^P and X_{12}^P as functions of s for the case of identical spheres ($\lambda = 1$). Note that the singular behavior of X_{11}^P (and X_{12}^P) is proportional to the corresponding resistance functions X_{11}^A, etc., relating forces to translational velocities. In Table 4.1 we give the results of summing the series (4.13)–(4.14) for $P_{\alpha\beta}^X$ to 300 terms. We can estimate the rate of convergence by making a comparison with sums to 200 terms, and that shows that the results are generally accurate to 4 significant figures.

4.5 The functions $X_{\alpha\beta}^Q$

4.5.1 Method of reflections

If sphere 1 deforms at a rate $\boldsymbol{E}_1 = E_1(\boldsymbol{kk} - \frac{1}{3}\boldsymbol{I})$ the pressure at the center of sphere 2 is

$$p = \tfrac{10}{3} a_1^3 \mu E_1 / r^3 .$$

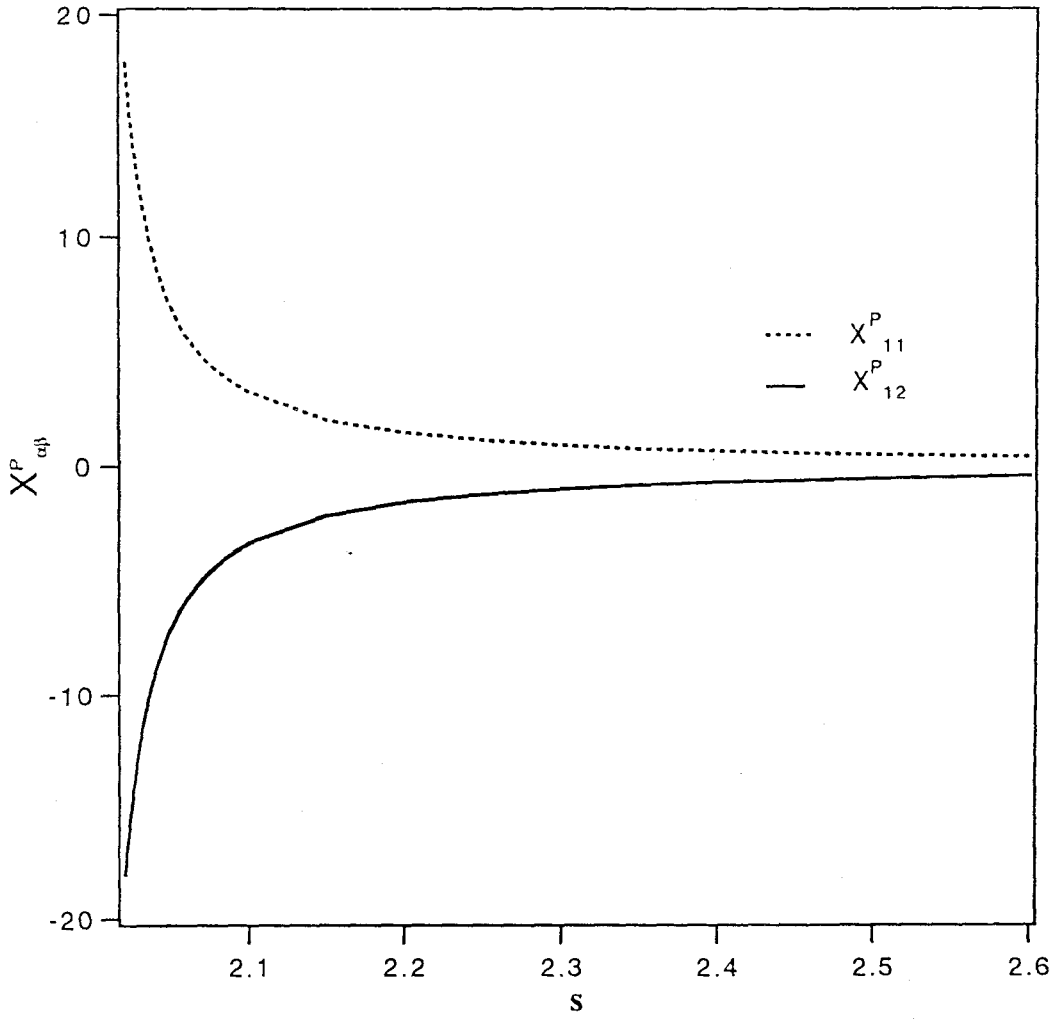

Figure 4.1: The functions X_{11}^P and X_{12}^P relating velocities to the trace of the first moment of the surface force distribution for equal-sized spheres are plotted against the separation distance scaled to the particle radius.

Hence,

$$S_2 = 4\pi a_2^3 \tfrac{10}{3} a_1^3 \mu E_1 / r^3 = \pi (a_1 + a_2)^3 \mu X_{21}^Q \tfrac{2}{3} E_1 \,,$$

and therefore

$$X_{21}^Q = \frac{8}{(1+\lambda)^3} \frac{20\lambda^3}{(1+\lambda)^3 s^3} \,.$$

There will be an ambient flow $(5/3)a_1 E_1 (a_1^2/r^2)\boldsymbol{d}$ created by sphere 1 which will lead to an induced S_1 of

$$S_1 = 8\pi a_1^3 \mu X_{11}^Q \tfrac{2}{3} E_1 = -\pi (a_1 + a_2)^2 X_{12}^P \tfrac{5}{3} (a_1^3/r^2) E_1 \,,$$

implying

$$X_{11}^Q = \frac{30\lambda}{(1+\lambda)^4 s^4} \,.$$

4.5.2 Twin multipole expansions

The calculation in Jeffrey (1992) used the problem

$$\boldsymbol{E}_\alpha = E_\alpha (\boldsymbol{kk} - \tfrac{1}{3}\boldsymbol{I}) \,,$$

together with the condition

$$a_1 E_1 = a_2 E_2 \,.$$

This means that

$$S_1 = 8\pi\mu a_1^3 X_{11}^Q \tfrac{2}{3} E_1 + \pi\mu (a_1 + a_2)^3 X_{12}^Q \tfrac{2}{3} E_2 \,,$$

and therefore

$$S_1 = \tfrac{16}{3}\pi\mu a_1^3 E_1 (X_{11}^Q + \frac{(1+\lambda)^3}{8\lambda} X_{12}^Q).$$

From this we find

$$X_{11}^Q + \frac{(1+\lambda)^3}{8\lambda} X_{12}^Q = \sum_{n=1}^{\infty}\sum_{p=0}^{\infty}\sum_{q=0}^{\infty} \tfrac{5}{2} P_{npq} t_2^{p+n} t_1^{q+1}.$$

The complementary problem adds a factor $(-1)^{n+p+q+3}$ to the summation, so we conclude

$$X_{11}^Q(s,\lambda) = \sum_{\substack{m=0 \\ m \text{ even}}}^{\infty} \frac{f_m(\lambda)}{(1+\lambda)^m s^m}, \tag{4.15}$$

and

$$X_{12}^Q(s,\lambda) = \frac{8}{(1+\lambda)^3} \sum_{\substack{m=1 \\ m \text{ odd}}}^{\infty} \frac{f_m(\lambda)}{(1+\lambda)^m s^m}, \tag{4.16}$$

where

$$f_0 = f_1 = f_2 = 0, f_3 = 20\lambda^3,$$

$$f_4 = 30\lambda, f_5 = 90\lambda^4,$$

$$f_6 = -72\lambda + 270\lambda^2 + 680\lambda^3,$$

$$f_7 = 720\lambda^4 + 810\lambda^5 + 864\lambda^6,$$

$$f_8 = 864\lambda^2 + 3888\lambda^3 + 7446\lambda^4 + 7128\lambda^5 + 3456\lambda^6.$$

4.5.3 Lubrication theory

We expect

$$\begin{aligned} 8\pi a_1^3 \mu X_{11}^Q \tfrac{2}{3} E_1 &= a_1 \boldsymbol{F} \cdot \boldsymbol{d} - a_1 \int (\boldsymbol{n} + \boldsymbol{d}) \cdot \boldsymbol{\sigma} \cdot \boldsymbol{n} \, dA \,, \\ &= 4\pi a_1^3 X_{11}^G E_{zz} - a_1 \int (\boldsymbol{n} + \boldsymbol{d}) \cdot \boldsymbol{\sigma} \cdot \boldsymbol{n} \, dA \,, \end{aligned}$$

and we obtain

$$X_{11}^Q = g_1 \xi^{-1} + g_2 \ln \xi^{-1} + Q_{11}^X + g_3 \xi \ln \xi^{-1} \,, \tag{4.17}$$

$$X_{12}^Q = g_4 \xi^{-1} + g_5 \ln \xi^{-1} + Q_{12}^X + g_6 \xi \ln \xi^{-1} \,, \tag{4.18}$$

where

$$g_1 = \tfrac{3}{2}\lambda^2/(1+\lambda)^3,$$

$$g_2 = \tfrac{3}{20}(\lambda + 2\lambda^2 - 9\lambda^3)/(1+\lambda)^3,$$

$$g_3 = \frac{5 - \lambda - 201\lambda^2 + 251\lambda^3 - 184\lambda^4}{280(1+\lambda)^3},$$

$$g_4 = 12\lambda^3/(1+\lambda)^6,$$

$$g_5 = \tfrac{12}{5}(-2\lambda^2 + \lambda^3 - 2\lambda^4)/(1+\lambda)^6,$$

$$g_6 = \frac{-65\lambda + 34\lambda^2 - 411\lambda^3 + 76\lambda^4 - 44\lambda^5}{35(1+\lambda)^6}.$$

As a check on our working we have the identity

$$4X_{11}^P(1+\lambda)(1+\tfrac{1}{2}\xi) - 8X_{11}^Q - (1+\lambda)^3 X_{12}^Q = O(1) \,.$$

4.5.4 Arbitrary separations

As before, we have the following expressions for Q_{11}^X and Q_{12}^X defined in equations (4.17)-(4.18):

$$Q_{11}^X = -\tfrac{1}{4}g_1 - g_3 + \sum_{\substack{m=2 \\ m \text{ even}}}^{\infty} \left[\frac{\tilde{f}_m(\lambda)}{(1+\lambda)^m} - g_1 - \frac{2g_2}{m} + \frac{4g_3}{m(m+2)} \right], \tag{4.19}$$

and

$$\frac{(1+\lambda)^3}{8} Q_{12}^X = \tfrac{1}{4}g_1 + g_2 \ln 4 - 2g_3 + \sum_{\substack{m=1 \\ m \text{ odd}}}^{\infty} \left[\frac{\tilde{f}_m(\lambda)}{(1+\lambda)^m} - g_1 - \frac{2g_2}{m} + \frac{4g_3}{m(m+2)} \right]. \tag{4.20}$$

4.5.5 Results for $X_{\alpha\beta}^Q$

To illustrate the behavior of the pressure moment, in Figure 4.2 we plot X_{11}^Q and X_{12}^Q as functions of s for the case of identical spheres ($\lambda = 1$). Again, the singular behavior as $s \to 2$ is proportional to the corresponding force-rate of strain coupling X_{11}^G, etc. In Table 4.2 we give the results of summing the series (4.19)-(4.20) for $Q_{\alpha\beta}^X$ to 300 terms. We can estimate the rate of convergence by making a comparison with sums to 200 terms, and that shows that the results are generally accurate to 4 significant figures.

4.6 Osmotic pressure in a dilute suspension

We determine the correction to the osmotic pressure of a dilute suspension of Brownian hard spheres. Batchelor (1977) determined the Brownian contribution to the

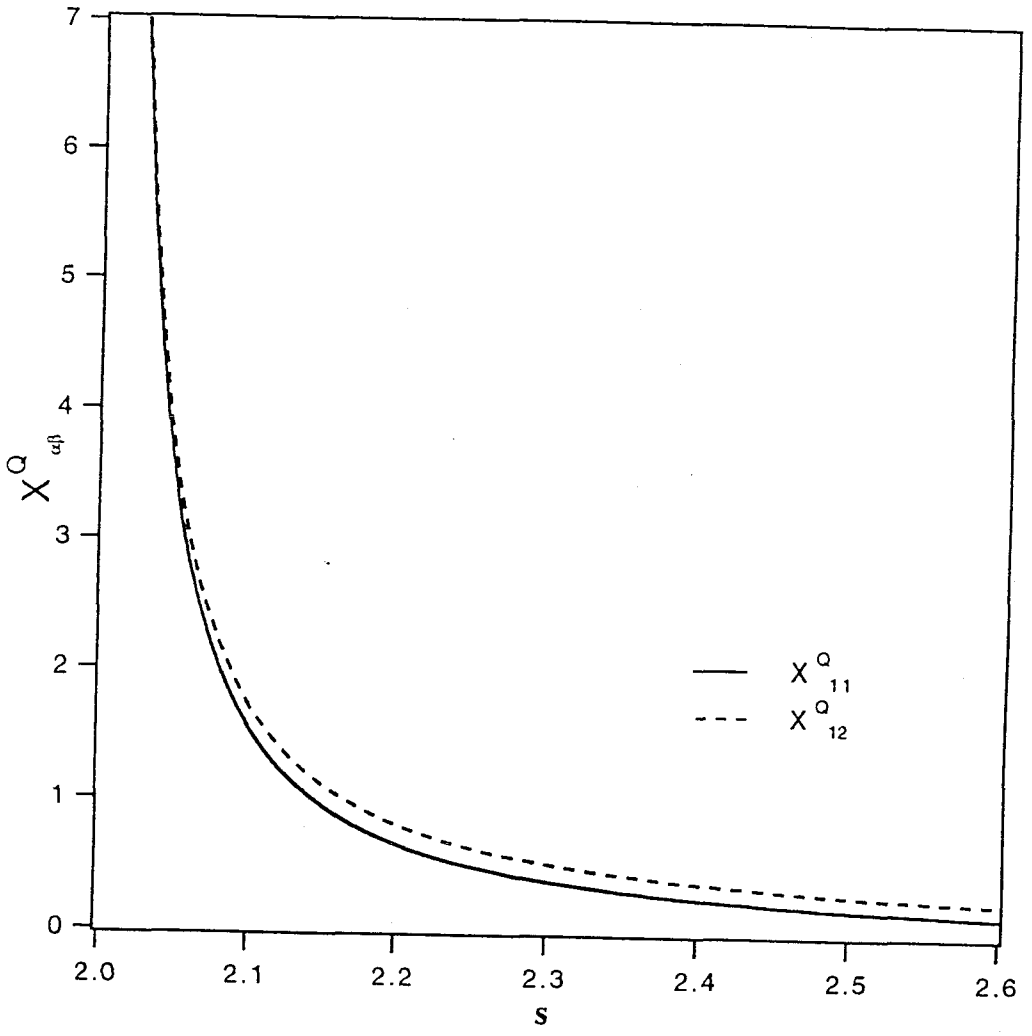

Figure 4.2: The functions X_{11}^Q and X_{12}^Q relating the rate of strain to the trace of the first moment of the surface force distribution for equal-sized spheres are plotted against the separation distance scaled to the particle radius.

λ	Q^X_{11}	Q^X_{12}	Q^X_{21}	Q^X_{22}
1	-0.0799	0.1329	0.1329	-0.0799
2	0.1581	0.1314	0.1332	-0.0413
3	0.5166	0.1219	0.1263	-0.0000
4	0.8686	0.1088	0.1146	0.0186
5	1.1875	0.0959	0.1020	0.0262
10	2.3350	0.0528	0.0571	0.0254
20	3.5543	0.0226	0.0244	0.0138
100	6.2409	0.0018	0.0020	0.0013

Table 4.2: Values of the function $Q^X_{\alpha\beta}(\lambda)$, with λ the size ratio of the two spheres, appearing in the asymptotic form of $X^Q_{\alpha\beta}$ for small separation.

bulk deviatoric stress, and here we complete that calculation for the isotropic stress.

In the presence of Brownian motion there are two contributions to the bulk stress which can be written as (Brady 1993, Brady & Bossis 1988)

$$\langle \boldsymbol{\Sigma} \rangle = -nkT\boldsymbol{I} + 2\mu\langle \boldsymbol{E} \rangle + n[\langle \boldsymbol{S}^E \rangle + \langle \boldsymbol{S}^B \rangle], \tag{4.21}$$

where $\langle \boldsymbol{E} \rangle$ is the bulk rate of strain in the material and the rate-of-strain and Brownian stresslets are given by

$$\langle \boldsymbol{S}^E \rangle = -\langle \boldsymbol{R}_{SU} \cdot \boldsymbol{R}_{FU}^{-1} \cdot \boldsymbol{R}_{FE} - \boldsymbol{R}_{SE} \rangle : \langle \boldsymbol{E} \rangle \,, \tag{4.22}$$

$$\langle \boldsymbol{S}^B \rangle = -kT\langle \nabla \cdot (\boldsymbol{R}_{SU} \cdot \boldsymbol{R}_{FU}^{-1}) \rangle \,. \tag{4.23}$$

In (4.22)–(4.23) $\boldsymbol{R}_{FU}$, $\boldsymbol{R}_{SU}$, etc. are the hydrodynamic resistance tensors that couple the hydrodynamic force/torque to the particle velocities ($\boldsymbol{R}_{FU}$), the stresslets to the velocities ($\boldsymbol{R}_{SU}$), etc. (see Brady & Bossis 1988). Here we have assumed that the

stresslets are *not* traceless, in contrast to the convention in the past, because we wish to determine the trace or pressure. In (4.21)–(4.23) k is Boltzmann's constant, T is the absolute temperature and n is the number density of suspended particles.

The osmotic or suspension pressure, Π, is defined mechanically as minus one third the trace of the bulk stress:

$$\Pi = nkT + nkT\langle \nabla \cdot \boldsymbol{A} \rangle + n\langle \boldsymbol{B} \rangle : \langle \boldsymbol{E} \rangle \,, \tag{4.24}$$

where the hydrodynamic functions $\boldsymbol{A}$ and $\boldsymbol{B}$ are defined by

$$\boldsymbol{A} = \tfrac{1}{3}\boldsymbol{P} \cdot \boldsymbol{R}_{FU}^{-1} \,, \tag{4.25}$$

$$\boldsymbol{B} = \tfrac{1}{3}(\boldsymbol{P} \cdot \boldsymbol{R}_{FU}^{-1} \cdot \boldsymbol{R}_{FE} - \boldsymbol{Q}) \,, \tag{4.26}$$

and $\boldsymbol{P}$ and $\boldsymbol{Q}$ are the pressure functions defined in (4.3). The procedure of obtaining (4.26) from (4.22) shows that $\boldsymbol{P} = \boldsymbol{I} : \boldsymbol{R}_{SU}$ and $\boldsymbol{Q} = \boldsymbol{I} : \boldsymbol{R}_{SE}$, where the resistance functions $\boldsymbol{R}_{SU}$ and $\boldsymbol{R}_{SE}$ are regarded as the *complete* relations between particle kinematics and the stresslets, as we are not restricting the hydrodynamic stress to be traceless.

Under equilibrium conditions (when $\langle \boldsymbol{E} \rangle \equiv 0$) the osmotic pressure is given by the first two terms on the right-hand side of (4.24) which may be shown to give precisely the osmotic pressure defined thermodynamically in terms of the free energy or interparticle potential (Brady 1993). When a shear flow is applied, the suspension microstructure is distorted from its equilibrium isotropic form, and both the Brown-

ian, $nkT\langle\nabla\cdot\boldsymbol{A}\rangle$, and rate-of-strain, $n\langle\boldsymbol{B}\rangle : \langle\boldsymbol{E}\rangle$, contributions to the osmotic pressure are nonzero. When the amplitude of the shearing motion is small, the distortion of the structure is linear and proportional to $\langle\boldsymbol{E}\rangle$, which occurs to leading order in the Péclet number, $Pe = 6\pi\mu a^3\dot{\gamma}/kT$, where $\dot{\gamma} = |\langle\boldsymbol{E}\rangle|$, some measure of the rate of strain, for example the largest principal strain rate.

Although one might expect an $O(Pe)$ correction to the osmotic pressure, general considerations show that at equilibrium $\langle\boldsymbol{B}\rangle$ must be proportional to the isotropic tensor, which contracts with $\langle\boldsymbol{E}\rangle$ to give zero. (The trace of $\boldsymbol{E}$ is zero from the incompressibility of the material.) Thus, a nonzero, non-isotropic $\langle\boldsymbol{B}\rangle$ must be proportional to $\langle\boldsymbol{E}\rangle$, and hence proportional to Pe. Since the rate-of-strain contribution to the osmotic pressure is already proportional to $\langle\boldsymbol{E}\rangle$ (*cf.* (4.24)), it is $O(Pe^2)$. This $O(Pe^2)$ rate-of-strain contribution can be determined from the $O(Pe)$ deformation to the structure, which we now do for a dilute suspension of Brownian hard spheres.

In a similar way, the $O(Pe)$ deformation to the structure results in a contribution to $\langle\nabla\cdot\boldsymbol{A}\rangle$ that averages to the isotropic tensor times $\langle\boldsymbol{E}\rangle$, and this again gives zero. Presumably, the next term in the development of the deformation of the microstructure is $O(Pe^2)$ and this would then give a nonzero, $O(Pe^2)$, Brownian contribution to the osmotic pressure. Here we shall only calculate the $O(Pe)$ deformation to the microstructure and thus only the $O(Pe^2)$ rate-of-strain contribution to the osmotic pressure.

For a dilute suspension of Brownian hard spheres, Batchelor (1977) showed that it is sufficient to consider the interactions between only two particles alone in the fluid.

The relevant microstructural quantity is the pair-distribution function $g(\boldsymbol{r})$, which satisfies the following Smoluchowski equation:

$$\nabla \cdot \boldsymbol{D} \cdot \nabla g - Pe \nabla \cdot \boldsymbol{U} g = 0\,, \tag{4.27}$$

with

$$g \sim 1 \quad \text{as} \quad r \to \infty\,,$$

$$\boldsymbol{d} \cdot [\boldsymbol{D} \cdot \nabla g - Pe \cdot \boldsymbol{U} g] = 0 \quad at \quad r = 2\,.$$

Here, $\boldsymbol{D} = kT\boldsymbol{R}_{FU}^{-1}$ is the relative diffusivity of two particles and $\boldsymbol{U}$ is the relative velocity due to the imposed shear flow, $\boldsymbol{U} = \boldsymbol{R}_{FU}^{-1} \cdot \boldsymbol{R}_{FE} : \langle \boldsymbol{E} \rangle$. (Care must be taken to insure that the appropriate combinations of $\boldsymbol{R}_{FU}^{-1}$ etc. for two particles are taken to form the relative diffusivity and velocity in (4.27).) All lengths have been made dimensionless by the particle radius a, the velocity by $\dot{\gamma}a$, and the time by the diffusive time scale a^2/D_0, where $D_0 = kT/6\pi\mu a$ is the diffusivity of an isolated particle. The Péclet number in (4.27) measures the relative importance of shear and Brownian forces.

The equilibrium solution of (4.27) is the Boltzmann distribution

$$g_0 = 1\,,$$

to $O(\phi)$. The perturbation to the equilibrium structure will be linear in $\langle \boldsymbol{E} \rangle$ and

therefore we define, writing $\langle \boldsymbol{E} \rangle \equiv \dot{\gamma} \langle \hat{\boldsymbol{E}} \rangle$,

$$g = g_0 \left(1 - Pef(s) \tfrac{1}{2} \boldsymbol{d} \cdot \langle \hat{\boldsymbol{E}} \rangle \cdot \boldsymbol{d} \right) , \tag{4.28}$$

where, to leading order in Pe, f satisfies

$$\frac{d}{ds} \left(s^2 G \frac{df}{ds} \right) - 6Hf = -s^2 W , \tag{4.29}$$

with

$$G \frac{df}{ds} = 0 \quad \text{at} \quad s = 2, \quad \text{and} \quad f \to 0 \quad \text{as} \quad s \to \infty .$$

Here, G and H are the radial and tangential components of the relative diffusivity $\boldsymbol{D}$, and may be written in terms of the mobility functions relating velocity to force as

$$G(s) = x_{11}^a(s) - x_{12}^a(s),$$

$$H(s) = y_{11}^a(s) - y_{12}^a(s),$$

and W is defined by

$$\nabla \cdot \boldsymbol{U} = W(s) \left(\boldsymbol{d} \cdot \langle \hat{\boldsymbol{E}} \rangle \cdot \boldsymbol{d} \right) .$$

Batchelor (1977) wrote W in terms of two functions $\mathcal{A}$ and $\mathcal{B}$ (Batchelor & Green 1972) which relate the rate of strain to the axisymmetric and nonaxisymmetric motions, respectively, for a pair of particles (note that $\mathcal{A}$ and $\mathcal{B}$ are to be distinguished

from $\boldsymbol{A}$ and $\boldsymbol{B}$ of (4.25) and (4.26)):

$$W(s) = 3(\mathcal{B}(s) - \mathcal{A}(s)) - s\frac{d\mathcal{A}}{ds}.$$

For equal-sized spheres, the functions $\mathcal{A}$ and $\mathcal{B}$ may be expressed in terms of nondimensionalized (see Kim & Karrila 1991) resistance and mobility functions as

$$\mathcal{A}(s) = \frac{4}{s}(x^g_{11} - x^g_{12}) = \frac{4}{3s}(X^G_{11} - X^G_{12})(x^a_{11} - x^a_{12}),$$

and

$$\mathcal{B}(s) = \frac{8}{s}(y^g_{11} - y^g_{12}) = \frac{8}{s}\{\tfrac{1}{3}(y^a_{11} - y^a_{12})(Y^G_{11} - Y^G_{12}) - (y^b_{11} - y^b_{12})(Y^H_{11} + Y^H_{12})\},$$

with $x^g_{\alpha\beta}$ and $y^g_{\alpha\beta}$ the functions relating the stresslet on particle α to the force on particle β in the formulation of Kim & Mifflin (1985), $X^G_{\alpha\beta}$ and $Y^G_{\alpha\beta}$ the resistance functions relating force to rate of strain and so forth. Equation (4.29) was solved by Batchelor (1977) (a factor of 1/2 in (4.28) is included so the form agrees with that work) and we have repeated the calculation here in order to have numerical values of f for integration in (4.30) below. Note that f decays as s^{-3} for large s.

In the hydrodynamic contribution to the osmotic pressure for two spheres, $\boldsymbol{B}$ can be expressed as

$$\boldsymbol{B} = B(s)(\boldsymbol{dd} - \tfrac{1}{3}\boldsymbol{I}),$$

where

$$B(s) = \frac{8\pi a^3 \mu}{3}[(X_{11}^P - X_{12}^P)\frac{s\mathcal{A}(s)}{4} - (X_{11}^Q + X_{12}^Q)].$$

Since the perturbation to g is proportional to $\boldsymbol{dd}:\langle \boldsymbol{E} \rangle$, the angular integration implied in the ensemble average of $\boldsymbol{B}$ will result in a term proportional to $\langle \boldsymbol{E} \rangle : \langle \boldsymbol{E} \rangle$. When $B(s)$ is normalized with $8\pi a^3 \mu/3$ and the averaging is expressed as a probability integral over the pair-distribution function, we have

$$n\langle \boldsymbol{B} \rangle : \langle \boldsymbol{E} \rangle = -\frac{1}{15\pi}\frac{kT}{a^3} Pe^2 \phi^2 \int_2^\infty B(s) f(s) s^2 ds \langle \hat{\boldsymbol{E}} \rangle : \langle \hat{\boldsymbol{E}} \rangle . \tag{4.30}$$

Note that the integral in (4.30) is absolutely convergent as $f \sim s^{-3}$ and $B(s) \sim s^{-3}$ for large s; also, note that the integrand is finite at contact as the singularities in the P and Q functions cancel. Calculation of the integral gives

$$n\langle \boldsymbol{B} \rangle : \langle \boldsymbol{E} \rangle = \frac{2.1}{15\pi}\frac{kT}{a^3} Pe^2 \phi^2 \langle \hat{\boldsymbol{E}} \rangle : \langle \hat{\boldsymbol{E}} \rangle .$$

Alternatively, the result could be expressed as $0.84 Pe \phi^2 \mu \dot{\gamma} \langle \hat{\boldsymbol{E}} \rangle : \langle \hat{\boldsymbol{E}} \rangle$, corresponding to a hydrodynamic, rather than thermal, scaling of the stress. In Figure 4.3, the nondimensional $B(s)$ and the integral on the right hand side of (4.30) as a function of the upper limit of integration are plotted; the latter, labeled I, illustrates that the majority of the contribution is due to particles within two radii of the reference particle.

A brief consideration shows why the $\langle \boldsymbol{B} \rangle : \langle \boldsymbol{E} \rangle$ contribution is positive. Two particles approaching one another along the compressional axis in a straining flow

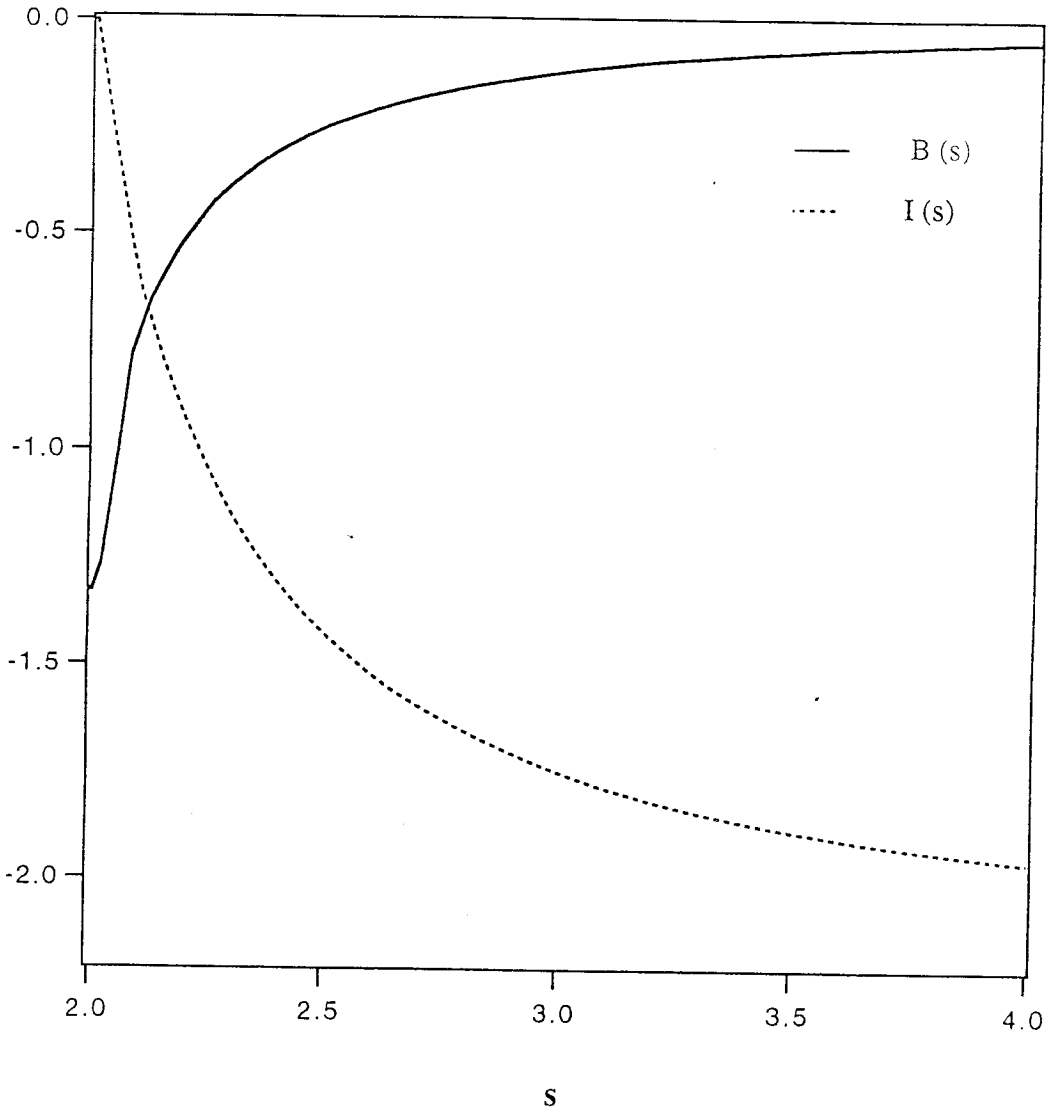

Figure 4.3: The function $B(s)$, solid line, and $\int_2^s r^2 f(r) B(r)\, dr$ from equation (4.30), dashed line labeled I, are plotted against dimensionless particle separation s. $B(s)$ has value -1.33 at $s = 2$ and the limiting value of I is -2.1.

must force fluid out of the intervening region, and the pressure moment for this interaction will be positive. For the case of two particles moving away from each other along an extensional axis, the moment is therefore negative, based on the reversibility of Stokes flow, and tangibly because fluid must be "sucked" into the region between the particles. The equilibrium structure is distorted by the weak straining, however, so that a second particle lies preferentially along the compressional axis relative to a reference particle, as will be seen from a study of the pair distribution (4.28). As a result, the average pressure from the interaction is positive.

4.7 Suspension pressure in a sheared lattice

In this second example, we show the behavior of the pressure as a function of particle volume fraction for a sheared simple cubic lattice of spheres. The volume fractions illustrated are: $\phi = 0.10, 0.30, 0.41$, and 0.45. For a suspension of force- and torque-free nonBrownian spheres, the suspension pressure is given by the rate-of-strain contribution in (4.24) only:

$$\Pi = \langle \boldsymbol{B} \rangle : \langle \boldsymbol{E} \rangle = \tfrac{1}{3} \langle \boldsymbol{P} \cdot \boldsymbol{R}_{FU}^{-1} \cdot \boldsymbol{R}_{FE} - \boldsymbol{Q} \rangle : \langle \boldsymbol{E} \rangle \,. \tag{4.31}$$

Equation (4.31) is the general form for the rate-of-strain pressure in any suspension, not just a periodic lattice. For a random suspension, for example that given by a hard-sphere microstructure, $\langle \boldsymbol{B} \rangle = \alpha(\phi)\boldsymbol{I}$, with $\boldsymbol{I}$ the isotropic tensor, and this contracts with $\langle \boldsymbol{E} \rangle$ to give zero. For an undeformed simple cubic lattice, $\langle \boldsymbol{B} \rangle$ is also

proportional to $\boldsymbol{I}$ and there is no pressure. When the lattice is sheared along one of the lattice vectors, however, the instantaneous lattice is not simple cubic, but rather rhombohedral, and there is a nonzero pressure. As the lattice structure periodically repeats itself, the pressure must return to zero in one period. For small ϕ, this occurs by the pressure taking positive values in the first half of the cycle and then negative values for the second half, as shown in Figure 4.4 for $\phi = 0.10$ and $\phi = 0.30$. The curves are antisymmetric about the midpoint of the cycle. At larger volume fractions, the values are seen to begin negative as the lattice is sheared away from registry; the curve is always antisymmetric about the midpoint of the cycle. This change of sign in the trace of the first moment as the particle fraction is increased may possibly be related to the negative second order coefficient in the series expansion in ϕ of the viscosity for a simple cubic lattice (Nunan & Keller 1984). We see the pressure increases with volume fraction as expected (the pressure is $O(\phi^2)$ at low ϕ; we have plotted the instantaneous value of the pressure moment for a chosen particle, so the dependence on ϕ is linear), although the change in sign at incipient strain at around $\phi = 0.41$ leads to small values of the pressure for volume fractions near $\phi = 0.41$.

The procedure used to calculate the pressure interactions for the lattice structure involves an accounting for near- and far-field interactions essentially equivalent to that used in the Stokesian Dynamics method for evaluating the grand resistance tensor (Brady & Bossis 1988). Expanding the force density as a series of moments about the particle centers in the integral formulation for the pressure (Kim & Karrila 1991, Ladyzhenskaya 1963), a "far-field" estimate for the pressure at the particle

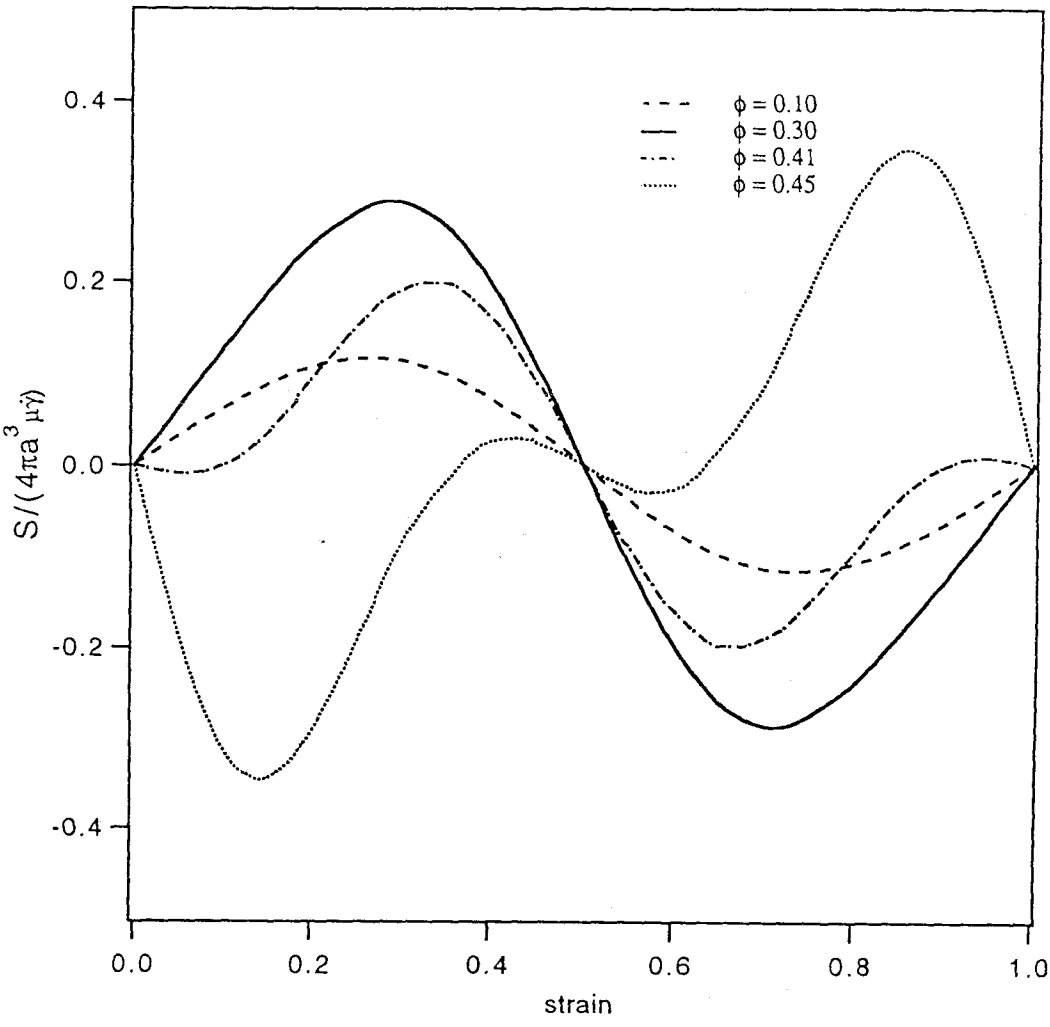

Figure 4.4: Values of the trace of the first moment of the force distribution upon a sphere (of radius a) are plotted as a function of total strain for an initially simple cubic lattice undergoing simple shear at shear rate $\dot{\gamma}$ in fluid of viscosity μ; the motion is along a lattice vector. Volume fractions shown are $\phi = 0.10$, 0.30, 0.41, and 0.45. The lattice is at registry at zero strain and returns to registry first at a strain of unity. The trace is identically zero at registry and the midpoint of the cycle. The values are antisymmetric about the midpoint, and hence average to zero for a cycle; note the change of sign with incipient strain occurring near $\phi \doteq 0.41$.

of interest due to the moments on the other particles is calculated. We truncate the moment expansion at the level of the stresslet, which is calculated by Stokesian Dynamics. When the interparticle distance is small, there is significant error in this approximation. For close pairs, the resistance functions $\boldsymbol{P}$ and $\boldsymbol{Q}$ reported here are used to calculate the trace for the particles as prescribed by (4.3); in the flow of the lattice, there is no deviation of particle velocities from the bulk flow, so only $\boldsymbol{Q}$:$\boldsymbol{E}$ contributes. The contributions to the pressure at a reference sphere by all neighbors within a distance $s = 4$ are calculated in this manner ($s = 4$ being an arbitrary choice), and are added to the far-field estimate. For close pairs, this double counts that portion of the near-field interaction which is captured by the truncated moment expansion. The leading error in the moment expansion is due to neglect of the change to the pressure environment of a reference sphere by the induced quadrupole upon a neighboring sphere, which behaves as s^{-8}. Hence, we subtract from the sum the terms in the resistance formulation of $O(s^{-7})$ and larger. It should be noted that the pressure environment experienced by a particle due to the stresslet on a second particle behaves as s^{-3}, with s the separation distance; the interactions would be nonconvergent if simply summed pairwise. Thus, the method of O'Brien (1979) for renormalization of nonconvergent hydrodynamic interactions is applied, with Ewald summation employed to speed convergence of the resulting expression (see Beenakker 1986).

4.8 Concluding remarks

The functions presented here make it possible to calculate the isotropic stress associated with rigid particle interactions in low-Reynolds-number flow. As the examples in the preceding sections illustrate, the functions may be applied in either analytical or computational contexts. These examples were restricted to systems where the particle phase was under the influence of hydrodynamic and Brownian forces only. In general, suspensions with interparticle forces (electrostatic, for example) will have a stress contribution associated with these forces. Hence, (4.21) will be replaced by

$$\langle \boldsymbol{\Sigma} \rangle = -nkT\boldsymbol{I} + 2\mu\langle \boldsymbol{E} \rangle + n[\langle \boldsymbol{S}^E \rangle + \langle \boldsymbol{S}^B \rangle + \langle \boldsymbol{S}^P \rangle], \tag{4.32}$$

with

$$\langle \boldsymbol{S}^P \rangle = -\langle (\boldsymbol{R}_{SU} \cdot \boldsymbol{R}_{FU}^{-1} + x\boldsymbol{I}) \cdot \boldsymbol{F}^P \rangle,$$

where $\boldsymbol{F}^P$ is the total nonhydrodynamic force exerted by the other particles upon the reference particle. The suspension pressure, mechanically defined to be negative one third of the trace of the bulk stress, for a system with hydrodynamic, Brownian, and specific interparticle forces is

$$\Pi = nkT + nkT\langle \nabla \cdot \boldsymbol{A} \rangle + n\langle \boldsymbol{x} \cdot \boldsymbol{F}^P \rangle + n\langle \boldsymbol{B} \rangle : \langle \boldsymbol{E} \rangle + n\langle \boldsymbol{A} \cdot \boldsymbol{F}^P \rangle, \tag{4.33}$$

with (4.25) and (4.26) for $\boldsymbol{A}$ and $\boldsymbol{B}$. The $n\langle \boldsymbol{x} \cdot \boldsymbol{F}^P \rangle$ term is the familiar xF^P pressure just as found in molecular systems, and the last two terms are the contributions from

hydrodynamics.

Efforts to model two-phase flow have made use of the concept of "particle phase pressure." This quantity has not, to date, been placed on firm footing for viscously dominated suspensions; authors have given heuristic arguments for the scaling of the pressure with respect to system parameters (Jenkins & McTigue 1990) or have stated that the particle interactions give rise to a positive pressure (Batchelor 1988), without apparent justification. With the functions presented here, the pressure interactions of suspended particles in Stokes flow may be calculated. The roles of the strain rate and particle velocities are made clear as is the fact that an induced pressure requires at least two particles. This work will, it is hoped, provide a means for rational investigation of the role of the particle phase pressure in macroscopic models of two-phase flow.

Chapter 5

Pressure-driven flow of a suspension: buoyancy effects

Abstract

Dynamic simulation of pressure-driven flow of a nonneutrally-buoyant suspension has been performed by Stokesian Dynamics. Channel flow at zero Reynolds number of a monodisperse nonBrownian suspension of spheres in a monolayer was studied for a range of three parameters: bulk particle areal fraction, ϕ_A^b, dimensionless gravitational parameter, $B = (U^0/\langle u \rangle)(H/a)^2$, and dimensionless channel width H/a. Here, U^0 is the Stokes settling velocity of an isolated sphere, $\langle u \rangle$ is the mean velocity of the suspension, H is the channel width, and a is the particle radius. From an initially uniform distribution, a range of behavior in the fully-developed flow is observed depending upon the value of B. For small B, shear-induced migration dominates buoyancy effects, and a layer at large ϕ_A is formed in the center of the channel. For sufficiently strong gravitation, particles settle rapidly to form a concentrated layer which is transported along the bottom of the channel by shearing. At intermediate values of B, shear-induced migration of particles to the center of the channel occurs simultaneously with gravitational settling. In the lower portion of the channel, these fluxes are opposed and lead to nonmonotonic variation of particle fraction, with ϕ_A increasing away from the lower wall to a maximum near or even above the centerline and then rapidly decreasing, typically vanishing to leave clear fluid adjacent to the upper wall. These results are in qualitative agreement with the small amount of experimental data in the literature on such systems. The flow has been modeled using macroscopic balance equations presented by Nott & Brady (1994) to determine ϕ_A, $\langle u \rangle$, and T. The predictions of the model agree well with simulations of the flow.

5.1 Introduction

Flowing suspensions are found in many natural and applied settings. In the design of processes involving suspensions, the variety of rheological responses of suspensions presents a number of challenges. Dependence of the viscosity and other rheological coefficients upon the particle volume fraction ϕ is strong, and even suspensions with weak interparticle forces and weak Brownian motion exhibit nonNewtonian behavior, including normal stress differences (Gadala-Maria 1979) and time-dependent viscosity (Gadala-Maria & Acrivos 1980). These rheological phenomena relevant in a suspension at homogeneous conditions are compounded in inhomogeneously-sheared suspensions by shear-induced particle migration, first investigated in detail by Leighton & Acrivos (1987*b*). This irreversible migration of noncolloidal particles from regions of high shear rate to low can result in very nonuniform particle concentration fields, and the pervasiveness of inhomogeneous flows in processes—pipe flow is the obvious and most important example—makes it an issue of importance for process design. If particles and fluid are not of the same density, settling (or rising) occurs simultaneously with shear-induced particle migration in an inhomogeneous flow, and the bulk flow thus depends upon the relative strength of the buoyancy forces to shearing forces.

This work has a dual purpose. The first is to provide basic information about the influence of particle buoyancy in inhomogeneous suspension flow, and the second is to test the suspension-flow model presented by Nott & Brady (1994) (hereafter referred to as NB) in a flow which includes buoyancy. The specific flow we have investigated is the pressure-driven flow of a suspension of heavy particles in a channel (there

is no loss of generality in assuming the particles more dense than the fluid). The flow was simulated by Stokesian Dynamics over a range of the relevant dimensionless parameters, which are the bulk particle areal fraction ϕ_A^b (ϕ_A^b appears rather than bulk volume fraction ϕ^b because we simulate flow in a monolayer), the ratio of channel width to particle size H/a, and $B = (U^0/\langle u \rangle)(H/a)^2$, where U^0 is the Stokes settling velocity of an isolated particle and $\langle u \rangle$ is the average velocity of the suspension; B characterizes the relative strength of buoyancy to viscous shearing effects. The model equations were solved to obtain predictions of the fully-developed flow for similar ranges of the parameters. We will see that the agreement between the simulation results and model predictions is good over a range of B, thus validating the model for a range of flow conditions which had previously not been considered. There is little experimental work that is directly comparable with our simulations of channel flow. While there is no replacement for physical experiments, confidence that the simulation results represent realistic behavior is well-founded: Stokesian Dynamics simulations by Phung (1993) yield excellent agreement for the suspension viscosity determined experimentally by van der Werff (1990); simulations by Bossis & Brady (1984) and Phung (1993) find particle microstructure in good qualitative agreement with that determined in experiments by Parsi & Gadala-Maria (1987). For pressure-driven flow, there is good qualitative agreement between the simulations of NB and the experiments by Koh, Hookham & Leal (1994).

An interesting and rather unusual density stratification occurs as the result of the competition between buoyancy forces and shear-induced migration in a pressure-

driven flow. It is found that relatively heavy material flows stably above lighter, despite constant fluctuations. A density stratification of this sort is illustrated by Figure 5.1, reproduced in adapted form from Altobelli, Givler & Fukushima (1991), a study in which nuclear magnetic resonance (NMR) imaging of the velocity and particle fraction in pressure-driven tube flow was performed. Shear-induced migration results in a maximum in ϕ near the center of the tube, similar to the results of the experiments by Koh *et al.* (1994). The results of this work are particularly interesting, however, because of the difference between the particle density*, $\rho_p = 1.03$ g cm^{-3}, and the fluid density, $\rho_f = 0.88$ g cm^{-3}. Thus, the suspension of large ϕ near the center of the tube is in fact *denser* than the more dilute material below. In work we discuss below, Zhang & Acrivos (1994) have modeled the flow in the experiments of Altobelli *et al.* (1991) showing that the volume-fraction profiles of Figure 5.1 can be explained by the balance of shear-induced migration and gravitational settling, and their model also predicts a nonaxial mean secondary flow. Our simulations demonstrate that a density stratification similar to that found by Altobelli *et al.* (1991) occurs in channel flow with heavy particles over a range of ϕ_A^b and B.

The flow in the present study may be described as one of a class of viscous resuspension phenomena, which have provided motivation for suspension-flow modeling. In resuspension, a settled layer of heavy particles expands in height and flows due to a shear flow over the layer. Resuspension phenomena at large Reynolds numbers, such as those which transport sand and silt in surf zones, are well-known. In

*Other experimental parameters included mean particle diameter, 0.762 mm; bulk particle volume fraction 0.4; fluid viscosity, 3.84 Poise, average velocity, 7.05 cm s^{-1}; and inner diameter of the tube, 2.54 cm.

contrast to these inertially-dominated phenomena, viscous resuspension occurs at small Reynolds number where inertia has negligible influence. Leighton & Acrivos (1986) showed that the steady-state height of a viscously-suspended layer could be estimated from a balance between the gravitational settling and a Fickian diffusive flux of particles to regions of smaller ϕ. The particles were assumed to be too large for Brownian diffusion to play a significant role, hence the diffusivity of this model is the shear-induced diffusivity driven by hydrodynamic interactions. This gradient- or collective-diffusivity is to be distinguished from the closely related shear-induced self-diffusivity first recognized and studied by Eckstein, Bailey & Shapiro (1977).

Leighton & Acrivos (1987*a*) improved the experimental technique of Eckstein *et al.* (1977), and showed that cross-stream migration of particles could be phenomenologically related to fluxes that were caused by gradients in both shear rate, $\dot{\gamma}$, and ϕ (Leighton & Acrivos 1987*b*). This "diffusive flux" phenomenology was used by Schaflinger, Zhang & Acrivos (1990) in modeling a suspension of dense particles in shear and pressure-driven channel flow, but these authors included only the particle flux due to $\nabla\phi$. The model showed some success, but for pressure-driven flow the model predicted that all particles would lie below the velocity maximum, a result which is sharply contradicted by the simulations of the present study. Because the the cross-stream flux at the maximum in velocity (*i.e.*, where $\dot{\gamma} = 0$) is solely gravitational settling, the particles must be predicted to lie below the velocity maximum in the fully-developed channel flow. Phillips *et al.* (1992) used the diffusive-flux model, including also the flux of particles due to $\nabla\dot{\gamma}$ to successfully predict both rates of

variation and steady-state values for ϕ in inhomogeneous shear flows. However, there was a notable discrepancy from experimental results for pressure-driven flow, as the model predicted that, regardless of the bulk particle fraction, ϕ would take on a cusp-like maximum with $\phi = \phi_m$ at the location of the velocity maximum, where ϕ_m is the maximum packing fraction.

More recent modeling of the pressure-driven tube flow with heavy particles by Zhang & Acrivos (1994), including fluxes of particles due to $\nabla\dot{\gamma}$ and $\nabla\phi$ as well as gravitational settling, shows excellent agreement with the experiments of Altobelli *et al.* (1991). One might argue, based on this agreement, that the model will predict the profiles of ϕ we observe in channel flow, with particles above the velocity maximum. This argument is, however, difficult to justify because a study of the model for this flow shows it would require a cross-stream flux proportional to $\nabla\dot{\gamma}$ to balance the gravity-driven flux where $\dot{\gamma} = 0$; the same mechanism that drives a flux toward the velocity maximum to yield the aphysical cusp of Phillips *et al.* (1992) would now have to drive particles away from this point. While resuspension in tube flow is more complicated than in channel flow, $\dot{\gamma} = 0$ in channel flow for all points at some height, and it is therefore a more stringent test of basic aspects of a flow model. The flux balance in the fully-developed channel flow is one-dimensional and the excess weight of the relatively dense suspension at the center of the channel must be supported by a stress variation directly related to the shear-induced migration. Thus the manner in which migration is incorporated into the model is thus isolated for scrutiny. The success of Zhang & Acrivos (1994) in modeling tube flow may be due to the three-

dimensional nature of the flow as azimuthal circulation is induced by the density stratification.

The failure of the diffusive-flux model at points where the shear rate vanishes, in particular the aphysical prediction of a cusplike maximum in pressure-driven flow, prompted NB to model the particle pressure, Π, in terms of the suspension temperature, T, rather than in terms of $\dot{\gamma}$, where $T = \langle \boldsymbol{u}' \cdot \boldsymbol{u}' \rangle_p$ (defined pointwise) is the mean square of the scalar particle velocity fluctuations[†]. Following Jenkins & McTigue (1990), NB assert that Π is proportional to $\sqrt{T}$. This modeling is based upon the low-Reynolds-number hydrodynamic resistance functions relating the pressure moments on spheres to the particle and bulk motions determined by Jeffrey, Morris & Brady (1993). Although in principle a rigorous theory of the nonlocality could perhaps be developed, NB showed that a balance equation for T including diffusive transport may be deduced from the equation for the rate of dissipation of energy in the suspension. Judging from the results of its application, this simple means of capturing the nonlocal dependence of the normal stresses on $\dot{\gamma}$ appears to be sound. In brief, the model asserts that T is generated at points where $\dot{\gamma}$ is large and is transported diffusively if not spatially constant, and the constitutive relation of the *pi* to $\sqrt{T}$ renders the stress nonlocal in $\dot{\gamma}$.

We have simulated the pressure-driven flow of a suspension over a range of B to assess the dependence of the flow behavior upon the relative strength of settling to shear-induced migration. With respect to B, a wide range of behavior is observed,

[†]There is no potential for confusion of the meaning of the symbol T here, as the particles are assumed nonBrownian and the absolute temperature is never considered.

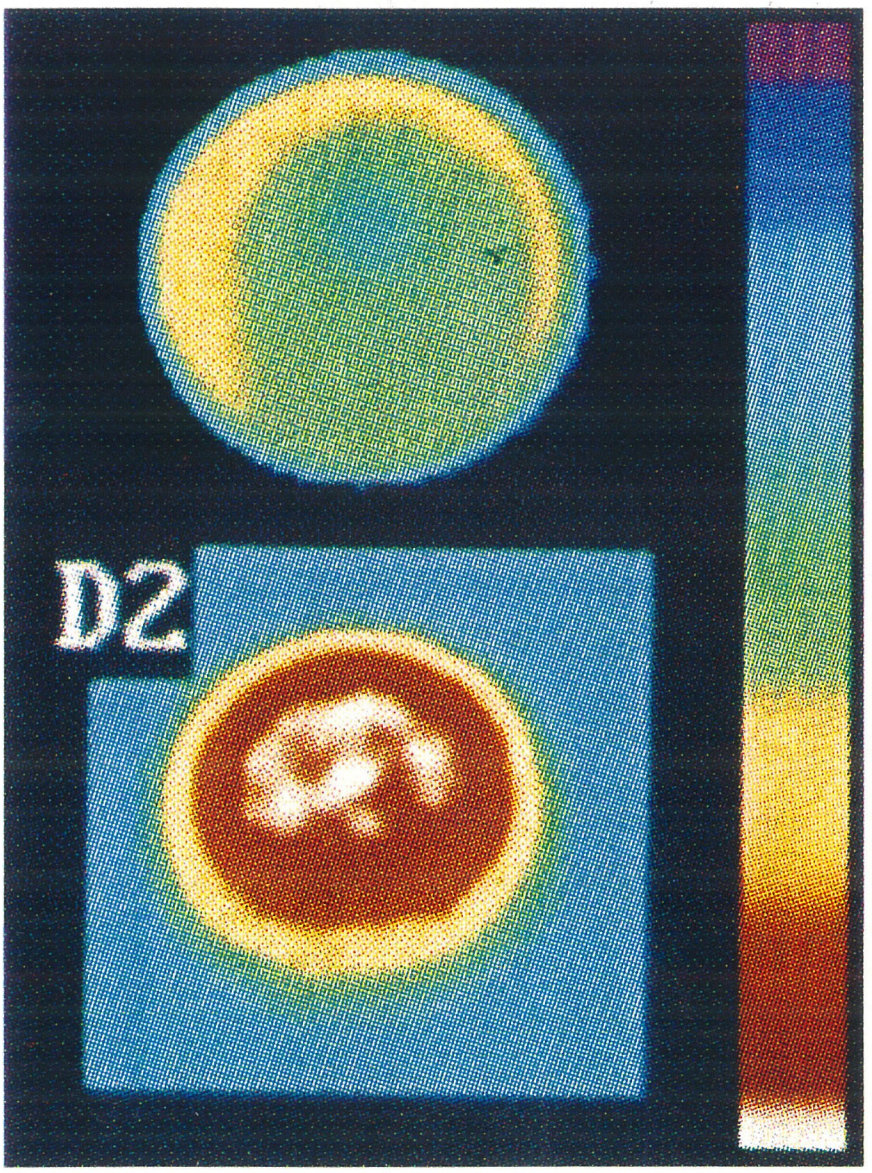

Figure 5.1: Reproduction from Altobelli, Givler & Fukushima (1991) of false-color images from NMR imaging of pressure-driven tube flow of a suspension of heavy particles at an average particle volume fraction of $\phi = 0.4$. The particle fraction is represented by the upper image and the velocity by the lower image, with the scale at right used for both: particle fraction increases and velocity decreases in the vertical.

from the neutrally-buoyant suspension ($B = 0$), in which a highly-concentrated layer of particles forms at the center of the channel, to the formation of a settled layer of particles which are transported along the bottom of the the channel by shear for sufficiently large B, with the value at which a shear layer occurs for $\phi_A^b = 0.4$ being $B \approx 20$. At small and intermediate B, a stable flow of heavy material over light like that illustrated by Figure 5.1 occurs; this is observed even for $B > 15$ at $\phi_A^b = 0.4$, and for larger B at higher ϕ_A^b. The bulk flow depends strongly upon ϕ_A^b: for small ϕ_A^b at a fixed B, the buoyancy is much more important relative to shear-induced migration than at larger concentrations. At fixed B and ϕ_A^b, the velocity and particle fraction profiles are essentially identical at $H/a = 18.32$ and $H/a = 30.54$. Therefore, fixing B effectively yields dynamic similarity for flows of the same suspension (the same ϕ_A^b) at different channel widths; the residual influence of H/a is weak, with the primary effect being that T is larger in the center of the channel for narrower channels due to the strong influence of the walls. Over a wide range of conditions, the suspension balance model successfully predicts the behavior observed in simulations. providing confidence that the modeling is sound, and the constitutive relations capture dependence on ϕ correctly.

We begin in §5.2 by presenting a basic scaling analysis of the flow of interest. In §5.3, application of Stokesian Dynamics to this flow is discussed and the simulation results are presented. Predictions of the flow behavior by the model are compared with simulation results in §5.4, followed by a summary and discussion.

5.2 Scaling analysis

We consider pressure-driven flow at vanishing Reynolds number of a nonBrownian suspension of spheres in Newtonian fluid. The particles are of equal or greater density than the fluid, and interact both hydrodynamically and through repulsive interparticle forces, the latter vanishing at surface separations much smaller than the particle size. The inhomogeneous shear rate in pressure-driven flow causes particle migration to the center of the channel, while the particles to settle. For an initially uniform particle fraction flowing in an arbitrarily long tube, which is the situation in our simulations, variations in the streamwise direction vanish on average, and the ϕ profile evolves in time in a manner which depends on the relative strength of shear-driven to buoyancy-driven fluxes.

An estimate of the timescale for bulk evolution of the particle fraction is useful for experimental and applicational purposes. When buoyancy forces is negligible, the fully-developed flow of an inertialess noncolloidal suspension is independent of the flowrate, and it is lengths or strains, rather than times, which are relevant. Under these conditions, NB showed (using an argument due to Leighton & Acrivos 1987*b*) that fully-developed pressure-driven channel flow should be expected only after a distance of $O[(H/a)^2 H]$. The argument holds that particles migrate a distance of $O(H)$ by a random-walk process characterized by the shear-induced self-diffusivity (Eckstein *et al.* 1977) which scales, on dimensional grounds, as $\dot{\gamma} a^2 \mathcal{D}(\phi)$, where $\mathcal{D}$ is a dimensionless function. Diffusive motion of lengthscale H occurs in a time $H^2/(\dot{\gamma} a^2 \mathcal{D})$, while $\dot{\gamma} H$ is a representative velocity scale, and the product of these time and velocity

scales yields the flowrate-independent $(H/a)^2 H/\mathcal{D}$ as an estimate of the development length. For $\phi > 0.3$, $\mathcal{D} \approx 0.1$ from the experiments of Leighton & Acrivos 1987*a* and Stokesian Dynamics simulations of Phung (1993). When particle buoyancy is relevant to the flow behavior, the estimate of NB for a neutrally-buoyant suspension serves as an upper limit on the lengthscale for evolution of ϕ. The rate of development is understandably more rapid for very dense particles as settling dominates the migration process.

We define a dimensionless parameter B characterizing the relative strength of buoyancy to shearing forces as the ratio of the times for a particle to diffuse and to settle a distance of $O(H)$. A shear-driven random walk of $O(H)$ takes a time of $O(H^2/\dot{\gamma}a^2) = O(H/\langle u \rangle a^2)$, with $\dot{\gamma} = \langle u \rangle / H$, while Stokes settling velocity yields an estimate of H/U^0 for the settling time, and thus

$$B \equiv \left(\frac{U^0}{\langle u \rangle}\right)\left(\frac{H}{a}\right)^2 . \tag{5.1}$$

The Stokes settling velocity is $U^0 = 2(\rho_p - \rho_f)ga^2/9\eta$ with $g = |\boldsymbol{g}|$ the magnitude of the gravitational acceleration, so that B may also be written

$$B = \frac{2(\rho_p - \rho_f)gH^2}{9\eta\langle u \rangle} = O\left(\frac{(\rho_p - \rho_f)g}{\nabla p}\right).$$

Note that B is inversely proportional to the Shields parameter κ that was used by Schaflinger *et al.* (1990).

The parameters B, bulk particle fraction ϕ^b, and dimensionless channel width

H/a characterize the channel flow of a suspension. The bulk particle areal fraction ϕ_A^b is often used in this work, because we simulate suspension flow in a monolayer, and a simple rescaling discussed in §5.4 allows constitutive relations developed for the three-dimensional description to be applied to a monolayer. Interparticle forces are neglected in the dimensional analysis, because NB showed the range—the surface-to-surface distance, ϵ, at which the force becomes negligible—of the forces has no discernible effect upon the suspension flow, provided $0 < \epsilon/a \ll 1$. As discussed in §5.3, repulsive interparticle forces do inhibit hydrodynamic clustering and influence flow behavior.

We note that at the particle fraction of $\phi_A^b = 0.4$, gravity has a scarcely discernible influence upon suspensions with $B < 1$, while at the other extreme, $B = 20$ represents an upper limit of the range of interesting behavior, as the particles settle into an ordered layer along the lower wall of the channel for $B > 20$. In general as ϕ_A^b is reduced, a given value of B has a larger influence, because the resuspension of particles depends on two-particle interactions which scale as ϕ_A^2.

Consideration of the influence of shear-induced particle migration shows that a density stratification with heavy material over light is to be expected. In a neutrally-buoyant suspension, particles migrate to the center of the channel where $\dot{\gamma}$ is small. If ρ_p increases by a small fraction, the immediate and correct expectation is that the ϕ profile will be slightly perturbed and the concentrated suspension at the center of the channel will therefore be denser than the dilute material below. Were this not the case, the condition of neutral buoyancy would be unstable and therefore probably

unobservable.

5.3 Simulation

Stokesian Dynamics simulations of pressure-driven channel flow were performed for a range of ϕ_A^b and B, at two values of H/a. Complete descriptions of Stokesian Dynamics are given by Brady, Phillips, Lester & Bossis (1988) and by Brady & Bossis (1988), while the application of the method to pressure-driven flow was demonstrated by NB, so we present only a brief treatment of the method before turning to the simulation results.

5.3.1 Simulation method

The Stokesian Dynamics method for simulation of suspension flow is based upon the solution of two-sphere problems at low Reynolds number, yet captures important aspects of the many-body nature of hydrodynamic interactions. This is possible because hydrodynamic interactions may be decomposed into short-ranged lubrication interactions and long-ranged mobility interactions. Mobility interactions are computed as an expansion in moments about the particles' centers of the hydrodynamic force density exerted on their surfaces. In application, the expansion must be truncated. We truncate after the first moment, where the zeroth moment is the net force on a particle, and the first moment consists of the antisymmetric torque and the symmetric stresslet. Faxén's laws (Kim & Karrila 1991) for the motion of a particle in given velocity fields are used along with the moment expansion to construct the grand

mobility tensor $\mathcal{M}^{\infty}$. To simulate a medium of infinite extent, a unit cell containing a finite number of particles is periodically replicated throughout space. Interactions between all particles are summed, with Ewald's summation technique (Beenakker 1986) used to speed convergence. The grand mobility tensor is inverted to give a far-field approximation, $\mathcal{R}^{\infty} = (\mathcal{M}^{\infty})^{-1}$, of the grand resistance tensor $\mathcal{R}$. It is in this inversion that many-body interactions are incorporated: while the construction of $\mathcal{M}^{\infty}$ was performed pairwise, the inversion sums the series of reflected interactions between all particles. Near-field lubrication interactions are added to the grand resistance tensor in pairwise fashion, with the portion of the near-field interaction captured by the far-field approximation subtracted to avoid double-counting, thus yielding the grand resistance tensor $\mathcal{R}$. Note that $\mathcal{R}$ is a function only of the particle configuration.

The hydrodynamic forces, torques, and stresslets on the N particles in the unit cell are related through $\mathcal{R}$ to the particle velocity fluctuations and the average rate of strain by

$$\begin{pmatrix} \boldsymbol{F} \\ \boldsymbol{S} \end{pmatrix} = -\mathcal{R} \cdot \begin{pmatrix} \boldsymbol{u} - \langle \boldsymbol{u} \rangle \\ -\langle \boldsymbol{e} \rangle \end{pmatrix}, \tag{5.2}$$

where

$$\mathcal{R} = \begin{bmatrix} \boldsymbol{R}_{FU} & \boldsymbol{R}_{FE} \\ \boldsymbol{R}_{SU} & \boldsymbol{R}_{SE} \end{bmatrix}. \tag{5.3}$$

In equation (5.2), $\boldsymbol{u}$ is the $6N$ vector of particle velocities (translational and rotational); $\langle \boldsymbol{u} \rangle$ and $\langle \boldsymbol{e} \rangle$ are the average velocity and the average rate of strain, respectively, of the bulk suspension; $\boldsymbol{F}$ is the vector of hydrodynamic forces and torques and $\boldsymbol{S}$ is the N-particle stresslet exerted by the fluid on the particles. Couplings in

(5.3) are indicated by subscripts: $\boldsymbol{R}_{FU}$ is the resistance tensor coupling force/torque to velocity, $\boldsymbol{R}_{SE}$ is the tensor coupling the stresslet to rate of strain, and the others are clear from these.

Simulation of pressure-driven flow requires simulating a boundary. This can be done either through a numerical approximation of a flat wall as discretized flat patches (Durlofsky & Brady 1987) or by allowing a group of the N particles, say N_w, to mimic a wall by moving together at a fixed velocity. The latter method is simpler because the hydrodynamic interaction between a "wall" particle and a suspended "interior" particle is no different from that between two suspended particles, whereas in the flat-wall approach the interaction of a sphere with the wall must be numerically approximated. Despite the simplicity, this method was shown by NB to capture the essential physical features of the flow and is used here. The N particles are divided into the N_w which make up the wall, and the remaining $N_i = N - N_w$ suspended particles. The unit cell is schematically illustrated (along with the wall particles of a neighboring image cell) in Figure 5.2. The wall particles are constrained to move at a prescribed velocity, while the interior particles move freely in the x- and y-directions in such a way that the net force (hydrodynamic plus nonhydrodynamic) on each is zero in accordance with inertialess flow. The quantities to be determined are thus the forces on the wall particles and the velocities of the interior particles. The bulk strain rate $\langle \boldsymbol{e} \rangle$ is set to zero, and the average suspension velocity $\langle \boldsymbol{u} \rangle$ is prescribed; a pressure gradient is established to drive the flow, and this pressure gradient balances the force necessary to maintain the wall particle velocities, thus

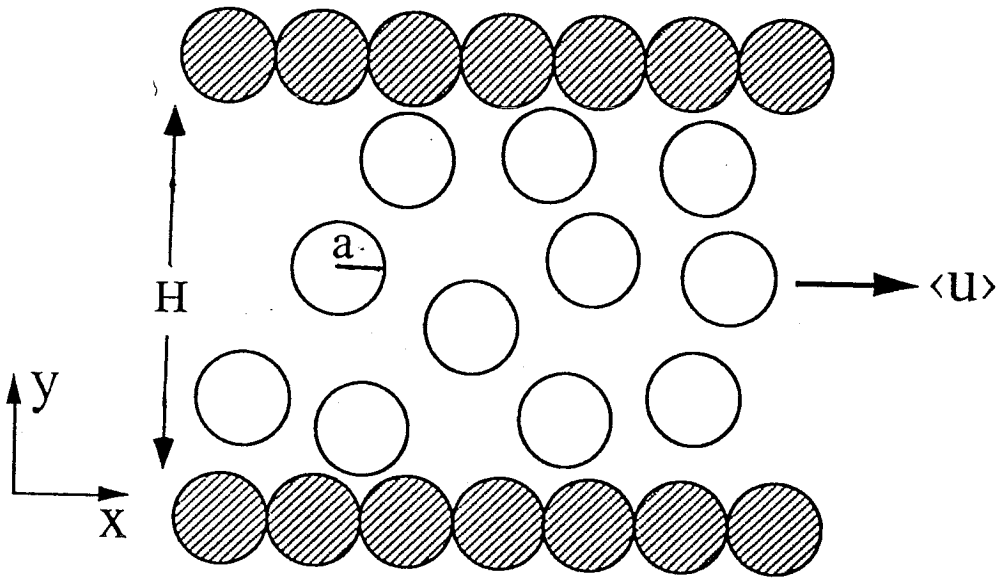

Figure 5.2: Schematic representation of the unit cell employed in the simulation of a pressure-driven channel flow of nonneutrally buoyant particles. The shaded wall particles are fixed while the unshaded interior particles are free to move in the x-y plane. Gravity acts in the negative y-direction. Only the particles of one wall are within the unit cell: the second wall is included for appearance.

satisfying the requirement of the overall momentum balance that the net force upon the unit cell vanish. Buoyancy is incorporated by exerting a constant force $\boldsymbol{F}_g$ upon each particle. Pairwise interparticle forces, denoted $\boldsymbol{F}_{IP}$, are also included, and these are discussed further below.

Fixing the wall velocity at zero, the equation of motion for the particles is

$$\begin{pmatrix} \boldsymbol{F}^w \\ \boldsymbol{F}^i \end{pmatrix} = \begin{pmatrix} \boldsymbol{F}^w \\ 0 \end{pmatrix} = - \begin{bmatrix} \boldsymbol{R}^{ww}_{FU} & \boldsymbol{R}^{wi}_{FU} \\ \boldsymbol{R}^{iw}_{FU} & \boldsymbol{R}^{ii}_{FU} \end{bmatrix} \cdot \begin{pmatrix} -\langle \boldsymbol{u} \rangle \\ \boldsymbol{u}^i - \langle \boldsymbol{u} \rangle \end{pmatrix} + \begin{pmatrix} \boldsymbol{F}^w_{IP} \\ \boldsymbol{F}^i_{IP} \end{pmatrix} + \begin{pmatrix} 0 \\ \boldsymbol{F}_g \end{pmatrix}. \tag{5.4}$$

We have decomposed $\boldsymbol{R}_{FU}$, denoting couplings by superscripts: $\boldsymbol{R}^{ww}$ is the resistance tensor denoting the interaction among wall particles, $\boldsymbol{R}^{wi}$ denotes the interaction of wall with interior particles, and so forth. Solving (5.4) for the suspended particle velocities yields

$$\frac{d\boldsymbol{x}^i}{dt} = \boldsymbol{u}^i = \langle \boldsymbol{u} \rangle + (\boldsymbol{R}^{ii}_{FU})^{-1} \cdot (\boldsymbol{R}^{iw}_{FU} \cdot \langle \boldsymbol{u} \rangle + \boldsymbol{F}^i_{IP} + \boldsymbol{F}_g), \tag{5.5}$$

where $\boldsymbol{x}^i$ is the N_i-particle position vector. Having constructed the resistance tensor, the positions are updated using (5.5) and the procedure is repeated. The near-field lubrication portion of the resistance tensor varies significantly for small relative motions of the particles, and is updated at each step in the evolution, whereas the far-field approximation obtained as the mobility invert $\mathcal{R}^{\infty}$ changes significantly only for relative motions of neighboring particles on the order of the particle size and is updated less frequently.

The set of ordinary differential equations (5.5) is completely coupled in the sense

that the motion of any particle depends upon the position of all other particles in the unit cell. Hydrodynamic interactions are nonlinear in particle position, and thus, as pointed out by NB, these equations exhibit deterministic chaos which leads readily to irreversible behavior.

Interparticle forces

Repulsive interparticle forces influence the bulk flow rather dramatically, apparently through disruption of the development of clusters of particles. Yet the range of these forces has essentially no influence, provided the range remains small relative to the particle size. In the simulations, pairwise repulsive forces are incorporated with the force on particle α due to particle β given by

$$\boldsymbol{F}_{\alpha\beta} = F_0 \frac{\tau e^{-\tau\epsilon}}{1 - e^{-\tau\epsilon}} \boldsymbol{d}_{\alpha\beta}, \tag{5.6}$$

where $\epsilon = r/a - 2$ is the dimensionless distance between the sphere surfaces, and $\boldsymbol{d}_{\alpha\beta}$ is the unit vector directed from sphere α to sphere β. The parameter τ determines the range of the force, while the product $F_0\tau$ fixes the strength. This interparticle force was used in the simulations of NB, who observed essentially identical results for the rate of particle migration and the eventual steady state as τ varied from 100 to 10^4. In the absence of repulsive forces ($\tau \to \infty$), however, clusters of particles formed which spanned the channel, thus disrupting smooth shearing and altering the migration process. Here, we also find that repulsive forces have a qualitative influence on the flow, as illustrated by the results of simulations with interparticle forces ($\tau = 1000$

and $F_0\tau = 0.6$) and without at $\phi_A^b = 0.4$, $H/a = 30.54$, and $B = 11.75$ presented in Figure 5.3. Particle fraction, velocity, and suspension temperature profiles from the two simulations are plotted against the y-coordinate scaled by the channel width H. Also plotted, in (b), is the parabolic velocity profile for Newtonian fluid at the same volumetric flux. When the short-ranged repulsive forces (the force scaled by $6\pi\eta a\langle u\rangle$ is unity at a surface separation of about 5×10^{-5} particle radius) are absent, a concentrated and slowly-sheared layer of particles lies adjacent to the lower wall. Conditions change abruptly at the top of the layer, with a rapid increase in $\dot{\gamma}$, a similarly rapid increase of T to a maximum followed at further increase in y by a smooth but rapid decrease. While ϕ_A decreases immediately, it then increases with increasing y as the result of shear-induced migration within the channel of truncated width formed by the concentrated layer and the upper wall.

We offer the following explanation for this behavior. Particle surfaces approach very closely without interparticle forces, allowing formation of persistent clusters bound together by lubrication forces. At nonzero B, the clusters sediment to create a relatively concentrated and therefore very viscous layer, so that $\dot{\gamma}$ is reduced and the rate at which the clusters are torn apart is slowed. This apparently allows the clusters to become more tightly packed and ordered, contributing further to the development and stability of the concentrated layer.

All further results reported are from simulations which include interparticle forces of very short range. Weak Brownian motion, short-ranged interparticle forces or surface irregularities disrupt the influence of lubrication to some degree in any suspen-

sion (the influence of Brownian motion and repulsive forces upon the microstructure is analyzed in Chapter 3) and thus we believe the flow behavior of most noncolloidal suspensions (excepting, of course, those which have attractive interactions) is best represented by simulations including these forces.

5.3.2 Results

The simulations elucidate flow behavior as a function of ϕ_A^b, H/a, and the buoyancy parameter B defined by (5.1). Our discussion is focused on values of B ranging from 3.4 to 16.8. At the moderate concentrations we have studied, smaller values of B yield flow much like that in the case of a neutrally-buoyant suspension, which was studied in detail by NB. For B in excess of about 20, the particles settle into a well-ordered layer, and larger values of B would yield only similar behavior with perhaps eventual cessation of shearing of the particle layer. The yield stress which would be indicated by cessation was not investigated.

We discuss nine simulations, with conditions and selected results summarized in Table 5.1. The simulations are labeled in column 1. Input parameters are listed in columns 2-7: ϕ_A^b, H/a, and B are given in columns 2-4, respectively; the number of particles and the number making up the wall in the unit cell are listed in columns 5 and 6, respectively; and column 7 lists $F_0\tau$, the leading constant in the interparticle force. Taking $F_0\tau = 1.0$ and 0.6 for $H/a = 18.32$ and 30.54, respectively, the repulsive force has the same relative magnitude with respect to the shear rate for all simulations, because $\langle u \rangle$ is fixed. The time, t_{ss}, required to achieve a steady fully-developed flow

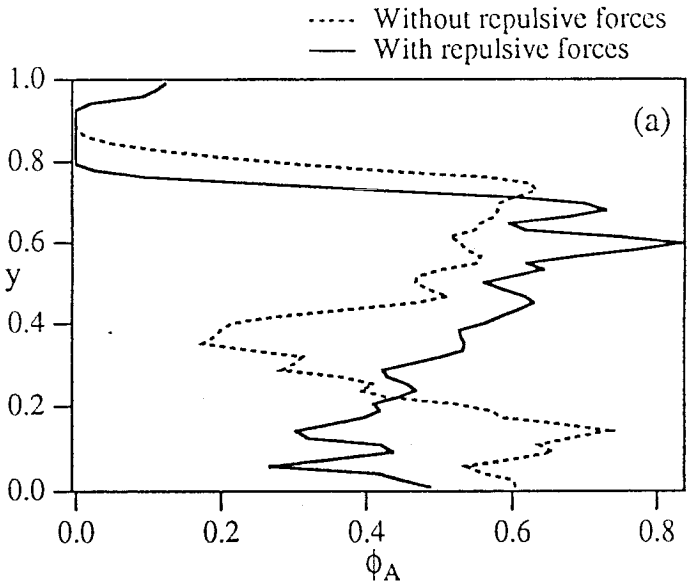

Figure 5.3: Comparison of profiles of the (a) particle areal fraction ϕ_A, (b) particle velocity u, and (c) suspension temperature T for $B = 11.75$, $H/a = 30.54$ and bulk areal particle fraction $\phi_A^b = 0.4$, for simulations with short-ranged repulsive interparticle forces, solid curves, and without these forces, dashed curves; (b) and (c) are on the following page. The parabolic profile of a Newtonian fluid at the same volumetric flux is shown in (b).

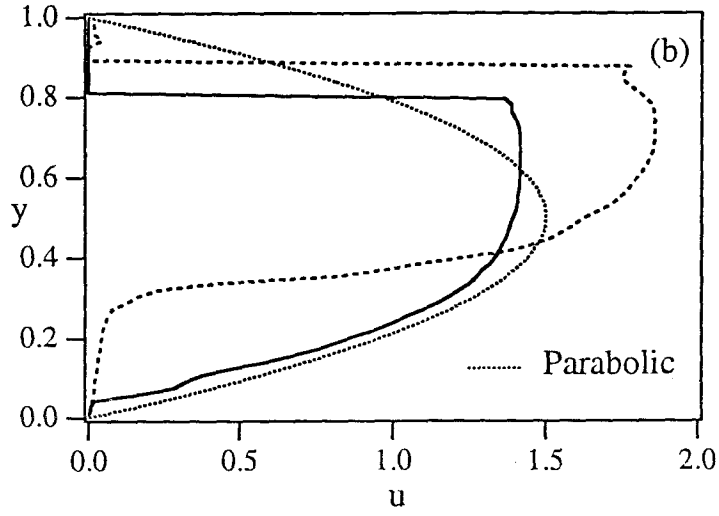

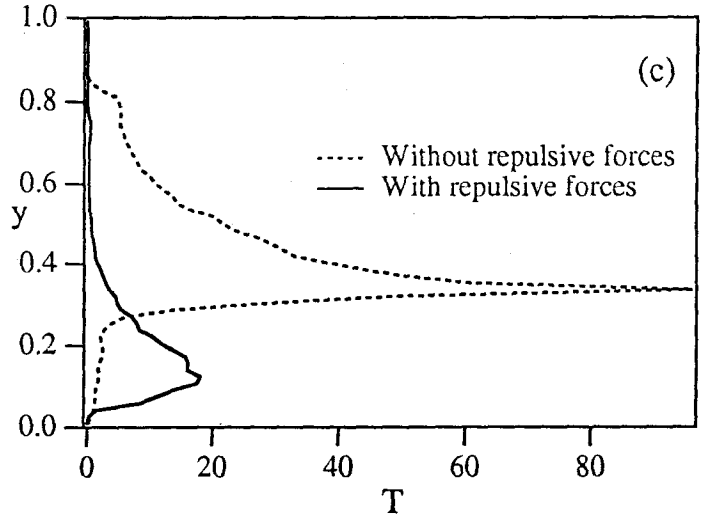

For caption, see previous page.

Simulation	ϕ_A^b	H/a	B	N	N_w	$F_0\tau$	t_{ss}	$\bar{h}_\infty$	Q_p
A	0.4	30.54	0	79	9	0.6	12000	0.49	1.20
B	0.4	30.54	3.4	79	9	0.6	4000	0.46	1.17
C	0.4	30.54	11.7	79	9	0.6	4000	0.40	1.14
D	0.4	30.54	16.8	79	9	0.6	3500	0.35	0.97
E	0.2	30.54	11.7	44	9	0.6	3200	0.21	0.62
F	0.6	30.54	11.7	114	9	0.6	4000	0.45	1.07
G1	0.4	18.32	3.4	51	9	1.0	1600	0.43	1.05
G2	0.4	18.32	3.4	51	9	1.0	2000	0.45	1.02
H	0.4	18.32	3.4	102	18	1.0	1800	0.46	1.14

Table 5.1: Summary of the simulations discussed. Columns 2-7 list input parameters, column 8 lists the times to achieve fully-developed flow, and columns 9-10 provide qualitative measures of the resulting bulk flow. Simulations G1 and G2 differ only in the separation between the monolayers: in G1 the layers are adjacent, while in G2 they are separated by four particle radii.

is given in column 8, with time made dimensionless by scaling with $a/\langle u\rangle$. Columns 9 and 10 provide qualitative measures of the fully-developed flow behavior. In column 9 is the average distance, scaled by H, of the suspended particles from the lower wall, denoted $\bar{h}_\infty$. Column 10 lists the particle flux normalized by its value for a uniformly dispersed suspension,

$$Q_p = \frac{1}{\phi_A^b \langle u\rangle} \int_0^1 \phi_A(y) u(y) dy. \tag{5.7}$$

We present profiles of ϕ_A, $\langle u\rangle$, and T averaged over 500 dimensionless time units, with averaging begun after the flow is fully-developed based on the criterion that $\bar{h}_\infty$ ceases to decrease. Lengths are scaled with a, velocities with $\langle u\rangle$, forces with $6\pi\eta a\langle u\rangle$, suspension temperature with $(\langle u\rangle a/H)^2$, and stresses with $\eta\langle u\rangle/H$, where η is the fluid viscosity.

Influence of particle buoyancy

We present in Figure 5.4 the particle fraction, velocity, and suspension temperature profiles in the fully-developed flow for simulations at $H/a = 30.54$, $\phi_A^b = 0.4$, and $B = 0$, 3.4, 11.7, and 16.8 (simulations A, B, C, and D in order of increasing B).

The profiles for the neutrally-buoyant suspension in simulation A are essentially symmetric about the channel centerline, with large ϕ_A near the center of the channel caused by shear-induced particle migration. For $B > 0$, competition at the bottom of the channel between settling and migration yield a density stratification with relatively heavy material above light for simulations B, C, and D; adjacent to the upper wall, both fluxes are directed down, resulting in a clear fluid layer for $B > 0$. On average, $\bar{h}_\infty$ decreases as B increases, indicating that particles lie progressively closer to the lower wall, but note that the maximum in ϕ_A is at larger y for simulations B, C, and D relative to simulation A (the point at which the maximum ϕ_A occurs in simulation B is close to $y = 0.5$, but the center of the concentrated region lies above this point). The large values of ϕ_A near the centerline in simulation A are reduced at nonzero B, because ϕ_A is increased near the lower wall, resulting in better "contact" between suspension and wall. This generates greater fluctuational motion in the interior of the channel and loosens the particle packing.

Figure 5.4 (b) shows that reduction of ϕ_A near the center of the channel lessens the blunting of the velocity. For $B > 0$, it is a general result that the maximum velocity occurs above the channel centerline, because the increase in ϕ_A at the bottom of the channel due to particle settling results in increased effective viscosity. Hence, $\dot{\gamma}$ is

reduced and the approach to the maximum from the lower wall of the channel is slower than from the upper.

The upper portion of the channel becomes devoid of particles and T, measured only over the particles, drops to zero here. Though there certainly remains fluctuational motion in the fluid, this is not sampled by our method. In the lower portion of the channel, the region where T exceeds unity widens while the maximum T grows as the gravity is increased. This may be attributed to stronger interaction of the suspension with the wall, as well as to the increased number and intensity of interactions between suspended particles, as ϕ_A increases.

Influence of particle fraction

We present in Figure 5.5 the particle areal fraction, velocity, and suspension temperature profiles in the fully-developed flow at $B = 11.7$ and $H/a = 30.54$ for $\phi_A^b = 0.2$, 0.4, and 0.6 (simulations are labeled E, C, and F in order of increasing ϕ_A^b).

The flow behavior depends strongly upon ϕ_A^b. In Figure 5.5 (a), we see that the particles have sedimented into a shear layer in the fully-developed flow at $\phi_A^b = 0.2$, simulation E; shear rate, ϕ_A, and T are all roughly constant within this layer. Surprisingly, the particle fraction adjacent to the lower wall, for $y = 0$ to $y \approx 0.2$, is larger for simulation E than simulation C at $\phi_A^b = 0.4$. Above $y \approx 0.35$, the particle fraction in simulation E drops rapidly to zero, while the particle fraction in simulation C increases, indicating that at this B shear-induced particle migration is important for $\phi_A^b = 0.4$, but has little influence for $\phi_A^b = 0.2$.

For both simulations C and F, the maximum in ϕ_A lies above the centerline, so

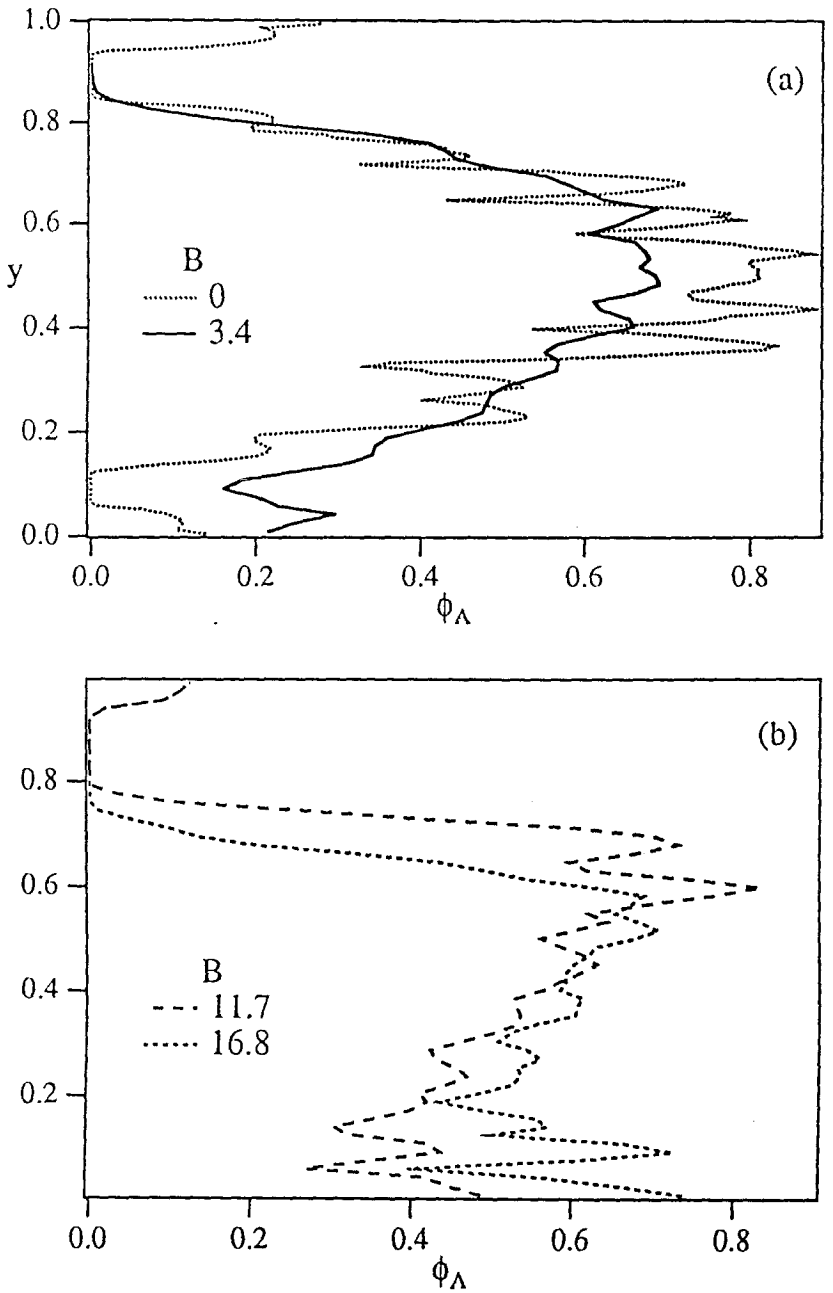

Figure 5.4: Comparison of profiles of the (*a* and *b*) particle areal fraction ϕ_A, (*c*) particle velocity u, and (*d*) suspension temperature T, for $\phi_A^b = 0.4$, $H/a = 30.54$, and $B = 0$, 3.4, 11.7 and 16.8 (simulations A, B, C, and D); (*c*) and (*d*) appear on the following page.

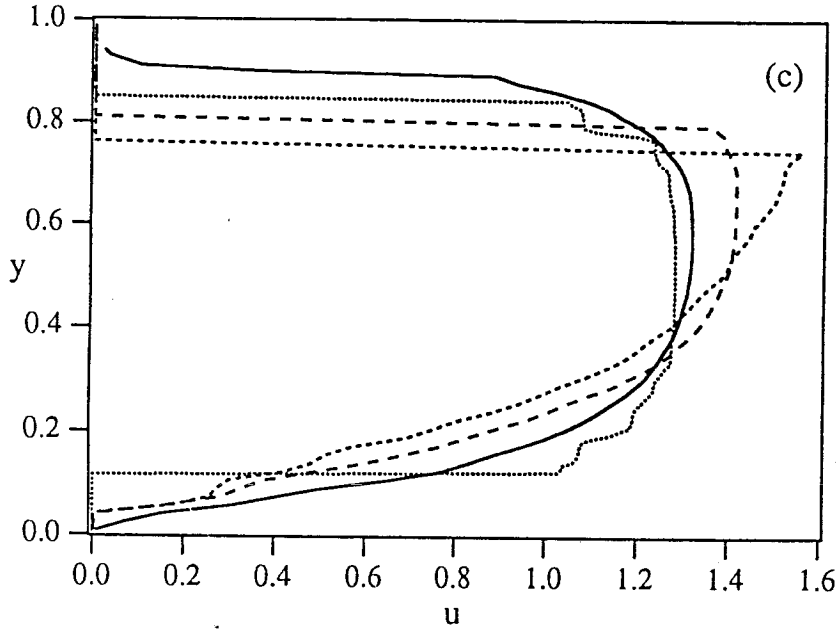

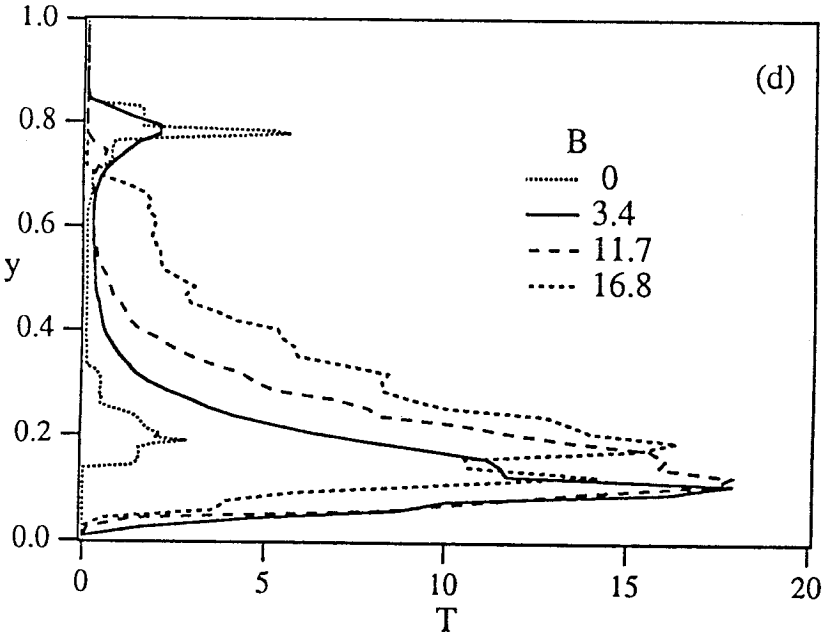

For caption, see previous page.

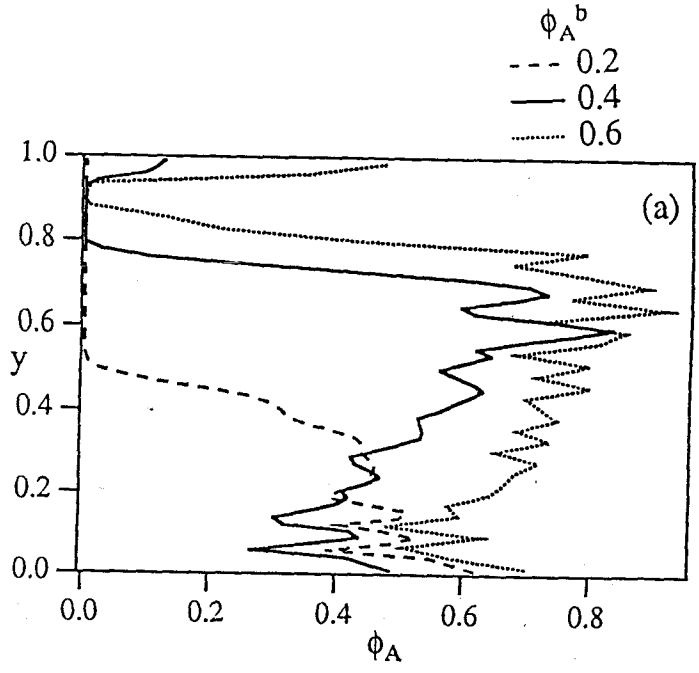

Figure 5.5: Comparison of profiles of the (a) particle areal fraction ϕ_A, (b) particle velocity u, and (c) suspension temperature T, for $B = 11.7$, $H/a = 30.54$, and $\phi_A^b = 0.2$, 0.4, and 0.6 (simulations E, C, and F); (b) and (c) are on the following page.

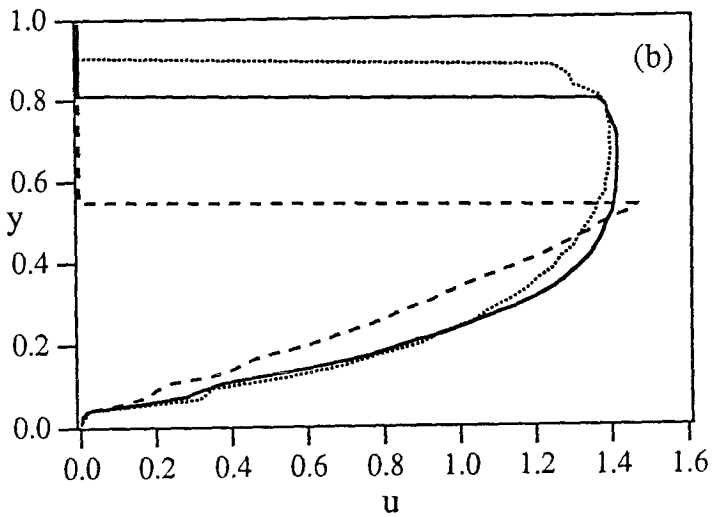

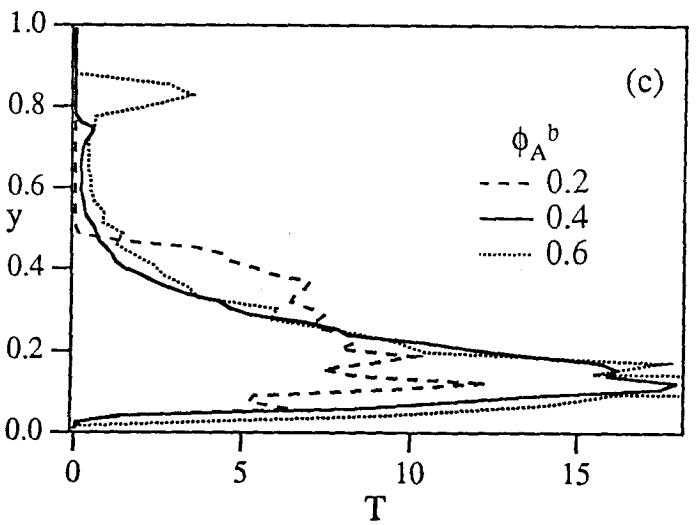

For caption, see previous page.

that relatively dense material flows over light. Note that in simulations C and F, rapid shearing near the lower wall generates larger values of T than in simulation E. The fluctuational motion in the dilute layer is apparently related to the suspension of the denser material.

Influence of channel width

We present in Figure 5.6 the results of simulations at $\phi_A^b = 0.4$ and $B = 3.4$ for $H/a = 18.32$ and $H/a = 30.54$, simulations G1 and B, respectively.

The flow behavior depends weakly upon H/a relative to the dependence upon ϕ_A^b and B. This implies that to a good approximation for these and, presumably, larger values of H/a, the suspension may be treated as a continuum in this bounded flow. Our definition of B (recall the scaling of B with $(H/a)^2$; see Eq. (5.1)) effectively reduces the influence of buoyancy, as evidenced by the similarity of the profiles of ϕ_A and u from simulations B and G1 in Figure 5.6 (a) and (b), respectively. The profiles of T do, however, show evidence of the finite size of the particles: in Figure 5.6 (c), we see that smaller values of T at the center of the channel occur for the larger H/a, and that the width of the region adjacent to the wall where T varies rapidly scales roughly as a/H, with T of simulation G1 reaching a maximum relatively farther from the wall than in the wider channel. These observations are consistent with the findings of NB for the influence of H/a for $B = 0$.

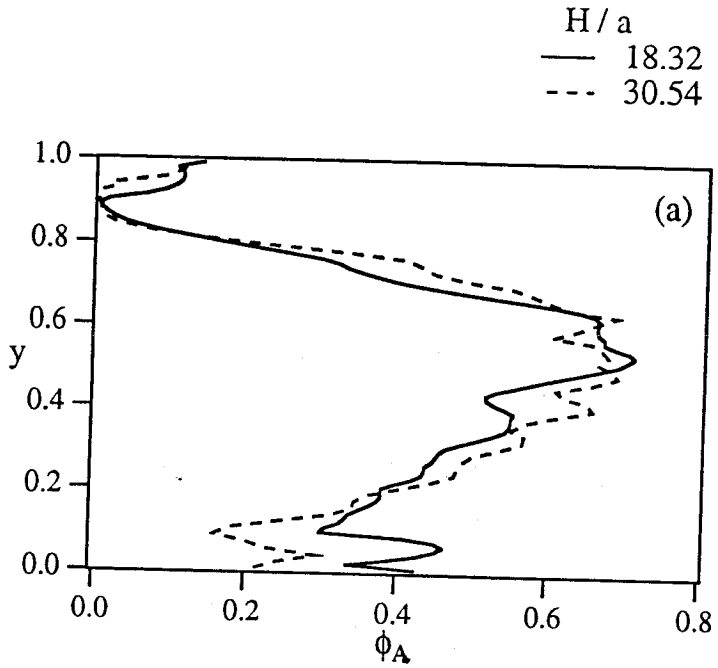

Figure 5.6: Comparison of profiles of the (a) particle areal fraction ϕ_A, (b) particle velocity u, and (c) the suspension temperature T, for $\phi_A^b = 0.4$, $B = 3.4$, $H/a = 18.32$ and $H/a = 30.54$ (simulations G1 and B, respectively); (b) and (c) are the previous page. The parabolic velocity profile of a Newtonian fluid at the same volumetric flux is shown in (b).

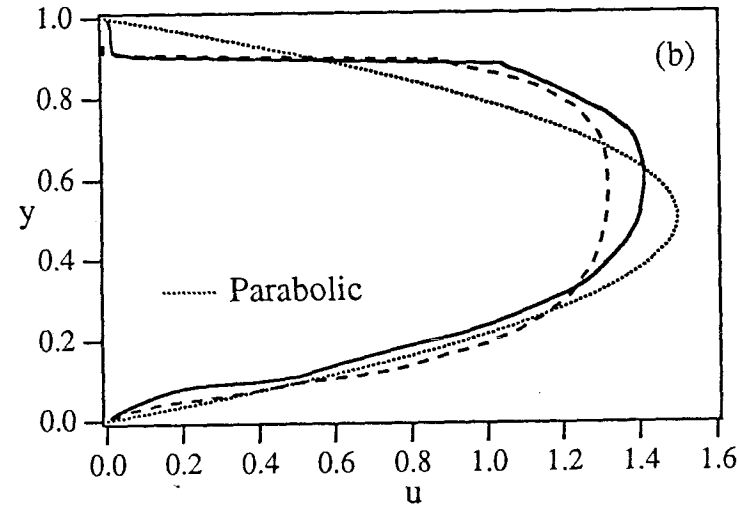

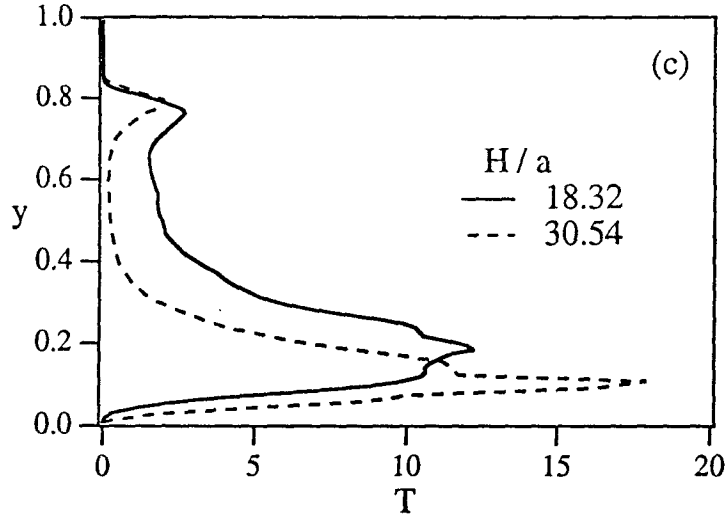

For caption, see previous page.

Simulational parameters: separated monolayers and size of the unit cell

We have studied the influence of varying the separation between monolayers and the size of the simulational unit cell for fixed ϕ_A^b and H/a. The studies were motivated by the observation of NB that, with other parameters held constant, T was systematically larger for larger N, the number of particles in the unit cell, a result which they could not explain. As noted in §5.3, the unit cell is periodically replicated in all directions, so that when the cell is a single particle diameter in thickness, particles essentially form cylinders in the direction perpendicular to the plane of motion, resulting in a quasi-two-dimensionality that was considered a potential source of the anomalous finding. By increasing the width of the unit cell in this direction, while maintaining the restriction of motion within the plane of the monolayer for the particles, this geometrical feature is broken, but we find that the dependence of T upon N remains and therefore is not due to this feature of the simulations. It remains possible that the anomalous dependence results from constraining the motions of particles to the plane of the monolayer, and fully three-dimensional simulations of channel flows should be undertaken to determine if the cause of the anomaly is this restriction.

A summary of the results of this investigation are presented in two figures. First consider Figure 5.7, which compares the results of simulation G2, in which monolayers of suspension are separated by a clear fluid layer of four particle diameters, with those of simulation G1, in which particles are directly adjacent to their nearest images in the z-direction. Both simulations are at the conditions $B = 3.4$, $\phi_A^b = 0.4$, and $H/a = 18.32$. The only systematic difference is a slightly smaller u over the entire

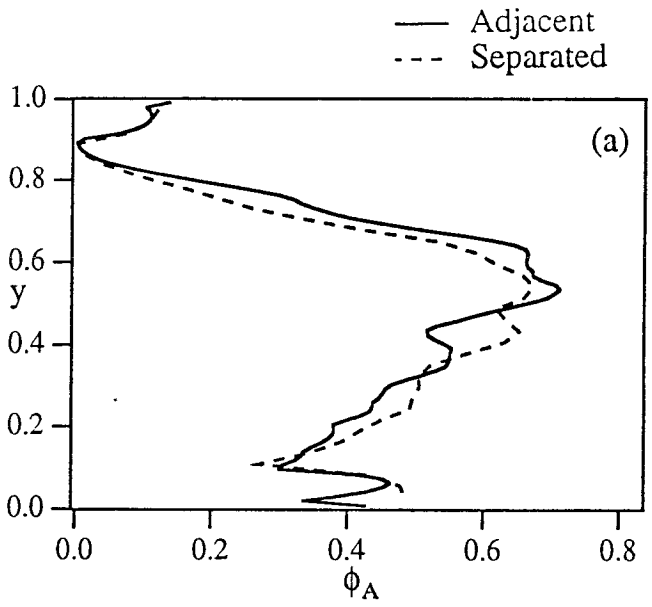

Figure 5.7: Comparison of profiles of the (a) particle areal fraction ϕ_A, (b) particle velocity u, and (c) suspension temperature T, for simulations G1 and G2 at $\phi_A^b = 0.4$, $B = 3.4$, and $H/a = 18.32$; (b) and (c) are on the following page. The monolayers of G1 are directly adjacent, solid curves, while those of G2 are separated by a layer of clear fluid of four particle diameters, dashed curves.

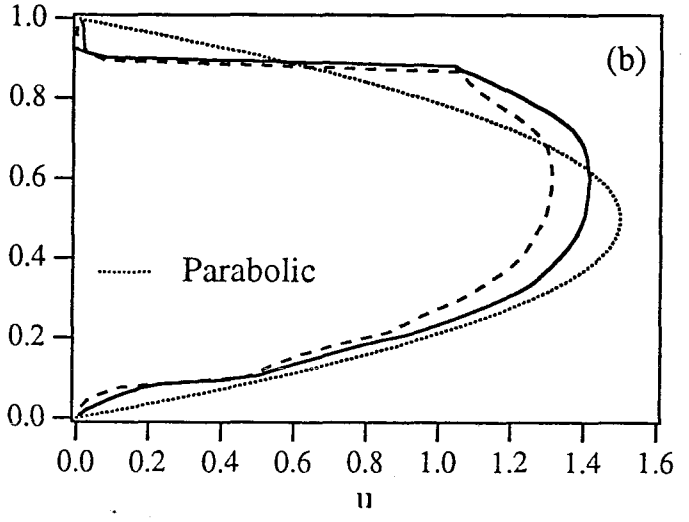

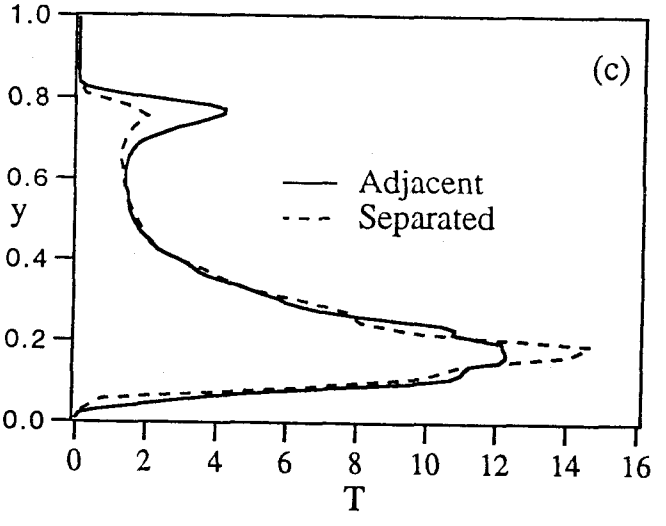

For caption, see previous page.

channel in simulation G2, a result discussed in the following paragraph. Now consider Figure 5.8, in which the results of simulation G1 with $N = 51$ are compared with those of simulation H with $N = 102$, but all other conditions are the same (the unit cell of simulation H is twice the length in the flow direction of the unit cell of simulation G1), and there is no clear fluid layer between the monolayers of suspension. No systematic difference is observed in the profiles of ϕ_A and u for these simulations. However, in Figure 5.8 (c), the profile of T for simulation H is larger over the entire channel than in simulation G1, with the difference most pronounced near the peaks in T. Because simulations G1 and G2 showed essentially no difference in T, the anomalous dependence of T upon N is not explained by the simulation of monolayers lying directly adjacent to one another.

The difference in the velocity profiles in simulations G1 and G2 is due simply to the fact that resistance to flow is less within the clear fluid than the suspension layers. The clear fluid is lower in viscosity and, on average, farther from the fixed wall particles than the monolayers of suspension, so that at a given x and y, the velocity is larger in the clear fluid than in the suspension layers, yet satisfies the specified $\langle u \rangle$.

5.4 Suspension flow modeling

The suspension-balance model outlined by NB is used to predict the fully-developed flow, with model predictions presented together with simulation results at the same conditions to facilitate evaluation of the success of the model. Predictions for conditions not simulated are also presented.

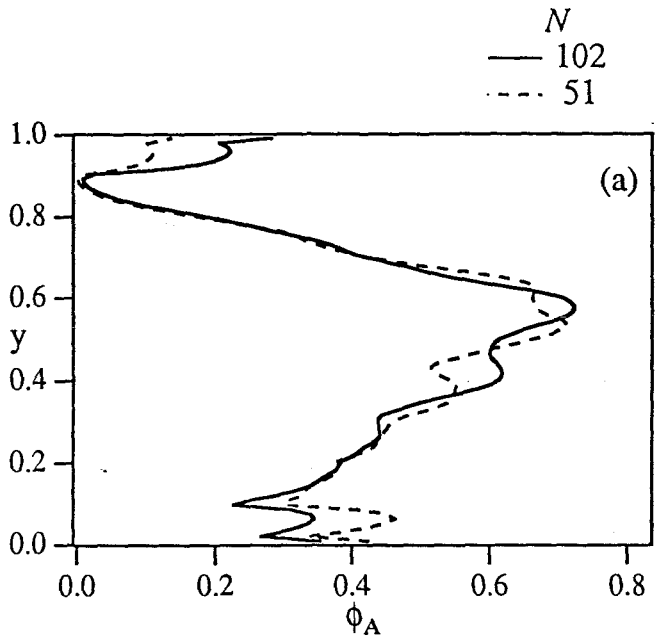

Figure 5.8: Comparison of profiles of the (a) particle areal fraction ϕ_A, (b) particle velocity u, and (c) the suspension temperature T, for simulations G1 ($N = 51$, dashed curves) and H ($N = 102$,, solid curves) at $\phi_A^b = 0.4$, $B = 3.4$, and $H/a = 18.32$; (b) and (c) are the following page.

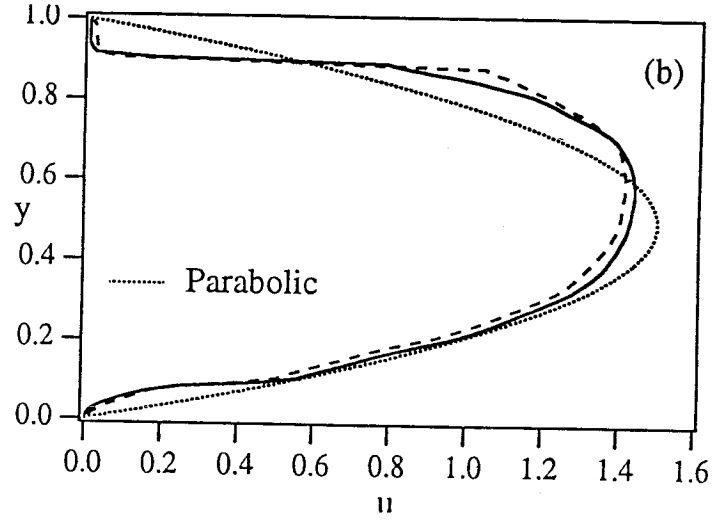

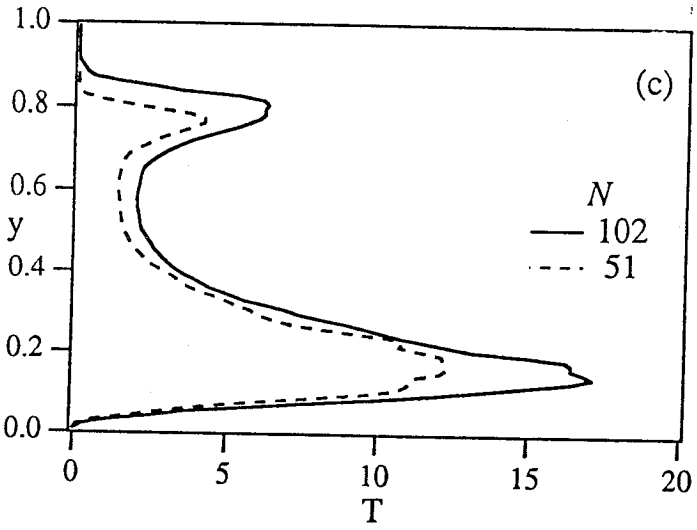

For caption, see previous page.

5.4.1 Balance equations and constitutive laws

Following the derivation in NB, we have the conservation of mass and momentum for the particle phase,

$$\frac{\partial \phi}{\partial t} + \nabla \cdot \phi \langle \boldsymbol{u} \rangle_p = 0, \tag{5.8}$$

and

$$\rho_p \phi \frac{D_p \langle \boldsymbol{u} \rangle_p}{Dt} = \langle \boldsymbol{b} \rangle_p + \langle \boldsymbol{F} \rangle_p + \nabla \cdot \langle \boldsymbol{\Sigma} \rangle_p, \tag{5.9}$$

respectively, where the material derivative in (5.9) follows the particles $D_p/Dt = \partial/\partial t + \langle \boldsymbol{u} \rangle_p \cdot \nabla$.

We are interested in the case where the particle density differs from that of the fluid. The average body force on the particles per unit volume is $\rho_p \boldsymbol{g} \phi$, but only the differential body force $(\rho_p - \rho_f)\boldsymbol{g}\phi$ is relevant to the particle dynamics, as a constant body force $\rho_f g$ at all points can be absorbed into a linearly varying isotropic stress which is hydrostatically stable. Hence, the body force in (5.9) is $\langle \boldsymbol{b} \rangle_p = (\rho_p - \rho_f)\boldsymbol{g}\phi$.

The average hydrodynamic force per unit volume on the particle phase is $\langle \boldsymbol{F} \rangle_p$, which is modeled from a consideration of its expression in terms of a low-Reynolds-number resistance tensor and the deviation of the particle velocity from the suspension average,

$$\begin{aligned} \langle \boldsymbol{F} \rangle_p &= -n \langle \boldsymbol{R}_{FU} \cdot (\boldsymbol{u} - \langle \boldsymbol{u} \rangle) \rangle_p \\ &\approx -n \langle \boldsymbol{R}_{FU} \rangle_p \cdot (\langle \boldsymbol{u} \rangle_p - \langle \boldsymbol{u} \rangle) \\ &\approx -6\pi\eta a n f(\phi)^{-1} (\langle \boldsymbol{u} \rangle_p - \langle \boldsymbol{u} \rangle), \end{aligned} \tag{5.10}$$

where n is the particle number density. The hindered settling function, $f(\phi)$, is the ratio of the settling velocity of a particle in bulk sedimentation relative to the Stokes settling velocity of an isolated particle; $f(\phi)$ has been measured experimentally (see the review by Davis & Acrivos 1985) and by Stokesian Dynamics simulation (Phillips, Brady & Bossis 1988).

The particle contribution to the suspension stress is given (Brady 1993*a*) by

$$\langle \boldsymbol{\Sigma} \rangle_p = \langle \boldsymbol{S} \rangle_p + \tfrac{1}{2}\boldsymbol{\epsilon}\cdot\langle \boldsymbol{L}^{ext} \rangle_p - \langle \boldsymbol{x}^i \boldsymbol{b}^i \rangle_p - \tfrac{1}{2}\rho_p \langle \boldsymbol{r}\boldsymbol{a} + \boldsymbol{a}\boldsymbol{r} \rangle_p - \rho_p \langle \boldsymbol{u}'\boldsymbol{u}' \rangle_p. \tag{5.11}$$

In (5.11), $\langle \boldsymbol{S} \rangle_p$ is the hydrodynamic stresslet; $-\langle \boldsymbol{x}^i \boldsymbol{b}^i \rangle_p$ is the stress due to nonhydrodynamic interparticle forces; $-\rho_p \langle \boldsymbol{u}'\boldsymbol{u}' \rangle_p$ is the particle contribution to the inertial Reynolds stress; $\frac{1}{2}\boldsymbol{\epsilon}\cdot\langle \boldsymbol{L}^{ext} \rangle$ is the antisymmetric stress which results from the application of an external torque $\langle \boldsymbol{L}^{ext} \rangle_p$ upon the particles with $\boldsymbol{\epsilon}$ the unit alternating tensor; and the stress resulting from the moment about the particle centers ($\boldsymbol{r} = \boldsymbol{x} - \boldsymbol{x}^i$, with $\boldsymbol{x}^i$ the center of the i^{th} particle) of the local acceleration is $-(\rho_p/2)\langle \boldsymbol{r}\boldsymbol{a} + \boldsymbol{a}\boldsymbol{r} \rangle_p$. The hydrodynamic stresslet (Batchelor 1970) is given by

$$\boldsymbol{S}_i = \tfrac{1}{2}\int_{A_i} [\boldsymbol{r}\boldsymbol{\sigma}\cdot\boldsymbol{n} + \boldsymbol{\sigma}\cdot\boldsymbol{n}\boldsymbol{r}] dA,$$

where $\boldsymbol{n}$ is the normal projecting out of the particle and A_i is the surface of particle i. The stresslet is a continuum concept, and is the only stress contribution without a direct counterpart in the expression for the stress in a molecular system (Irving & Kirkwood 1950) for molecules of finite size.

No external torque is applied to the particles, and we consider low-Reynolds-number flows, so that both the acceleration and Reynolds stresses are negligible. Thus, the constitutive law for the particle stress is

$$\langle \boldsymbol{S} \rangle_p = -\Pi \boldsymbol{I} + 2\eta\eta_p(\phi)\langle \boldsymbol{e} \rangle \tag{5.12}$$

in which Π is the particle contribution to the pressure, $\eta_p = \eta_s - 1$ is the particle viscosity made dimensionless with the fluid viscosity, and $\langle \boldsymbol{e} \rangle$ is the bulk rate of strain. In general, a term representing normal stress differences must be included in (5.12) as discussed by NB, but is omitted because normal stress differences play no role in the fully-developed flow in a straight channel. While it was shown by Jeffrey *et al.* (1993) that the particle contribution to the pressure could be written as

$$\Pi = -\tfrac{1}{3}\boldsymbol{I}:\langle \boldsymbol{S} \rangle_p = \langle \boldsymbol{P}\cdot(\boldsymbol{u} - \langle \boldsymbol{u} \rangle) - \boldsymbol{Q}:\langle \boldsymbol{e} \rangle \rangle_p, \tag{5.13}$$

in which $\boldsymbol{P}$ and $\boldsymbol{Q}$ are the hydrodynamic resistance tensors relating particle velocity and the bulk flow to the isotropic stress, respectively, we constitutively relate Π to the fluctuational motion of the particles alone. In a flow with homogeneous rate of strain, T can be written in terms of $\langle \boldsymbol{e} \rangle$, and relating Π to T alone or to $\langle \boldsymbol{e} \rangle$ alone is equivalent. If, however, we relate Π to the local $\langle \boldsymbol{e} \rangle$ alone, it will vanish at the velocity maximum in a pressure-driven flow, leading to an aphysical prediction of a cusplike maximum in ϕ_A, as shown by Phillips *et al.* (1992). Thus, as first suggested

by Jenkins & McTigue (1990), we relate the pressure to T as

$$\Pi = \eta a^{-1} p(\phi) \sqrt{T}, \tag{5.14}$$

in which Π is proportional to the square root of the suspension temperature (and hence linear in velocity) because it is a viscously-generated stress.

The suspension-averaged velocity $\langle \boldsymbol{u} \rangle$ is governed by the ensemble average of the mass and momentum conservation equations, taken over all points in the suspension. For incompressible materials, these equations are

$$\nabla \cdot \langle \boldsymbol{u} \rangle = 0, \tag{5.15}$$

and

$$\frac{D\langle \rho \boldsymbol{u} \rangle}{Dt} = \langle \boldsymbol{b} \rangle + \nabla \cdot \langle \boldsymbol{\Sigma} \rangle, \tag{5.16}$$

where the material derivative in this case, $D/Dt = \partial/\partial t + \langle \boldsymbol{u} \rangle \cdot \nabla$, follows the suspension-averaged motion. The expression for the suspension stress is of the same form as (5.11) for the particle stress, with averaging now over the entire suspension. The constitutive law for the suspension stress is thus

$$\begin{aligned} \langle \boldsymbol{\Sigma} \rangle &= -\langle p \rangle_f \boldsymbol{I} + 2\eta \langle \boldsymbol{e} \rangle + \langle \boldsymbol{\Sigma} \rangle_p \\ &= -(\Pi + \langle p \rangle_f) \boldsymbol{I} + 2\eta \eta_s(\phi) \langle \boldsymbol{e} \rangle, \end{aligned} \tag{5.17}$$

where $\langle p \rangle_f$ is the average pressure in the fluid.

To determine the stress in (5.14), we must determine T. An equation governing T is deduced from a consideration of the balance equation for kinetic energy of the entire suspension. Multiplying the velocity $\boldsymbol{u}$ in a scalar product with Cauchy's equation, taking the suspension average of the resulting equation and subtracting from it the scalar product of $\langle \boldsymbol{u} \rangle$ with the average momentum equation for the suspension, (5.16), yields (Batchelor 1970)

$$\frac{D\langle \rho(u')^2 \rangle}{Dt} = \langle \boldsymbol{b}' \cdot \boldsymbol{u}' \rangle + \langle \boldsymbol{\Sigma} \rangle : \langle \boldsymbol{e} \rangle - \langle \dot{\Phi} \rangle - \nabla \cdot \langle \boldsymbol{\Sigma}' \cdot \boldsymbol{u}' \rangle. \tag{5.18}$$

On the right-hand side of (5.18), $\langle \boldsymbol{b}' \cdot \boldsymbol{u}' \rangle$ and $\langle \boldsymbol{\Sigma} \rangle : \langle \boldsymbol{e} \rangle$ represent the rates of working by fluctuating interparticle and body forces and by the mean bulk stress, respectively, $\langle \dot{\Phi} \rangle$ is the average rate of viscous dissipation of mechanical energy into heat, and the final term is the divergence of the flux vector of microscopic kinetic energy.

The equation (5.18) is used to motivate the form of the equation governing T. The dissipation rate for a low-Reynolds-number suspension is given by (Brady & Bossis 1988)

$$\dot{\Phi} = \begin{pmatrix} \boldsymbol{u} - \langle \boldsymbol{u} \rangle \\ -\langle \boldsymbol{e} \rangle \end{pmatrix} \cdot \begin{bmatrix} \boldsymbol{R}_{FU} & \boldsymbol{R}_{FE} \\ \boldsymbol{R}_{SU} & \boldsymbol{R}_{SE} \end{bmatrix} \cdot \begin{pmatrix} \boldsymbol{u} - \langle \boldsymbol{u} \rangle \\ -\langle \boldsymbol{e} \rangle \end{pmatrix}. \tag{5.19}$$

The dissipation consists of a term $\langle \boldsymbol{u}' \cdot \boldsymbol{R}_{FU} \cdot \boldsymbol{u}' \rangle$, where $\boldsymbol{u}' = \boldsymbol{u} - \langle \boldsymbol{u} \rangle$, which is due to the fluctuational motion of the particles relative to the local mean motion of the material, a term $\langle \boldsymbol{e} \rangle : \langle \boldsymbol{R}_{SE} \rangle : \langle \boldsymbol{e} \rangle$ due to the particles moving "affinely" with the average bulk motion and terms due to the coupling of the fluctuational motion to the bulk.

The fluctuational dissipation is proportional to the suspension temperature

$$\langle \boldsymbol{u}' \cdot \boldsymbol{R}_{FU} \cdot \boldsymbol{u}' \rangle \sim 6\pi\eta a f(\phi)^{-1} T, \tag{5.20}$$

a fact that is used to model the dissipation as proportional to T. By introducing a Newtonian constitutive law for the stress, the flux vector appears in a form which suggests modeling by a Fourier law,

$$-\langle \boldsymbol{\Sigma}' \cdot \boldsymbol{u}' \rangle \sim -\eta\eta_p \langle \boldsymbol{u}' \nabla \cdot \boldsymbol{u}' \rangle \sim -\eta\kappa(\phi)\nabla T, \tag{5.21}$$

in which the conductivity coefficient $\kappa(\phi)$ is proportional to the particle viscosity $\eta_p(\phi)$. We discard the dissipation due to affine motion and use the constitutive models expressed by (5.20) and (5.21) to deduce the following equation for the particle fluctuational motion,

$$c(\phi)\frac{DT}{Dt} = \beta(\phi)\langle \boldsymbol{b}' \cdot \boldsymbol{u}' \rangle + \langle \boldsymbol{\Sigma} \rangle_p : \langle \boldsymbol{e} \rangle - \eta\alpha(\phi)a^{-2}T - \nabla \cdot \kappa(\phi)\nabla T. \tag{5.22}$$

Keeping the rate of working unchanged while discarding the affine dissipation requires introduction of phenomenological coefficients: $c(\phi)$ is analogous to a heat capacity, $\alpha(\phi)$ describes the magnitude of T in a homogeneous shear flow, and $\beta(\phi)$ together with $\alpha(\phi)$ gives T in a homogeneous sedimentation. The average particle stress $\langle \boldsymbol{\Sigma} \rangle_p$ appears on the right of (5.22) because the fluid dissipation is associated with the discarded affine motion.

Closure of the governing equations requires sprecification of the ϕ-dependent functions η_s, p, c, α, β, and κ. For the suspension viscosity, we take

$$\eta_s(\phi) = \left(1 - \frac{\phi}{\phi_m}\right)^{-2}, \tag{5.23}$$

which differs only through the exponent of -2 (rather than -1.82) from Krieger's (1972) correlation of experimental data, and the particle viscosity is given by $\eta_p = \eta_s - 1$. The other ϕ-dependent functions, all recently defined by NB, can be determined from independent experiments or simulations. All except the "conductivity" coefficient $\kappa(\phi)$ can be determined from experiments at homogeneous conditions. This work has yet to be performed, however, and the coefficients used here are modeled.

The pressure function is recommended by NB as

$$p(\phi) = \phi^{1/2}\eta_p(\phi), \tag{5.24}$$

with the leading $\phi^{1/2}$ included so that for $\phi \to 0$, $\Pi = O(\phi^2)$ (T is proportional to ϕ for $\phi \to 0$), in agreement with the analysis of Jeffrey *et al.* (1993). The factor of $\phi^{1/2}$ was omitted here, taking $p(\phi) = \eta_p(\phi)$. This relation for $p(\phi)$ works well for moderately- to highly-concentrated suspensions, but convergence difficulties in the numerical solution were encountered for $\phi_A^b < 0.15$, suggesting that the neglected dependence is significant for small ϕ.

The coefficients in the equation governing T are

$$\alpha(\phi) = \frac{k_\alpha \eta_p(\phi)}{\phi}, \quad \text{and} \quad \kappa(\phi) = k_\kappa \eta_p(\phi), \tag{5.25}$$

where k_α and k_κ are constants. The coefficient $c(\phi)$ is not needed here because we consider only the fully-developed flow; $\beta(\phi)$ is also not needed because there is no average phase slip in the fully-developed flow and we assume the interparticle forces to have the effect only of inhibiting cluster formation.

The model equations are made dimensionless by scaling lengths with H, velocities with $\langle u \rangle \sim |\nabla \langle p \rangle| H^2/\eta$, and T with $(a/H)^2 \langle u \rangle^2$. We define $\epsilon \equiv a/H$. For steady, fully-developed channel flow variations are only in the cross-stream, *i.e.* y, direction, and the dimensionless particle momentum balances are

$$\frac{d}{dy}\left(\eta_p(\phi)\frac{d\langle u_x \rangle_p}{dy}\right) + 1 = \tfrac{9}{2}\epsilon^{-2}\phi f^{-1}(\phi)(\langle u_x \rangle_p - \langle u_x \rangle), \tag{5.26}$$

and

$$\frac{d}{dy}\left(p(\phi)\sqrt{T}\right) = -B\phi, \tag{5.27}$$

where B is the buoyancy parameter defined by (5.1). An immediate simplification is obtained by assuming $\epsilon^2 \ll 1$, an assumption consistent with describing the particulate phase as an effective continuum. In this case, the x-momentum balance (5.26) states $\langle u_x \rangle_p = \langle u_x \rangle + O(\epsilon^2)$: in the fully-developed flow, there is negligible slip between the average particle and suspension average velocities. The equation governing

the velocity is thus the x-momentum balance for the entire suspension,

$$\frac{d}{dy}\left(\eta_s(\phi)\frac{d\langle u_x\rangle}{dy}\right) = -1. \tag{5.28}$$

At steady state, the equation governing T is

$$\eta_p(\phi)\left(\frac{d\langle u\rangle}{dy}\right)^2 - \alpha(\phi)T + \epsilon^2\frac{d}{dy}\left(\kappa(\phi)\frac{dT}{dY}\right) = 0. \tag{5.29}$$

Here and in the following, we omit the subscript x on the velocity. We carry out the differentiation in (5.27) to yield

$$p'\frac{d\phi}{dy} + \frac{p}{T}\frac{dT}{dy} = \frac{-B\phi}{\sqrt{T}}, \tag{5.30}$$

where $p' = dp/d\phi$. For $B = 0$, this equation is linear in T, but this is no longer the case for $B > 0$. Thus, particle buoyancy introduces a new type of nonlinearity to the model equations, with the other nonlinearity being due to the ϕ-dependent coefficents.

Boundary conditions on $\langle u\rangle$ and T and an integral condition on ϕ must be specified. The boundary conditions on the velocity are no slip at both walls,

$$u = 0 \quad \text{at} \quad y = 0 \quad \text{and} \quad y = 1, \tag{5.31}$$

while the particle fraction must sum to the bulk value,

$$\int_0^1 \phi_A(y)dy = \phi_A^b. \tag{5.32}$$

The conditions on T prove to be more problematic. Simulations and a consideration of the hydrodynamic interactions of particles with the walls suggest that the boundary condition should be $T = 0$ at the walls. However, NB showed that this forces ϕ_A to take on its maximum value $\phi_{A,m}$ (areal fraction is used because of the modeling of a monolayer) at the wall to generate the finite particle pressure necessary to satisfy the y-momentum balance, and this does not agree with observed results. Here, we apply an *ad hoc* condition intended to reflect in a simple fashion the physical influence of the wall, which is to hydrodynamically damp the fluctuational motion and substantially reduce the value of T in the immediate vicinity of the wall. This condition is

$$T_w = \frac{\eta_p(\phi_w)}{\alpha^*}\left(\frac{du}{dy}\right)^2 \quad \text{at} \quad y = 0 \quad \text{and} \quad y = 1, \tag{5.33}$$

where the subscript w indicates the limiting value as the wall is approached from the suspension, and α^* is larger than $\alpha(\phi_w)$ by an arbitrarily chosen factor of 20. Thus, the wall is represented as a region of particles near maximum packing. This condition forces T to be small but finite at the wall and we will see that it yields good agreement with simulation results. The coupled set of ordinary differential equations (5.27-5.29) are solved subject to the conditions (5.31-5.33) for ϕ, $\langle u \rangle$, and T.

To generate model predictions for comparison with the simulational results, the

constitutive laws are modified for use in determining the areal fraction ϕ_A. As shown by NB, the constitutive laws reported above are satisfactory for use in predicting areal fraction if ϕ and ϕ_m are replaced by ϕ_A and $\phi_{A,m}$, where $\phi_{A,m}$ is the maximum random packing fraction of circles in a plane, determined by Kausch, Fesko & Tschoegl (1971) to be $\phi_{A,m} \approx 0.83$.

A finite-difference scheme is used to solve the second-order equations (5.28) and (5.29) for $\langle u \rangle$ and T, respectively. The y-momentum equation is a first-order equation for ϕ_A, and the linearized difference equation in the numerical solution is solved analytically using a summing factor analogous to the integrating factor used for first-order linear differential equations (see Bender & Orszag 1978, p. 38). Simulations show that for sufficiently large B, there is a region with no particles adjacent to the upper wall, a result which the continuum equations can not predict. Thus, we set the particle fraction to zero if it falls below 10^{-3}, and find this *ad hoc* method entirely satisfactory. The solution is computed on a one-dimensional grid of 500 nodes.

The set of equations is solved by a nested-iteration algorithm. This procedure begins with assumption of a particle fraction profile $\phi_A^{(0)}(y)$ having the desired bulk fraction ϕ_A^b. This particle fraction is inserted to the x-momentum equation, which is solved to yield the velocity field $u^{(0)}(y)$. This velocity field is used in the temperature equation, which is solved for $T^{(0)}(y)$. The field $T^{(0)}(y)$ is substituted to the linearized y-momentum equation, which is iterated with systematic increase or decrease of $\phi_A(0)$ until the average particle fraction is ϕ_A^b, with the field satisfying this condition denoted $\phi_A^{(1)}(y)$. This nested iteration completes the first overall iteration, and $\phi_A^{(1)}(y)$ is used

in the x-momentum equation to begin the second. The procedure is continued until convergence is achieved, with our convergence criterion being that the integrated absolute difference between two subsequent $\phi_A^{(i)}$ is less than a specified tolerance of one-half of a percent.

5.4.2 Model predictions

We present model predictions for two conditions simulated and a composite of the predictions for varying B. Also, we present predictions at conditions which require excessive simulation time at present capacity.

In Figure 5.9, the predicted fully-developed flow at $B = 3.4$, $\phi_A^b = 0.4$, and $H/a = 30.54$ is presented together with the results of simulation B, at the same conditions. The model predictions were fitted to the simulation results at these conditions using k_α and k_κ as fitting parameters, with the appropriate values found to be

$$k_\alpha = 0.815, \quad \text{and} \quad k_\kappa = 0.8, \tag{5.34}$$

substantially larger than the values of $k_\alpha = 0.19$ and $k_\kappa = 0.17$ used by NB; the values given by (5.34) were used in all of the modeling reported here. The agreement between the model predictions and the results of simulation B is very good. There is a clear fluid layer above $y \approx 0.82$. The model predicts a similar particle-fraction profile with the value of ϕ_A just beneath the clear fluid predicted accurately. The location of the maximum ϕ_A and the small local maximum in T above the channel centerline are both accurately predicted. The velocity from the model solution is

extremely close to the particle velocity of the simulation, and has the merit of also predicting the velocity in the fluid layer.

In Figure 5.10, the model predictions are compared with simulation results at $\phi_A^b = 0.6$, $H/a = 30.54$, and $B = 8.4$. The bulk particle fraction has been increased by one-half and B by a factor of roughly 2.5 from their values at the conditions for which k_α and k_κ were fitted. For an example of the change in conditions, note that $\eta_s(\phi_A^b)$ increases by a factor of 3.5. Model predictions remain in good agreement with the simulation results. Prediction of ϕ_A is less accurate than in the prior case, but the qualitative features are captured correctly. In the ϕ_A profile from simulation in Figure 5.10 (a), considerable ordering is seen at the channel center. Ordering can not be predicted by this model, and because the model assumes smooth shearing of the suspension at all $\phi_A < \phi_{A,m}$, the sticking of particles to the walls observed in the simulation results in an understandable disparity between the predicted and observed u. Remarkably, the maximum in T is correctly predicted to lie above the channel centerline.

A composite of the predicted fully-developed flow profiles for $\phi_A^b = 0.4$ and $H/a = 30.54$ over a range of B are shown in Figure 5.11. Note the large difference between the predicted flows at $B = 25$ and 25.5, and that the maximum in T undergoes nonmonotonic variation with respect to B. Apparently, as ϕ_A at the lower wall increases with B, the reduction in shear rate is outstripped by the growth in intensity of particle interactions until $B \approx 25$. At larger values of gravity, the increased viscosity reduces $\dot{\gamma}$ enough to cause T in this region to drop dramatically. Between

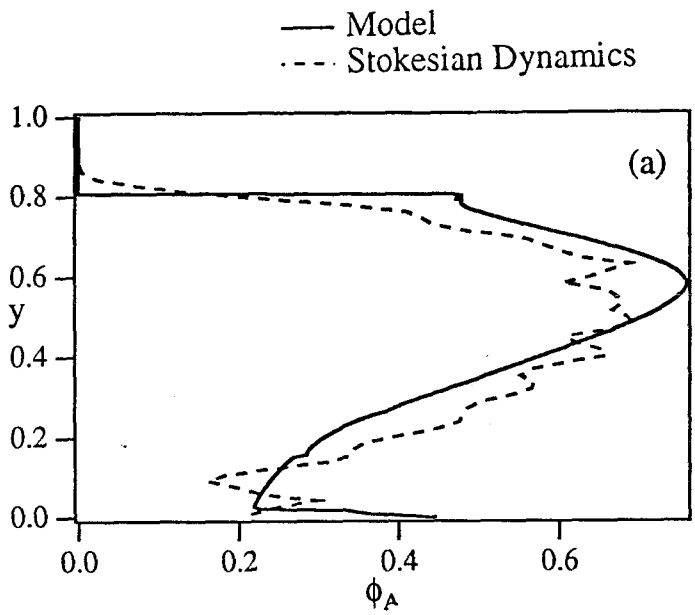

Figure 5.9: Model predictions and Stokesian Dynamics simulation results for the fully-developed flow of a suspension at $\phi_A^b = 0.4$, $B = 3.4$, and $H/a = 30.54$. Profiles of (a) the particle fraction ϕ_A, (b) the velocity u (of the entire suspension in the case of the model, particles for the simulation) and (c) suspension temperature T are shown; (b) and (c) are the following page. The parabolic velocity profile of a Newtonian fluid at the same volumetric flux is shown in (b).

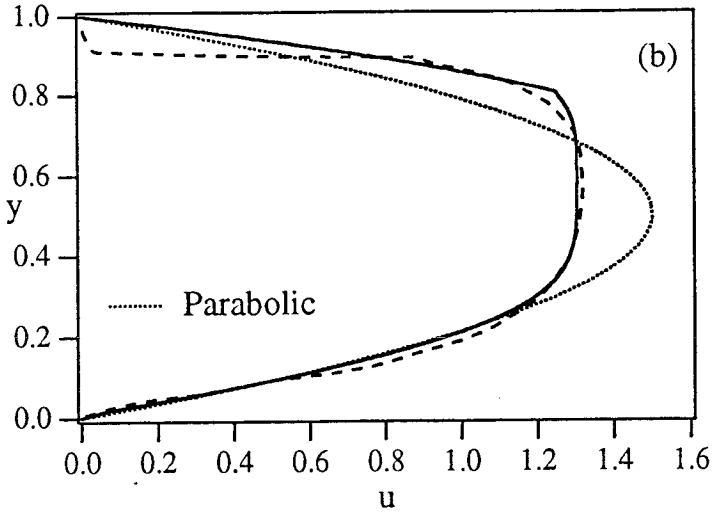

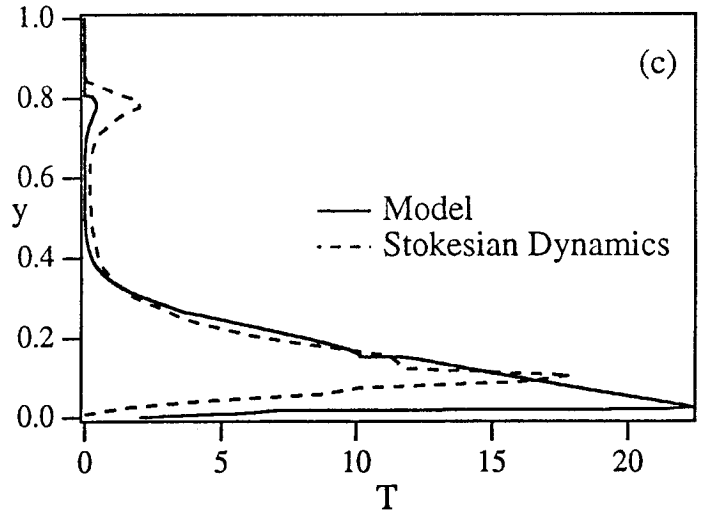

For caption, see previous page.

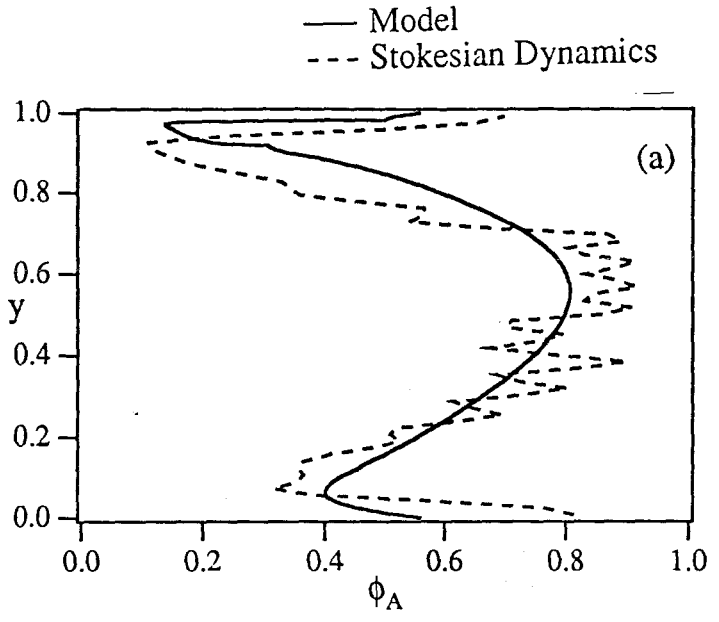

Figure 5.10: Model predictions and Stokesian Dynamics simulation results for the fully-developed flow of a suspension at $\phi_A^b = 0.6$, $B = 8.4$, and $H/a = 30.54$. Profiles of the (a) particle fraction ϕ_A, (b) velocity u (of the entire suspension in the case of the model, particles for the simulation), and (c) suspension temperature T are shown; (b) and (c) are on the following page. The parabolic profile of a Newtonian fluid at the same volumetric flux is shown in (b).

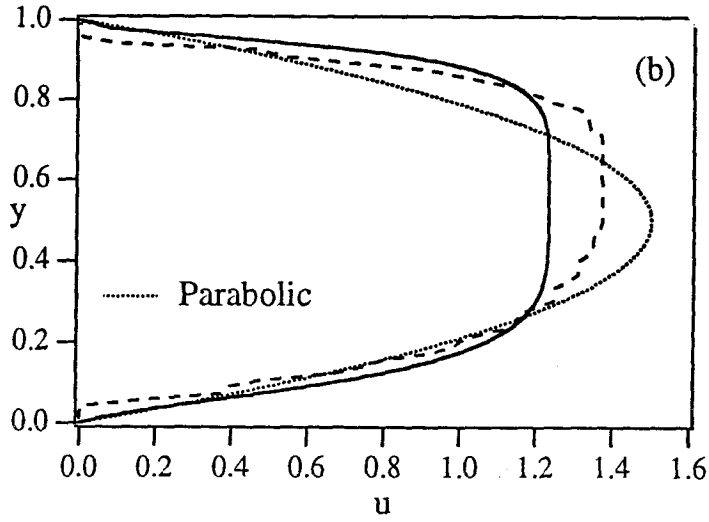

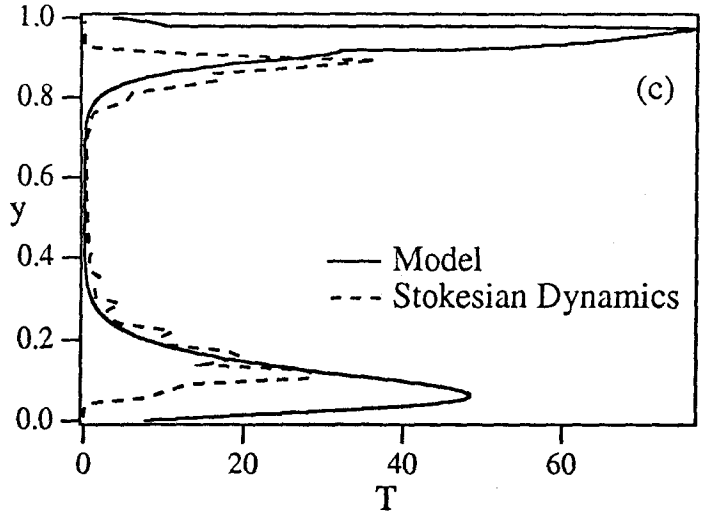

For caption, see previous page.

$B = 10.2$ and 25, the upper surface of the suspended layer of particles falls below the suspension velocity maximum, and for the larger values of B, the majority of the volumetric flux in the channel occurs in the clear fluid layer, with particles transported in a shear layer.

The model does not accurately reflect the reduction in both the maximum particle fraction and degree of blunting as B is increased that was demonstrated by simulations A-D (see Figure 5.4). Figure 5.11 illustrates that the model predicts only a slight reduction in the maximum ϕ_A in going from $B = 3.4$ to 10.2, and consequently predicts an almost indiscernible change in the u profiles. It is possible that this could be remedied by an increase in the value of k_κ, but this would entail also a change in the value of k_α.

Based on the agreement of model predictions with simulation results at conditions well-removed from those at which k_κ and k_α were determined, we conclude that the modeled coefficients accurately capture the ϕ dependence. Thus, we may with some confidence predict flows for which simulation and experimental data are lacking. This is especially useful for conditions which would be prohibitively time-consuming to simulate. Predictions for the conditions $\phi_A^b = 0.6$, $H/a = 100$, and $B = 5$ are presented in Figure 5.12. The particle fraction is predicted to be close to $\phi_{A,m}$ in a wide layer, with consequent extreme blunting of the velocity profile and essentially vanishing T. This layer is supported by a rapidly-sheared layer in which ϕ_A is more dilute and T is large.

The model equations converge to legitimate solutions for $\phi_A^b > 0.15$. At smaller

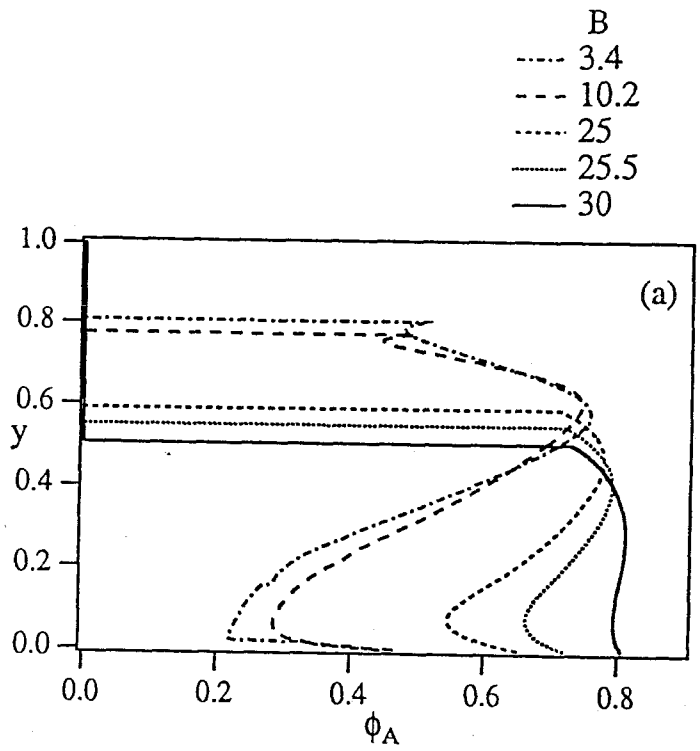

Figure 5.11: Model predictions for the fully-developed flow of a suspension at $\phi_A^b = 0.6$, $H/a = 30.54$, and a range of B. Profiles of (a) particle fraction ϕ_A, (b) suspension velocity u, and (c) suspension temperature T are shown; (b) and (c) are on the following page.

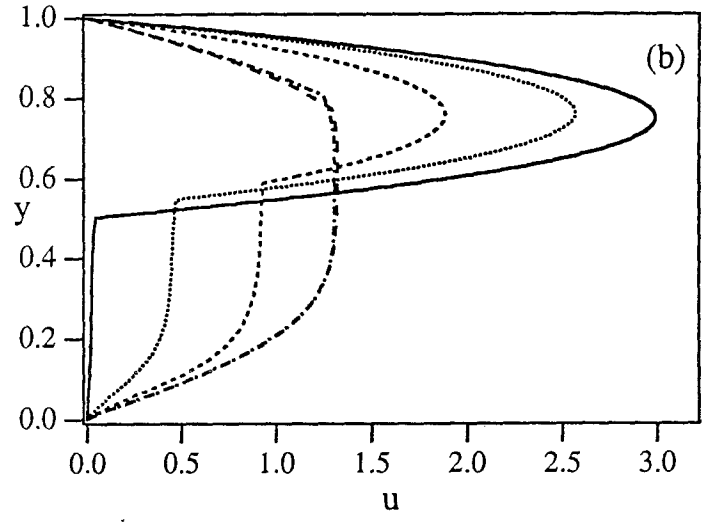

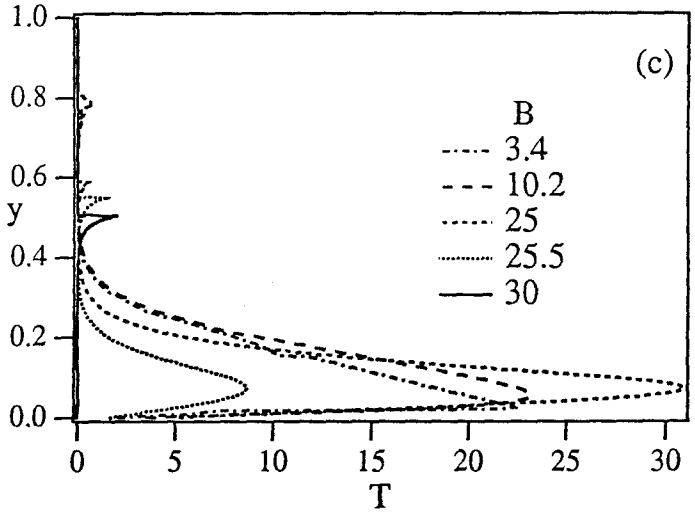

For caption, see previous page.

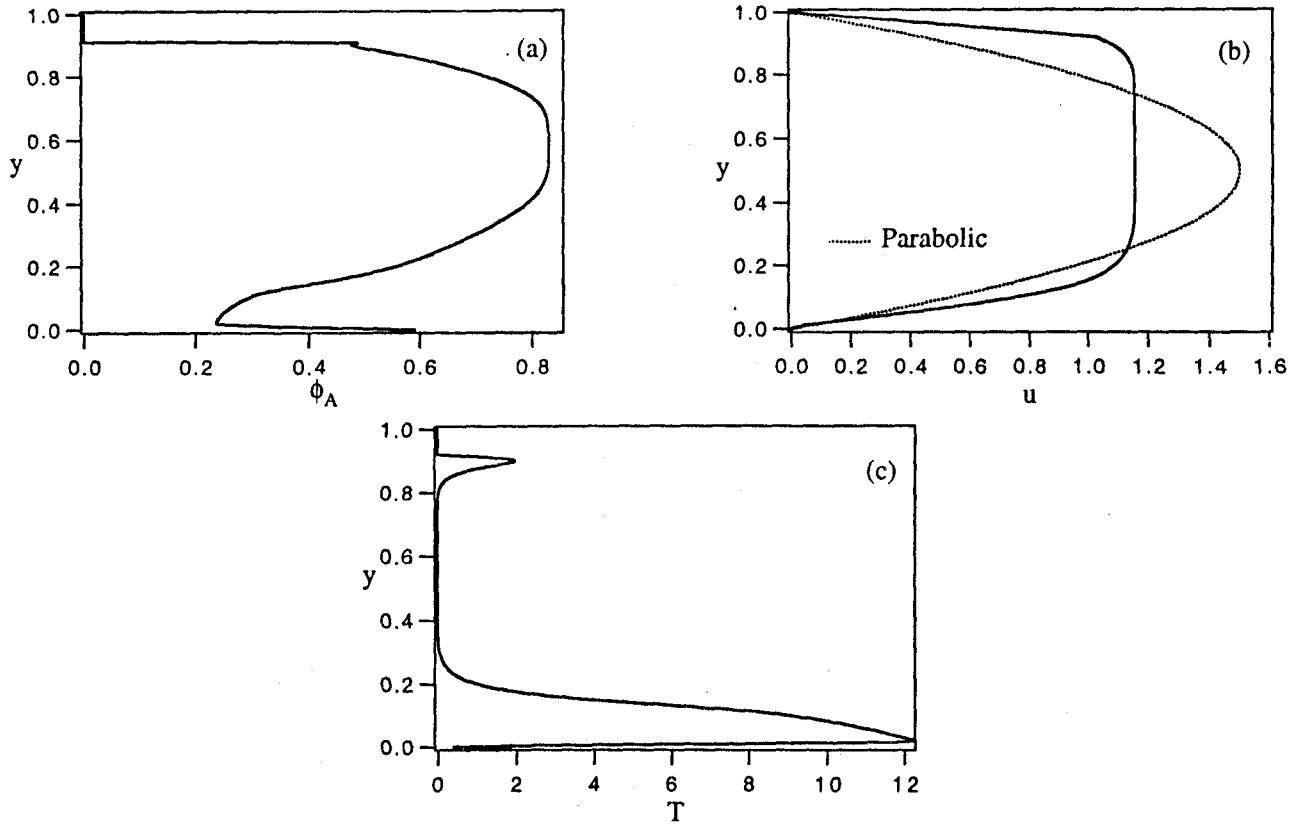

Figure 5.12: Model predictions for the fully-developed flow of a suspension at $\phi_A^b = 0.6$, $B = 5$, and $H/a = 100$: (a) particle fraction ϕ_A, (b) the suspension velocity u, and (c) suspension temperature T. The parabolic profile of a Newtonian fluid at the same volumetric flux is shown in (b).

particle fractions, the model as implemented in this study typically failed to converge. One possible cause of this failure, noted in §5.4.1, is the omission of $\phi^{1/2}$ in the constitutive law $p(\phi) = \phi^{1/2}\eta_p(\phi)$. Further study of the functional forms of $p(\phi)$, $\alpha(\phi)$, and $\kappa(\phi)$ (in particular for $\phi \to 0$) is needed in order to assess whether the cause of difficulty is this omission, inappropriate forms of other coefficients of the model for small ϕ, or the method of solution of the governing equations.

5.5 Summary and concluding remarks

Channel flow of a suspension of dense particles flowing in a monolayer was simulated by Stokesian Dynamics over a range of the bulk particle areal fraction ϕ_A^b, dimensionless channel width H/a, and buoyancy parameter $B = (U^0/\langle u \rangle)(H/a)^2$. The simulations provide basic information which is unavailable from present experimental results. Direct comparisons between simulation results and predictions of the flow by the suspension balance model have established the validity of the model under conditions where buoyancy is relevant. Buoyancy effects can be continuously varied, and a large range of behavior is exhibited. For intermediate to large values of B, the fully-developed flow is quite unlike that of a neutrally-buoyant suspension in pressure-driven flow. Good agreement between simulation and model predictions with flow behavior over a range of B and ϕ_A^b, with model parameters fitted at a single condition, indicates that the constitutive modeling proposed is based upon correct physical principles.

Pressure-driven flow of a suspension of dense particles results in the interesting

and somewhat surprising phenomenon of a relatively heavy material flowing over light, first shown by Altobelli *et al.* (1991). Zhang & Acrivos (1994) have used the diffusive-flux phenomenology of Leighton & Acrivos (1987*b*) to predict this flow, finding excellent agreement with the experiments of Altobelli *et al.* (1991) for the fully-developed flow. They also find that the model predicts a mean secondary non-axial flow; it does not, however, appear that the model based upon diffusive flux could predict the density stratification seen in the channel flow simulations. Aphysical predictions (Phillips *et al.* 1992) of the diffusive-flux model result from its locality in $\dot{\gamma}$. The suspension-balance model we use achieves a nonlocality in $\dot{\gamma}$ indirectly by assuming the particle pressure to depend on the suspension temperature as $\sqrt{T}$. An equation for T, whose form is deduced by physical arguments from the balance equation governing the microscopic kinetic energy in the suspension presented by Batchelor (1970), includes diffusion of T, so that fluctuational motion is produced in regions of large $\dot{\gamma}$, with diffusive transport to regions of small or zero $\dot{\gamma}$.

Simulations show that the flow behavior depends strongly upon both ϕ_A^b and B, but only weakly upon H/a. The weakness of the dependence on H/a is largely due to the fact that the influence of particle size has been included in B; consistent with the finding of NB for $B = 0$, the primary influence of H/a at nonzero B is upon the suspension temperature, as T is larger in the weakly-sheared regions for smaller H/a and varies rapidly near the walls in a layer whose thickness scales roughly as a/H. At fixed ϕ_A^b and H/a, increasing B has the expected effect of driving particles toward the lower wall, but the maximum ϕ_A often lies above the channel centerline:

shear-induced migration causes the particles to move toward the velocity maximum, which lies above the centerline because of the increased η_s (and hence reduced $\dot{\gamma}$) near the lower wall. As a result, there is heavy suspension over light, and this occurs for a wide range of B for moderate concentrations. The strong dependence of the flow behavior on ϕ_A^b is understandable given the strong dependence of the viscosity upon particle fraction.

Confidence in suspension-flow modeling in which T is a variable of central importance is increased by the success of the suspension-balance model in this study. We have tested the model over a range of conditions and it should be noted also that a new type of nonlinearity in T is introduced by particle buoyancy (see Eq. (5.30)). The equation for T, unlike the others, was deduced rather than derived, and its boundary conditions caused some difficulties in the original application. The success with which the model predicted the T field, including some unexpected behavior, indicates that the physical arguments used in deducing the equation are sound. The *ad hoc* boundary condition applied to T is also successful and, although unsatisfying because it is retains considerable freedom in its specification, accurately reflects the hydrodynamic damping effect of a solid boundary. With the work of NB and the present investigation establishing the validity of this model in a straight channel, it would be of interest to know its predictions for other geometries, including rheometric flows and curved channels or pipes.

Bibliography

Abramowitz, M. & Stegun, I. A. 1972 *Handbook of Mathematical Functions.* Dover.

Acrivos, A., Batchelor, G. K., Hinch, E. J., Koch, D. L. & Mauri, R. 1992 Longitudinal shear-induced diffusion of spheres in a dilute suspension. *J. Fluid Mech.* **240**, 651.

Acrivos, A. & Taylor, T.D. 1962. Heat and mass transfer from single spheres in Stokes flow. *Phys. Fluids*, **5**, 387.

Altobelli, S. A., Givler, R. C. & Fukushima, E. 1991 Velocity and concentration measurements of suspensions by nuclear-magnetic-resonance imaging *J. Rheol.* **35**, 721.

Batchelor, G. K. 1970 The stress system in a suspension of force-free particles. *J. Fluid Mech.* **41**, 545.

Batchelor, G. K. 1976 Brownian diffusion of particles with hydrodynamic interaction. *J. Fluid Mech.* **74**, 1.

Batchelor, G. K. 1977 The effect of Brownian motion on the bulk stress in a suspension of spherical particles. *J. Fluid Mech.* **83**, 97.

Batchelor, G. K. 1979 Mass transfer from a particle suspended in fluid with a steady linear ambient velocity distribution. *J. Fluid Mech.* **95**, 369.

Batchelor, G. K. 1982 Sedimentation in a dilute polydisperse system of interacting spheres. Part 1. General theory. *J. Fluid Mech.* **119**, 379.

Batchelor, G. K. 1988 A new theory of the instability of a uniform fluidized bed. *J. Fluid Mech.* **193**, 75.

Batchelor, G. K. & Green, J. T. 1972*a* The hydrodynamic interactions of two small freely-moving spheres in a linear flow field. *J. Fluid Mech.* **56**, 375.

Batchelor, G. K. & Green, J. T. 1972*b* The determination of the bulk stress in a suspension of spherical particles to order c^2. *J. Fluid Mech.* **56**, 401.

Batchelor, G. K. & Wen, C. S. 1982 Sedimentation in a dilute polydisperse system of interacting spheres. Part 2. Numerical results. *J. Fluid Mech.* **124**, 495. Corrigendum 1983 *J. Fluid Mech.* **137**, 467.

Beenakker, C. W. J. 1986 Ewald sum of the Rotne-Prager tensor. *J. Chem. Phys.* **85**, 1581.

Beenakker, C. W. J. & Mazur, P. 1984 Diffusion of spheres in a concentrated dispersion II. *Physica* A **126**, 349.

Bender, C. M. & Orszag, S. A. 1978 *Advanced Mathematical Methods for Scientists and Engineers.* McGraw-Hill.

Berne, B. J. & Pecora, R. 1976 *Dynamic Light Scattering.* Wiley.

Blawzdziewicz, J. & Szamel, G. 1993 Structure and rheology of semidilute suspension under shear. *Phys. Rev. E.* **48**, 4632.

Bossis, G. & Brady, J. F. 1984 Dynamic simulation of sheared suspensions. I. General method. *J. Chem. Phys.* **80**, 5141.

Bossis, G. & Brady, J. F. 1987 Self-diffusion of Brownian particles in concentrated suspensions under shear. *J. Chem. Phys.* **87**, 5437.

Brady, J. F. 1993 Brownian motion, hydrodynamics and the osmotic pressure. *J. Chem. Phys.* **98**, 3335.

Brady, J. F. 1994 The long-time self-diffusivity in concentrated colloidal dispersions. *J. Fluid Mech.* **272**, 109.

Brady, J. F. & Bossis, G. 1988 Stokesian Dynamics. *Ann. Rev. Fluid Mech.* **20**, 111.

Brady, J. F. & Bossis, G. 1985 The rheology of concentrated suspensions in simple shear by numerical simulation. *J. Fluid Mech.* **155**, 105.

Brady, J. F., Phillips, R. J., Lester, J. C., & Bossis, G. 1988 Dynamic simulation of hydrodynamicallyinteracting suspensions. *J. Fluid Mech.* **195**, 257.

Brady, J. F. & Vicic, M. A. 1995*a* Normal stresses in colloidal dispersions. *J. Rheol.* **39**, 545.

Brady, J. F. & Vicic, M. A. 1995*b* Personal communication.

Brenner, H. 1980 Dispersion resulting from flow through spatially periodic porous medium. *Phil. Trans. Roy. Soc.* (London) **A297**, 81.

Carrier, G. F. & Pearson, C. E. 1988 *Partial Differential Equations.* Academic.

Davis, R. H. 1992 Effects of surface roughness on a sphere sedimenting through a dilute suspension of neutrally buoyant spheres. *Phys. Fluids* A **4**, 2607.

Davis, R. H. & Acrivos, A. 1985 Sedimentation of noncolloidal particles at low Reynolds numbers. *Ann. Rev. Fluid Mech.* **17**, 91.

Duffy, J. W. 1984 Diffusion in shear flow. *Phys. Rev.* A **30**, 1465.

Durlofsky, L. & Brady, J. F. 1989 Dynamic simulation of bounded suspensions of hydrodynamically interacting spheres. *J. Fluid Mech.* **200**, 39.

Eckstein, E. C., Bailey, D. G. & Shapiro, A. H. 1977 Self-diffusion in shear flow of a suspension. *J. Fluid Mech.* **79**, 191.

Elrick, D. E. 1962 Source functions for diffusion in uniform shear flow. *Aust. J. Phys.* **15**, 283.

Foister, R. T. & Ven, T. G. M. van de 1980 Diffusion of Brownian particles in shear flows. *J. Fluid Mech.* **96**, 105.

Frankel, I. & Brenner, H. 1991 Generalized Taylor dispersion phenomena in unbounded homogeneous shear flows. *J. Fluid Mech.* **230**, 147.

Frankel, N. A. & Acrivos, A. 1968 Heat and mass transfer from small spheres and cylnders freely suspended in shear flow. *Phys. Fluids* **11**, 1913.

Gadala-Maria, F. 1979 *The Rheology of Concentrated Suspensions.* Ph.D. thesis, Stanford University.

Gadala-Maria, F. & Acrivos, A. 1980 Shear-induced structure in a concentrated suspension of solid spheres. *J. Rheol.* **24** (6), 799.

Hansen, J. P. & McDonald, I. R. 1986 *Theory of Simple Fluids.* Academic.

Irving, J. H. & Kirkwood, J. G. 1950 The statistical mechanical theory of transport processes IV. The equations of hydrodynamics. *J. Chem. Phys.* **18**, 817.

Jeffrey, D. J. 1988 Stresslet resistance functions for low Reynolds number flow using deformable spheres. *Z. Angew. Math. Phys.*, **40**, 1.

Jeffrey, D. J. 1992 The calculation of the low Reynolds number resistance functions for two unequal spheres. *Phys. Fluids* A, **4**, 16.

Jeffrey, D. J. & Corless, R. M. 1988 Forces and stresslets for the axisymmetric motion of nearly touching unequal spheres. *Physicochem. Hydrodynamics* **10**, 461.

Jeffrey, D. J., Morris, J. F. & Brady, J. F. 1993 The pressure moments for two spheres in a low-Reynolds-number flow. *Phys. Fluids* A **5**, 2317.

Jeffrey, D. J. & Onishi, Y. 1984 Calculation of the resistance and mobility functions for two unequal rigid spheres in low-Reynolds-number flow. *J. Fluid Mech.* **139**, 261.

Jenkins, J. T. & McTigue, D. F. 1990 Transport processes in concentrated suspensions: the role of particle fluctuations. In *Two phase flows and waves* (ed. D. D. Joseph and D. G. Schaeffer). Springer.

Jones, R. B. & Burfield, G. S. 1982 Memory effects in the diffusion of an interacting polydisperse suspension. Part 1. *Physica* A. **111**, 562.

Kausch, H. H., Fesko, D. G. & Tschoegl, N. W. 1971 The random packing of circles in a plane. *J. Colloid Interface Sci.* **37**, 603.

Kim, S. & Karrila, S. J. 1991 *Microhydrodynamics: Principles and Selected Applications.* Butterworth-Heinemann.

Kim, S. & Mifflin, R. T. 1985 The resistance and mobility functions of two equal spheres in low-Reynolds-number flow. *Phys. Fluids* **28**, 2033.

Koch, D. L. 1990 Kinetic theory for a monodisperse gas-solid suspension. *Phys Fluids A* **2**, 1711.

Koh, C. J., Hookham, P. & Leal, L. G. 1994 An experimental investigation of concentrated suspension flows in a reactangular channel. *J. Fluid Mech.* **266**, 1.

Krieger, I. M. 1972 Rheology of monodisperse latices. *Advan. Colloid Interface. Sci.* **2**, 111.

Ladd, A. J. C. 1990 Hydrodynamic transport coefficients of random dispersions of hard spheres. *J. Chem. Phys.* **93**, 3483.

Ladyzhenskaya, O. A. 1963 *The Mathematical Theory of Viscous Incompressible Flow.* Gordon and Breach.

Leal, L. G. 1973 On the effective conductivity of a dilute suspension of spherical drops in the limit of low particle Péclet number. *Chem. Eng. Comm.* **1**, 21.

Leal, L. G. 1992 *Laminar Flow and Convective Transport Processes.* Butterworth-Heinemann.

Leighton, D. & Acrivos, A. 1986 Viscous resuspension. *Chem. Engng. Sci.* **41**, 1377.

Leighton, D. & Acrivos, A. 1987*a* Measurement of self-diffusion in concentrated suspensions of spheres. *J. Fluid Mech.* **177**, 109.

Leighton, D. & Acrivos, A. 1987*b* The shear-induced migration of particles in concentrated suspensions. *J. Fluid Mech.* **181**, 415.

Mauri, R. & Acrivos, A. 1995 Personal communication.

Miguel, M. san & Sancho, J. M. 1979 Brownian motion in shear flow. *Physica* **A99**, 357.

Nott, P. R. & Brady, J. F. 1994 Pressure-driven suspension flow: Simulation and theory. *J. Fluid Mech.* **275**, 157.

Novikov, E. A. 1958 Concerning turbulent diffusion in a stream with transverse gradient of velocity. *Appl. Math. Mech. (P.M.M.)* **22**, 412. In Russian.

Nunan, K. C. & Keller, J. B. 1984 Effective viscosity of a periodic suspension. *J. Fluid Mech.* **142**, 269.

O'Brien, R. W. 1979 A method for the calculation of the effective transport properties of interacting particles. *J. Fluid Mech.* **139**, 261.

Ottewill, R. H. & Williams, N. St. J. 1987 Study of particle motion in concentrated dispersions by tracer diffusion. *Nature* **325**, 232.

Parsi, F. & Gadala-Maria, F. 1987 Fore-and-aft asymmetry in a concentrated suspension of solid spheres *J. Rheol.* **31**, 725.

1992)]Phill Phillips, R. J., Armstrong, R. C., Brown, R. A., Graham, A. & Abbott, J. R. 1992 A constitutive model for concentrated suspensions that accounts for shear-induced particle migration. *Phys Fluids* A **4**, 31.

Phillips, R. J., Brady, J. F., & Bossis, G. 1988 Hydrodynamic transport properties of hard-sphere dispersions. I. Suspensions of freely mobile particles. *Phys. Fluids* **31**, 3462.

Phung, T. N. 1993 *Behavior of Concentrated Colloidal Dispersions by Stokesian Dynamics.* Ph.D. thesis, California Institute of Technology.

Proudman, I. & Pearson, J. R. A. 1957 Expansions at small Reynolds number for the flow past a sphere and a circular cylinder. *J. Fluid Mech.* **2**, 237.

Pusey, P. N. 1991 Colloidal suspensions. In *Liquids, Freezing, and Glass Transition* (ed. J. P. Hansen, D. Levesque, and J. Zinn-Justin). Elsevier.

Pusey, P. N. & Megen, W. van 1983 Measurement of the short-time self-mobility of particles in concentrated suspensions. Evidence for many-particle hydrodynamic interactions. *J. Phys.* (Paris) **44**, 285.

Qiu, X., Ou-Yang, H.D., Pine, D.J. & Chaikin, P.M. 1988 Self-diffusion of interacting colloids far from equilibrium. *Phys. Rev. Lett.* **61**, 2554.

Rallison, J. M. & Hinch, E. J. 1986 The effect of particle interactions on dynamic light scattering from a dilute suspension. *J. Fluid Mech.* **167**, 131.

Russel, W. B. 1993 Dynamics of concentrated colloidal dispersions: statistical mechanical approaches. In *Particulate Two-Phase Flow* (ed. M. Roco). Butterworths.

Russel, W. B. & Glendinning, A. B. 1981 The effective diffusion coefficient detected by dynamic light scattering. *J. Chem. Phys.* **74**, 948.

Russel, W., Saville, D. A. & Schowalter, W. R. 1989 *Colloidal Dispersions.* Cambridge.

Schaflinger, U., Acrivos, A. & Zhang, K. 1990 Viscous resuspension of a sediment within a laminar and stratified flow. *Int. J. Multiphase Flow* **16**, 567.

Tabatabaian, M. & Cox, R. G. 1991 Effect of contact forces on sedimenting spheres in Stokes flow. *Int. J. Multiphase Flow* **17**, 395.

Taylor, G. I. 1953 Dispersion of soluble matter in solvent flowing slowly through a tube. *Proc. R. Soc. Lond.* A **219**, 186.

Wallis, G. B. 1969 *One-dimensional Two-phase Flow.* McGraw-Hill.

Werff, J. C. van der 1990 *The Rheology of Hard-Sphere Dispersions.* Ph.D. thesis, University of Utrecht.

Woodcock, L. V. 1981 Glass transition in the hard sphere model and Kauzman's paradox. *Ann. NY Acad. Sci.* **37**, 274.

Zhang, K. & Acrivos, A. 1994 Viscous resuspension in fully developed laminar pipe flows. *Int. J. Multiphase Flow* **20**, 579.